ISSN 2007-2422

Tecnología y Ciencias del Agua

• Índice de revistas mexicanas de investigación científica y tecnológica del Consejo Nacional de Ciencia y Tecnología (Conacyt)

Incluida en Thomson Reuters Science Citation Index® (ISI) • Expanded Thomson Reuters Research Alert® (ISI) • EBSCO • ProQuest • Elsevier • Redalyc

Vol. VIII, núm. 2, marzo-abril de 2017

Tecnología y Ciencias del Agua

Consejo Editorial

Comité Editorial

©***TECNOLOGÍA Y CIENCIAS DEL AGUA***, vol. VIII, núm. 2, marzo-abril de 2017, es una publicación bimestral editada por el Instituto Mexicano de Tecnología del Agua, Paseo Cuauhnáhuac 8532, Colonia Progreso, Jiutepec, Morelos, C.P. 62550, teléfono +52 (777) 3 29 36 00, extensión 474, www.imta.gob.mx/tyca, fsalinas@tlaloc.imta.mx. Editor responsable, Nahún Hamed García Villanueva; Reserva de Derecho al Uso Exclusivo No. 04-2011-083111404500-203 e ISSN 2007-2422, ambos otorgados por el Instituto Nacional de Derechos de Autor. Responsable de la última actualización de este número, Subcoordinación de Difusión y Divulgación, Lic. Francisco José Salinas Estrada, Paseo Cuauhnáhuac 8532, Colonia Progreso, Jiutepec, Morelos, C.P. 62550. Fecha de la última modificación, 15 de abril de 2017.

Tecnología y Ciencias del Agua constituye la continuidad de las revistas *Irrigación en México* (1930-1946); *Ingeniería hidráulica en México* (1947-1971); *Recursos hidráulicos* (1972-1978), e *Ingeniería hidráulica en México*, segunda época (1985-2009); *Tecnología y Ciencias del Agua*, antes *Ingeniería hidráulica en México* (2010-2011).

ISSN 2007-2422

Para comentarios a la Coordinación Editorial, dé clic aquí

Tecnología y Ciencias del Agua

Vol. VIII, núm. 2, marzo-abril de 2017

Para suscripciones, dé clic aquí

Portada: lagunas de Cotacotani, Andes, Chile. Localizadas a 4 495 metros de altura, las lagunas de Cotacotani se consideran una de los cuerpos de agua a mayor altitud en la Tierra. Son alimentadas por agua de deshielo que fluye de los glaciares del volcán Parinacota (6 348 metros de altura).

Foto: Bernhard Edmaier.

Cover: Located at an altitude of 4 495 metres, the Cotacotani Lakes are among the highest lakes on earth. They are fed by meltwater which flows down from the glaciers of Parinacota Volcano (6,348 metres).

Photo: Bernhard Edmaier.

Palacio de Verano cerca de Beijing, China.

Foto: Fernando Leyva Calvillo.

Contenido

Artículos técnicos

Contents

Technical articles

Relationships between floods and social fragmentation: A case study of Chiayi, Taiwan

• Yung-Jaan Lee •
Chung-Hua Institution for Economic Research, Taiwan

• Li-Pei Peng* • Ting-Jay Lee •
National Taiwan University, Taiwan
*Corresponding author

Abstract

Lee, Y.-J. Peng, L.-P., & Lee, T.-J. (March-April, 2017). Relationships between floods and social fragmentation: A case study of Chiayi, Taiwan. *Water Technology and Sciences* (in Spanish), *8*(2), 5-18.

The social vulnerability approach has been recognized as one of the most important tools for exploring contexts and coping strategies in relation to contemporary disasters. However, social vulnerability is such a multi-faceted and complex construct that scholars from different fields have not reached consensus on how best to measure it, and discussions on this issue continue. Some scholars consider that this approach can manifest the role of human agency. However, given a lack of historical observations, interpreting the causes of disasters through event-based perspectives cannot easily reflect the institutional mechanism behind disaster events. Thus, this study applies a social fragmentation concept to represent the opposite of social integration and depicts the trend of social fragmentation based on historical data from 1983–2011 in the Chiayi County, Taiwan. Furthermore, this study overlays the trend of social fragmentation and the flood map at the township level using the GIS technique. Four types of social fragmentation are identified, namely "continuous high social fragmentation," "transformed social fragmentation," "fluctuating social fragmentation" and "continuous low social fragmentation". The study suggests that the social fragmentation approach can play a supplementary role in measuring the social vulnerability indicator.

Keywords: Floods, social fragmentation, social vulnerability, disaster, overlay analysis.

Resumen

Lee, Y.-J. Peng, L.-P., & Lee, T.-J. (marzo-abril, 2017). Las relaciones entre las inundaciones y la fragmentación social: un estudio de caso de Chiayi, Taiwán. Tecnología y Ciencias del Agua, 8*(2), 5-18.*

El enfoque de la vulnerabilidad social ha sido reconocido como una de las herramientas más importantes para explorar contextos y estrategias de afrontamiento en relación con los desastres contemporáneos. Sin embargo, la vulnerabilidad social es un constructo tan multifacético y complejo, que estudiosos de diversas disciplinas no han llegado a un consenso sobre la mejor manera de medirlo y continúa el debate sobre dicha cuestión. Algunos estudiosos consideran que este enfoque puede manifestar el papel de la intervención humana. Sin embargo, dada la falta de observaciones históricas, interpretar las causas de los desastres a través de perspectivas basadas en eventos no puede reflejar el mecanismo institucional detrás de tales eventos. Así, el presente estudio aplica el concepto de fragmentación social para representar lo opuesto de la integración social. Asimismo, muestra la tendencia de la fragmentación social con base en datos históricos de 1983 a 2011 en el condado de Chiayi, Taiwán. Por otra parte, se superpone a la tendencia de la fragmentación social y elabora un mapa de inundación a nivel municipal mediante la técnica de SIG. Se identifican cuatro tipos de fragmentación social, a saber: " fragmentación social alta continua," "fragmentación social transformada," "fragmentación social fluctuante" y "fragmentación social baja continua". El estudio sugiere que el enfoque de la fragmentación social puede desempeñar un papel complementario en la medición del indicador de vulnerabilidad social.

***Palabras clave**: inundaciones, fragmentación social, vulnerabilidad social, desastres, análisis de superposición.*

Received: 13/05/2016
Approved: 22/09/2016

Introduction

All cities —even those in wealthy countries— are vulnerable to disasters and extreme climate events, and their resilience and capacity to cope vary markedly (Seto, Parnell, & Elmqvist, 2013). Therefore, achieving urban sustainability and resilience is a priority for all governments (Sukhdev, 2013). Recently, besides the physical vulnerability approach, the social vulnerability approach has been proposed as a crucial perspective in discussing the causes of contemporary disasters, because it stresses human agency when discussing the issues of environmental change, or the occurrence of disaster (Lee, 2014; Khan, 2012).

Some researchers have suggested that given identical natural hazards, the consequent damage will be more severe when the social system is more vulnerable (Cutter 1996; Cutter, Boruff, & Shirley, 2003; Mendes, 2009; Menoni, Molinari, Parker, Ballio, & Tapsell, 2012; Turner *et al*., 2003). Thus, because the structural characteristics of social systems moderate various impacts of disasters, discourse on disasters is considered a social construct rather than a simple natural event (Adger, Brooks, Bentham, Agnew, & Eriksen, 2004; Adger *et al*., 2011; Cutter, 1996; Cutter, Mitchell, & Scott, 2000; Cutter *et al*., 2003; Khan, 2012; Tierney, 2007).

Some scholars have noted that the traditional epistemology of disaster was based on an "event-based" perspective that overemphasized specific disaster events such as typhoons or earthquakes. However, it is easy to overlook that many disasters have human causes. For instance, overuse or improper use of slopelands owing to urbanization can cause building collapses and landslides. Focusing solely on a disaster event or its immediate impact excludes consideration of human agency (Tierney, 2007).

The institutional roots of disasters thus are difficult to improve, and consequently social vulnerability researchers consider the "process of vulnerability" necessary to understand the causes of disasters (Turner *et al*., 2003). Such understanding of disasters can help establish more local-contextual strategies to respond to disasters, environmental changes and sustainable lifestyles (Turner *et al*., 2003). Hence, only by understanding disasters from the perspectives of trajectory and process, is it possible to clarify the limitations and possibilities for human action when facing changes in social-environmental systems.

On the other hand, rural-urban mobility has increased urbanization in both developing and newly developed countries. Socio-economic articulation is also increasing between larger and smaller urban communities (Barbieri & Carr, 2005). Indeed, a hallmark of contemporary urbanization is that urban areas are growing faster and larger than before, and in new geographic locations (Fragkias, Güneralp, Seto, & Goodness, 2013). Furthermore, since the 1990s, urbanization has led to clear trends of an ageing rural population and shrinking working population in the agriculture, forestry and fisheries sectors (Kohsaka, Shih, Saito, & Sadohara, 2013). Consequently, the most vulnerable residents tend to be socioeconomically deprived. Such residents also tend to live in informal or traditional settlements, located in areas at the greatest risk for flooding or landslides, and also for eviction during environmental crises (Nagendra, Sudhira, Katti, & Schewenius, 2013).

Social fragmentation refers to the social organization or structure of a neighborhood, where a highly fragmented neighborhood influences social connections within the neighborhood and between residents, with potential consequences for the quality of social life (Ivory, Collings, Blakely, & Dew, 2011). The social fragmentation construct fits broadly into the social properties of neighborhoods, along with the more commonly used social cohesion and capital constructs. However, few studies have examined social fragmentation can be used to examine the relationship with vulnerability.

This study applies social fragmentation to explore the integration of a social system to supplement social vulnerability index. Furthermore, this study examines whether longitudinal data can represent the trend of

• ISSN 2007-2422

social fragmentation and potential responses in the face of natural hazards in Chiayi County, Taiwan, a newly industrialized country.

Social vulnerability, social fragmentation and disaster

Vulnerability has become an important concept in elucidating the condition of a system or its vulnerability to damage from hazards (Lee, 2014). Vulnerability is "the degree to which a system is susceptible to, or unable to cope with, adverse effects of climate change, including climate variability and extremes. Vulnerability is a function of the character, magnitude and rate of climate change and variation to which a system is exposed, its sensitivity, and its adaptive capacity" (IPCC, 2001, 2007). Vulnerability is a function of exposure to a stressor, the effect of that stressor (also named potential impact or sensitivity) and recovery potential (also termed adaptive capacity or resilience) (Adger, 2006; Lange, Sala, Vighi, & Faber, 2010; Dwyer, Zoppou, Nielsen, Day, & Roberts, 2004; Sonwa, Somorin, Jum, Bele, & Nkem, 2012; Turner *et al*., 2003). In short, vulnerability is exposure to unforeseen events, incidents and stress, and the difficulty of coping with them (Elmqvist *et al*., 2013). Analysis of vulnerability provide an effective approach to promoting corrective actions to reduce impacts from disasters by supporting coping strategies and facilitating adaptation (Kelly & Adger, 2000).

There are three processes related to vulnerability, namely the production and application of knowledge related to vulnerability, and the answering of questions related to interactions between the first two processes. These three processes exist due to multi-faceted and dynamic of vulnerability. The range of focal points differs dramatically among different disciplines, and the degree of interest influences both the production and application of knowledge related to vulnerability (Lee, 2014).

Due to the multiple dimensions and high levels of abstraction, definitions of vulnerability vary among different knowledge fields and disciplines (Cutter & Finch, 2008; Khan, 2012; Menoni *et al*., 2012). Vulnerability can be either physical (or biophysical) or socio-economic (Adger *et al*., 2004; Birkmann, 2006; Cutter, 1996; European Commission, 2011; Tate, Burton, Berry, Emrich, & Cutter, 2011). Physical vulnerability resembles that was devoted to the traditional impact method, which is based on natural science, and stresses the risk of exposure to risks associated with natural hazards (Adger *et al*., 2004; Cutter, 1996; Cutter *et al*., 2003). In contrast, social vulnerability denotes the state that exists before disasters (Finch, Emrich, & Cutter, 2010; Schmidtlein, Shafer, Berry, & Cutter, 2011), and includes social, economic, political and institutional components (European Commission, 2011). Therefore, the social vulnerability is the characteristics of social system and represents the wellbeing of residents. The more social vulnerability may increase the impacts of natural hazards on the society. Furthermore, while the hazards happened, residents may be inadequate to recover from their vulnerable state, and probably fall into worse conditions while facing coming hazards.

Therefore, considering social vulnerability as a planning tool and utilizing it to planning practices can motivate sustainable planning and human life. The sustainability of treating social vulnerability as a planning tool is important for responding to climate change, because of the difficulty of forecasting environmental trends. Social systems on various geographical scales must develop their own capacities to respond to extreme weather events. Only by doing so can the social capacity building become a real and long-term adaptation strategy. Social vulnerability thus can respond to environmental changes and disasters that impact social systems, and can remind government agencies, the private sector and residents to base developmental strategies on social conditions — particularly when facing with the development of highly vulnerable places.

Furthermore, the complexity of disasters means the content and application of social vulnerability needs to be a developing concept.

ISSN 2007-2422 •

Certain factors have been recognized as crucial determinants of the degree of a social system, such as personal property, age, density of buildings, single department economics, race, ethnicity, etc. However, few studies have attempted to conceptualize these factors or thoroughly examine the relationships between the main factors and the changes in those relationships.

Considering the regional characteristics of disasters, most studies have found it difficult to determine the weightings of measurement items. Consequently, most social vulnerability studies primarily measure social vulnerability without weighting (Cutter, 1996; Cutter *et al*., 2003; Mendes, 2009). Although measurement methods can provide an abstract picture of the vulnerability of a social system, such an approach cannot easily display details and other potential characteristics. Such measurements and the lack of historical data may neglect potential heterogeneity in terms of the role of human agency among social systems and the reflection of institutional mechanisms.

On the other hand, the origins of the term "social fragmentation" can be found in the work of Durkheim, who is widely considered the "father" of sociology (Emirbayer 2002; Syme 2000). Generally, social fragmentation was more significant than deprivation in explaining small area variations for mental rather than physical health outcomes (Ivory *et al*., 2011; Evans, Middleton, & Gunnell, 2004).

Social fragmentation appears to be the preferred term, and is generally defined as the inverse of social integration (Evans *et al*., 2004) or social cohesion (Cramm, Van Dijk, & Nieboer, 2013; Fagg *et al*., 2008). There is also little reference to the wider research on the processes of anomie or social fragmentation at a societal level, such as work on urbanization (Ivory *et al*., 2011) or changes in societal structure and anomie (Makinen, 2000).

Social fragmentation represents weak social solidarity and a lack of social support, whereby individuals who belong to a highly social fragmented society can hardly cope with the difficulties they face. Thus it can be assumed that to some extent, a system based on high social integration is better able to respond to disaster or recover from damage. The other crucial point is that social fragmentation, which denotes the degree of social integration of a social system, must result from long-term societal development. That is to say, local residents with more social fragmentation could be uneasy to recover from natural hazards. But the social integration, contrary to concept of social fragmentation, could be the important tools for local residents to adapt to natural hazards. Therefore, like two sides to one coin, this paper highlights the indicators of social fragmentation to catch the whole concept.

High divorce rate, high migration rate and percentage of people living alone can cause high social fragmentation. Therefore, divorce rate, migration rate and percentage of people living alone provide effective measurements of social fragmentation (Dorling & Gunnell, 2003). On the other hand, the consolidation of the feed, seed, processed grain, and livestock industries has decreased the number of small businesses in rural areas. This decrease has contributed to the decrease in demand for labor. Rural areas that once provided employment for all young adults willing to work in challenging conditions now offer only partial employment. The situation is exacerbated by the decrease in services such as schools, shops, and cultural opportunities that accompanies the population decline, and the rising age of the remaining population further stresses social services in rural areas (Carr & Kefalas, 2009; Elmqvist *et al*., 2013).

Moreover, the rapid growth of the elderly population worldwide, and increasing urbanization, will influence international trends in living arrangements, family structure, and the informal care-giving options available for older persons (Hokenstad & Roberts, 2010). Vulnerable socio-economic settlements, particularly slums, are likely to be especially affected by this double whammy of urbanization and climate change (D'Souza, 2011). Urbanization will result in poor infrastructure in rural areas, including in the areas of sanitation, treated water, and

• ISSN 2007-2422

accessibility to health facilities, and thus will further induce migration from rural to urban areas (Elmqvist *et al*., 2013). Therefore, out-migration can be seen as a root cause of social fragmentation in rural areas.

Marriage and social support limit the negative impacts of chronic illness (Elliott, Charyton, Sprangers, Lu, & Moore, 2011). Furthermore, single and unpaired individuals are more responsive to psychological stress than married individuals, consistent with a growing body of evidence suggesting that marriage and social support protect against stress (Maestripieri, Baran, Sapienza, & Zingales, 2010).

Data and Method

Study site

Chiayi County, one of the 22 municipalities and counties of Taiwan, is located on the west coast of the country. To the east of Chiayi County is Jade Mountain; to the west is the Taiwan Strait; to the south is Tainan County, and to the north is Yunlin County. Chiayi County has an area of 1,903 square kilometers, or 5.35% that of Taiwan. Chiayi County has 18 cities and townships (figure 1). Located in Central Southern Taiwan, Chiayi is easily accessible, particularly now the completion of the Taiwan High-Speed Rail has cut travel time to Taipei, the capital of Taiwan, to just one hour.

The population of Chiayi County was approximately 540 000 in 2013. The Tropic of Cancer runs through Chiayi, which has a different landscape to other places on the Tropic of Cancer, most of which are either dessert or semi-dessert while Taiwan is forested owing to the abundant rainfall brought by the trade wind and airstreams. Chiayi County has four notable geographic features: coastal, plains, hills and mountains.

Land subsidence and changes in the coastline are important issues in Taiwan (Chen, Wang,

Figure 1. Chiayi County, Taiwan.

ISSN 2007-2422 •

Hsu, Yu, & Kuo, 2010). Coastal land subsidence has continued unabated because most fish species raised in coastal fish farms require more than 80 percent fresh water, which is sourced underground. Chen and Kuo (2000) analyzed data from 1976 to 1996 and determined that sea-levels on the Chiayi coast rose approximately 1.92cm/year during that period, exceeding the global average. Ground subsidence has slowly decreased since the government implemented some control measures, and thus its contribution to rising sea-levels has also decreased. Although whether climate change is the cause of the rise in sea-level on the Chiayi coast cannot be determined, the existence of the phenomenon is undoubted. For example, the typhoon Mindulle attacked Taiwan in July, 2, 2004. Around 11,793 hectares of lands were flooded in Chiayi County. In June 12, 2005, the extremely torrential rain continued for several days, this area was serous flooded including 8,261 hectares of lands in Dongshi Township and 4,859 hectares of lands in Budai Township.

Variables and data resources

This study conducts two analyses. First, this study examines the historical trend of social fragmentation at the township level in Chiayi County by using longitudinal statistical data from 1983 to 2011. Second, this study performs overlay analyses of social fragmentation trends and flood maps. Using the map of social fragmentation trend as the base map, this study overlays a second layer, the flood map of Chiayi County, under the condition of rainfall exceeding 500 mm daily. According to the Central Weather Bureau of Ministry of Transportation and Communications in Taiwan, the extremely torrential rain means the accumulative rainfall up to the threshold of 500 mm daily or above. Thus, the rainfall threshold set to 500 mm daily. Through this strategy, this study examines the potential responsive capacity to major disasters at the township level.

This study suggests that high migration from rural areas manifests high social fragmentation. Accordingly, the rate of social increase is assumed to be negatively related with social fragmentation. On the other hand, marriage is considered to be a crucial factor that increases social integration in a social system (table 1).

To summarize, this study uses the rate of social increase, crude divorce rate and crude marriage rate to measure social fragmentation. Longitudinal data for these three variables were collected from the Department of Accounting and Statistics of Chiayi County Government from 1983 to 2011. To assess the responsive capacity of a social system to natural hazards, this study uses flood maps from Taiwan's Water Resources Agency for 2007 to 2011. The two data

Table 1. Variables and their relation to social fragmentation.

Construct	Variable	Relation to social fragmentation	Data source[1]
Social fragmentation	Rate of social increase [2]	Negative	Department of Accounting and Statistics, Chiayi County Government (1983-2011)[3]
	Crude divorce rate[4]	Positive	Department of Accounting and Statistics, Chiayi County Government (2000-2011)
	Crude marriage rate[5]	Negative	
Natural hazard risk	Floods	-- --	Water Resources Agency, Ministry of Economic Affairs (2007-2010)

Note: (1) Dapu Township has recently had extremely high social migration rates. To avoid confounding the index framework, this study excluded data from Dapu; (2) social increase rate = (in-migration rate) – (out-migration rate); (3) the original data of the rate of social increase are absent for 1988 and 1995; (4) crude divorce rate = (registered divorces/population of mid-year)*1 000 (5) Crude marriage rate = (registered marriages/population of mid-year)*1 000.

• ISSN 2007-2422

are transformed from long-term statistics to a stationary description of local characteristic. Thus, this study will not attempt to analyze the longitudinal statistical data year by year. Restated, the longitudinal statistical data are used for realizing the types of social fragmentation of social system, and the flood map data are used for mapping the spatial distribution of the natural hazards. By so doing, this study can examine different disaster exposure risks, trends in responsive capacities, and differences among townships.

Analysis Method

The analytical procedure comprises two steps. The first step is to analyze social fragmentation during 1983-2011. Meanwhile, the second step is to overlay the flood map on top of that of social fragmentation trends in Chiayi County by GIS.

To obtain meaningful comparisons among the three variables and integrate them into a social fragmentation index, this study subjects the variable to a standardization procedure whereby social fragmentation increases with decreasing social increase and marriage rate, and decreases with decreasing divorce rate. Therefore, before summing the standardized scores, this study reverses the direction of the standardized scores of divorce rate. Next, this study sums the standardized scores of variables and calculates the annual averages for each variable as an annual social fragmentation index. The longitudinal data is from 1983-2011. To clearly interpret the characteristics of social fragmentation, this study divides the 18-year period into six sub-periods, namely 1983-1985, 1986-1990, 19991-1995, 1996-2000, 2001-2005 and 2006-2011. This study sums the standardized scores and then averages them for each time period. Thus, due to the standardization procedure, the different longitudinal data could be utilized to explain the trend of social fragmentation in different periods. Furthermore, this study overlays the spatial distribution of flood maps and the six time period map of social fragmentation.

Results

According to the range of standardized scores of the rate of social increase from 1983 to 2011, Fanlu is the township with the highest in-migration, while Dongshi and Xikou are the townships with the highest out-migration. The townships that changed from out-migration to in-migration are Dalin, Lucao, Xinkang, Yizhu and Liujiao. Moreover, Zhuqi, Taibao and Minxiong show decreased in-migration. Finally, Puzi, Meishan, Zhongpu and Shuishang changed from in-migration to out-migration (tables 2 and 3).

Tables 4 and 5 list the standardized scores of crude divorce rate, which are original and not subject to reverse adjustment. The different range of standardized scores of divorce rate from 2000 to 2011 shows that townships with increased divorce rates are, ranked from low to high, Xikou, Dongshi, Yizhu, Xinkang, Zhongpu, Zhuqi and Alishan. Specifically, Xinkang, Zhongpu, Zhuqi and Alishan transformed from negative to positive values. Meanwhile, the townships with decreased divorce rates are Taibao, Dalin, Budai, Shuishang, Puzi, Liujiao and Meishan. Lucao, Minxiong and Fanlu changed from positive to negative values.

Based on the distribution of the range of standardized scores of marriage rate from 2000 to 2011, table 6 shows that the townships with increased marriage rate were Fanlu, Meishan, Minxiong, Taibao, Shuishang, Budai, Zhuqi, Zhongpu, Puzi and Alishan. Meanwhile, the townships with decreased marriage rate were Lucao, Dalin, Xinkang, Dongshi, Xikou, Liujiao and Yizhu. Townships where marriage rate changed from decreasing to increasing are Minxiong, Taibao, Zhuqi, Puzi and Alishan. Finally, marriage rate changed from increasing to decreasing in Minxiong, Taibao, Zhuqi, Puzi and Alishan (tables 6 and 7).

Tables 8 and 9 point out that townships with increased standardized social fragmentation scores include Alishan, Meishan, Zhuqi, Zhongpu, Shuishang and Minxiong. Meanwhile, townships with decreased standardized social

ISSN 2007-2422 •

Table 2. Range of the rate of social increase from 1983 to 2011.

Region	Township	Range of Z-score
Coast	Dongshi	0.63
	Budai	0.41
Plain	Liujiao	1.34
	Yizhu	1.04
	Lucao	0.97
	Shuishang	-1.89
	Xinhang	0.98
	Minxiong	-2.15
	Xikou	0.73
	Taibao	-0.31
	Dalin	0.77
	Puzi	-0.74
Hill-Mountain	Zhougpu	-1.81
	Zhuqi	-0.21
	Meishan	-0.77
	Fanlu	0.49
	Alishan	0.70

Table 3. Characteristics of the rate of social increase from 1983 to 2011.

Range	1983	2011	Characteristic	Township
Positive	+	+	Increased in-migration	Fanlu
	–	+	Out-migration to in-migration	Dalin, Lucao, Xinhang, Yizhu, Liujiao
	–	–	Decreased out-migration	Dongshi, Xikou
Negative	+	+	Decreased in-migration	Zhuqi, Taibao, Minxiong
	+	–	In-migration to out-migration	Puzi, Meishan, Zhougpu, Shuishang
	–	–	Increased out-migration	None

Note: Ranges of standardized scores are ranked sequentially from low to high.

Table 4. Range of crude divorce rate from 2000 to 2011.

Region	Township	Range of Z-score
Coast	Dongshi	0.88
	Budai	-0.18
Plain	Liujiao	-0.78
	Yizhu	1.02
	Lucao	-1.07
	Shuishang	-0.65
	Xinhang	1.02
	Minxiong	-2.08
	Xikou	0.41
	Taibao	-0.01
	Dalin	-0.10
	Puzi	-0.75
Hill-Mountain	Zhougpu	1.47
	Zhuqi	2.05
	Meishan	-0.80
	Fanlu	-2.50
	Alishan	7.01

Table 5. Characteristics of crude divorce rate from 2000 to 2011.

Range	2000	2011	Characteristic	Township
Positive	+	+	Increased divorce rate	Xikou, Dongshi, Yizhu
	–	+	Negative to positive	Xinhang, Zhougpu, Zhuqi, Alishan
	–	–	Increased divorce rate	None
Negative	+	+	Decreased divorce rate	Shuishang, Dalin
	+	–	Positive to Negative	Lucao, Minxiong, Fanlu
	–	–	Decreased divorce rate	Taibao, Budai, Puzi, Liujiao, Meishan

Table 6. Range of crude marriage rate from 2000 to 2011.

Region	Township	Range of Z-score
Coast	Dongshi	-1.21
	Budai	0.59
Plain	Liujiao	-2.18
	Yizhu	-2.36
	Lucao	-0.41
	Shuishang	0.55
	Xinhang	-1.12
	Minxiong	0.40
	Xikou	-1.26
	Taibao	0.49
	Dalin	-0.42
	Puzi	2.27
Hill-Mountain	Zhougpu	1.77
	Zhuqi	0.85
	Meishan	0.38
	Fanlu	0.11
	Alishan	3.51

Table 7. Characteristics of crude marriage rate from 2000 to 2011.

Range	2000	2011	Characteristic	Township
Positive	+	+	Increased marriage rate	Shuishang, Zhougpu
	–	+	Negative to positive	Minxiong, Taibao, Zhuqi, Puzi, Alishan
	–	–	Increased marriage rate	Fanlu, Meishan, Budai
Negative	+	+	Decreased marriage rate	Dongshi
	+	–	Positive to Negative	Xinhang, Xikou, Liujiao, Yizhu
	–	–	Decreased marriage rate	Lucao, Dalin

fragmentation scores include Taibao, Xinkang, Dalin, Puzi, Yizhu, Budai, Xikou, Dongshi, Fanlu, Lucao and Liujiao. Only Lucao had its standardized score change from negative to positive, while only Meishan and Zhuqi had their scores change from positive to negative.

Based on the trend of social fragmentation from 1983 to 2011, this study overlaid the map

ISSN 2007-2422 •

Table 8. Range of social fragmentation from 2000 to 2011.

Region	Township	Range of Z-score
Coast	Dongshi	0.75
	Budai	0.58
Plain	Liujiao	0.98
	Yizhu	0.52
	Lucao	0.90
	Shuishang	-1.43
	Xinhang	0.11
	Minxiong	-1.73
	Xikou	0.70
	Taibao	0.09
	Dalin	0.26
	Puzi	0.38
Hill-Mountain	Zhougpu	-1.29
	Zhuqi	-0.48
	Meishan	-0.17
	Fanlu	0.81
	Alishan	-0.04

Table 9. Characteristics of social fragmentation from 2000 to 2011.

Range	2000	2011	Characteristic	Township
Positive	+	+	Decreased fragmentation	Taibao, Puzi, Fanlu
	–	+	Negative to positive	Lucao
	–	–	Decreased fragmentation	Xinhang, Dalin, Yizhu, Budai, Xikou, Dongshi, Liujiao
Negative	+	+	Increased fragmentation	Zhougpu, Shuishang, Minxiong
	+	–	Positive to negative	Meishan, Zhuqi
	–	–	Increased fragmentation	Alishan

of social fragmentation score with the flood map (figure 2), thus revealing four types of social fragmentation trend. Type one is characterized by social fragmentation scores that remain continually below the average for all townships. Such types can be represented as "continuous high social fragmentation," which includes Dongshi, Budai, Yizhu, Lucao, Puzi, Liujiao and Xinkang. Type Two is characterized by social fragmentation scores that change from positive to negative, indicating increased social fragmentation. Type Two is labeled "transformed social fragmentation," and includes Shuishang and Zhongpu. Type Three exhibits fluctuating social fragmentation, and includes Dalin, Meishan, Zhuqi, Fanlu and Alishan, and this type is termed "fluctuating social fragmentation." Finally, Taibao is categorized as Type Four because of its higher social fragmentation score than the average of all townships. Type Four thus is named "continuous low social fragmentation".

Discussions

The social fragmentation is an important factor of social vulnerability concept. Comparing to the concept which is a comprehensive measure, the

• ISSN 2007-2422

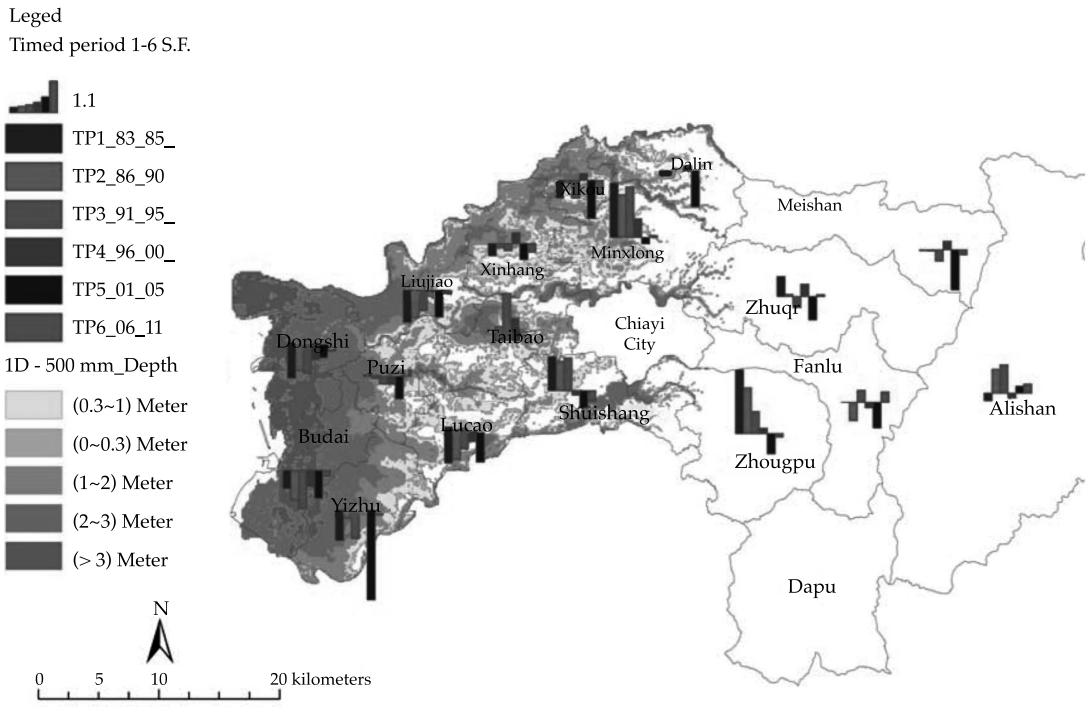

Figure 2. Overlay analysis of the trend of social fragmentation in six time-periods.

social fragmentation may specifically reflect on the degree of social integration of social system. The less social fragmentation, or let's say, the more social integration is a chance to overcome the natural hazards at local level. Thus, instead of social vulnerability, this paper highlights the relationship between social fragmentation and natural hazards.

In addition, the social fragmentation is able to reflect the local characteristics, but hard to manifest them onto spatial distribution. Thus, this paper will contribute to mapping the longitudinal indicators of social fragmentation on the spatial distribution. The efforts help to illustrate the local characteristics of social structure in the map and to explain how flood map interact with the trends of social fragmentation as well. This paper identifies four types of social fragmentation, including "continuous high social fragmentation," "transformed social fragmentation," "fluctuating social fragmentation" and "continuous low social fragmentation."

This study adopts migration and marriage as indicators of social fragmentation, because the decision of migration and marriage are usually based on the household units. Thus, the migration and marriage indicators are able to represent local characteristics in the household. Another social system is a community basis. Communities represent local characteristics among the households. Although this study cannot capture them owing to data availability, however, the other indicator including neighborhood, organizational mobilization, social network, trust, etc. will be suitable for the chosen factors of social fragmentation for future studies.

Conclusions

Individuals and institutions should move from "crisis fighters" to "proactive and systematic risk managers" (World Bank, 2013). After all, understanding more about the changes of

ISSN 2007-2422 •

human society can help mitigate and adapt to future disasters. This study identifies four types of social fragmentation that include "continuous high social fragmentation," "transformed social fragmentation," "fluctuating social fragmentation" and "continuous low social fragmentation." Of the four types, "continuous high social fragmentation" is located in coastal Chiayi. Meanwhile, "transformed social fragmentation" is clustered in the plain area. "Fluctuated social fragmentation" occurs in the hill-mountain area. Finally, "continuous low social fragmentation" occurs only in Taibao City, because it is the county capital and located in the core of the county.

Clearly studies may overlook such potential social fragmentation if the longitudinal trend analysis is missing. Restated, trend analysis is required to clarify different characteristics of social fragmentation. Analysis of changing trends based on the longitudinal data as well as the loss maps of flood disasters thus can avoid the limitations of the event-based perspective on discussing disaster, and can also provide historical and local contexts for further insights into human agency and the institutional mechanism of natural hazards.

Unlike the traditional social vulnerability approach of using indicator measurements, this study suggests that social fragmentation is related to social integration in terms of social systems. The social fragmentation approach thus can help adjust the shortage of indicator measurements.

Some interesting follow-up analysis can be performed to identify more appropriate variables that can be used to calculate social fragmentation, and that can help identify the relationships between social fragmentation and social vulnerability, the two factors that determine differences in resilience and adaptation between cities, counties and countries. Furthermore, analysis of social fragmentation and physical vulnerability dynamics by land type category can help to assess the specificity of each profile and confirm the study classification.

References

Adger, W. N., Brooks, N., Bentham, G., Agnew, M., & Eriksen, S. (2004). *New indicators of vulnerability and adaptive capacity.* Norwich: UK Tyndall Centre for Climate Change Research (Technical Report 7).

Adger, W. N. (2006). Vulnerability. *Global Environmental Change*, *16*(3), 268-281.

Adger, W. N., Brown, K., Nelson, D. R., Berkes, F., Eakin, H., Folke, C., Galvin, K., Gunderson, L., Goulden, M., O'Brien, K., Ruitenbeek, J., & Tompkins, E. L. (2011). Resilience implications of policy responses to climate change. *Wiley Interdisciplinary Reviews: Climate Change*, *2*(5), 757-766.

Barbieri, A. F., & Carr, D. L. (2005). Gender-specific out-migration, deforestation and urbanization in the Ecuadorian Amazon. *Global and Planetary Change*, 47, 99-110.

Birkmann, J. (2006). *Measuring vulnerability to natural hazards - towards disaster resilient societies*. Tokyo: United Nations University Press.

Carr, P. J., & Kefalas, M. J. (2009). *Hollowing out the middle: The rural brain drain and what it means for America*. New York: Random House Publishing Group.

Chen, C. H., Wang, C.H., Hsu, Y. J., Yu, S. B., & Kuo, L. C. (2010). Correlation between groundwater level and altitude variations in land subsidence area of the Choshuichi Alluvial Fan, Taiwan. *Engineering Geology*, *115*(1-2), 122-131.

Chen, W. J., & Kuo, C. T. (2000). Sea level fluctuation in west Taiwan. *Journal of Coastal research*, 34, 635-641.

Cramm, J. M., Van Dijk, H. M., & Nieboer, A. P. (2013). The importance of neighborhood social cohesion and social capital for the well being of older adults in the community. *The Gerontologist, 53*(1), 142-152.

Cutter, S. L. (1996). Vulnerability to environmental hazards. *Progress in Human Geography*, *20*(4), 529-539.

Cutter, S. L., Mitchell, J. T., & Scott, M. S. (2000). Revealing the vulnerability of people and places: A case study of Georgetown County, South Carolina. *Annals of the Association of American Geographers*, *90*(4), 713-737.

Cutter, S. L., Boruff, B. J., Shirley, W. L. (2003). Social vulnerability to environmental hazards. *Social Science Quarterly*, *84*(2), 242-261.

Cutter, S. L., & Finch, C. (2008). Temporal and spatial changes in social vulnerability to natural hazards. *PNAS*, *105*(7), 2301-2306.

Dorling, D., & Gunnell, D. (2003). Suicide: The spatial and social components of despair in Britain 1980-2000. *Transactions of the Institute of British Geographers*, *28*(4), 442-460.

D'Souza, J. (2011). *Vulnerability assessment of urban marginalised communities: A pilot study in Bangalore slum areas* (pp. 1-54). Mumbai: Centre for Environment and

• ISSN 2007-2422

Documentation and Indian Network on Ethics and Climate Change.

Dwyer, A., Zoppou, C., Nielsen, O., Day, S., & Roberts, S. (2004). Quantifying social vulnerability: A methodology for identifying those at risk to natural hazards. *Geoscience Australia, 2004*(14).

Elliott, J. O., Charyton, C., Sprangers, P., Lu, B., & Moore, J. L. (2011). The impact of marriage and social support on persons with active epilepsy. *Epilepsy & Behavior*, *20*(3), 533-538.

Elmqvist, T., Goodness, J., Marcotullio, P. J., Parnell, S., Sendstad, M., Wilkinson, C., Fragkias, M., Güneralp, B., McDonald, R. I., Schewenius, M., & Seto, K.C. (2013). *Urbanization, biodiversity and ecosystem services: Challenges and opportunities*. London: Springer.

European Commission (Seventh Framework Programme) (2011). *ENSURE: Enhancing resilience of communities and territories facing natural and na-tech hazards, EU*. Orléans. France: European FP7 project. European Commission.

Evans, J., Middleton, N., & Gunnell, D. (2004). Social fragmentation, severe mental illness and suicide. *Social Psychiatry and Psychiatric Epidemiology*, *39*(3), 165-170.

Fagg, J., Curtis, S., Stansfeld, S. A., Cattell, V., Tupuola, A. M., & Arephin, M. (2008). Area social fragmentation, social support for individuals and psychosocial health in young adults: Evidence from a national survey in England. *Social Science & Medicine*, 66, 242-254.

Finch, C., Emrich, C. T., & Cutter, S. L. (2010). Disaster disparities and differential recovery in New Orleans. *Population and Environment*, 31, 179-202.

Fragkias, M., Güneralp, B., Seto, K. C., & Goodness, J. (2013). A synthesis of global urbanization projections (pp. 409-435). In: *Urbanization, biodiversity and ecosystem services: challenges and opportunities*. Elmqvist, T., Fragkias, M., Goodness, J., Güneralp, B., Marcotullio, P. J., McDonald, R. I., Parnell, S., Schewenius, M., Sendstad, M., Seto, K. C., & Wilkinson, C. (eds.). London: Springer.

Hokenstad, M. C., & Roberts, A. R. (2010. Social work's role in ensuring enabling and supportive environments for older persons: A global perspective. *Journal of Social Intervention: Theory and Practice*, *19*(2): 25-38.

IPCC (2001). Working group II contribution to the Intergovernmental Panel on Climate Change third assessment report. In: *Climate change 2001: Impacts, adaptation and vulnerability*. McCarthy, J., Canziani, O., Leary, N., Dokken, D. *et al*. (eds.). Cambridge: Cambridge University Press.

IPCC (2007). Working group II contribution to the Intergovernmental Panel on Climate Change fourth assessment report. In: *Climate change 2007: Impacts, adaptation and vulnerability*. Parry, M. L., Canziani, O. F., Palutikof, J. P. *et al*. (eds.). Cambridge: Cambridge University Press.

Ivory, V. C., Collings, S.C., Blakely, T., & Dew, K. (2011). When does neighbourhood matter? Multilevel relationships between neighbourhood social fragmentation and mental health. *Social Science & Medicine*, 72, 1993-2002.

Kelly, P. M., & Adger, W. N. (2000). Theory and practice in assessing vulnerability to climate change and facilitating adaptation. *Climatic Change*, *47*(4), 325-352.

Khan, S. (2012). Vulnerability assessments and their planning implications: A case study of the Hutt Valley, New Zealand. *Natural Hazards*, 64, 1587-1607.

Kohsaka, R., Shih, W., Saito, O., & Sadohara, S. (2013). Local assessment of Tokyo: Satoyama and Satoumi - traditional landscapes and management practices in a contemporary urban environment (pp. 92-105). In: *Urbanization, biodiversity and ecosystem services: Challenges and opportunities*. Elmqvist, T., Fragkias, M., Goodness, J., Güneralp, B., Marcotullio, P. J., McDonald, R. I., Parnell, S., Schewenius, M., Sendstad, M., Seto, K. C., & Wilkinson, C. (eds.). London: Springer.

Lange, H. J. D., Sala, S., Vighi, M., & Faber, J. H. (2010). Ecological vulnerability in risk assessment - A review and perspectives. *Science of the Total Environment*, 408, 3871-3879.

Lee, Y.-J. (2014). Social vulnerability indicators as a sustainable planning tool. *Environmental Impact Assessment Review*, 44, 31-42.

Maestripieri, D., Baran, N. M., Sapienza, P., & Zingales, L. (2010). Between- and within-sex variation in hormonal responses to psychological stress in a large sample of college students. *Stress*, *13*(5), 413-424.

Makinen, I. H. (2000). Eastern European transition and suicide mortality. *Social Science and Medicine*, *51*(9), 1405-1420.

Mendes, J. M. O. (2009). Social vulnerability indexes as planning tools: Beyond the preparedness paradigm. *Journal of Risk Research*, *12*(1), 43-58.

Menoni, S., Molinari, D., Parker, D., Ballio, F., & Tapsell, S. (2012). Assessing multifaceted vulnerability and resilience in order to design risk-mitigation strategies. *Natural Hazards*, 64, 2057-2082.

Nagendra, H., Sudhira, H. S., Katti, M., & Schewenius, M. (2013). Sub-regional assessment of India: effects of urbanization on land use, biodiversity and ecosystem services. In: *Urbanization, biodiversity and ecosystem services: Challenges and opportunities* (pp. 65-74). Elmqvist, T., Fragkias, M., Goodness, J., Güneralp, B., Marcotullio, P. J., McDonald, R. I., Parnell, S., Schewenius, M., Sendstad, M., Seto, K. C., & Wilkinson, C. (eds.). London: Springer.

Schmidtlein, M. C., Shafer, J. M., Berry, M., & Cutter, S. L. (2011). Modeled earthquake losses and social vulnerability in Charleston, South Carolina. *Applied Geography*, 31, 269-281.

Seto, K. C., Parnell, S., & Elmqvist, T. (2013). A global outlook on urbanization (pp. 1-12). In *Urbanization, biodiversity and ecosystem services: Challenges and opportunities*. Elmqvist, T., Fragkias, M., Goodness, J., Güneralp, B., Marcotullio, P.

J., McDonald, R. I., Parnell, S., Schewenius, M., Sendstad, M., Seto, K. C., & Wilkinson, C. (eds.). London: Springer.

Sonwa, D. J., Somorin, O. A., Jum, C., Bele, M. Y., & Nkem, J. N. (2012). Vulnerability, forest-related sectors and climate change adaptation: the case of Cameroon. *Forest Policy and Economics*, 23, 1-9.

Sukhdev, P. (2013). Preface. In: *Urbanization, biodiversity and ecosystem services: Challenges and opportunities*. Elmqvist, T., Fragkias, M., Goodness, J., Güneralp, B., Marcotullio, P. J., McDonald, R. I., Parnell, S., Schewenius, M., Sendstad, M., Seto, K. C., & Wilkinson, C. (eds.). London: Springer.

Tate, E., Burton, C. G., Berry, M., Emrich, T., & Cutter, S. L. (2011). Integrated hazards mapping tool. *Transactions in GIS*, *15*(5), 689-706.

Tierney, K. J. (2007). From the margins to the mainstream? Disaster research at the crossroads. *Annual Review of Sociology*, 33, 503-525.

Turner, B. L., Kasperson, R. E., Matson, P. A., McCarthy, J. J., Corell, R. W., Christensen, L., Eckley, N., Kasperson, J. X., Luers, A., Martello, M. L., Polsky, C., Pulsipher, A., & Schiller, A. (2003). A framework for vulnerability analysis in sustainability science. *Proceedings of the National Academy of Sciences*, *100*(14), 8074-8079.

World Bank (2013). Risk and opportunity: Managing risk for development. *World Development Report 2014*. Washington, DC: World Bank.

Author´s institutional address

Ph.D. Yung-Jaan Lee

Chung-Hua Institution for Economic Research
75 Chang-Hsing St., Taipei
10672 Taipei, Taiwan, PR China
Telephone: +886 (2) 2735 6006
Fax: +886 (2) 2735 6035
yungjaanlee@gmail.com

Ph.D. Li-Pei Peng
Ph.D. Ting-Jay Lee

National Taiwan University
Department of Bio-Industry Communication and Development
No. 1, Section 4, Roosevelt Rd, Da'an District, Taipei City
10617 Taipei, Taiwan, PR China
Telephone: +886 (2) 3366 2939
Fax: +886 (2) 2363 5879
lipei@ntu.edu.tw
tinjay@hotmail.com

Haga clic aquí para escribir al autor

• ISSN 2007-2422

Effect of drip irrigation with saline water on the construction of shelterbelts for soil and groundwater protection in the hinterland of the Taklimakan Desert, China

• Jinglong Fan*# •
Xinjiang Institute of Ecology and Geography Chinese Academy of Sciences
#These author contributed equally to this work
*Corresponding author

• Yaping Wei •
Xinjiang Institute of Ecology and Geography, Chinese Academy of Sciences/University of Chinese Academy of Sciences

• Xinwen Xu# •
Xinjiang Institute of Ecology and Geography Chinese Academy of Sciences
#This author contributed to this work equally with the corresponding author

• Xinghu Yang •
Xinjiang Institute of Ecology and Geography, Chinese Academy of Sciences/University of Chinese Academy of Sciences

Abstract

Fan, J., Wei, Y., Xinwen, W., & Yang, X. (March-April, 2017). Effect of drip irrigation with saline water on the construction of shelterbelts for soil and groundwater protection in the hinterland of the Taklimakan Desert, China. *Water Technology and Sciences* (in Spanish), *8*(2), 19-30.

In order to perceive the effect of drip irrigation with saline water in the desert hinterland on plant growth of shelterbelts and underground environment (vadose zone and groundwater), by developing water-saving irrigation technology to ensure the scientifically substantiated utilization of water resources, four different irrigation cycle experiments (difference in irrigation period I: 12d; IV: 25d; II & III: 25d in the summer and the respective spring and autumn periods, which were the same: 15d and 20d, respectively) were carried out during the irrigation season in four different regions of well irrigation area. In this paper, regular on-site investigation was adopted to observe soil, water, and salt. Single-factor analysis of variance and least significant difference (LSD) are used to analyze the data acquired by the survey method and for measuring plant growth, complemented with the comparison of groundwater level and chemical index before and after irrigation. The results showed that the reduction of annual irrigation volume from 420 mm to 201.6 mm had almost no effect on plant growth and could save more than 50% of the water as compared to treatment I. Considering the impact on the height-growth of Tamarix, treatment II could be optimized, so that more than 30% of the water could be saved as compared to treatment I. Three days after irrigation, the salt was leached through

Resumen

Fan, J., Wei, Y., Xinwen, W., & Yang, X (marzo-abril, 2017). Efecto del riego por goteo con agua salina en la construcción de cortinas rompevientos para protección del suelo y las aguas subterráneas en el interior del desierto de Taklimakan, China. Tecnología y Ciencias del Agua, *8(2), 19-30*.

Con la finalidad de entender el efecto del riego por goteo con agua salina en el crecimiento de plantas de cortinas rompevientos y en el ambiente subterráneo del interior del desierto (zona no saturada y aguas subterráneas), mediante el desarrollo de tecnología de riego para asegurar el aprovechamiento científicamente justificado de los recursos hídricos, se efectuaron cuatro experimentos de riego en ciclo de ahorro de agua (diferencia en periodo de riego I: 12d; IV: 25d; II y III: 25d en verano; sus respectivos periodos de primavera y otoño fueron los mismos: de 15 d y 20 d, respectivamente) durante la temporada de riego en cuatro diferentes regiones del área de riego con agua de pozo. En este trabajo se adoptó la investigación regular in situ *para observar suelo, agua y salinidad. Se utiliza el análisis de varianza de un solo factor y la diferencia mínima significativa (LSD) para analizar los datos obtenidos por el método de encuesta y medir el crecimiento de las plantas, complementando lo anterior con la comparación de nivel de agua subterránea y el índice químico antes y después del riego. Los resultados mostraron que la reducción de volumen de riego anual de 420 a 201.6 mm casi no tuvo efecto en el crecimiento de las plantas, y podría ahorrar más de 50% de agua, en comparación con el tratamiento I. Si se considera el impacto en el crecimiento de altura de Tamarix, el tratamiento II podría ser optimizado, por lo que se podría ahorrar más de un 30% del agua, en comparación con el tratamiento I. Tres días después del riego, la sal se lixivia a través del cuerpo del suelo a las aguas subterráneas;*

the soil body into the groundwater. The groundwater level in the shelterbelt area, total dissolved solids (TDS), and total hardness exhibited an upward trend. Six days after irrigation, the high salt concentration region was found at a depth of 0–30 cm.

Keywords: Drip irrigation with saline water, shelterbelts, vadose zone, groundwater, Taklamakan Desert.

el nivel de agua subterránea en el área de la cortina rompevientos, los sólidos disueltos totales (SDT) y la dureza total mostraron una tendencia ascendente. Seis días después del riego, la región de alta concentración de sales se encontró a una profundidad de 0 a 30 centímetros.

***Palabras clave**: riego por goteo con agua salina, cortina rompevientos, zona no saturada, aguas subterráneas, desierto de Taklamakan.*

Received: 14/01/2016
Approved: 26/10/2016

Introduction

In the arid and semi-arid regions of China, many hydrological changes have occurred due to the impact of climate change and human activities (Zhao & Cheng, 2002; Huang & Pang, 2010), particularly the irrigation projects with use of groundwater. Groundwater in the arid areas plays an important role in ensuring the stability of the desert and oasis ecosystem (Naumburg, Mata-Gonzalez, Hunter, Mclendon, & Martin, 2005; Mu Oz-Reinoso, 2001; Gullison & Bourque, 2001). Tarim Desert Highway shelterbelt ecological engineering project is the longest artificial shelterbelt system crossing drifting desert. It has been completed 436 km protection forest in the Taklimakan desert, sometimes known as "the green corridor". Groundwater resources in the desert region are very precious, and various environmental problems could arise without optimal use and effective conservation (Zhang, 2004). One of the most pertinent issues in achieving water saving irrigation is to study the formation and movement pattern of water in the vadose zone. The thickness of vadose zone along desert highway is different, and the irrigation system for shelterbelts is the same, which is conducive to the convenient management of water resources, but is also an indirect waste of groundwater resources (Han, Cao, Yimit, Xu, & Zhang, 2012). Currently, there have been few reports on the effect of irrigation with saline water on the growth of artificial forest and groundwater environment (Li, Lei, Zhao, Xu, & Li, 2015; Zhang, 2016). These studies not only help deepen the scientific insight into the SPAC (soil-plant-atmosphere continuum) (Shaozhong, 1994), but also have important guiding significance for groundwater pollution control as well as ecological and environmental engineering projects (Guswa, Celia, & Rodriguez-Iturbe, 2002; Scott, 2001).

The volume of irrigation water and the salt distribution in soil profile can affect the salt leaching process (Swarajyalakshmi, Gurumurthy, & Subbaiah, 2003), so the soil salt dynamics has been extensively explored (Xu, Li, & Wang, 2006; Zhou, Xu, Lei, & Li, 2006; Miyamoto, Chacon, Hossain, & Martinez, 2005; Mousavi, Soltani-Gerdefaramarzi, & Mostafazadeh-Fard, 2010). However, most of the laboratory studies were focused on the effect of water and soil properties on the response to irrigation, while there is scarce information on the impact of drip irrigation with saline water on the growth, soil, and groundwater of *Tamarixramosissima* and *Haloxylonammodendron* forests under desert environment. Therefore, the purpose of this study is to evaluate the impact of drip irrigation with saline water on plant growth in shelterbelts and underground environment in the study area under natural conditions. In this study, four

irrigation experiments with different water treatments were set up in which water volume decreased gradually, and the cross-sectional distribution of water and salt for each treatment and ultimate impact on the groundwater environment were analyzed. Finally, an approach for water conservation and the observed differences between various treatments were described.

Experimental

Study area

The Taklimakan desert is the largest desert in China, at the same time, is the world's second-largest drifting desert, and covers an area of 33.7 square kilometers (Sun & Liu, 2006). It is located in the center of Tarim basin in northwest China. This basin is a major area for producing oil and gas resources in China. The Tarim Desert Highway crosses the Taklimakan desert from south to north. The shelterbelt forests were built on both sides of the highway with the width of 72-78m. Due to the distance of the road across, the drifting desert is the longest in the world (Alles, 2012), so it is listed in the Guinness Book of Records.

From north to south, Tarim Desert Highway sequentially crosses five major geomorphic units-compound transverse dune area, dome-shaped dune area, high compound longitudinal dune area, compound longitudinal dune area, and compound transverse dune area (Lei *et al*., 2008). The study area is located in a dome-shaped dune area and the geomorphic unit has a total length of about 20 km, and the groundwater level is generally around 2 m. The water supply for the shelterbelt is basically groundwater with total dissolved solids (TDS) was 4.138 g/l and pH value is 7.21. The main pipe was used to convey the water from the ground while the branch pipe diverted the water with drippers installed on the drip tube for irrigation. The Aeolian sandy soil is fine sand, the soil bulk density of peripheral plantations is 1.43 g/cm^3, and the soil porosity is 45.55%.

Test design

In order to effectively use the groundwater characteristics of the regions with relatively rich groundwater resources and to achieve water-saving irrigation, three additional water supply schemes for conservation of water resources were proposed based on the original irrigation system for shelterbelt project. As shown in figure 1, the entire shelterbelt land irrigated by well water was divided into four regions: region I with the existing irrigation system and regions II, III, and IV with modified irrigation systems for the comparison with region I (table 1).

Since the Tarim Desert Highway Ecological Shelterbelt Project completion in 2005, the annual irrigation cycle from March to October was used for the shelterbelt. Under the condition of sufficient water resources for the spring and autumn irrigations, the above irrigation period was elongated, so that plants were under water stress compared to the original irrigation system. The growth of plants in different regions was monitored, in order to achieve effective water conservation without affecting plant growth. The specific experimental design is shown in table 1.

The data in table 1 are calculated as follows:

Annual irrigation times (W_{IT}):

$$W_{IT} = \frac{90}{W_{IP_1}} + \frac{90}{W_{IP_2}} + \frac{60}{W_{IP_3}} \quad (1)$$

Irrigation water (W_{IW}):

$$W_{IW} = W_{IT} \times 6 \times 3.5 \times 10^{-3} \quad (2)$$

Water conservation rate (W_{CR}). We set irrigation treatment I′ for $W_{IW} = W_{IWCK}$:

Then:

$$W_{CR} = \frac{W_{IWCK} - W_{IW\_n}}{W_{IWCK}} \quad (3)$$

ISSN 2007-2422

Table 1. Experimental design for different irrigation treatments.

Irrigation treatment	Irrigation time/h	Irrigation period/d			W_{IT}	W_{IW}/mm	W_{CR}/%
		Mar.- May.	Jun. - Aug.	Sep.- Oct.			
I	6	12	12	12	20	420.0	-
II	6	15	25	15	13.6	285.6	32.0
III	6	20	25	20	11.1	233.1	44.5
IV	6	25	25	25	9.6	201.6	52.0

Here the number of days with irrigation is 240 from March to October. The water volume that drips out of emitters is 3.5×10^{-3} m^3 per hour. The control area of the drip water emitter is 1 m^2. The single irrigation time is 6 hours per emitter. W_{IP} *is* irrigation period/interval, W_{IP_1}, W_{IP_2}, W_{IP_3} are March to May, June to August, and September to October irrigation periods, respectively; *n* is *II*, *III*, *IV*.

Measurement and analysis

The effect that saline water irrigation to the groundwater was observed by four wells from the emitter every 30 cm called 1, 2, 3, 4, and set a control check (CK) observation well in bare sandy land around 100 meters away (figure 1). It reflected cumulative-change values by subtracting groundwater level and chemical indicators (TDS, pH, total alkalinity & total hardness) before the irrigation from the corresponding value after irrigation, where TDS were tested by using the 180 ºC drying weight method (APHA-AWWA-WEF, 1998). Measurement of pH was performed using a pH meter (Model PHS-3C, Shanghai Lici Ltd., China). Total alkalinity was determined by titration with acid (Larocque *et al*., 2016). Total hardness was determined by an EDTA complexometry.

The effect of the irrigation to the groundwater level was observed every day in an irrigation period 12d. It measured by releasing a probe connected with a multimeter by dual-cable wire into the well pipe. The multimeter was switched to the resistance shift. When the probe touched the water table, the cable was marked at the height of the well head, and the distance between the mark and the probe was measured after retrieval. The subtraction of the *n*th water table observation H_n data from the initial observation data H_0 gave the relative water level at the *n*th observation (H_0–H_n) to each observation wells.

Seedling investigation method was used for shelterbelts trees during the whole growing season, ten representative plants were randomly selected by human from *Tamarixramosissima* and *Haloxylonammodendron* respectively, and three indicators of plant height, crown width, and diameter at the ground level were measured. The One-Way ANOVA and least significant difference (LSD) method were used to analyze the influence of irrigation water for plant growth using SAS statistical software (version 9.1, SAS Institute Inc.).

Regular on-site investigation method was adopted to observe the soil salt in the experiment area on 1d, 6d, and 9d after irrigation. Soil electrical conductivity (EC) exhibiting a linear relationship with soil salinity within the study area (Wang, Xu, Lei, Li, & Wang, 2010), the respective EC value was measured, in order to assess the soil salinity, by a SY-3 conductivity-thermometer (Institute of Soil Science, Chinese Academy of Sciences, 1987) with the weight of water: soil = 5:1 (Han, Cao, Yimit, Xu, & Zhang, 2012). The soil samples were collected at depths of 0, 5, 15, 25, 35, 55, 75 and 95 cm under the emitter with the horizontal distances of 0 to 150 cm every 30 cm from the emitter. Three samples per each fixed point were used to measure EC.

• ISSN 2007-2422

In each experimental area, a 2 m long Soil moisture observation tube was embedded into soil under emittter made of aluminum/plastic composite pipe of 50 mm in diameter. Soil moisture was determined via neutron probes (Gardner & Kirkham, 1952) with five replicates after irrigation, then the mean value of replications was used as the soil water content. This rapid, *in situ*, nondestructive means of measuring soil moisture profiles in forestry (Wells & Fityus, 2011) was used in this work to determine soil moisture at 10-cm intervals from the soil surface to a depth of 180 cm.

Results and discussion

Spatial distribution of soil water and salt under different irrigation conditions

Water spatial distribution

Four different irrigation cycle experiments during irrigation season were carried out in four different regions of well irrigation area (table 1). According to figure 2, after the irrigation, the soil water content in region I with the original irrigation system reached saturation at

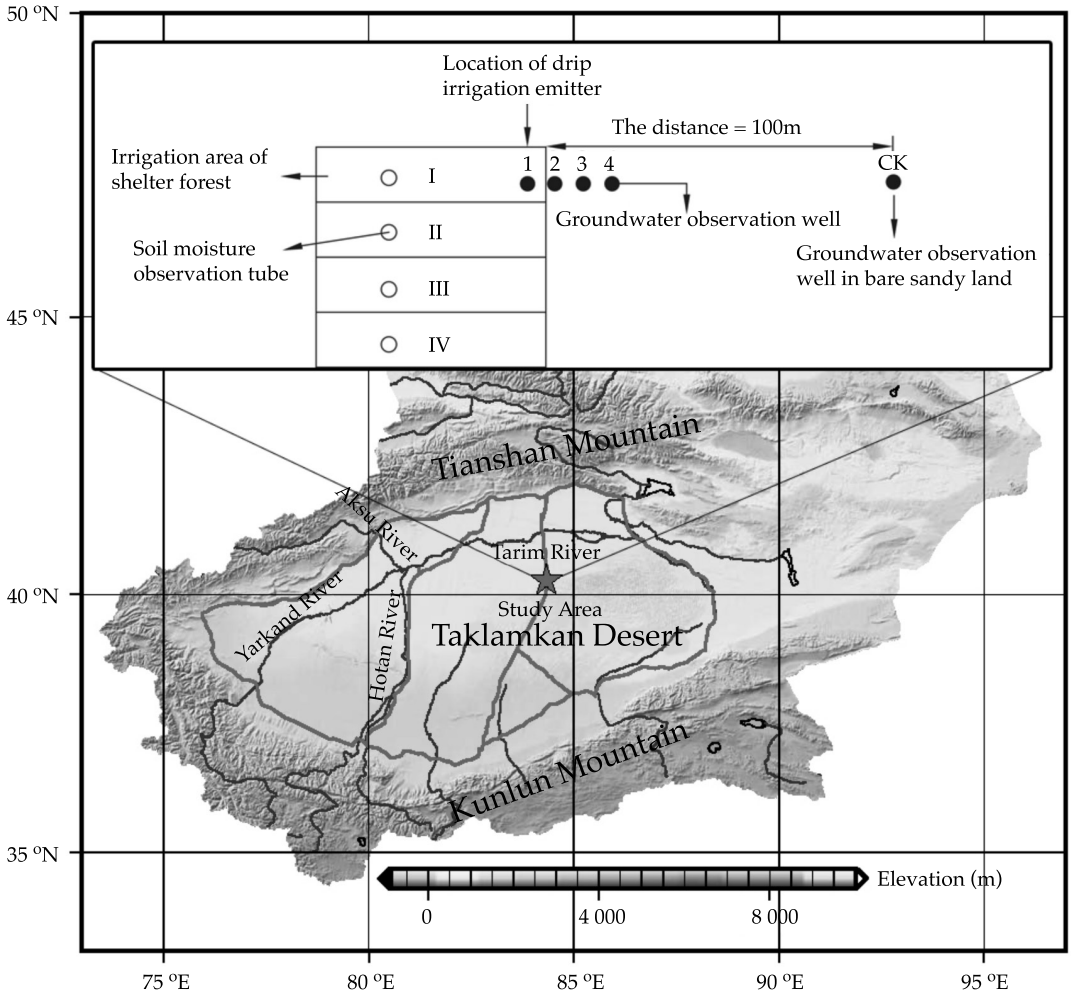

Figure 1. Schematic diagram of the experimental layout.

Tecnología y Ciencias del Agua, vol. VIII, núm. 2, marzo-abril de 2017, pp. 19-30
ISSN 2007-2422

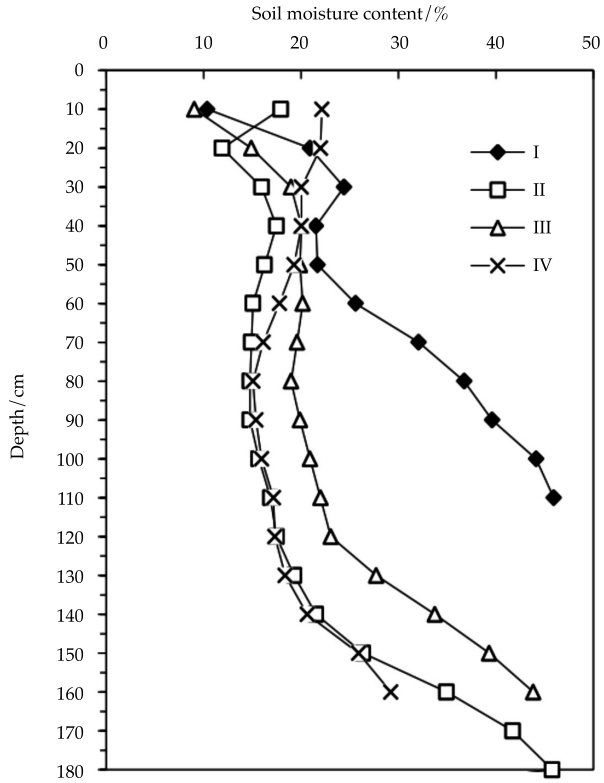

Figure 2. Differences in the soil water content under different irrigation treatments.

a depth of 100 cm, while the soil water content in regions III, II, and IV reached saturation at depths of 160, 180, and 160 cm, respectively. Due to the shallow groundwater in the entire irrigation area, an aquifer is present within 180 cm soil depth, while the groundwater depths of four irrigated areas were different. The shallowest and the deepest groundwater depths were found in regions I and IV, respectively, with a gap of about 60 cm. Therefore, irrigation has a relatively high impact on the surface soil water, but a feeble one on deep soil water; the soil water content of each region can be maintained at a high level with the soil porosity of 45.55%.

Salt temporal change

Since shelterbelt plants have high tolerance to soil salinity, plant could grow normally under various irrigation systems, and soil salinity increases from spring to autumn (Huang *et al*., 2015). Due to multiple repeated irrigation cycles, salts dissolved in irrigation water may increase soil salinity, resulting in a salinity level higher than that tolerated by the plant (Zhang *et al*., 2008), so understanding of the patterns of the salt migration and accumulation is very important. For example, the pattern in salt migration of region I was studied by continuous salinity monitoring within the irrigation cycle. As shown in figure 3(b), 3d after irrigation, the total soil salinity was significantly reduced, as compared to that in figure 3(a) and there was no significant salt accumulation. Most of the salt was infiltrated with the soil water from the range defined by the dashed line in figure 3(a) (*i.e.* the range from the surface to 20 cm) through the vadose zone into groundwater body. As can be seen from figure 3(c), over the course of evaporation and water redistribution, the salt

• ISSN 2007-2422

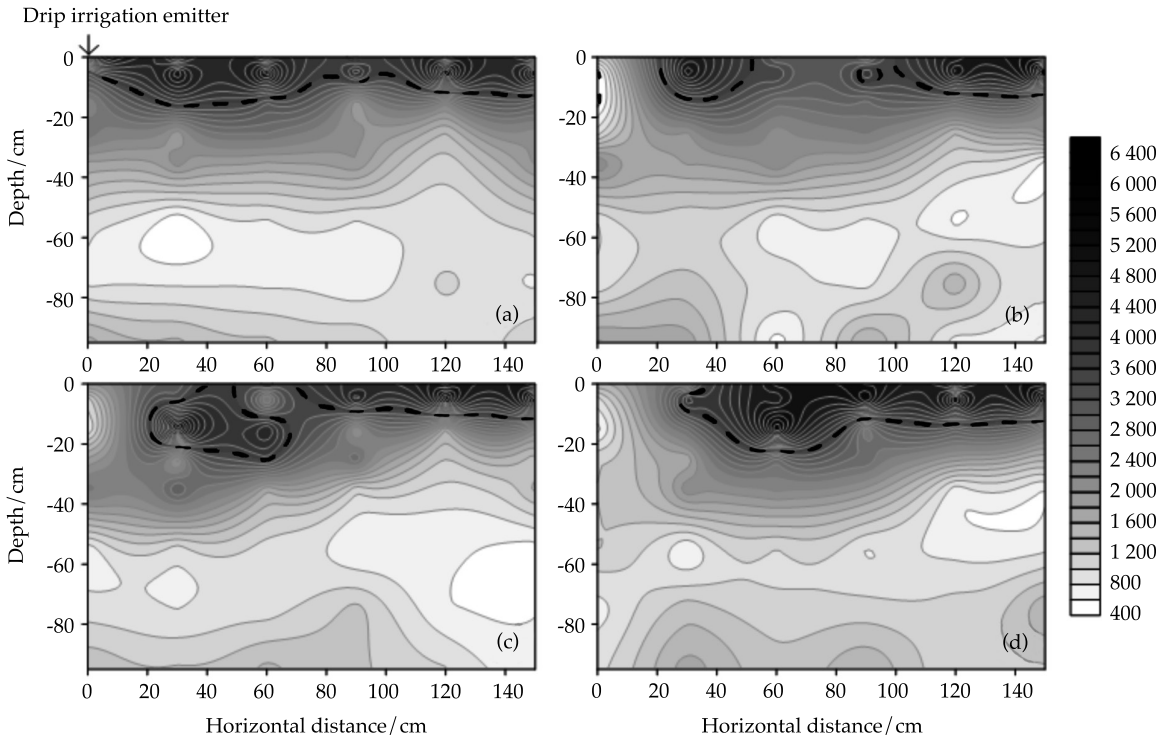

Figure 3. Soil salt migration process within the irrigation cycle (a) Isoline of soil electrical conductivity one day after irrigation; (b) Isoline of soil electrical conductivity three days after irrigation; (c) Isoline of soil electrical conductivity six days after irrigation; (d) Isoline of soil electrical conductivity nine days after irrigation.

gradually moved from the lower layer to the upper one in the vadose zone, and was accumulated in a depth range from 0~25 cm (dotted line) on day 9. Figure 3(d) shows that salt was continuously accumulated in the surface soil body at a horizontal distance of 20-140 cm from the dripper and a depth of about 20 cm.

Differences in plant growth under various irrigation volumes

With the survey method for shelterbelt tree seedlings, ten representative plants were randomly selected for the measurement of plant height, crown width, and diameter at the ground level. These characterization parameters are used to reflect the impact of different irrigation systems on plant growth. Single-factor analysis of variance was used to analyze the data from statistical experiments, and the respective results are presented in table 2.

The comparative analysis of the above results revealed no significant differences on all indicators of various treatments, except for plant height of *Tamarixramosissima.* This indicates that various irrigation systems have no significant effect on plant growth. The plant height difference for *Tamarixramosissima* can be assessed using the multiple comparison procedure among groups, which yields the results as shown in table 3. As can be seen, no significant difference was found between regions I and II, while there were differences found between region I and region III or region IV at the significance level of 5%. At a high significance level of 1%, there were differences between regions I and III.

Table 2. Variance analysis of the increment in plant growth with different irrigation treatments for selected plants.

Irrigation treatment	*Haloxylon*			*Tamarix*		
	Height/cm	Crown width/cm	Diameter at the ground level/mm	Height/cm	Crown width/cm	Diameter at the ground level/mm
I	158.6	119.4 × 117.9	18.245	78.8	107.5 × 105.7	10.325
II	172.3	183.3 × 208.8	27.664	73.0	120.3 × 118.7	8.691
III	151.0	108.0 × 106.0	14.560	123.0	112.0 × 116.7	16.680
IV	133.2	124.6 × 121.2	23.256	123.0	181.5 × 165.5	18.744
F value	0.4150	2.2190	0.6570	10.6670	1.1720	2.6960
P value	0.7441	0.1210	0.5893	0.0019*	0.3684	0.1024

Note: * There is significant difference at $p = 0.05$; in the plant height, crown width, and diameter at the ground level.

Table 3. Analysis of height difference of *Tamarixramosissima* using the multiple comparison procedure (LSD).

Treatment	Average value	Significance level of 5%	High significance level of 1%
I	78.8333	B	B
II	73.0000	B	B
III	123.0000	A	A
IV	123.0000	A	AB

Impact on groundwater

Groundwater level

The values of the groundwater level changes at different observation wells during each irrigation period were obtained by subtracting the groundwater level after irrigation from the groundwater level before irrigation (figure 4). According to the changes in the groundwater level at different observation wells, the water levels in the four groundwater observation wells in the shelterbelt area showed an upward trend. The highest water level at No. 1 observation well was reached on day 10, and the highest water levels at the remaining three observation wells were reached on day 9. On the other hand, no obvious change pattern was found in the groundwater level in the observation well CK that was located in the original sands outside of the shelterbelt. According to observational data, the largest and the smallest rises of water levels were 0.022 m (No. 3 observation well) and 0.001 m (No. 1 observation well), respectively, indicating that irrigation can raise groundwater levels, but this effect is feeble, resulting only in few centimeter changes.

Groundwater chemistry

In this study, groundwater chemistry was indicated by pH, TDS, total hardness and total alkalinity (Salem, Atwia, & El-Horiny, 2015). The value of cumulative-change as relative comparison was carried out to obtain the change values compared with the initial value, such as heavy metal accumulation (Unterbrunner *et al*., 2007), plant relative growth yield (Keyantash, & Dracup, 2002), cumulative precipitation (Alkhayri & Albahrany, 2004), etc. Figure 5 shows that the main characteristic changes in groundwater chemistry were reflected on the changes in TDS and total hardness. The changes in the above mentioned two indicators decreased within the shelterbelt area, while the changes of the same two values increased for the bare sandy land outside of shelterbelt land (the change was positive). Therefore, under the influence of irrigation

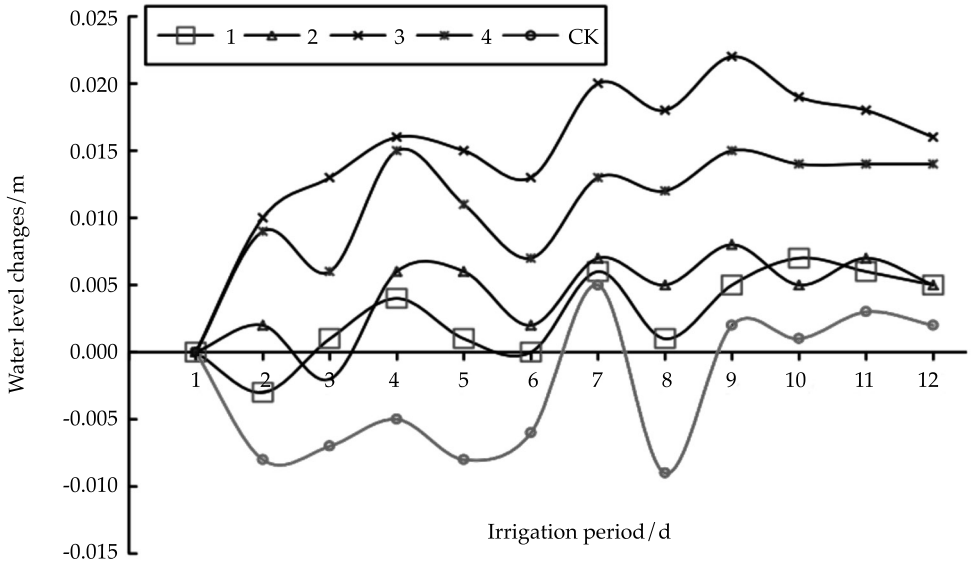

Figure 4. Changes in groundwater level at different observation wells in the shelterbelt area.

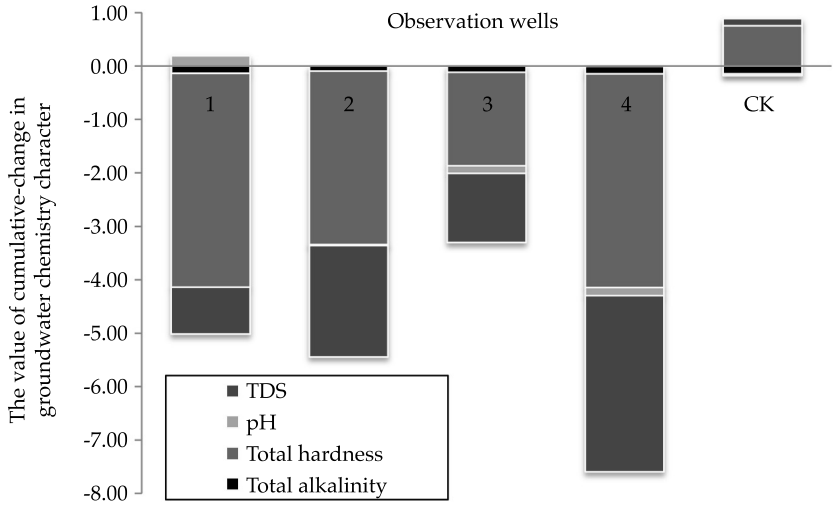

Figure 5. Cumulative changes in each indicator of water chemistry at different observation wells in the shelterbelts area.

projects, the groundwater environment in the local areas allowed the TDS and total hardness of groundwater in the shelterbelt area covered by the irrigation system to exhibit the significant upward trend. However, values of pH and total alkalinity showed no significant changes.

Discussion

In this study, we have designed a water-saving irrigation test at the desert shelterbelt land irrigated by groundwater was designed. There were 4 testing treatments have used to study the

effect of the distributions of different irrigation schedules to soil moisture and salt, plant growth and groundwater chemical. It was revealed that the irrigation has a relatively high impact on the surface soil moisture, but a feeble one on deep soil. The study of soil moisture in the direction perpendicular to the horizon indicates that the soil moisture varies slightly below a soil depth of 100 cm (Wang *et al*., 2008). With the same age of forest, the soil moisture gradually increases from surface to deep soil (Zhang *et al*., 2008). Other studies have shown that the distributions of the soil water content at the capillary saturation zone were determined by groundwater, while vegetation could affect the soil salinity, but not soil moisture (Wang *et al*., 2012).

The soil salt was continuously accumulated to the surface soil body at a horizontal distance of 20-140 cm from the dripper and a depth of about 20 cm. It is in agreement with the salt accumulation at the shifting aeolian sandy soil surface (Zhang, 2008), and has different temporal dynamics in an irrigation cycle (Zhang, 2016). In addition, some other factors also influence the spatial distribution of soil salinity such as soil spatial variability, groundwater salt content (Huang *et al*., 2015; Rose, Konukcu, & Gowing, 2005), because the clay soil is suitable to adsorb soluble salt ions (Brantley S L. Geology, 2008).

Some studies indicate that average soil moisture above 6% in shelterbelts along the Tarim Desert Highway can meet the requirement for plant growth (Unterbrunner *et al*., 2007). By our water-saving irrigation test, the plant growth was not abnormal, while average soil moisture above 21%, and 32% of water could be saved when the irrigation treatment in region II was used. Based on this work results, more efficient irrigation methods can be elaborated for similar applications.

Conclusions

Irrigation has relatively large impact on the water content of surface soil, but has little effect on deep soil water content. In the layer with root distribution, the soil water content of each region could be maintained at a high level. Three days after irrigation, the entire soil salinity was significantly decreased, as compared to that before irrigation, indicating that most salt was infiltrated with water via the range from soil surface to 30 cm entering the groundwater body. The groundwater level, TDS and total hardness exhibited an upward trend in the shelterbelt area.

The plant growth showed no significant variations under the impact of various irrigation treatments. Based on the analysis of variance, the response in the radial growth of *Tamarixramosissima* tree trunk is more sensitive to water stress. Therefore, if the statistical results obtained are verified and the height growth issue of *Tamarixramosissima* is disregarded, then at least 50% or more of water as well as the corresponding manpower and resources could be saved when the entire area was irrigated with the irrigation system in region IV. If the above issue is considered, 32% of water could be saved if the irrigation system of region II was used.

The results in this paper can provide a very good theoretical support on the sustainability study on desert shelterbelt systems, and also show practical significance in the study of the relationship between shelterbelt irrigation volume and shelterbelt tree growth. However, the investigation on the status of shelterbelt plant growth is affected by subjective factors, including standard plant selection, judgement of observation staff, and differences in readings, and objective factors, including observation tools, micro-topography, soil heterogeneity and observation time. The results of statistical analysis can be affected to some degree. Therefore, in order to obtain more accurate data, it is necessary to strengthen the standardized operation for observers, adopt a more scientific and convenient measurement instruments, increase the observation density, and increase observed sample density. Therefore, the data from a longer scientific observation is still needed for validation.

• ISSN 2007-2422

Acknowledgments

This study is jointly funded by National Natural Science Foundation of China, No. 41301038, 31300449, 41471222 and the Research Projects of the Tarim Branch of Petro China Company Limited, No. 971014060006.

Author contributions

Jinglong Fan designed the study and analyzed the experimental data, wrote and edited the paper.Yaping Wei, XinwenXu andXinghu Yang provided the plan and suggestions on writing and editing this paper. All authors have read and approved the manuscript.

Conflicts of interest

The authors declare no conflict of interest.

References

Alkhayri, J. M., & Albahrany, A. M. (2004). Growth, water content, and proline accumulation in drought-stressed callus of date palm (J). *Biologia Plantarum*, *48*(1), 105-108.

Alles, D. L. (2012). *China's desert*. Available online: http://fire.biol.wwu.edu/trent/alles/ChinaDeserts.pdf.

APHA-AWWA-WEF (1998). *Standard methods for the examination of water and wastewater* (20th ed). Washington, DC: American Public Health Association.

Brantley S L. Geology (2008). Understanding soil time. *Science*, *321*(5895), 1454-1455.

Gardner, W., & Kirkham, D. (1952). Determination of soil moisture by neutron scattering. *Soil Sci*., 73, 391Y401.

Gullison, J. J., & Bourque, C. (2001). Spatial prediction of tree and shrub succession in a small watershed in Northern Cape Breton Island, Nova Scotia, Canada. *Ecol. Model*, 137, 181-199.

Guswa, A. J., Celia, M. A., & Rodriguez-Iturbe, I. (2002). Models of soil moisture dynamics in ecohydrology: A comparative study. *Water Resources Research*, 38, 1-5.

Han, W., Cao, L., Yimit, H., Xu, X., & Zhang, J. (2012). Optimization of the saline groundwater irrigation system along the Tarim Desert Highway Ecological Shelterbelt Project in China. *Ecological Engineering*, *40*(3), 108-112.

Huang, T., & Pang, Z. (2010). Changes in groundwater induced by water diversion in the Lower Tarim River, Xinjiang Uygur, NW China: Evidence from environmental isotopes and water chemistry. *J. Hydrol*., 387, 188-201.

Huang, Y., Wang, Y., Zhao, Y., Xu, X., Zhang, J., & Li, C. (2015). Spatiotemporal distribution of soil moisture and salinity in the Taklimakan Desert highway shelterbelt. *Water*, *7*(8), 4343-4361.

Institute of Soil Science, Chinese Academy of Sciences (1987). *Soil Physical and Chemical Property Analysis* (in Chinese). Shanghai: Shanghai Science and Technology Press, 196-233.

Keyantash, J., & Dracup, J. A. (2002). The quantification of drought: An evaluation of drought indices. *Bulletin of the American Meteorological Society*, *83*(8), 1167-1180.

Larocque, M., Ferlatte, M., Pellerin, S., Cloutier, V., Munger, J., Paniconi, C., & Quilet, A. (2016). Chemical and botanical indicators of groundwater inflow to Sphagnum-dominated peatlands. *Ecological Indicators*, *64*, 142-151.

Lei, J., Li, S., Fan, D., Zhou, H., Feng, G., Qiu, Y., Bo, X., Shang, L., Du, W., & Yan, Z. (2008). Classification and regionalization of the forming environment of windblown sand disasters along the Tarim Desert Highway. *Chinese Sci. Bull*., 53, 1-7.

Li, C., Lei, J., Zhao, Y., Xu, X., & Li, S. (2015). Effect of saline water irrigation on soil development and plant growth in the Taklimakan Desert Highway shelterbelt. *Soil & Tillage Research*, 146, 99-107.

Miyamoto, S., Chacon, A., Hossain, M., & Martinez, I. (2005). Soil salinity of urban turf areas irrigated with saline water: I. Spatial variability. *Landscape\s&\surban Planning*, 71, 233-241.

Mousavi, S. F., Soltani-Gerdefaramarzi, S., & Mostafazadeh-Fard, B. (2010). Effects of partial rootzone drying on yield, yield components, and irrigation water use efficiency of canola (*Brassica napus L.*). *Paddy & Water Environment Journal of the International Society of Paddy & Water Environment Engineering*, 8, 157-163.

Mu Oz-Reinoso, J.C. (2001). Vegetation changes and groundwater abstraction in SW Do09ana, Spain. *J. Hydrol*., 242, 197-209.

Naumburg, E., Mata-Gonzalez, R., Hunter, R.G., Mclendon, T., & Martin, D. W. (2005). Phreatophytic vegetation and groundwater fluctuations: A review of current research and application of ecosystem response modeling with an emphasis on Great Basin vegetation. *Environ Manage*, 35, 726-740.

Rose, D. A., Konukcu, F., & Gowing, J. W. (2005). Effect of water table depth on evaporation and salt accumulation from saline groundwater. *Soil Research*, *43*(5), 565-573.

Salem, Z. E., Atwia, M. G., & El-Horiny, M. M. (2015). Hydrogeochemical analysis and evaluation of groundwater in the reclaimed small basin of Abu Mina, Egypt. *Hydrogeology Journal*, 23(8), 1781-1797.

Scott, H. D. (2001). Soil Physics: Agricultural and Environmental Applications. *Soil Sci*., 166, 717-718.

Shaozhong, K. (1994). *Theory of water transport in soil-plant-atmosphere continuum and its application*. Beijing: China Water & Power Press.

Sun, J., & Liu, T. (2006). The age of the Taklimakan Desert. *Science*, 312, 1621.

Swarajyalakshmi, G., Gurumurthy, P., & Subbaiah, G. V. (2003). Soil salinity in south India: Problems and solutions. *Journal of Crop Production*, *7*, 247-275.

Wells, T., & Fityus, S. (2011). Neutron soil moisture probe operation in saline environments. *Soil Science*, *176*(12), 642-651.

Unterbrunner, R., Puschenreiter, M., Sommer, P., Wieshammer, G., Tlustos, P., Zupan, M., & Wenzel, W. (2007). Heavy metal accumulation in trees growing on contaminated sites in Central Europe. *Environmental Pollution*, *148*(1), 107-114.

Wang, Y., Xu, X., Lei, J., Li, S., Zhou, Z., Chang, Q., Wang, L., Gu, F., Qiu, Y., & Xu, B. (2008). The dynamics variation of soil moisture of shelterbelts along the Tarim Desert highway. *Chinese Science Bulletin*, *53*(S2), 102-108.

Wang, Y., Xu, X., Lei, J., Li, S., & Wang, X. (2010). Analysis on properties of topsoil salinity along the shelterbelts of the Tarim Desert highway (in Chinese). *Arid Zone Research*, *27*(1), 51-56.

Wang, Z., Li, G., Li, X., Shan, S., Zhang, J., Li, S., & Fan, J. (2012). Characteristics of moisture and salinity of soil in Taklimakan Desert, China. *Water Science & Technology*, *66*(6), 1162-70.

Xu, X., Li, B., & Wang, X. (2006). Progress in study on irrigation practice with saline groundwater on sand lands of Taklimakan Desert Hinterland. *Chinese Sci. Bull.*, 51, 161-166.

Zhang, G. (2004). Groundwater crisis and sustainable agricultural development in north China. *Arid Land Geography*, 27, 437-441.

Zhang, J., Xu, X., Lei, J., Jin, Z., Li, S., Gu, F., Qiu, Y., Xu, B., Liu, S., Du, W., Yan, Z., & Wang, Y. (2008). Effect of drip-irrigation with salinity water on soil environment of the Trim Desert highway shelterbelt (in Chinese, with English abstract). *Transactions of the CSAE*, *24*(10), 34-39.

Zhang, J., Xu, X., Lei, J., Sun, S., Fan, J., Li, S., Gu, F., Qiu, Y., & Xu, B. (2008). The salt accumulation at the shifting aeolian sandy soil surface with high salinity groundwater drip irrigation in the hinterland of the Taklimakan Desert. *Science Bulletin*, *53*(S2):63-70.

Zhang, J., Wang, Y., Zhao, Y., Xu, X., Lei, J., & Li, S. (2016). Spatial-temporal distribution of soil salt crusts under saline drip irrigation in an artificial desert highway shelterbelt. *Water*, *8*(2), 35, DOI: 10.3390/w8020035.

Zhao, W., & Cheng, G. (2002). Review of several problems on the study of eco-hydrological processes in arid zones. *Chinese Sci. Bull.*, *47*, 353-360.

Zhou, Z., Xu, X., Lei, J., & Li S. (2006). Ecological stability of Tarim Desert Highway shelterbelt. *Chinese Science Bulletin*, 51, 153-160.

Author´s institutional address

Ph.D. Jinglong Fan

Xinjiang Institute of Ecology and Geography,
Chinese Academy of Sciences
818 South Beijing Road, Urumqi, Xinjiang, 830011,
PR China
Telephone: +86 (991) 7823 146
Fax: +86 (991) 7885 357
fanjl@ms.xjb.ac.cn

BSc. Yaping Wei

Xinjiang Institute of Ecology and Geography Chinese Academy of Sciences/ University of Chinese Academy of Sciences
818 South Beijing Road, Urumqi, Xinjiang, 830011,
PR China
Telephone: +86 (991) 7823 146
Fax: +86 (991) 7885 357
weiypingya@163.com

BSc. Xinwen Xu

Xinjiang Institute of Ecology and Geography,
Chinese Academy of Sciences
818 South Beijing Road, Urumqi, Xinjiang, 830011,
PR China
Telephone: +86 (991) 7823 146
Fax: +86 (991) 7885 357
sms@ms.xjb.ac.cn

MSc.Xinghu Yang

Xinjiang Institute of Ecology and Geography,
Chinese Academy of Sciences
818 South Beijing Road, Urumqi, Xinjiang, 830011,
PR China
Telephone: +86 (991) 7823 146
Fax: +86 (991) 7885 357
429726240@qq.com

University of Chinese Academy of Sciences
19A Yuquan Road, Beijing 100049,
PR China

Haga clic aquí para escribir al autor

• ISSN 2007-2422

Particle size distribution and settling velocity of sediments in water diverted from the Yellow River during border-strip irrigation

• Jinshan Li •
Xi'an University of Technology, Xi'an/Henan Key Laboratory of Water-Saving Agriculture, Farmland Irrigation Research Institute of Chinese Academy of Agricultural Sciences

• Liangjun Fei * •
Xi'an University of Technology, Xi'an, China
Corresponding author

• Zhen Chen • Xiulu Sun •
Henan Key Laboratory of Water-Saving Agriculture, Farmland Irrigation Research Institute of Chinese Academy of Agricultural Sciences

Abstract

Li, J., Fei, L., Chen, Z., & Sun, X. (March-April, 2017). Particle size distribution and settling velocity of sediments in water diverted from the Yellow River during border-strip irrigation. *Water Technology and Sciences* (in Spanish), *8*(2), 31-41.

Diversion of river water for irrigation is an important factor in sustainable agricultural development in the Yellow River basin. This study examines patterns in the advance of sediment in irrigation water diverted from the Yellow River during border-strip irrigation. An irrigation experiment was carried out on a 1.8 m-wide strip and a 2.7 m-wide strip of a fruit field in order to observe the advance rate of irrigation water, the distribution of settled sediment, and the concentration and particle size distribution of sediment in the water flow. The settling velocity of sediment particles was then calculated using an empirical formula. The results show that the irrigation water gradually slowed as it advanced along the strip length, and the amounts of deposited particles decreased from the top ends of the strips to their bottom ends. The decrease was especially sharp on the section of each strip between 40 and 120 m from the water pipe outlet. Overall, the size of particles carried by the irrigation water fell within the range of 0.004 to 0.016 mm, with coarse and fine particles making up small proportions of the sediment. The concentration of coarse particles was higher at the top ends than at the bottom ends, while the concentration of fine particles was higher at the bottom ends than at the top ends. Water content in the soil at several locations varied significantly before and after irrigation, and the deposition of sediment was found to exert a great influence on the infiltration of irrigation water. The particle size distribution of the sediment deposited along the strips accords with the law of sedimentation in that coarse particles accumulated primarily at the top ends of the strips as a result of high settling velocity. Moreover, the results demonstrate

Resumen

Li, J., Fei, L., Chen, Z., & Sun, X. (marzo-abril, 2017). Distribución del tamaño de partículas y velocidad de sedimentación en el agua desviada del río Amarillo para riego por amelgas. Tecnología y Ciencias del Agua, *8(2), 31-41.*

La desviación de agua de río para riego es un factor importante en el desarrollo agrícola sostenible en la cuenca del río Amarillo. El presente estudio examina los patrones de avance de sedimentos en el agua de riego desviada del río Amarillo en el riego por amelgas. Se llevó a cabo un experimento de riego en una amelga de 1.8 m y otra de 2.7 m de ancho en un campo frutal, con el fin de observar la tasa de avance del agua de riego y la distribución de sedimentos asentados, así como la concentración y distribución del tamaño de partículas de sedimento en el flujo de agua. Posteriormente, la velocidad de sedimentación de las partículas se calculó mediante una fórmula empírica. Los resultados muestran que el agua de riego se redujo poco a poco, a medida que avanzaba a lo largo de las amelgas y la cantidad de partículas depositadas disminuyó de los extremos superiores a los extremos inferiores de éstas. La disminución fue especialmente marcada en la sección de cada amelga entre 40 y 120 m de la salida del tubo de agua. En general, el tamaño de partículas arrastradas por el agua de riego estuvo dentro del rango de 0.004 a 0.016 mm. Una pequeña proporción del sedimento estaba formada por partículas gruesas y finas. La concentración de partículas gruesas fue mayor en los extremos superiores que en los extremos inferiores, mientras que la concentración de partículas finas fue mayor en los extremos inferiores. El contenido hídrico del suelo en varios lugares varió significativamente antes y después del riego, y la deposición de sedimentos ejerció una gran influencia sobre la infiltración del agua de riego. La granulometría de los sedimentos depositados a lo largo de las amelgas concuerda con la ley de sedimentación en que las partículas gruesas se acumulan principalmente en los extremos superiores de las melgas, como resultado de la alta velocidad de sedimentación. Por otra parte, los resultados demuestran que es factible simplificar el flujo de agua sobre el campo a canal abierto

that it is feasible to simplify the water flow over the field to open-channel flow when calculating settling velocity. However, the formula for calculating settling velocity needs further modification to take into account the influences of flume rate and the scouring action of irrigation water on the surface sediment deposited on the strips.

Keywords: Water diverted from the Yellow River, border-strip irrigation, sediment, particle size distribution, settling velocity.

al calcular la velocidad de sedimentación. Sin embargo, la fórmula para calcular la velocidad de sedimentación necesita una modificación adicional, al tener en cuenta las influencias de la tasa de flujo y la acción erosiva del agua de riego en el sedimento superficial depositado en las melgas.

***Palabras clave**: agua desviada del río Amarillo, riego por amelgas, sedimento, distribución de tamaño de partículas, velocidad de sedimentación.*

Received: 20/04/2016
Approved: 11/10/2016

Introduction

The Yellow River, often referred to as China's mother river, plays an important role in industrial and agricultural development throughout its drainage basin. The river water has been diverted for irrigation for over 2000 years. Since the river has high sediment loads, the issue of sediment control necessarily arises whenever Yellow River water diversion (YRWD) is discussed (Jiang *et al*., 2015). Most existing research on sediment carried by Yellow River water focuses on river regulation works (Hu, Cao, Guo, & Chen, 2008), providing in-depth analyses of movement patterns of sediments, probability of incipient motion of sediments, and the flow velocity for incipient motion (Zhang, 2012; Fan, Zhong, & Wu, 2012; Li, Jiang, Zheng, & Zhang, 2012). A primary purpose of YRWD is to provide farm irrigation water, thereby ensuring sustainable agricultural development in the Yellow River basin (Duan, 1997). Given that sediment-laden water from the Yellow River is directly channeled to fields, many studies have provided insight into how to dredge channels and utilize sediments (Zhou & Wang, 2010; Wang, Hu and Zhou, 2010; Wang, Li, & Wang, 1997). However, little research has been done on the diverted river water applied to fields.

Diversion of Yellow River water for irrigation is an important component of YRWD. All provinces lying along the Yellow River have large areas irrigated by river water, including the Hetao, Shizuishan, Zuncun, and Weishan irrigation areas that are famous across the country. Despite that fact that they have brought remarkable agricultural benefits, these irrigation projects are beset by problems arising from the sediment in the river water. For example, some water-saving irrigation techniques such as sprinkler irrigation, micro-sprinkler irrigation, and drip irrigation require relatively high water quality because the irrigation devices are prone to blockage. In fact, sprinkler irrigation typically requires the sediment concentration in irrigation water to be lower than 0.2 kg/m^3, and the criteria for drip and micro-sprinkler irrigation are even stricter. These problems require more work for the application of water-saving irrigation techniques in areas irrigated by the Yellow River (Shi, Zhang, Huang, & Zhao, 2000). In addition, previous research into the movement patterns of river sediment in irrigation water concentrated on the infiltration of muddy water; the findings suggested that higher sediment concentrations and smaller particle sizes lead to lower infiltration rates (Bie, Cao, & Chang, 2015). A study conducted by Fei Liangjun *et al.* (Fei & Wang, 1998) at the end of the 20th century

revealed that, during border-strip irrigation, the irrigation method significantly affected the infiltration of muddy irrigation water into the soil.

Surface irrigation is still the primary irrigation technique practiced in areas watered by the Yellow River. However, few studies have looked at the accumulation and distribution of sediment on fields during border-strip irrigation, and even fewer studies have examined the mechanisms of incipient motion and deposition of sediment on fields. This study was conducted to investigate the distribution of settled sediment on fields irrigated with water diverted from the Yellow River, as well as the infiltration of the water into the soil. The settling of sediment particles during border-strip irrigation was analyzed using methods presented in related studies. This study is expected to provide support for irrigation projects that involve diverting water from the Yellow River.

Materials and methods

A survey of the study area

The field experiment presented in this paper was carried out in 2015 in the Zuncun irrigation area, which is located in the Sushui River basin within Yuncheng City, Shanxi Province. The irrigation area extends 145 km in the east-west direction and 30 km in the north-south direction. The YRWD project in this area is a Type I large-scale hydraulic engineering project for flood control, irrigation, and water supply; furthermore, it constitutes the largest YRWD project in Shanxi Province. This area features an irrigation system consisting of pipelines and ditches. Irrigation water is diverted from the Yellow River via low pressure pipelines and then distributed to fields through U-shaped concrete ditches.

The experimental field is located in Chuhou Township, Yuncheng City. The soil in the field primarily consists of loam and clay, and its complete mechanical composition is displayed in table 1. The uppermost 1 m of soil has an average dry bulk density of 1.4 g/cm^3 and a field capacity of 21.4%. Because the properties of sediments carried by the Yellow River vary across regions and seasons, the water diverted from the Yellow River in this study was analyzed to determine the composition of the sediment (see table 1) prior to the irrigation experiment.

The experimental field includes a narrow strip with dimensions of 1.8 × 300 m and the other with dimensions of 2.7 × 300 m. These are typical dimensions for the Zuncun irrigation area. Fruit trees are planted on the borders, and the areas between the borders are irrigated using the traditional border-strip irrigation

Table 1. Mechanical composition of the soil.

Soil depth (cm)	Percentages of different particle sizes (%)			Name of soil texture (International system)
	Clay (< 0.002 mm)	Silt (0.002-0.02 mm)	Sand (0.02-2 mm)	
0	6.33	34.61	59.06	Sandy loam
0-10	12.93	44.92	42.15	Loam
10-20	12.19	43.5	44.31	Loam
20-30	16.38	42.13	41.49	Loamy clay loam
30-40	16.04	47.83	36.13	Silty clay loam
40-50	83.39	16.61	0	Heavy clay
50-60	29.8	67.72	2.48	Silty clay
60-70	74.43	25.57	0	Heavy clay
70-80	36.06	62.35	1.59	Silty clay
80-90	81.76	18.24	0	Heavy clay
90-100	87.2	12.8	0	Heavy clay

ISSN 2007-2422

Table 2. Composition of the sediment in the Yellow River water.

Percentages of particle size ranges									Median particle size (mm)	Average particle size (mm)	Sediment concentration (kg/m³)
Particle size (mm)	< 0.125	< 0.062	< 0.031	< 0.016	< 0.008	< 0.004	< 0.002	< 0.001	0.009	0.015	1.567
Percentage (%)	100.0	98.1	86.3	68.2	46.9	27.5	13.6	5.6			

technique. Figure 1 illustrates the layout of the experimental field. Before the experiment, the slope of the field along the strip length was measured using a leveling instrument, and the average slope was calculated to be 1/1000.

Experimental methods

After the preliminary work was complete, water diverted from the Yellow River was applied to the field on June 19 and July 30, and relevant experimental parameters were determined. The rate of inflow was measured using a Parshall flume. The bottom of the Parshall flume were covered with sediments, which was swept by a broom, and rinsed off thoroughly with water when the irrigation event was done. Specific parameters and methods used in the experiment are as follows:

1. During the experiment, marker posts were set up along the length of the strips at intervals of 10 m. The time required for irrigation water to cover the majority of the surface around each post was recorded using a stopwatch, in order to determine advance time.
2. Monitoring points were designated along the length of each strip at intervals of 40 m. Three Trime tubes were embedded in the soil at each point to monitor variations in soil water content within the soil profiles (see figure 1). Soil samples were collected two days before irrigation, and two days and five days after irrigation. Then time-domain reflectometry (TDR) was used to determine the volumetric water content within the soil profiles at the monitoring points at depths from 10 to 100 cm. The TDR was calibrated

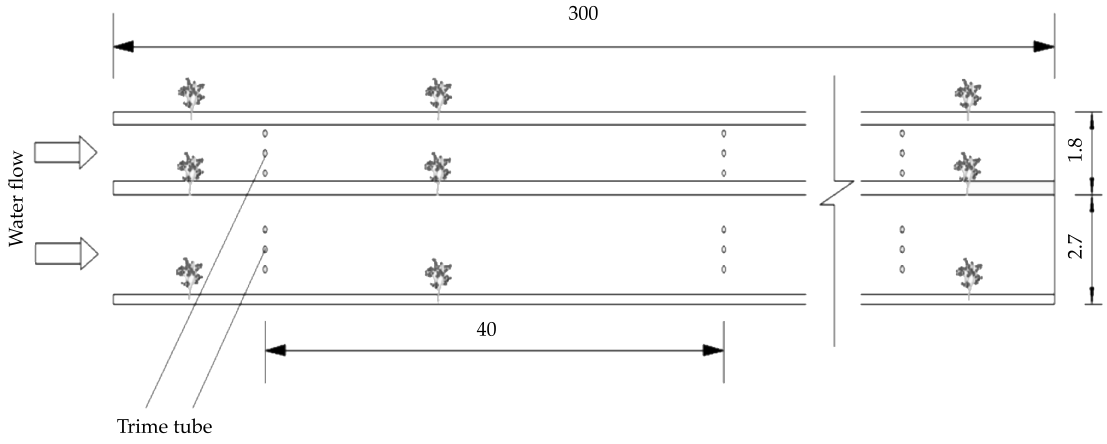

Figure 1. Layout of the experimental field.

• ISSN 2007-2422

three times, compared with oven dry method for soil water content, during the experimental period. Every steps as follow: insert the TDR probe and the soil auger into soil and let them stay parallel, meanwhile measure the TDR and the soil moisture content. And choose three different time periods when the soil moisture content is different, such as 2 days before irrigation, 2 days after irrigation, 15 days after irrigation. The relation curve was obtained between soil moisture content and soil depth calibration.

3. The advance rate and settling speed of sediment in the irrigation water were measured during and after irrigation. The specific procedures are as follows:
   a) Before irrigation, pieces of double-layered gauze (10 × 20 cm) were positioned on the surface of the strips at intervals of 40 m along their length. After irrigation, the sediment accumulated on the gauze was weighed and then taken to the laboratory for particle size analysis.
   b) During irrigation, water samples were collected at the outlets of the water pipes and from locations 0 m, 40 m, 120 m, 200 m, and 280 m from the top end of each strip. Then the concentration and particle size distribution of the sediment in the water samples were analyzed.
   c) Two days after irrigation, undisturbed soil samples were collected from the strips at intervals of 40 m along their length, and their dry bulk densities were measured.

Calculation methods

In existing research, settling velocities of sediment particles are typically calculated using empirical formulas, and various calculation methods are available. Existing comparative studies (Fan *et al*., 2012; Li, He, Zhu, & Huang, 2014) point out that the formula obtained by Weiming Wu (Wu & Wang, 2006) through an intensive regression analysis of the settling velocity of irregular particles, as well as the formula used to calculate the probability of incipient motion of sediments are commonly used and can produce satisfactory results. The calculation and analysis performed in this study suggest that introducing a shape factor into Wu's formula can yield a universal formula for determining settling velocity, but the method proposed by Fan, Zhong and Wu (2012) is more applicable to the case of sediment in irrigation water diverted from the Yellow River. In this study, a settling velocity calculation was performed to verify Fan's method. A comparison of the calculation results with the measured data suggests that water flow over the strips can be simplified to open-channel flow. The relationship of the settling velocity of particles to the Shields number and other parameters can be expressed as follows:

$$\frac{\omega}{u_*} = \frac{\sqrt{\left(25+1.2d_*^2-5\right)^{1.5}}}{\Theta^{0.5}d_*^{1.5}} \qquad (1)$$

where the Shields number is given by $\Theta = \Delta hJ/D$, in which h is water depth, $d_* = (\Delta g/v^2)^{1/3}D$, J is the slope of water surface, and D represents dimensionless particle size. In $\Delta = (\rho_s - \rho)/\rho$, ρ_s is the sediment density, ρ is the fluid density, g is gravitational acceleration, and v is the fluid's kinematic viscosity.

The friction velocity of a fluid is normally calculated using the equation, $U_* = \sqrt{gHj}$ where J denotes the hydraulic slope, H is water depth, and g is gravitational acceleration (Liu, Li, & Wang, 2005).

Results and analyses

Analysis of advance rate of irrigation water

As figure 3 shows, the advance rate of water flow over the field gradually decreased along the strip length. The advance rate over the first 80 m of the narrow strip was significantly higher than the rate over the same section of the wide strip. The water underwent a rapid increase in advance rate as it flowed over the section of the

ISSN 2007-2422

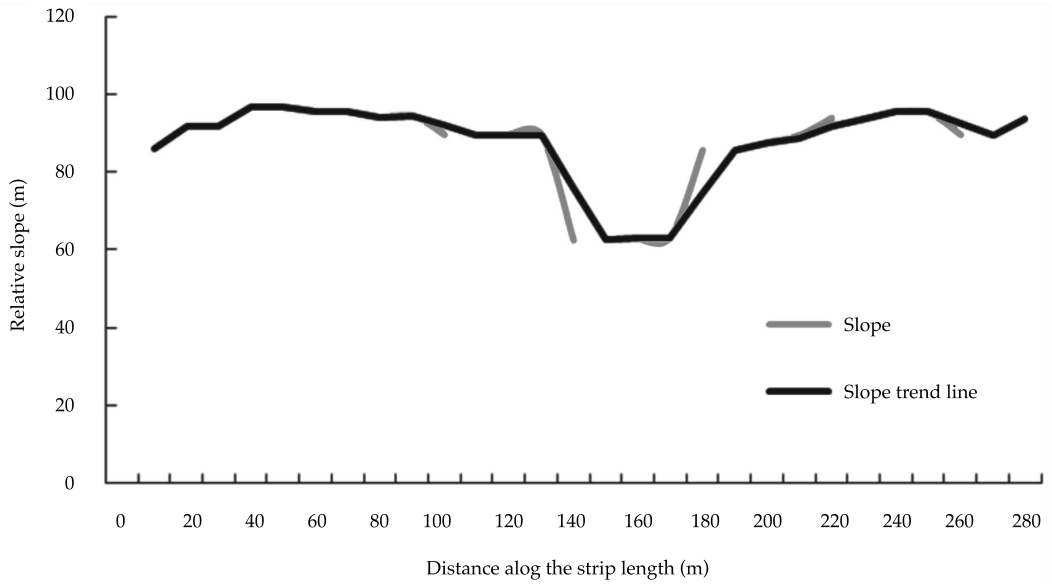

Figure 2. Slope along the strip length and its trend line.

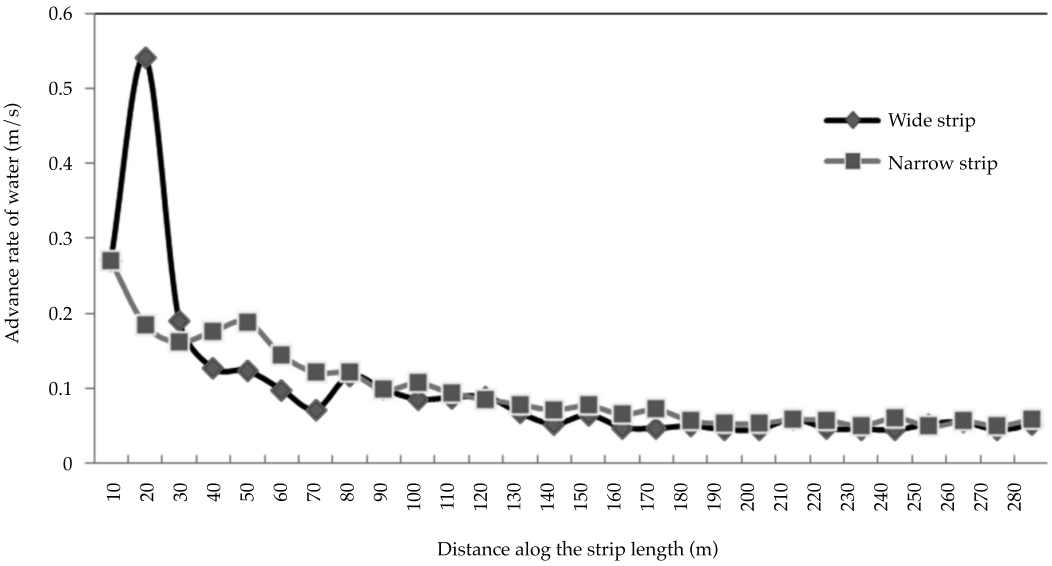

Figure 3. Distribution of advance rate of water along the strip length.

wide strip between 10 and 20 m, as is evident from the high slope on this section of the graph. No significant difference in advance rate was found between the wide and narrow strips after the water advanced over 200 m.

Distribution of sediment on the strips

As figure 4 shows, the sediment concentration in the irrigation water declined as the water moved forward over the two strips, with the

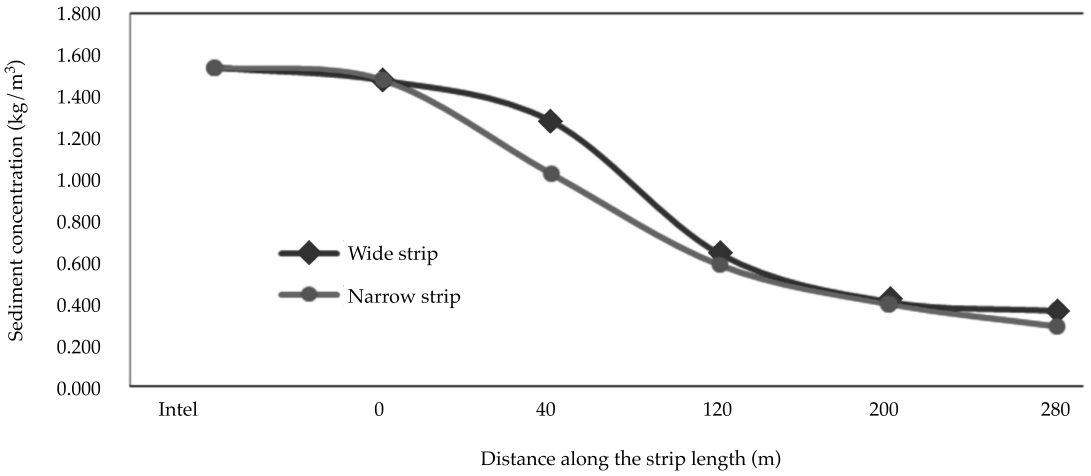

Figure 4. Distribution of sediment concentration along the strip length.

result that the sediment concentrations were significantly higher at the top ends of the strips than at the bottom ends. The decrease in sediment concentration was sharp over the 0 to 120 m section of each strip, while it was relatively slower over the 120 to 180 m section, indicating that the majority of the sediment carried by the irrigation water settled at the top ends of the strips. This pattern of variation was especially marked on the narrow strip, a finding that can possibly be attributed to the higher flow rate and thus the higher sediment concentration in the irrigation water at the top end of the narrow strip.

Particle size distribution of sediment in water flow over the strips

Figures 5 and 6 show that the particle sizes class of sediments carried by the irrigation water largely fell within the range of 0.004 to 0.016 mm, while coarse and fine particles accounted for only small fractions of the sediments. The concentration of coarse particles was higher at the top ends of the strips than at the bottom ends, while the concentration of fine particles was higher at the bottom ends than at the top ends. This suggests that coarse particles settled out of the fluid earlier than fine particles, with the result that the slower-settling fine particles advanced further with the water flow. The irrigation water at the bottom ends contained more sediment particles ranging from 0.001 to 0.008 mm in size than the water at the top ends, because parts of the surface sediment that had settled on the strips were scoured away by the moving water. Further analysis and research is needed to find out why particles in this size range were mobilized by the water flow.

Figure 7 shows the variations in soil water content before and after irrigation at three monitoring points on each strip, located at the top end, middle section, and bottom end. Before irrigation, the water content in the topsoil was about 20%, indicating a need for irrigation. Meanwhile, soil deeper than 60 cm varied slightly in water content, roughly around 23%. On the first and second days after irrigation, the topsoil exhibited marked increases in water content. At the three monitoring points, the overall soil water content on the first day after irrigation was very close to the water content on the second day after irrigation. The topsoil's water content increased more than 5% compared to the level before irrigation, and the deeper layers also demonstrated noticeable increases in water

ISSN 2007-2422

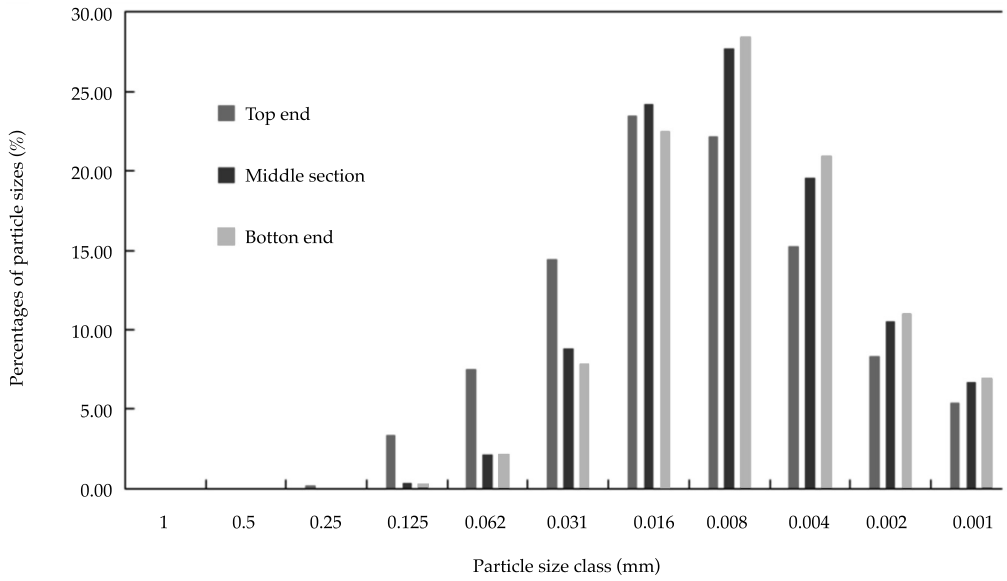

Figure 5. Particle size distribution of sediment in water flow over the wide strip.

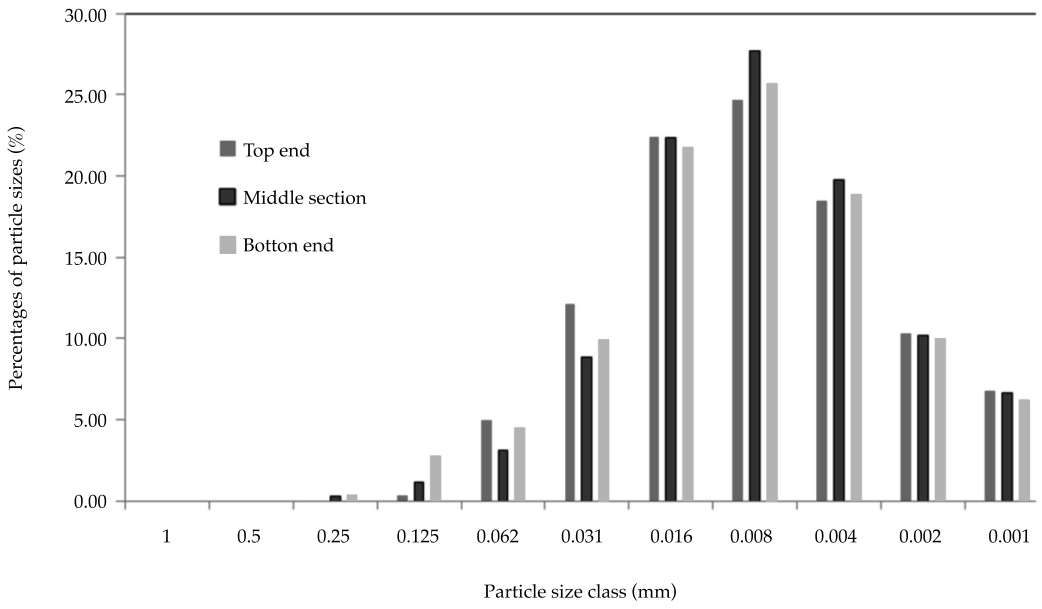

Figure 6. Particle size class distribution of sediment in water flow over the narrow.

content. Differences were noted between the soil water contents on the first and second days after irrigation, despite their similar overall trends. For example, in the top and middle sections, the water content in the deep soil layer was slightly higher on the second day after irrigation than on the first day; at the top end, however, the topsoil water content on the second day after irrigation

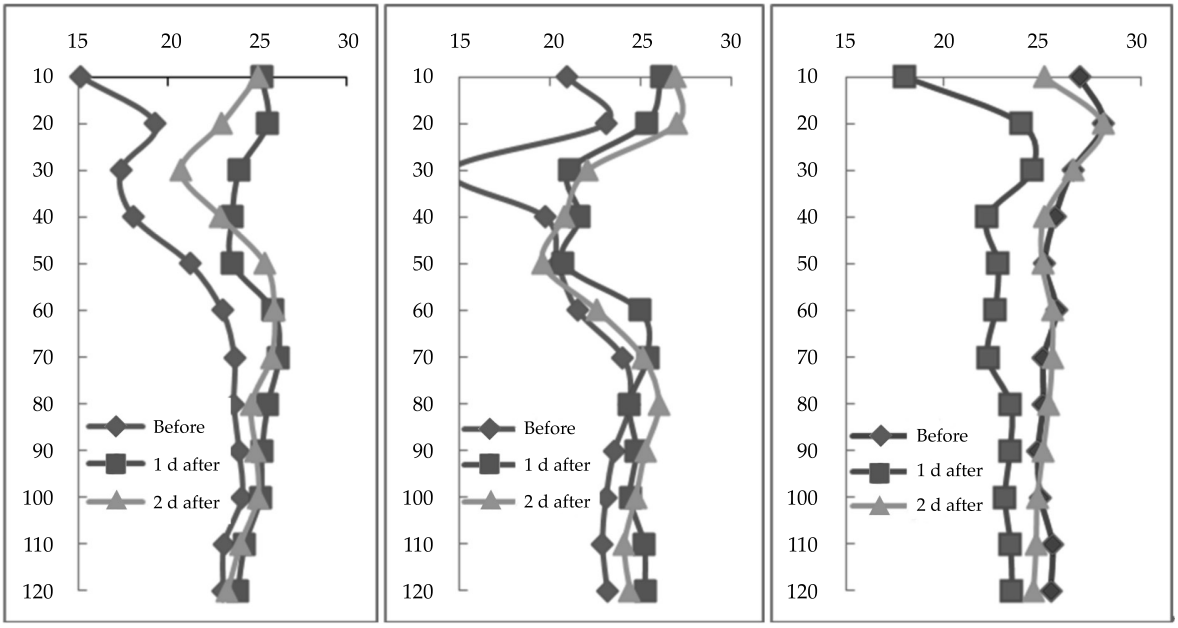

Figure 7. Soil water content in different locations before and after irrigation.

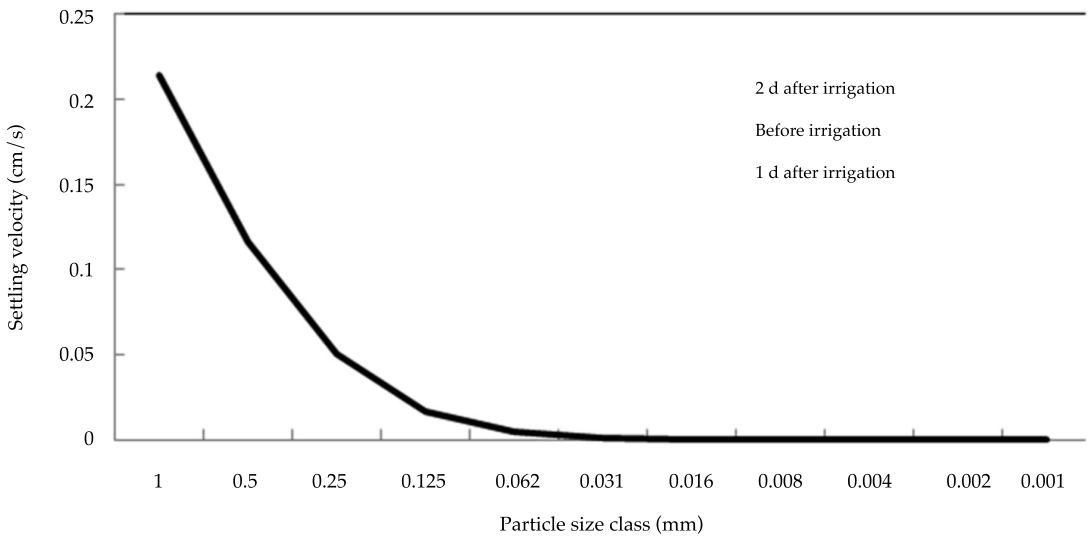

Figure 8. Average settling velocity of particles of different sizes class.

was significantly lower than that on the first day. This result occurred because the water at the top end nearly disappeared as it advanced to the middle and bottom of the strips.

Analysis of settling velocity

Based on the sediment particle size class distribution in the irrigation water, the settling

velocities of particles of different sizes were calculated using the formula presented in Section of Calculation methods. The settling velocity was found to be affected primarily by the sediment's density and particle size, water temperature, water depth, and strip width. The density of the sediment did not change as the irrigation water moved forward. After the water was channeled to the field, the water temperature tended to remain stable, rendering its influence on the water flow negligible. The water depth and the strip's slope changed a lot during the advance of the irrigation water, and water depth also affected the friction velocity of the flow ($U_* = \sqrt{gHj}$) and the Shields number ($\Theta = \Delta hJ/D$). Water depth in the formula canceled out during the formula derivation, implying that it has no influence on settling velocity. However, the strip's slope varied significantly along the strip length and the slope variation was closely correlated with the settling velocity. Ultimately, particle size was the main factor affecting the settling velocity of the sediment in the irrigation water: The settling velocity decreased as the particle size decreased.

Conclusions

During the border-strip irrigation experiment, the amounts of settled sediment varied significantly from the top ends of the strips to their bottom ends. The amounts of sediment settled at the top ends of the wide strip and narrow strip were, respectively, 4.2 times and 5.3 times the amounts settled on the bottom ends. The advance rate of the sediment also changed significantly from the top end to the bottom end of each strip, indicating that the advance rate was affected not only by the strip's slope, but also by the flow rate and infiltration of water into the soil.

The amounts of deposited particles decreased along the strip length from top to bottom. The decrease was especially marked on section of each strip between 40 and 120 m.

The particle size distribution of the sediments deposited along the strips accords with the law of sedimentation; coarse particles accumulated primarily at the top ends as a result of high settling velocity. The existence of coarse particles in the sediment at the bottom ends suggests that the advance of irrigation water was a relatively complex process associated with the scouring action of the water flow on the surface particles deposited on the strips. Further research is needed to explore this issue.

It was feasible to represent the water flow over the strips as open-channel flow when calculating the settling velocity of the sediment particles. However, the formula for calculating settling velocity requires further modification to take into account the influences of flume rate as well as the scouring action of the moving water on the surface sediment deposited on the strips.

References

Bie, Y., Cao, H., & Chang, Z. (2015). Analysis of the characteristics and causes of the increase of soil moisture content under muddy water irrigation with different sediment gradations. *Water Saving Irrigation*, 10, 12-18.

Duan, Z. (1997). Optimal deployment of sediment is necessary to ensure sustainable development of projects of Yellow River water diversion for irrigation. *Sediment Research*, 2, 57-60.

Fan, N., Zhong, D., & Wu, B. (2012). Determination of probability of incipient motion of sediment using a probability density function. *Journal of Tsinghua University (Science and Technology)*, 6, 766-770.

Fei, L., & Wang, W. (1998). Experimental study on the intermittent infiltration of silt laden water in surge flow border irrigation . *Journal of Hydraulic Engineering*, 5, 66-71.

Hu, C., Cao, W., Guo, Q., & Chen, J. (2008). Progress and prospect on sediment study. *China Water Resources*, 21, 56-59.

Jiang, E., Cao, Y., Dong, Q. *et al*. (2015). Long term effects of the Yellow River sediment resources utilization. *Yellow River*, 2, 1-5, 12.

Li, J., Jiang, E., Zheng, B., & Zhang, Y. (2012). Statistical analysis of threshold velocity of sediment particles. *Sediment Research*, 3, 15-20.

Li, M., He, Y., Zhu, G., & Huang, C. (2014). Comparative analysis of settling velocity formulas for sand. *Port and Waterway Engineering*, 6, 6-9.

Liu, C., Li, D., & Wang, X. (2005). Experimental study on friction velocity and velocity profile of open channel flow. *Journal of Hydraulic Engineering*, 8, 950-955.

• ISSN 2007-2422

Shi, Z., Zhang, J., Huang, H., & Zhao, R. (2000). Discussion on methods for disposal of sediment in the Yellow River water used in water-saving irrigation. *Water Saving Irrigation*, 1, 12-14, 43.

Wang, Y., Hu, C., & Zhou, Z. (2010). Long-distance and distributed mode of sediment deployment of lower Yellow River and its evaluation indexes. *Journal of Hydraulic Engineering*, 7, 764-770.

Wang, Y., Li, X., & Wang, B. (1997). Sediment movement and causes of siltation in representative areas irrigated by the Yellow River. *Journal of Hydraulic Engineering*, 7, 14-19, 37.

Wu, W., & Wang, S. Y. (2006). Formulas for sediment porosity and settling velocity. *Journal of Hydraulic Engineering*, 132, 858-862.

Zhang, H. (2012). A unified formula for incipient velocity of sediment. *Journal of Hydraulic Engineering*, 12, 1387-1396.

Zhou, Z., & Wang, Y. (2010). Optimal deployment of sediment resource in irrigation districts of Yellow River and its application. *Journal of Hydraulic Engineering*, 9, 1018-1023.

Author´s institutional address

Jinshan Li

Ph.D. candidate
Henan Key Laboratory of Water-Saving Agriculture
Farmland Irrigation Research Institute
of Chinese Academy of Agricultural Sciences,
Xinxiang 453002, PR China
Telephone: +86 (0373) 3393 248
lijinshan72@126.com

Ph.D. Liangjun Fei

Xi'an University of Technology,
Xi'an, China, PR, China
Telephone: +86 (029) 8773 2335
feiliangjun2008@163.com

Zhen Chen

Ph.D. candidate
Henan Key Laboratory of Water-Saving Agriculture,
Farmland Irrigation Research Institute of Chinese
Academy of Agricultural Sciences
Xinxiang 453002, PR China
Telephone: +86 (0373) 3393 207
chenzhen@caas.cn

Xiulu Sun

Ph.D. candidate
Henan Key Laboratory of Water-Saving Agriculture,
Farmland Irrigation Research Institute of Chinese
Academy of Agricultural Sciences
Xinxiang 453002, PR China
Telephone: +86 (0373) 3393 105
sunxiulu@caas.cn

Haga clic aquí para escribir al autor

Calle de Beijing, China.

Foto: Fernando Leyva Calvillo.

Phytoextraction potential of wetland plants for Copper in Water Bodies

• Zhiwen Luo •
Chongqing University, China
Sichuan University of Sciences & Engineering, China

• Xingzhong Yuan* •
Chongqing University, China
*Corresponding author

• Xiangying Chen • Xiaoxia Cui •
Sichuan University of Sciences & Engineering, China

Abstract

Luo, Z., Yuan, X, Chen, X., & Cui, X. (March-April, 2017). Phytoextraction potential of wetland plants for Copper in Water Bodies. *Water Technology and Sciences* (in Spanish), *8*(2), 43-50.

Copper is the most common heavy metal contaminant in the environment. Wetland construction engineering and technology have been used to control water pollution due to their low cost and efficiency and the hydrophytes have been the most important constituents of wetland construction. In this experiment, during April of 2014, Cu^{2+} accumulation content in different parts of *Acorus calamus* and *Phragmites australis* were investigated based on hydroponic experiments of different Cu^{2+} concentration solutions. Cu^{2+} concentrations in the water body were 0, 10, 25, 60, 100, 200 and 500 mg/l, respectively. The results showed that there were significant Cu^{2+} concentration differences between the above- and below-ground parts of *Acorus calamus* and *Phragmites australis*. Cu^{2+} content in the above- and below-ground parts of wetland plants increased with hydroponic solution Cu^{2+} concentrations, resulting in a significantly positive correlation between Cu^{2+} content and concentrations of hydroponic solutions. There was a significant difference in Cu^{2+} content in the wetland plants under all hydroponic solution Cu^{2+} concentrations. *Acorus calamus* exhibited the greatest Cu^{2+} accumulation in above- and below-ground parts. *Acorus calamus* and *Phragmites australis* can be selected for application on the phytoremediation of water polluted by heavy metals due to their excellent Cu^{2+} accumulation ability.

Keywords: *Acorus calamus*, *Phragmites australis*, Cu^{2+}, accumulation.

Resumen

Luo, Z., Yuan, X, Chen, X., & Cui, X. (marzo-abril, 2017). Potencial de fitoextracción de plantas de humedales para el cobre en cuerpos de agua. Tecnología y Ciencias del Agua, *8(2), 43-50.*

El cobre es el metal pesado contaminante más común en el medio ambiente. La ingeniería y tecnología de construcción de humedales se han utilizado para el control de la contaminación del agua debido a su economía y eficiencia, y las hidrófitas han sido los componentes más importantes de la construcción de humedales. En este estudio, llevado a cabo en abril de 2014, se investigó la acumulación de Cu^{2+} *en diferentes partes de* Acorus calamus *y* Phragmites australis *mediante métodos hidropónicos de soluciones con diferentes concentraciones de* Cu^{2+}*. Las concentraciones de* Cu^{2+} *en el cuerpo de agua fueron de 0, 10, 25, 60, 100, 200 y 500 mg/l. Los resultados mostraron que existen diferencias significativas en la concentración de* Cu^{2+} *entre las partes de* Acorus calamus *y* Phragmites australis *que están por encima y las que están por debajo del suelo. El contenido de* Cu^{2+} *en las partes de arriba y debajo del suelo de plantas de humedal aumentó con solución hidropónica de* Cu^{2+}*, dando por resultado una correlación significativamente positiva entre el contenido de* Cu^{2+} *y las concentraciones de soluciones hidropónicas. Hubo una diferencia significativa en el contenido de* Cu^{2+} *en las plantas de humedal con todas las concentraciones de* Cu^{2+} *en solución hidropónica.* Acorus calamus *exhibió la mayor acumulación de* Cu^{2+} *en las partes por encima y por debajo del suelo.* Acorus calamus *y* Phragmites australis *se pueden seleccionar para su aplicación en fitoremediación de aguas contaminadas por metales pesados debido a su excelente capacidad de acumulación de cobre.*

Palabras clave: Acorus calamus, Phragmites australis, *Cu^{2+}, acumulación.*

Received: 16/02/2016
Approved: 22/09/2016

Introduction

Heavy metals are harmful to aquatic ecosystems, and remain in the environment for a long time (Ameh & Akpah, 2011; Bissenbaev, Ishchenko, Taipakova, & Saparbaev, 2011; Tanhan, Kruatrachue, Pokethitiyook, & Chaiyarat, 2007). Copper is a toxic heavy metal pollutant that quickly accumulates in animals and humans through the food chain, which seriously affects the metabolism of the human body. The human body releases Cu^{2+} very slowly, causing damage to bodily organs that are irreversible. Therefore, Cu^{2+} pollution treatment has become an urgent subject. Traditional methods of treatment to heavy metal pollution in soil mainly use the mixing of soil, leaching method, chemical modifiers, and so on. Not only are these physical and chemical methods expensive, they cannot be applied into small areas and cause second pollution. Such methods cannot fundamentally solve the Cu2+ pollution in soil. (He, Huang-Xiao, & Chen, 2011; Visioli & Marmiroli, 2013; Mirza, Hossain, & Masayuki, 2010). In recent years, people have found the bioconcentration ability of some plants to heavy metals. It is a high efficiency, environmental protection and cost control measures to use such plants as phytoremediation of heavy metal pollution. This treatment measure has very broad application prospects (Engelen, Sharpe-Pedler, & Moorhead, 2007; Chaumont *et al*., 2012; Rajkumar, Sandhya, Prasad, & Freitas, 2012; Zhou *et al*., 2007).

The calamus (*Acorus calamus L.*) and reed (*Phragmites australis*) are common across China's natural wetlands. The high Cu^{2+} absorption features of these two plants species provide scientific basis for phytoremediation of heavy metal pollution in water bodies.

Materials and methods

Acorus calamus and *Phragmites australis* were collected from the Fuxi River basin of Sichuan Province, China.

In April of 2014, the experiment was carried out with hydroponic cultivation in a ventilated plastic shed. Foam boards were placed on the clean plastic barrels with three holes to serve as a plant carrier. Three plants of similar height were selected from each species and transplanted into the foam carriers, and the root of the plants were immersed in the nutrient solution with the modified Hoagland formula: 945 mg/l $Ca(NO_3)_2{\cdot}4H_2O$, 506 mg/l KNO_3, 80 mg/l NH_4NO_3, 136 mg/l KH_2PO_4, 493 mg/l $MgSO_4$, 2.5 ml Fe-EDTA, 5 ml trace element solution (0.83 mg/l KI, 6.2 mg/l H_3BO_4, 22.3 mg/l $MnSO_4$, 8.6 mg/l $ZnSO_4$, 0.25 mg/l Na_2MoO_4, 0.025 mg/l $CuSO_4$, 0.025 mg/l $CoCl_2$), pH = 6.0.

After two weeks of continued growth of the plant's, the $Cu(NO_3)_2$ was added to the aqueous solution according to the concentration gradient: 7 concentration process of 0, 10, 25, 60, 100, 200 and 500mg/l. Each of concentration process was repeated six times.

The well-growing plants were collected after three weeks and divided into above- and below-ground parts. They were washed with distilled water and deionized water twice, treated with deactivation enzymes at 105°C, and dried to a constant weight for eight hours at 70°C. After drying, weighing, grinding and digestion, the plant samples were determined Cu^{2+} concentration by atomic absorption spectrophotometer.

Copper retention rate was calculated by formula (1) (Xia & Shu, 2001).

$$Cu^{2+}\ \text{retention rate}(\%) = (C1\text{-}C2)/C1 \times 100 \quad (1)$$

C1: Cu^{2+} content in underground part of plants, mg/kg.
C2: Cu^{2+} content in aboveground part of plants, mg/kg.

The experimental data was analyzed by variance analysis (ANOVA), LSD test, and correlation analysis between Cu^{2+} concentration of solution and enrichment concentration of plants by Origin 9.0 software.

Results and discussion

The Two-way ANOVA analysis of Cu^{2+} contents of the two emergent plants is as follows: The

• ISSN 2007-2422

plant species and the Cu^{2+} concen tration process significantly affected the accumulation of copper in plants. The analysis results were showed in table 1.

Calamus and reeds showed very significant differences at seven concentration processes for the Cu^{2+} accumulation capacity in different emergent plants. The Cu^{2+} accumulation content in different plant species (calamus and reeds) has significantly affected ($P < 0.01$). In addition, the interaction of different Cu^{2+} concentrations and plant species also significantly affects Cu^{2+} enrichment capacity of wetland plants ($P < 0.01$).

Table 2 shows Cu^{2+} accumulation in *Acorus calamus* and *Phragmites australis*.

Figure 1a and 1b indicated that the Cu^{2+} accumulation contents in calamus and reed showed significant differences. In general, Cu^{2+} accumulation amounts in calamus were significantly more than in the reed. The calamus has a stronger ability to absorb and transport Cu^{2+} than reed does.

The experiment results showed that the Cu^{2+} accumulation contents of calamus were significantly more than that of reed in both the above- and below-ground parts. The Cu^{2+} enrichment amounts in the underground parts of the two plant species were not significantly different at low Cu^{2+} concentrations (10 mg/l and 25 mg/l). Yet, the Cu^{2+} enrichment amounts in calamus were significantly more than that

Table 1. The ANOVA analysis of Cu^{2+} accumulation

	F	P
Concentration process	33.13**	<0.001
Plant species	5.99*	0.0028
Interaction	5.60*	0.0038

* Notes: ** indicates a significant difference at p = 0.001; *indicates a significant difference at p = 0.01

Table 2. Cu^{2+} accumulation in Acorus calamus and *Phragmites australis*.

Plant part	Cu^{2+} concentration (mg/l)	*Acorus calamus* (mg/kg)	*Phragmites australis* (mg/kg)
Aboveground	0	7.4[a]	122.79[b]
	10	115.09[a]	159.92[b]
	25	681.23[a]	143.61[b]
	60	899.17[a]	223.69[b]
	100	4 107.53[a]	198.39[b]
	200	6 208.5[a]	264.75[b]
	500	4 206.9[a]	349.73[b]
Underground	0	37.85[a]	113.17[b]
	10	282.73[a]	236.54[b]
	25	955.3[a]	768.41[b]
	60	2 980.97[a]	373.75[b]
	100	8 107.53[a]	429.22[b]
	200	4 271.03[a]	379.52[b]
	500	2 198.27[a]	448.83[b]

* Notes: Values with different letters in the same element of the same species and same column indicate a significant difference at $p = 0.05$ according to the LSD test.

ISSN 2007-2422

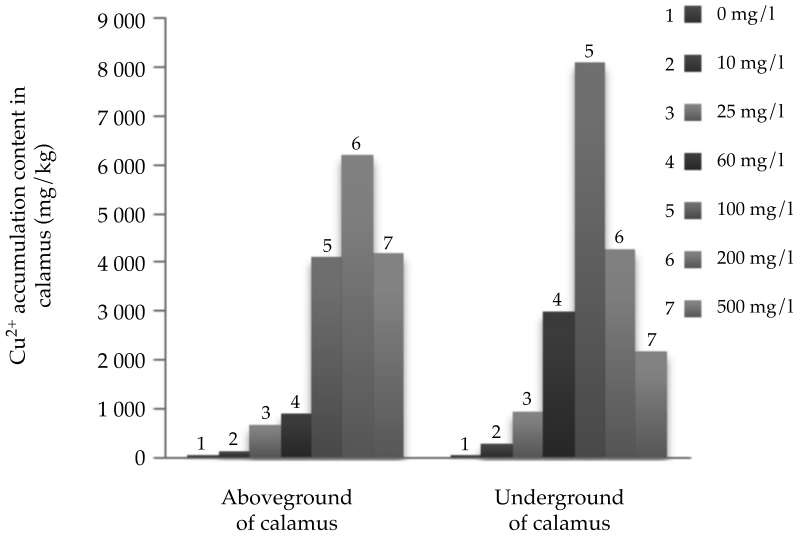

Figure 1a. The Cu^{2+} accumulation mean content in *calamus*.

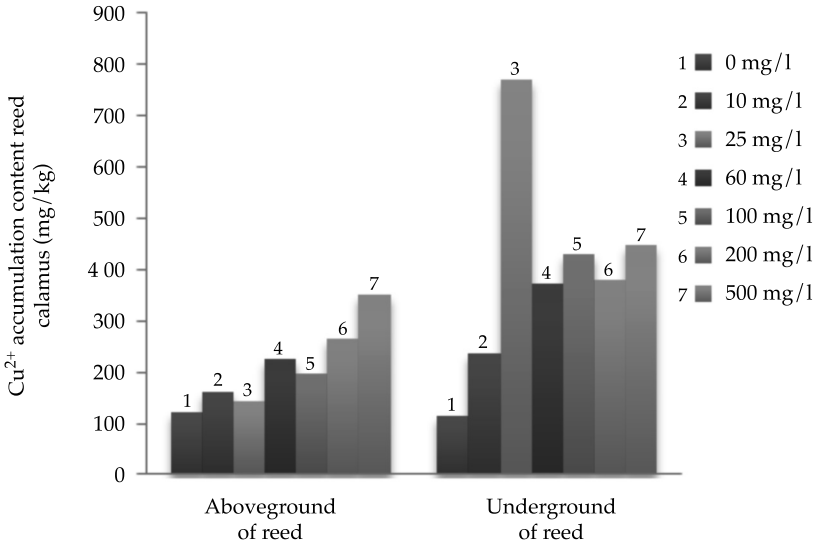

Figure 1b. The Cu^{2+} accumulation mean content in reeds.

in the reed at higher Cu^{2+} concentrations (60 mg/l, 100 mg/l, 200 mg/l and 500 mg/l). The aboveground parts of plants were similar to belowground parts

Overall, in lower concentrations (10 and 25 mg/l), Cu^{2+} accumulation quantity in Acorus calamus and Phragmites australis were similar at the 0.05 level. Cu^{2+} accumulation quantity in the above- and below-ground reed parts were significantly different at higher Cu^{2+} concentrations, but the same parts of the calamus were not significantly different. The two plant species showed different accumulation abilities at different Cu^{2+} concentrations; calamus

accumulated more Cu^{2+} than the reeds did, as shown in figure 1a and 1b.

The accumulation amount of Cu^{2+} in calamus and reed increased with the increase of pollutant concentration. At medium and low concentrations, the contents in the underground part of calamus were more than that in the aboveground part, and the average retention rate was more than 50%. However, it was the opposite at high concentrations (200 and 500 mg/l); the content in the underground parts was lower. The calamus has a strong ability to enrich and migrate Cu^{2+}. The content of underground part of reed was higher than that of aboveground parts at six concentration processes, indicating that the root system of reed had a strong retention effect on Cu^{2+}, and the average retention rate was more than 40% (table 3). There was no significant difference in mean retention rate between the two species.

The results of the correlation analysis of Cu^{2+} contents in the aboveground parts of calamus and hydroponic solution Cu^{2+} concentration showed that a maximum Cu^{2+} content was achieved when the concentration was 200mg/l. The variation curve of Cu^{2+} content in the underground and aboveground parts were similar. The optimum enrichment concentration for copper was 100mg/l (figure 2).

Table 3. Cu^{2+} retention rate of calamus and reed.

Cu^{2+} concentration(mg/l)	***Acorus calamus* (%)**	***Phragmites australis* (%)**
0	80.45	-8.50
10	59.29	32.39
25	28.69	81.31
60	69.84	40.15
100	49.34	53.78
200	-45.36	30.24
500	-91.37	22.08

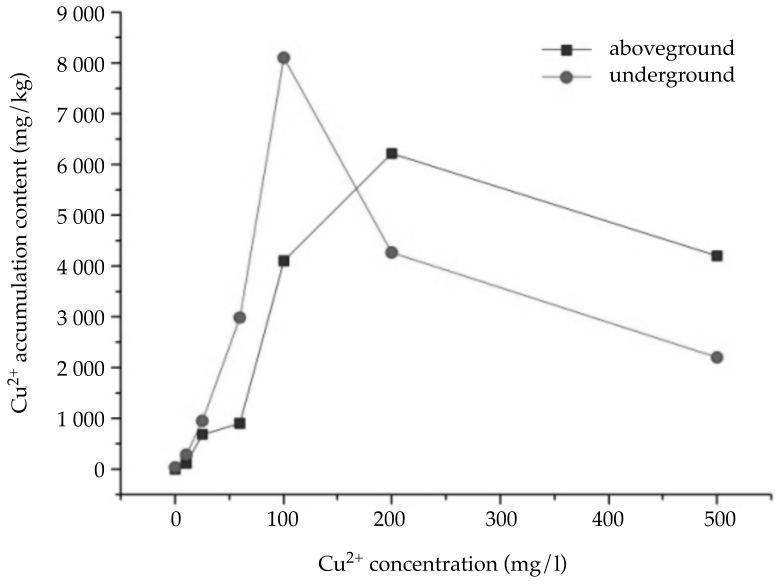

Figure 2. The correlation between Cu^{2+} accumulation content in *Acorus calamus* and Cu^{2+} concentration.

ISSN 2007-2422 •

Cu^{2+} accumulation contents in plants reaches a maximum with the increase of Cu^{2+} concentration in hydroponic solution. Cu^{2+} accumulation contents in plants decreased if the concentration exceeded the optimum enrichment concentration, indicating that the toxicity of heavy metals to plants has exceeded its tolerance, inhibiting plant growth and halting the accumulation of Cu^{2+}.

The Cu^{2+} enrichment amount in the aboveground of reed increased with the increase of Cu^{2+} concentration in the solution through the correlation analysis curve (figure 3). Cu^{2+} accumulation content showed slight fluctuations at low concentration processes (10, 25, 60 and 100 mg/l), but Cu^{2+} accumulation significantly increase as the hydroponic solution of Cu^{2+} concentration increased. Therefore, *Phragmites australis* showed good Cu^{2+} tolerance. Cu^{2+} content in the underground parts of reed gently increased as hydroponic solution Cu^{2+} concentration increased, showing a positive correlation relationship. The enrichment amount of Cu^{2+} in the underground part was significantly more than that in the aboveground part. As can be seen from figure 3, Cu^{2+} accumulation contents in the underground portion of reed fluctuated under low Cu^{2+} concentrations. As Cu^{2+} content increased, Cu^{2+} content stabilized and Cu^{2+} content reached its maximum in reeds.

The absorption of copper by calamus was higher than that of reed at seven concentration processes, but reed tolerance to high Cu^{2+} concentration was higher than calamus. Therefore, calamus is suitable for the ecological restoration of plants for medium and low concentration of heavy metal polluted water bodies.

According to the results of correlation analysis between Cu^{2+} content in plants and Cu^{2+} concentration in the hydroponic solution, the Cu^{2+} accumulation content(y) in aboveground and underground parts of *Acorus calamus* and *Phragmites australis* increased as Cu^{2+} concentration (x) increased; there was a significant positive correlation (table 4). Thisindicated that the concentration of heavy metals in the growing medium plays an important role that impacts plant absorption and heavy metal accumulation.

Cu^{2+} primarily accumulates in plant roots (Stolts & Gregor, 2002). This is because Cu^{2+} in roots is the primarily forms from precipitation. Additionally, there is ionic and complex states

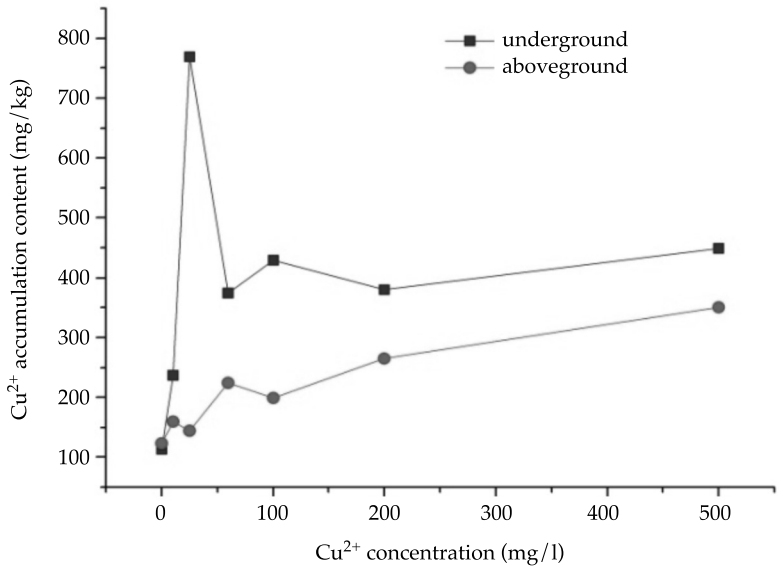

Figure 3. The correlation between Cu^{2+} accumulation content in *Phragmites australis* and Cu^{2+} concentration.

• ISSN 2007-2422

Table 4. Correlation of Cu^{2+} accumulation content in copper-contaminated water to wetland plants.

Plant	Plant part	Correlation Function	R^2
Acorus calamus	Aboveground	$4.4082 \times 10^{-16}x^{22.1631x^{-0.18477}}$	0.97386
	Underground	$2.7194 \times 10^{-16}x^{25.4253x^{-0.20935}}$	0.93498
Phragmites australis	Aboveground	$125.1777 + 7.04417x^{0.55753}$	0.85224
	Underground	$463.1011 - 370.54424x^{0.88195}$	0.45869

of Cu in the plant saps. It is difficult to transport Cu^{2+} in plant roots due to retention, passivation, or precipitation. Cu^{2+} accumulates in the root surface mainly in the form of microcrystals on cell walls. Plants accumulated them in the roots, which prevents harmful ions from inhibiting photosynthesis. In this study, Cu^{2+} accumulation quantities in the underground parts of the two wetland plants were significantly greater than those in the aboveground parts (Ren, Tao, & Yang, 2009).

Conclusions

The two wetland plant species showed strong Cu^{2+} enrichment abilities at different Cu^{2+} concentration conditions, both in under-ground microcrystals on cell walls. ons from and aboveground parts. The contents of Cu^{2+} in calamus and reed were significantly different at the same Cu^{2+} concentration. Among same type of wetland plants, while below 200 mg/l, Cu^{2+} accumulation increased as the Cu^{2+} concentration in the solutions increased.

Because they have the ability to effectively-absorb and enrich copper, both Acorus calamus and *Phragmites australis* can be used as selective species for phytoremediation of contaminated water bodies with heavy metal. The *Phragmites australis* has better tolerance to heavy metals Cu^{2+}, and compared to other plants, the *Acorus calamus* has stronger absorption and accumulation Cu^{2+} abilities (table 5). Overall, *Acorus calamus* is a better heavy metal contaminated water remediation plant than the *Phragmites australis*.

Acknowledgements

The research was supported by the Projects of Sichuan Province Science and Technology Support Program (2014GZ0132) and the Projects of the Education Department of Sichuan Province (16ZB0252).

References

Ameh, E. G., & Akpah, F. A. (2011). Heavy metal pollution indexing and multivariate statistical evaluation of hydrogeochemistry of River PovPov in Itakpe Iron-Ore mining area, Kogi State, Nigeria. *Advances in Applied Science Research*, 2(1), 33-46.

Bissenbaev, A. K., Ishchenko, A. A., Taipakova, S. M., & Saparbaev, M. K. (2011). Presence of base excision repair enzymes in the wheat aleurone and their activation in

Table 5. Possibilities accumulation ability of several plants for Cu^{2+} (Zhang, 2014).

Family	Plant	Possibilities of Cu^{2+} accumulation
Convolvulaceae	*Ipomoea alpina*	12 300 mg/kg
Scrophulariaceae	*Lindernia perennis*	9 322 mg/kg
Labiatae	*Gutenbergia katangense*	8 356 mg/kg
Cyperaceae	*Bulbostylis mucronata*	7 783 mg/kg
Amaranthaceae	*Pandiaka metallorum*	6 260 mg/kg
Leguminosae	*Vigna dolomitica*	3 000 mg/kg
Asteraceae	*Anisopappus davyi*	2 889 mg/kg
Pottiaceae	*Didymodon constricta*	1 962 mg/kg (Peng & Zhang, 2007)

cells undergoing programmed cell death. *Plant Physiology and Biochemistry*, *49*(10), 1155-1164.

Chaumont, A., Nickmilder, M., Dumont, X., Lundh, T., Skerfving, S., & Bernard, A. (2012). Associations between proteins and heavy metals in urine at low environmental exposures: Evidence of reverse causality. *Toxicology Letters*, *210*(3), 345-352.

Engelen, D. L. V., Sharpe-Pedler, R. C., & Moorhead, K. K. (2007). Effect of chelating agents and solubility of cadmium complexes on uptake from soil by *Brassica juncea*. *Chemosphere*, *68*(3), 401-408.

He, Q. X., Huang-Xiao, C., & Chen, Z. L. (2011). Influence of organic acids, complexing agents and heavy metals on the bioleaching of iron from kaolin using Fe (III)-reducing bacteria. *Applied Clay Science*, *51*(4), 478-483.

Mirza, H., Hossain, M. A., & Masayuki, F. (2010). Physiological and biochemical mechanisms of nitric oxide induced abiotic stress tolerance in plants. *American Journal of Plant Physicology*, *5*(6), 295-324.

Rajkumar, M., Sandhya, S., Prasad, M. N. V., & Freitas, H. (2012). Perspectives of plant-associated microbes in heavy metal phytoremediation. *Biotechnology Advances*, *30*(6), 1562-1574.

Peng, T., & Zhang, Z. (2007). Analyses of the contents of elements of five mosses and their substrates in Tongshankou Copper mine, Hubei Province, China. *Journal of Wuhan Botanical Research* (in Chinese), *25*(6), 596-600.

Ren, J., Tao, L., & Yang, Q. (2009). Accumulation ability of Phragmites australis, *Acorus calamus* and *Scirpus tabernaemontani* for Pb^{2+} in Water body. *Wetland Science*, 7, 255-260.

Stolts, E., & Gregor M. (2002). Accumulation properties of As, Cd, Cu, Pb and Zn by four wetland species growing in submerged mine tailings. *Environmental and Experimental Botany*, 47, 271-280.

Tanhan, P., Kruatrachue, M., Pokethitiyook, P., & Chaiyarat, R. (2007). Uptake and accumulation of cadmium, lead and zinc by Siam weed *Chromolaena odorata L.* King & Robinson. *Chemosphere*, *68*(2), 323-329.

Visioli, G., & Marmiroli, N. (2013). The proteomics of heavy metal hyperaccumulation by plants. *Journal of Proteomics*, *79*(4), 133-145.

Xia, H. P., Shu, W. S. (2001). Resistance to and uptake of heavy metals by *Vetiveria zizanioides* and *Paspalum notatumfrom* lead/zinc mine tailings. *Acta Ecologica Sinica* (in Chinese), 21, 1121-1129.

Zhang, J. (2014). Selection of Copper Hyperaccumulators. Beijing: Beijing Forestry University.

Zhou, S. B., Wang, C. J., Yang, H. J., Bi, D., Li, J. H., & Wang, Y. (2007). Stress responses and bioaccumulation of heavy metals by *Zizania latifolia* and *Acorus calamus*. *Acta Ecologica Sinica* (in Chinese), *27*, 281-287.

Author´s institutional address

Zhiwen Luo

Ph.D. Candidate
Chongqing University
College of Resources and Environmental Science
Chongqing 400044, PR China
and Sichuan University of Sciences & Engineering
College of Chemistry and Environmental Engineering
Zigong 643000, PR China
Telephone: +86 (23) 6510 2421(O)
luoyanlizw@sina.com

Xingzhong Yuan

Ph.D. and Professor, Chongqing University
College of Resources and Environmental Science
Chongqing 400044, PR China
Telephone: +86 (23) 6510 2421(O)
3612074@qq.com

Xiangying Chen

Bachelor, Sichuan University of Sciences & Engineering
College of Chemistry and Environmental Engineering
Zigong 643000, PR China
Telephone: +86 (813) 5505 863(O)
380148523@qq.com

Xiaoxia Cui

Bachelor, Sichuan University of Sciences & Engineering
College of Chemistry and Environmental Engineering
Zigong 643000, PR China
Telephone: +86 (813) 5505 863(O)
475121522@qq.com

Haga clic aquí para escribir al autor

Daily streamflow simulation based on the improved machine learning method

• Guangyuan Kan* •
China Institute of Water Resources and Hydropower Research, China/Tsinghua University, China
*Corresponding author

• Xiaoyan He • Liuqian Ding • Jiren Li •
China Institute of Water Resources and Hydropower Research, China

• Yang Hong •
Tsinghua University, China/University of Oklahoma, USA

• Minglei Ren* • Tianjie Lei* •
China Institute of Water Resources and Hydropower Research, China
*Corresponding authors

• Ke Liang •
Hohai University, China

• Depeng Zuo •
Beijing Normal University, China

• Pengnian Huang •
Nanjing University of Information Sciences & Technology, China

Abstract

Kan, G., He, X., Ding, L., Li, J., Hong, Y., Ren, M., Lei, T., Liang, K., Zuo, D., & Huang, P. (March-April, 2017). Daily streamflow simulation based on the improved machine learning method. *Water Technology and Sciences* (in Spanish), *8*(2), 51-60.

Daily streamflow simulation has usually been implemented by conceptual or distributed hydrological models. Nowadays, hydrological data, which can be easily obtained from automatic measuring systems, are more than enough. Therefore, machine learning turns into an effective and popular tool which is highly suited for the streamflow simulation task. In this paper, we propose an improved machine learning method referred to as PKEK model based on the previously proposed NU-PEK model for the purpose of generating daily streamflow simulation results with better accuracy and stability. Comparison results between the PKEK model and the NU-PEK model indicated that the improved model has better accuracy and stability and has a bright application prospect for daily streamflow simulation tasks.

Keywords: Machine learning, daily streamflow simulation, hydrological model, flood forecasting, global optimization.

Resumen

Kan, G., He, X., Ding, L., Li, J., Hong, Y., Ren, M., Lei, T., Liang, K., Zuo, D., & Huang, P. (marzo-abril, 2017). Simulación de caudales diarios mediante el método de aprendizaje automático mejorado. Tecnología y Ciencias del Agua, *8(2), 51-60.*

La simulación de caudales diarios se ha implementado por lo general mediante modelos hidrológicos distribuidos o conceptuales. En la actualidad, los datos hidrológicos, que pueden obtenerse con facilidad de sistemas automáticos de medición, son más que suficientes. Por lo tanto, el aprendizaje automático (machine learning) *se ha convertido en una herramienta eficaz y popular, muy adecuada para la tarea de simulación de caudales. En este trabajo se propone un método de aprendizaje automático mejorado denominado modelo PKEK, basado en el modelo NU-PEK, previamente propuesto para generar resultados de simulación de flujo diario más precisos y estables. Los resultados de la comparación entre el modelo PKEK y el modelo NU-PEK indican que el modelo mejorado ofrece mayor exactitud y estabilidad, y tiene un excelente potencial de aplicación en la simulación de caudales diarios.*

Palabras clave: *aprendizaje automático, simulación de caudales diarios, modelo hidrológico, inundación, pronósticos de inundación, optimización global.*

Received: 14/05/2016
Approved: 22/09/2016

Introduction

With the development of hydrological automatic measuring technology, the hydrological data become more and more sufficient nowadays. The best way to make full use of these big hydrological data is to adopt the machine learning method. The most popular machine learning methods, which have been widely used in the field of hydrological simulation, are the artificial neural network (ANN) and K-nearest neighbor (KNN) method (Li *et al*., 2014; Chen *et al*., 2017; Dong *et al*., 2015; Kan *et al*., 2016a, 2016b, 2016c, 2016d, 2016e; Lei *et al*., 2016; Li *et al*., 2016; Zuo *et al*., 2016). In previous literatures, we proposed an effective and efficient machine learning based streamflow simulation model, NU-PEK model, which is constituted by coupling the ANN and KNN methods. It has been successfully applied in the field of event-based hourly streamflow simulation task. However, when applied to daily streamflow tasks, its performance becomes poor significantly.

In order to overcome the poor performance problem of the NU-PEK model for daily streamflow simulation task, we proposed an improved machine learning based streamflow simulation model, named PKEK. The PKEK model is composed by partial mutual information (PMI) based input variable selection (IVS) module, the K-means clustering input vector clustering module, the ensemble artificial neural network (ENN) based output estimation module, and the KNN based output error estimation module. The PKEK model and the previously proposed NU-PEK model were applied in Chengcun catchment in China to compare the model performance and stability. Simulation results indicated that the improved model has better accuracy and stability, and has a bright application prospect for daily streamflow simulation task.

Watershed, hydrological and meteorological data utilized in this research

The daily streamflow simulation is carried on in the Chengcun catchment. The Chengcun catchment lies in the Qiantang River basin, Anhui province, China. It is located in the subtropical monsoon region and is a typical humid catchment. Rainfall mainly falls in the period from April to June. There are ten rainfall gauges located in this area. Observed daily rainfall, evaporation, and average discharges range from 1986 to 1994 were utilized as the calibration data, while data from 1995 to 1999 were utilized as the validation data. The watershed map, hydrological and meteorological characteristics for the Chengcun catchment are shown in figure 1 and table 1.

Methodology

K-means clustering algorithm

The *K*-means clustering is a famous and widely used partitioning and clustering method (MATLAB, 2012; Grigorios & Aristidis, 2014; Kapageridis, 2015). It is a method of vector quantization, originally from signal processing, that is popular for cluster analysis in data mining. *K*-means clustering aims to partition *n* observations into *K* clusters in which each observation belongs to the cluster with the nearest mean, serving as a prototype of the cluster. The *K*-means method is usually calibrated or trained by the iterative method which minimizes the sum of distances from each object to its cluster centroid over all clusters.

PEK model

The PEK model is a hybrid data-driven model (Kan *et al*., 2015a, 2015b) and is composed by ensemble artificial neural network (ENN) and *K*-nearest neighbor (KNN) algorithm. The PEK approximator functions as a general purpose function approximator. It can be applied for the simulation of the multi-input single-output (MISO) system mapping relationship. The PEK approximator is firstly proposed by Kan *et al*. (2015a, 2015b) and its detailed principle can be found in the corresponding literatures (Kan *et al*., 2015a, 2015b).

• ISSN 2007-2422

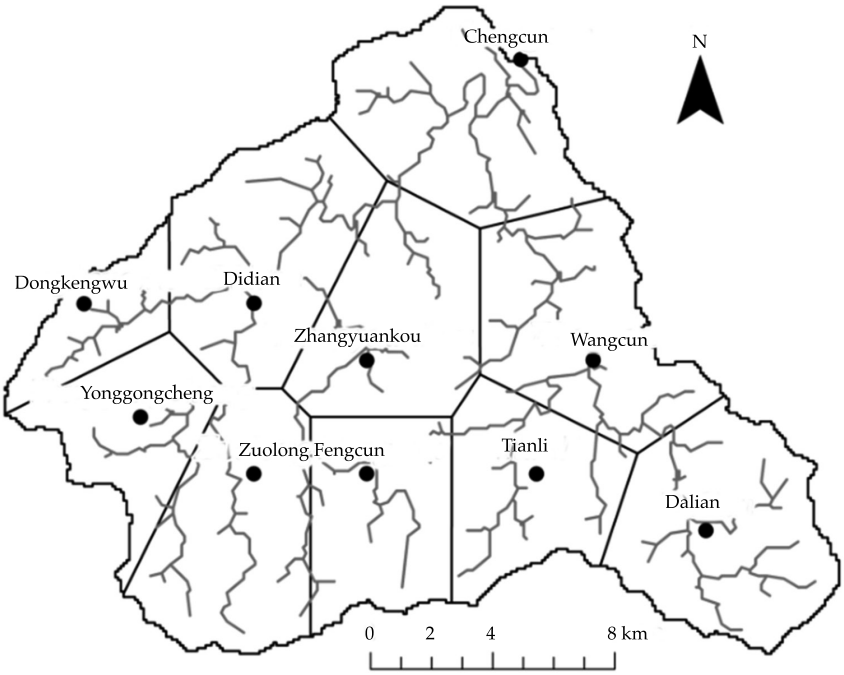

Figure 1. Watershed map for the Chengcun catchment.

Table 1. The hydrological and meteorological characteristics of the Chengcun catchment.

Area (km^2)	Annual mean rainfall (mm)	Annual mean evapotranspiration (mm)	Annual mean streamflow (m^3/s)
290	1 600	730.9	5 440.9

PKEK model

PKEK model is an improved version of the previously proposed PEK model. It is proposed for the purposed of improving the non-linear simulation capability of the PEK model. It is combined by the PMI-based input variable selection (IVS) module, the *K*-means clustering algorithm based input variable clustering module, and the ENN and KNN simulation module. The PKEK model can be seen as a hybrid approximator which composed by a *K*-means clustering module and multiple PEK modules. The simulation and calibration method of the PKEK model is as follows: The input variables are selected by the PMI-based separate IVS scheme to generate the selected input vectors. After that, each selected input vector is fed into the *K*-means clustering algorithm to determine which category it belongs to. After that, for each selected input vector, we choose a corresponding PEK module to calculate the output. In the PEK module, the output is estimated by the ENN, and the output error is estimated by the KNN regression. The final simulated output is the sum of the estimated output and output error. The calibration of the PKEK approximator is almost the same with the PEK approximator. The difference is that the *K*-means algorithm needs to be calibrated by an iterative method (Grigorios & Aristidis, 2014; Kapageridis, 2015).

ISSN 2007-2422 •

Non-updating RR simulation of the PKEK model

The non-updating modeling approach of the PKEK model is similar to the previously proposed NU-PEK model. The difference is the addition of the *K*-means clustering algorithm. The modeling approach of the PKEK model is as follows:

$$X_t^{(Q\_SIM)} = \left(Q_{t-1}^{(SIM)},\ Q_{t-2}^{(SIM)},\ \ldots,\ Q_{t-n_Q}^{(SIM)}\right)^T \quad (1)$$

$$X_t^{(SWCR)} = \left(SWCRs_t^{(1)},\ SWCRs_t^{(2)},\ldots,\ SWCRs_t^{(n_P)}\right)^T \quad (2)$$

$$X_t^{(S)} = \left(IVS_{Q\_SIM}\left(X_t^{(Q\_SIM)}\right),\ IVS_{SWCR}\left(X_t^{(SWCR)}\right)\right)^T \quad (3)$$

$$Q_t^{(EST)} = F_{EBPNN}\left[F_{K\text{-means}}\left(X_t^{(S)}\right)\right] \quad (4)$$

$$E_t^{(EST)} = F_{KNN}\left[Q_t^{(EST)}, F_{K\text{-means}}\left(X_t^{(S)}\right)\right] \quad (5)$$

$$Q_t^{(SIM)} = Q_t^{(EST)} + E_t^{(EST)} \quad (6)$$

where $X_t^{(Q\_SIM)}$ denotes the candidate simulated antecedent discharge (SAD) input vector; $X_t^{(SWCR)}$ denotes the candidate sliding window cumulative rainfall (SWCR) input vector; $Q_{t-1}^{(SIM)}$ denotes the SAD, i=1, 2, …, n_Q; $SWCRs_t^{(i)}$ denotes the SWCR with sliding window width i, i=1, 2, …, n_P; n_Q and n_P denote the order of the SAD and the SWCR respectively; IVS_{Q_SIM} denotes PMI-based IVS for candidate SAD input vector; IVS_{SWCR} denotes PMI-based IVS for candidate SWCR input vector; $X_t^{(S)}$ denotes the selected input vector; $Q_t^{(EST)}$ denotes the estimated output discharge associated with $X_t^{(S)}$; $E_t^{(EST)}$ denotes the estimated output discharge error associated with $X_t^{(S)}$; $Q_t^{(SIM)}$ denotes the simulated output discharge and it is the final prediction of the output discharge; F_{EBPNN} denotes the EBPNN discharge estimation; F_{KNN} denotes the KNN discharge error estimation; $F_{K\text{-means}}$ denotes the *K*-means clustering algorithm. The non-updating simulation procedure of the PKEK model for each flood event is almost the same with the NU-PEK model. The difference is that after the PMI-based separate IVS, the *K*-means clustering algorithm is executed to classify the input vector and fed it to different PEK module to calculate the forecasted discharge value.

Calibration of the PKEK model

The calibration of the PKEK model is almost the same with the NU-PEK model. The difference is the addition of the calibration of the *K*-means clustering method. The *K*-means algorithm is calibrated by the iterative method and this calibration process is repeated for 500 times with different initial parameters to avoid the local minimum problem. The optimal number of classes is determined by the Silhouette value. In this paper, approximately 70% of the flood events are utilized to create the calibration data and the remaining events are utilized to create the validation data.

Results and discussion

Model structure and parameter calibration

Input variable selection

Considered that we are studying the daily simulation, we set the order of SWCR and SAD (i.e. n_P and n_Q) equal to 10 and suppose 10 is large enough. This means that the rainfall will becomes runoff with a lag at most 10 days. After the IVS we have found that the lag time of most selected SADs are less than 10. Therefore, we

• ISSN 2007-2422

conform that the order of 10 is large enough to describe the mapping relationship between the rainfall and runoff data of the Chengcun catchment.

K-means clustering

We use the Silhouette value to optimize the best number of clusters. The Silhouette refers to a method of interpretation and validation of consistency with clusters of data. The technique provides a succinct graphical representation of how well each object lies within its cluster (Rousseeuw, 1987). The classification result show that the Silhouette value reaches the maximum value when the input samples are clustered into 3 clusters. Therefore, we divide the input sample into 3 clusters.

The PEK module

The PEK module are calibrated by the NSGA-II, LM, and cross-validation methods. The arithmetic parameters of the NSGA-II algorithm are set as: population size = 90, evolution generation total number =1000, crossover probability = 0.85, and mutation probability = 0.15. The arithmetic parameters of the LM method are set as suggested by the MATLAB software. As for the early stopping strategy, approximately 3/4 of the calibration data are utilized as the training set, and the remaining data are utilized as testing set. The maximum number of testing failures is set to 5. The lower and upper boundaries of K for the KNN algorithm are set to 1 and 300, and the K is optimized by the leave-one-out cross-validation method. Because we divide the input samples into 3 clusters, we construct a PEK module for each cluster for the PKEK model. The objective function used for the NSGA-II algorithm is mean squared error (MSE), mean squared value of the network parameters (MS), and hidden layer neuron number. The calibration results indicate that all the Pareto fronts distribute evenly which means that the optimization results is reasonable.

Model performance comparison

Scatter plots comparison

We use the scatter plots of the observed and simulated discharges and the regression R values to inspect the overall performance of the models. The scatter plots and the regression R values are demonstrated in figure 2.

As demonstrated in figure 2, as for the calibration period, the PKEK model obtains better result (R = 0.9634). The NU-PEK model obtains the worse result (R = 0.9539). It can be noticed that the data scatters of the PKEK model intensively lie close to the 45 degree line. The distribution of the data scatters of the PKEK model is relatively more uniform for small, middle, and large discharge values. These results indicate that the PKEK model generates the best result and obtains the most stable performance in the calibration period. As for the validation period, the PKEK model obtains the best result (R = 0.9296). The NU-PEK model obtains the worse result (R = 0.8912). As demonstrated in the figure 2, the data scatters of the PKEK model distributed normally around the 45 degree line. This result indicates that the simulation results of the PKEK model do not have bias to be larger or smaller and shows a very stable property. However, the simulated discharges of the NU-PEK model is larger than the observed values. This phenomenon becomes more obvious especially for large discharge values.

After analyzing the accuracy in calibration and validation period, the accuracy declination is also compared in this section. The PKEK model obtains better accuracy declination value (0.9296/0.9634 = 0.9649), and the NU-PEK model obtains worse accuracy declination value (0.8912/0.9539 = 0.9343). The comparison of accuracy declination value shows that although the PKEK model outperforms the original NU-PEK model and generates better forecasted results.

The analysis of the three models shows that the PKEK model can generate better overall

ISSN 2007-2422

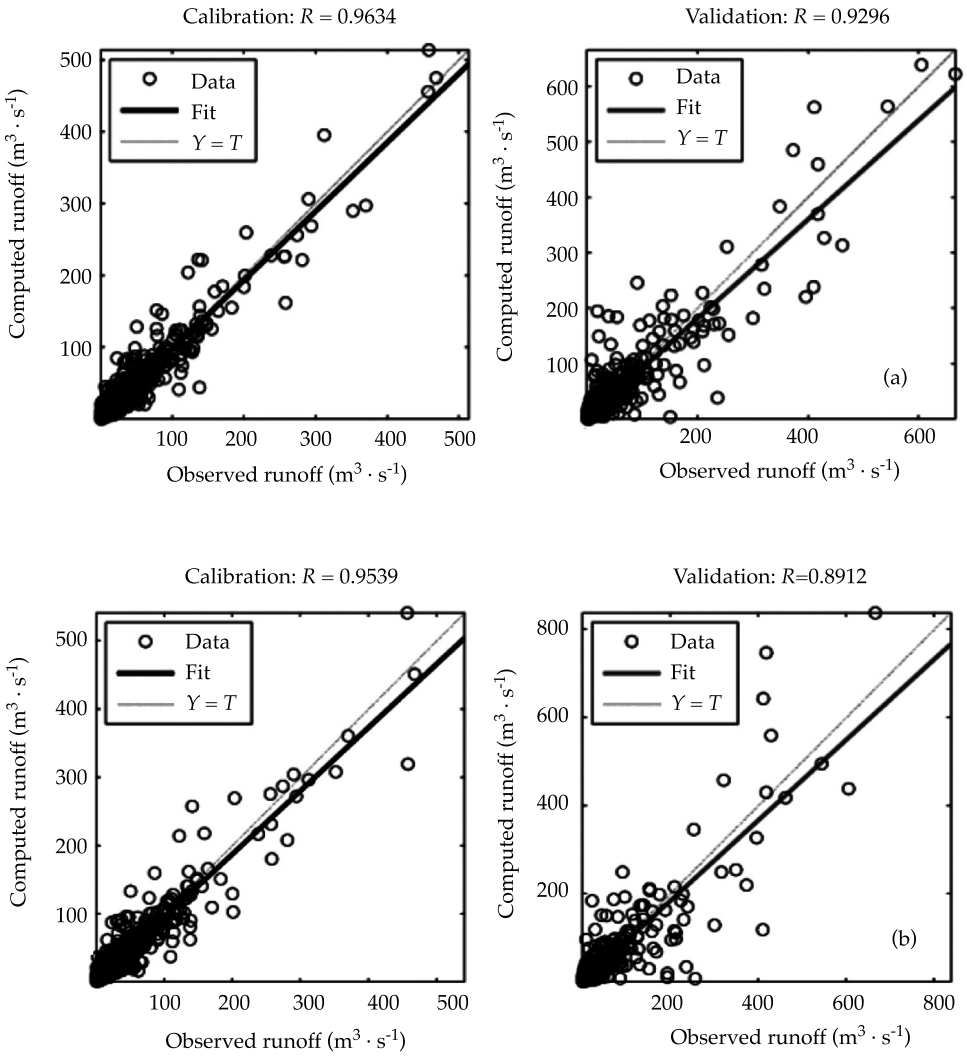

Figure 2. The scatter plots of the observed and simulated discharges and the regression *R* values: (A) PKEK model, (B) NU-PEK model.

results than the original NU-PEK model. As demonstrated in figure 2, for peak values, the PKEK model is much better than the NU-PEK model. The comparison results indicate that the PKEK model outperforms the NU-PEK model in Chengcun catchment and prove its satisfactory accuracy and stability.

Simulated hydrographs comparison

Figures 3 and 4 show the observed and simulated hydrographs in the calibration and validation period of the PKEK and NU-PEK models, respectively. Due to the space limitation, we only demonstrate two hydrographs for each model. They are year 1986 for calibration and year 1995 for validation, respectively. As shown in these figures, a further ascendency of the PKEK model is that the hydrographs simulated by the PKEK model are much smoother. The hydrographs simulated by the PKEK model are more consistent with the observed hydrographs. The improvement in hydrograph shape is owe to the inclusion of the SADs and is attributed to the

• ISSN 2007-2422

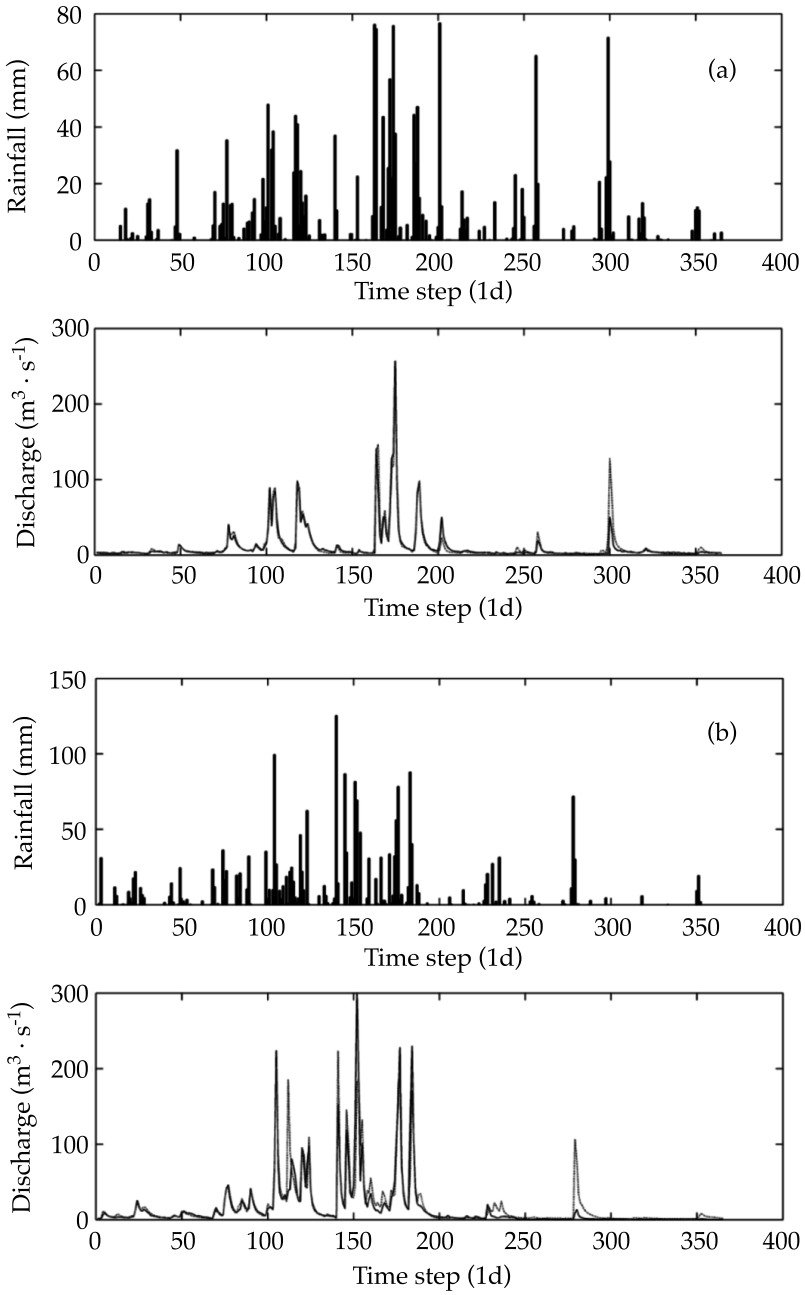

Figure 3. Observed and simulated hydrographs of the PKEK model: (a) Calibration; (b) Validation.

autoregressive characteristic of the ANN models. The ANN models place a higher weighting to the latest simulated discharge value utilized as inputs to the model. As a result, the model follows the general trend as prescribed by the simulated discharge.

Conclusions

An improved hybrid data-driven model, named PKEK, is proposed in this paper to overcome the disadvantages of the previously proposed NU-PEK model in daily RR simulation. For the

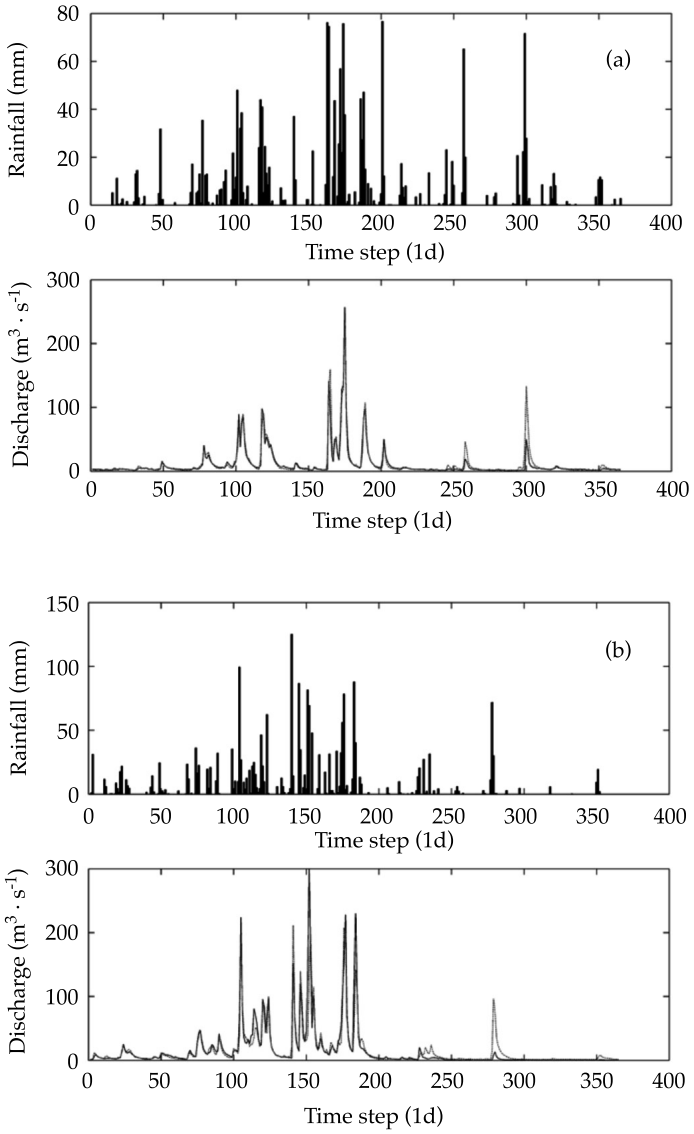

Figure 4. Observed and simulated hydrographs of the NU-PEK model: (a) Calibration; (b) Validation.

purpose of comparing performances of different models, the PKEK and NU-PEK models are applied to daily RR simulation in the Chengcun catchment. It can be remarked that the PKEK model is able to simulate generally much better runoff hydrograph than other models. From the application and analysis of the PKEK model, we can conclude that:

The PKEK model have all the advantages of the previously proposed NU-PEK model, including better calibration and validation non-updating simulation accuracy, automatic calibration without much impact from human experiences, good compromise between the sufficiency and parsimony of the input data, and good compromise between the simulation accuracy and topology complexity, and so on. Compared with the original NU-PEK model, the performance of the PKEK model becomes much better for the daily RR simulation. The improvement in the goodness-of-fit to the observed discharge of the PKEK model is

• ISSN 2007-2422

owed to the addition of the *K*-means clustering method combined with the utilization of multiple PEK modules. With the clustering method and multiple PEK modules, the PKEK model can simulate the characteristics of the RR relationship much precisely and it's forecasting capability and stability becomes better. Furthermore, the hydrographs simulated by the PKEK model are much smoother and more consistent with the observed hydrographs. The smoother performance of the PKEK model is attributed to the autoregressive nature of the ANN which allocates a higher weighting to the antecedent discharge inputs.

Acknowledgments

This research was funded by the IWHR Research & Development Support Program (JZ0145B052016), China Postdoctoral Science Foundation on Grant (Grant NO. 2016M600096, 2016M591214), Major International (Regional) Joint Research Project – China's Water and Food Security under Extreme Climate Change Impact: Risk Assessment and Resilience (G0305, 7141101024), International Project (71461010701), Study of distributed flood risk forecast model and technology based on multi-source data integration and hydro meteorological coupling system (2013CB036406), China National Flash Flood Disaster Prevention and Control Project (126301001000150068), Natural Science Foundation of China (41601569), Specific Research of China Institute of Water Resources and Hydropower Research (Grant Nos. Fangji 1240), and the Third Sub-Project: Flood Forecasting, Controlling and Flood Prevention Aided Software Development - Flood Control Early Warning Communication System and Flood Forecasting, Controlling and Flood Prevention Aided Software Development for Poyang Lake Area of Jiangxi Province (0628-136006104242, JZ0205A432013, SLXMB200902). We gratefully acknowledge the support of NVIDIA Corporation with the donation of the Tesla K40 GPU used for this research. Guangyuan Kan, Minglei Ren, and Tianjie Lei are the corresponding authors. Guangyuan Kan and Ke Liang contributed equally to this work. The author(s) declare(s) that there is no conflict of interest regarding the publication of this paper.

References

Chen, S., Kan, G., Liang, K., Li, J., Hong, Y., Zuo, D., Lei, T., Xu, W., Zhang, M., Shi, W., & Chen, X. (2017). Air quality analysis and forecast for environment and public health protection: a case study in Beijing, China. *Transylvanian Review*, *24*(12), 3575-3591.

Dong, J., Zheng, C., Kan, G., Wen, J., Zhao, M., & Yu, J. (2015). Applying the ensemble artificial neural network-based hybrid data-driven model to daily total load forecasting. *Neural Computing & Applications*, *26*(3), 603-611.

Grigorios, T., & Aristidis, L. (2014). The MinMax k-means clustering algorithm. *Pattern Recognition*, *47*(7), 2505-2516.

Kan, G., Yao, C., Li, Q., Li, Z., Yu, Z., Liu, Z., Ding, L., He, X., & Liang, K. (2015a). Improving event-based rainfall-runoff simulation using an ensemble artificial neural network based hybrid data-driven model. *Stochastic Environmental Research and Risk Assessment*. DOI: 10.1007/s00477-015-1040-6.

Kan, G., Li, J., Zhang, X., Ding, L., He, X., Liang, K., Jiang, X., Ren, M., Li, H., Wang, F., Zhang, Z., & Hu, Y. (2015b). A new hybrid data-driven model for event-based rainfall-runoff simulation. *Neural Computing & Applications*, *27*(2), DOI: 10.1007/s00521-016-2200-4.

Kan, G., He, X., Li, J., Ding, L., Zhang, D., Lei, T., Hong, Y., Liang, K., Zuo, D., Bao, Z., & Zhang, M. (2016a). A novel hybrid data-driven model for multi-input single-output system simulation. *Neural Computing & Applications*, DOI: 10.1007/s00521-016-2534-y.

Kan, G., Liang, K., Li, J., Ding, L., He, X., Hu, Y., & Mark, A. (2016b). Accelerating the SCE-UA global optimization method based on multi-core CPU and many-core GPU. *Advances in Meteorology*, 8483728, 10 pages. Recovered from http://dx.doi.org/10.1155/2016/8483728.

Kan, G., Lei, T., Liang, K., Li, J., Ding, L., He, X., Yu, H., Zhang, D., Zuo, D., Bao, Z., Mark, A., Hu, Y., & Zhang, M. (2016c). A multi-core CPU and many-core GPU based fast parallel shuffled complex evolution global optimization approach. *IEEE Transactions on Parallel and Distributed Systems*, DOI: 10.1109/TPDS.2016.2575822.

Kan, G., Zhang, M., Liang, K., Wang, H., Jiang, Y., Li, J., Ding, L., He, X., Hong, Y., Zuo, D., Bao, Z., & Li, C. (2016d). Improving water quantity simulation & forecasting to solve the energy-water-food nexus issue by using heterogeneous computing accelerated global optimization method. *Applied Energy*. Recovered from http://dx.doi.org/10.1016/j.apenergy.2016.08.017.

Kan, G., He, X., Ding, L., Li, J., Lei, T., Liang, K., & Hong, Y. (2016e). An improved hybrid data-driven model and its application in daily rainfall-runoff simulation. *IOP Conference Series: Earth and Environmental Science*, *46*(2016), 012029 (6th Digital Earth Summit), DOI: 10.1088/1755-1315/46/1/012029.

Kapageridis, I. K. (2015). Variable lag variography using K-means clustering. *Computers & Geosciences*, SI, B, 85, 49-63.

Lei, T., Pang, Z., Wang, X., Li, L., Fu, J., Kan, G., Zhang, X., Ding, L., Li, J., Huang, S., & Shao, C. (2016). Drought and

carbon cycling of grassland ecosystems under global change: A review. *Water*, 8, 460, DOI: 10.3390/w8100460.

Li, C., Cheng, X., Li, N., Du, X., Yu, Q., & Kan, G. (2016). A framework for flood risk analysis and benefit assessment of flood control measures in urban areas. *International Journal of Environmental Research and Public Health*, 13, 787, DOI: 10.3390/ijerph13080787.

Li, Z., Kan, G., Yao, C., Liu, Z., Li, Q., Yu, S. (2014). An improved neural network model and its application in hydrological simulation. *Journal of Hydrologic Engineering*, *19*(10), 04014019-1-04014019-17.

MATLAB (2012). *MATLAB documentation - user's manual, USA.*

Rousseeuw, P. J. (1987). Silhouettes: A graphical aid to the interpretation and validation of cluster analysis. *Computational and Applied Mathematics*, 20, 53-65.

Zuo, D., Cai, S., Xu, Z., Li, F., Sun, W., Yang, X., Kan, G., & Liu, P. (2016). Spatiotemporal patterns of drought at various time scales in Shandong Province of Eastern China. *Theoretical and Applied Climatology*, DOI: 10.1007/s00704-016-1969-5.

Author´s institutional address

Ph.D. Guangyuan Kan[#]

State Key Laboratory of Simulation and Regulation of Water Cycle in River Basin
China Institute of Water Resources and Hydropower Research
Research Center on Flood & Drought Disaster Reduction of the Ministry of Water Resources
Beijing 100038, PR China

Tsinghua University
Department of Hydraulic Engineering

State Key Laboratory of Hydroscience and Engineering
Beijing, 100084, PR China
No. 3 Yuyuantan South Road, Haidian district,
Beijing, PR China
Telephone: +86 13718606623
kanguangyuan@126.com
[#]Authors Guangyuan Kan and Ke Liang contributed equally to this work.

Prof. Xiaoyan He
Prof. Liuqian Ding
Prof. Jiren Li
Ph.D. Minglei Ren
Ph.D. Tianjie Lei

State Key Laboratory of Simulation and Regulation of Water Cycle in River Basin
China Institute of Water Resources and Hydropower Research
Research Center on Flood & Drought Disaster Reduction of the Ministry of Water Resources
Beijing 100038, PR China
No. 3 Yuyuantan South Road, Haidian district,
Beijing, PR China
68781991
68781956
68781593
68781798
Telephone: +86 15120098723
hexy@iwhr.com
dinglq@iwhr.com
ljrrsc@163.com
renml@iwhr.com
leitj@iwhr.com

Prof. Yang Hong

Tsinghua University
Department of Hydraulic Engineering State Key Laboratory of Hydroscience and Engineering
Beijing, 100084, PR China

University of Oklahoma
Department of Civil Engineering and Environmental Science
Norman, OK, United States
Tsinghua University, Haidian district
Beijing, PR China
68787394
hongyang@tsinghua.edu.cn

M.S. Ke Liang[#]

Hohai University
College of Hydrology and Water Resources
Nanjing 210098, PR China
No. 1 Xikang Road, Gulou District, Nanjing
Jiangsu Province, PR China
Telephone: +86 15295500581
liangkepapers@126.com
[#]Authors Guangyuan Kan and Ke Liang contributed equally to this work

Ph.D. Depeng Zuo

Beijing Normal University
College of Water Sciences
Beijing 100875, PR China
No. 19 Xinjiekouwai Street, Haidian District
Beijing, PR China
58801136
dpzuo@bnu.edu.cn

Ph.D. Pengnian Huang

Nanjing University of Information Sciences & Technology
College of Hydrometeorology
Nanjing, 210044, PR China
No. 219 Liuning Road, Nanjing,
Jiangsu Province, PR China
15951990472
002752@nuist.edu.cn

Reactivation of hypersaline aerobic granular sludge after low-temperature storage

• Yao Chen* •
University, Chongqing, China/ Cooperative Research Centres for Water Sensitive Cities and Monash University, Australia
*Corresponding author

• Jia-Yue Zhu • Yu Qin • Zhi-Min Zhang • Shao-Chun Yuan •
University, Chongqing, China

Abstract

Chen, Y., Zhu, J. Y., Qin, Y., Zhang, Z. M., & Yuan, S. C. (March-April, 2017). Reactivation of hypersaline aerobic granular sludge after low-temperature storage. *Water Technology and Sciences* (in Spanish), *8*(2), 61-70.

Reactivation of hypersaline aerobic granular sludge after low-temperature storage was studied by slowly increasing the organic loading. Results indicated that the basic external features of thawed hypersaline aerobic granules were still largely intact after a six-week low temperature storage, but the colors and internal structure changed greatly. Aerobic granules experienced a process of particle disintegration, fragmentary particles, filamentous bacteria-like particles, and dense granules during the recovery process. After more than one-month re-cultivation, the settling property, dehydrogenase activity, and nitrification properties of hypersaline aerobic granules returned to normal. During the re-cultivated process, the decentralized growth pattern of particles can be effectively controlled, and granules can grow compactly by controlling water alkalinity, aeration rate and reactor settling time.

Keywords: Hypersaline, aerobic granular sludge, filamentous bacteria, reactivation.

Resumen

Chen, Y., Zhu, J. Y., Qin, Y., Zhang, Z. M., & Yuan, S. C. (marzo-abril, 2017). Reactivación de lodo granular aerobio hipersalino después de almacenamiento a baja temperatura. Tecnología y Ciencias del Agua, 8*(2), 61-70.*

Se estudió la reactivación de lodo granular aerobio hipersalino después de su almacenamiento a baja temperatura, mediante el incremento progresivo de la carga orgánica. Los resultados indicaron que las características externas básicas de los gránulos aerobios hipersalinos descongelados permanecieron prácticamente intactas después de su almacenamiento a baja temperatura durante seis semanas, pero el color y las características de la estructura interna habían cambiado de modo significativo. Los gránulos aerobios presentaron desintegración y fragmentación de partículas, partículas parecidas a bacterias filamentosas y gránulos densos durante el proceso de recuperación. Después de más de un mes de recultivo, la propiedad de asentamiento, la actividad de la deshidrogenasa y las propiedades de nitrificación de los gránulos aerobios hipersalinos regresaron a la normalidad. Durante el proceso de recultivo, el patrón de crecimiento descentralizado de las partículas puede controlarse de manera eficaz y los gránulos pueden crecer en forma compacta mediante el control de la alcalinidad del agua, del índice de aireación y del tiempo de asentamiento en el reactor.

***Palabras clave**: lodo granular aerobio hipersalino, bacterias filamentosas, reactivación.*

Received: 20/05/2016
Approved: 22/09/2016

Introduction

Aerobic granular sludge, a special biofilm, is spontaneously formed of self-immobilization of microorganisms (De Kreuk, Pronk, & Van Loosdrecht, 2005; Adav, Lee, Show, & Tay, 2008). It has many incomparable advantages towards common activated sludge, such as: compact structure, good settling property, big biomass, microbial metabolism diversification, high activity and high resistance to toxicity and organic loading (Adav, Lee, Show, & Tay, 2008; Morales, Figueroa, Mosquera-Corral, Campos, & Méndez, 2012; Zhao, Huang, Zhao, & Yang,

2013). Therefore, it has been widely applied to the treatment of industrial wastewater (Adav, Lee, Show, & Tay, 2008; Moussavi, Barikbin, & Mahmoudi, 2010; Taheria, Khiadani, Amina, Nikaeen, & Hassanzadeh, 2012; Rosman, Anuar, Chelliapan, Md Din, & Ujang, 2014). However, during the reactor operating, there is idle frequently in aerobic granular sludge system because of accidents or other causes, and then granules will lose activity easily during long-term idle process. Thus it has a great significance to study the storage and activity recovery of aerobic granular sludge in its engineering application. In particular, the success development of storing aerobic granular sludge can extend application of aerobic granules as inoculums for rapid startup, and as microbial supplement to enhance treatment of bioreactor systems. There are reports on the reactivation of aerobic granular sludge and results have showed that aerobic granular sludge has a good stability and resiliency after the thawed granules have to be recovered successfully, and the activity of revived sludge can even return to the level of original state (Adav, Lee, & Tay, 2007; Lee, Chen, Show, Whiteley, & Tay, 2010; Gao, Yuan, & Liang, 2012; Lv *et al.*, 2013). However, to the authors' knowledge, there are no reports concerning the reactivation of aerobic granules after thawing under high salt stress.

In order to solve the problem mentioned above, high salt aerobic granules, which were cultivated successfully in laboratory scale column-type sequencing batch reactor (SBR) operating with synthesis saline wastewater (the NaCl content of 3%, calculated as weight to volume) in previous study, was took out to be washed by distilled water several times to remove the substrate on the surface of the granules, and then transferred into the polypropylene plastic bottles and kept in storage at 4 °C. After six-week storage in low temperature, the thawed aerobic granules were re-cultivated by controlling the organic loading to investigate the reactivation process of granules in this study. The aim of this study was expected to provide theoretical support for aerobic granular sludge as a novel technique for the biological treatment of saline wastewater in practical engineering.

Materials and methods

Reactor set-up

The column-type SBR reactor used in this study was made of Plexiglas (internal diameter of 4.8 cm, high of 105 cm and H/D ratio was 22) giving an operation volume of 1.9 L. Bottom aeration of the reactor was supplied by air pump, and the aeration rate was controlled to meet different level of dissolved oxygen (DO) in different experimental period. The reactor was operating for 12 h per cycle at a volumetric exchange ratio of 50%, included 2 min influent (via the reactor top), 3 min discharge, aeration and sedimentation for the remaining time, in which, the time of aeration and sedimentation should be adjusted to operating condition.

The reactor controlled the temperature needed in different reactivation of aerobic granular sludge by a heater, and a programmable logic controller was used to actuate and control the pump, heater, and the operating cycle. Inoculated sludge was provided from hypersaline aerobic granules (Chen, Yang, & Yu, 2013) in previous study, which were formatted from flocculent sludge in SBR reactors after more than two-month culture under high salt content of 3%. Detailed information about the characteristics of aerobic granules in this study is shown in table 1.

Synthetic substrate

In this test, each column was dosed with simulated wastewater, the compositions of which fed to the reactor were as follows: 3% of salt content, 849-4245 mg of glucose (900-4500 mg l^{-1} as chemical oxygen demand (COD) basis), 21.9-109.6 mg of KH_2PO_4 (5-25 mg l^{-1} as PO_4^{3-}-P basis), 171.7-858.8 mg of NH_4Cl (45-225 mg l^{-1} as NH_4^+-N basis), 266.7-1333.3 mg of $MgSO_4 \cdot 7H_2O$ (26-130 mg l^{-1} as Mg basis), 55.4-277 mg of $CaCl_2$

Tecnología y Ciencias del Agua, vol. VIII, núm. 2, marzo-abril de 2017, pp. 61-70
• ISSN 2007-2422

Table 1. Characteristics of hypersaline aerobic granules before storage.

Parameters	Index
Appearance	Deep yellow, smooth
Salt stress content (%)	3.0
Average particle diameter (mm)	0.89
Sludge volume index (SVI) (ml g^{-1})	30.23
Minimum settling velocity (MSV) (m h^{-1})	4.79
Dehydrogenase activity (DHA) (ugTF g^{-1}SS h^{-1})	39.27

(20-100 mg l^{-1} as Ca basis) and 0.1 ml of trace elements solution (Kishida, Kim, Tsuneda, & Sudo, 2006).

Experiments

The granules, which had been stored under a low temperature without DO and nutrients for 6 weeks, were taken out from the refrigerator to thaw in a temperature controlled at 15±0.5 °C. The microbes of the granular sludge were basically in a dormant state with low activity, and therefore, it was inappropriate for the granules to recover directly under a high loading. The influent substrate concentration was raised gradually by controlling COD/N ratio (20:1) to slowly increase the organic loading, and the DO level and temperature were improved accordingly to control the reactor operating in different phases. Detailed information about the SBR operation is shown in table 2.

Analytical methods

Dehydrogenase activity (DHA) of granular sludge was measured by 2, 3, 5-triphenyltetrazolium chloride (TTC) reduction method. The particle size distribution was analyzed according to Sauter formula as noted by Zhang *et al*. (2006). DO concentration in the bulk liquor was measured with a DO meter (HQ40d, HACH, USA). pH was determined by a pH meter (SENSION2, HACH, USA). MSV, SVI and NH_4^+-N were measured according to the standard methods (APHA, 2005).

Results and discussion

Appearance characteristics

Before low temperature storage, the average diameter and dispersion of hypersaline aerobic granules were 0.89 mm and 0.377 respectively. The deep yellow granules with homogeneous particles and smooth surface contained few fragmentary sludge or small particles, as showed in figure 1a. The apparent structure of granules basically remained an initial shape after storage, while the colors had turned to gray white or light yellow. Meanwhile, it was found that the granules were becoming to be loose by microscopy. When the reactor started up, the loose granules broke up constantly, and the break-up granules deteriorated into small pieces

Table 2. Operational parameters of the aerobic granular sludge reactor.

Phase	I	II	III	IV	V
Length of operation (cycles)	1-13	14-27	28-41	42-51	52-70
Organic loading (kg COD m^{-3} d^{-1})	0.90	1.12	1.50	2.25	4.50
DO (mg l^{-1})	4-5	4-5	5-6	5-6	5-6
Temperature (°C)	20±0.5	20±0.5	20±0.5	25±0.5	25±0.5

ISSN 2007-2422

to flow out with the upflow air stream. Meanwhile, it was even found that some fragmentary particles appeared, on which a large number of breeding filamentous bacteria were observed. With the running of reactor, small particles and fragmentary sludge were disappearing constantly, and then, overgrowth of filamentous bacteria on granules was effectively controlled. At the end of experiment (the 70th cycle), the loose surface of granules developed to smooth, with a little compact structure and the color recovered to yellow (figure 1b). Average particle size reached up to 0.99 mm and dispersion was only 0.376, which also indicated that revived aerobic granulation had a relative symmetrical particle distribution. Results show that granules experienced a process of particle disintegration, fragmentary particles, filamentous bacteria-like particles, and dense granules during more than one month recovery, and finally appearance of granular sludge recovered to initial characteristics before stored. During the re-cultivation, microbes of granules grew up rapidly, resulting in an increase of particles size.

Settling property

SVI is an index to measure the sedimentation performance of activated sludge, which can reflect the loose structure and the coagulation performance. Changes in parameters such as SVI and MSV for various operating phase are shown in figure 2.

As presented in figure 2, within 27 cycles after the reactor was in operation and begun to aerate, eventual fragmented sludge appeared in the reactor and settling property of granules deteriorated. The profile of SVI showed a rising trend during the operation phase I and II, which indicated the SVI reached up to the maximum of 95.21 ml g^{-1} and MSV fell down to the minimum of 0.26 m h^{-1} at the 27th cycle. Microscopic analysis revealed that massive filamentous bacteria multiplied surrounding the granules. In order to prevent the situation on a further deterioration, some strategies, such as improving influent organic loading, increasing the water alkalinity and aeration rate, and shortening reactor settling time and so on, were adopted to inhibit overgrowth of filamentous bacteria on granules and improve settling performance after operation phase II. Research showed that settling property was gradually taking a favorable turn after filamentous bacteria separated form granules and subsequently washed out with effluent form the reactor, and sludge bulking can be controlled effectively. Influent organic loading and temperature of reactor improved after operation cycle 41, with the result that sludge morphology changed with smooth

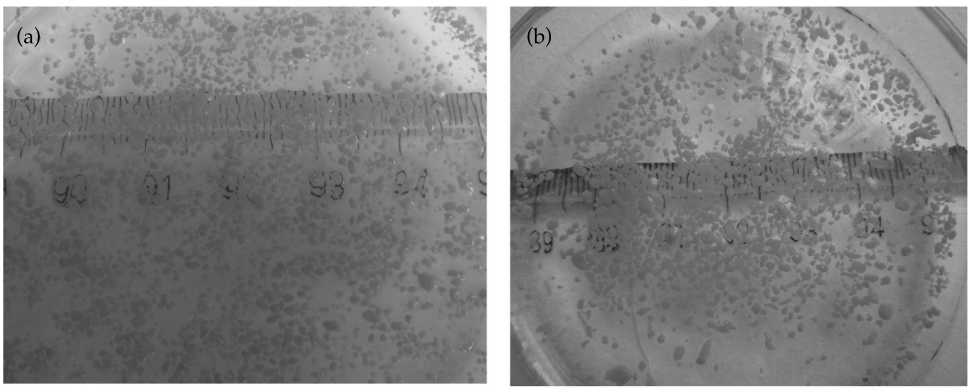

Figure 1. Appearance characteristic of hypersaline aerobic granular sludge before/after storage (a: before storage; b: after storage).

• ISSN 2007-2422

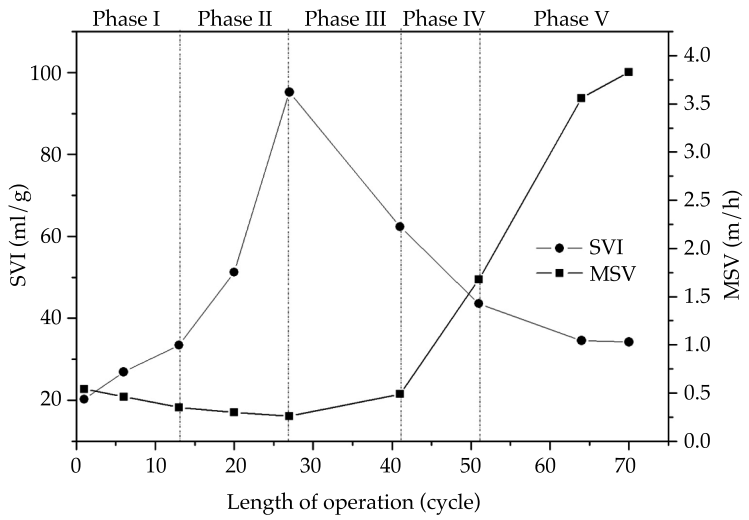

Figure 2. Variation of MSV and SVI during reactivation (organic loading of Phase I, II, III, IV and V is 0.90, 1.12, 1.50, 2.25 and 4.50 kg COD m^{-3} d^{-1}, respectively).

surface, settling property improved and small size granules declined continuously. When organic loading of reactor reached 4.50 kgCOD m^{-3} d^{-1}, the loading level of reactor operating before storage, the SVI and MSV was stable around 34 ml g^{-1} and 3.83 m h^{-1} respectively. It is considered that the settling performance of the thawed granules have recovered to the initial level before low temperature storage.

Experimental results show that activity of microorganism inner the thawed granules, especially activity of filamentous bacteria binding and connecting zoogloea bacteria in sludge during granulation was inhibited, caused by the short of nutrient substrate and DO in six-week-idle period. It was found that granular sludge morphology was on a loose structure and simultaneously a large number of fragmented microbe matrix appeared. With the running of SBR, aerobic granular sludge gradually disintegrated to floc sludge and then massive light and bulky granules were discharged form reactor on the selective pressure aeration shear and organic loading. Thereby, the settling property of granules in reactor performed an endlessly deteriorating trend. Although microbes in granules can grow rapidly with the improvement of organic loading (Wang, Zhang, & Wu, 2009), which indicates that formation of aerobic granule is a substrate loading rate-dependent process (Lee, Chen, Show, Whiteley, & Tay, 2010; Liu, Tay, & Liu, 2003), settling property had not been ameliorated with increasing organic loading to 1.12 kg COD m^{-3} d^{-1} after operation cycle 13. From the changes of sludge morphology, it was analyzed that the DO concentration in reactor seemed to be sufficiently high (reached 4 to 5 mg l^{-1}), but DO can't diffuse into the granules for it to be available to the bacteria located within the granule, easily resulting in a relative low DO concentration gradient and deficiency oxygen in granules, which can promote dominant filamentous growth in aerobic granular sludge SBR (Gaval & Pernell, 2003). Evidence shows that low-levels and moderate-levels of filamentous bacteria growth do not cause operational problems and may even stabilize the granule structure (Liu & Liu, 2006). However, overgrowth of filamentous bacteria as dominant microorganism in granular sludge was unwanted as it even led to eventual disintegration of aerobic granules. Therefore, results show

ISSN 2007-2422

that low diffusion of DO in aerobic granule is unfavorable to formation and stability of aerobic granules. In addition, rise of influent ammonium nitrogen (NH_4^+-N) concentration can also lead loose morphology and overgrowth of filamentous bacteria located on the outer layer of the granules (Liu & Liu, 2006; Liu, Yang, Pu, Liu, & Lan, 2009). When filamentous bacteria in/on granules became as dominant microbes in SBR, particles had presented in a decentralized growth pattern, dominated by filamentous inter-twine mode (Liu, Liu, & Tay, 2004; Wang, Li, & Wang, 2008). Unfortunately, there were short of sufficient extracellular polymeric substances (EPS), metabolic products accumulating on the surface of bacterial cells and bridging bacterial cells and other particulate matter into an aggregate (Adav, Lee, Show, & Tay, 2008; Liu, Liu, & Tay, 2004), to strengthen microbial structure, which can lead to granules disintegrated easily and then induced filamentous bulking (Chen, Yang, & Yu, 2013). Therefore, overcoming the occurrence of filamentous growth induced by a low DO level and increasing influent ammonia, some effective strategies had been adopted in this study, such as properly adding influent water alkalinity with $NaHCO_3$ to adapt initial pH value of 8.0±0.5, increasing aeration rate, shortening settling time and others, and then decentralized growth pattern of granules was availably controlled in the following operation phase. It was explained that increasing alkalinity of reaction system can contribute to the growth of non-filamentous bacteria on pH value of 8.0±0.5, and the propagation of zoogloea bacteria on a high DO level condition resulted in a competitive relationship with filamentous, which can inhibit the growth of filamentous. Moreover, filamentous bacteria breeding on granules was gradually cut off with the high upflow liquid stream, and then washed out on a short settling time of reactor. Furthermore, enhancing shear force of reaction system and shortening settling time can also improve cellular surface hydrophobicity of zoogloea bacteria and microbial activity, and promote cell to secrete more EPS content, which can facilitate cell-to-cell adhesion and strengthen microbial structure through polymeric matrices (Lee, Chen, Show, Whiteley, & Tay, 2010; Tay, Liu, & Liu, 2001; Liu & Tay, 2004). Whereas residuary filamentous in granules would enter inside to bind and connect with zoogloea bacteria, high density and good settling property granular sludge was thus formed.

DHA

Figure 3 shows the variation of DHA of granules during the whole reactivation process. The thawed granules had low activity after experiencing a low temperature idle phase, and DHA was low to 5.42 ugTF g^{-1}SS h^{-1}, only 1/8 of activity before storage. Heterotrophs in granules were prone to endogenous respiration and intracellular hydrolysis being short of DO and nutrients at cryogenic temperatures, which can explain why microbes in granular sludge lost growth activity during storing. With the running of reactor, zoogloea and filamentous bacteria in granules were in the condition of adequate nutrients and DO, and then activity of aerobic granules restored gradually. On cycle 27, DHA reached up to the maximum of 48.9 ugTF g^{-1}SS h^{-1}, exceeding the initial level, whereas settling property of granules dropped to the lowest level and dehydrogenase activity reached to the maximum, causing by overgrowth of massive filamentous bacteria on granules as dominant microbes. When some related measures were adopted to control overgrowth of filamentous, granular activity gradually decreased and stabilized at about 38 ugTF g^{-1}SS h^{-1}. Result indicates that activity of hypersaline granular sludge had recovered basically after more than one-month re-cultivated.

Nitrification characteristic

Hypersaline aerobic granules before storage have good nitrification property, and removal efficiency of NH_4^+-N is up to 81.8% at 225 mg l^{-1} of influent concentration. Change in the removal efficiency for NH_4^+-N by re-cultured thawed granules after cryogenic storage during reactivation is showed in figure 4.

• ISSN 2007-2422

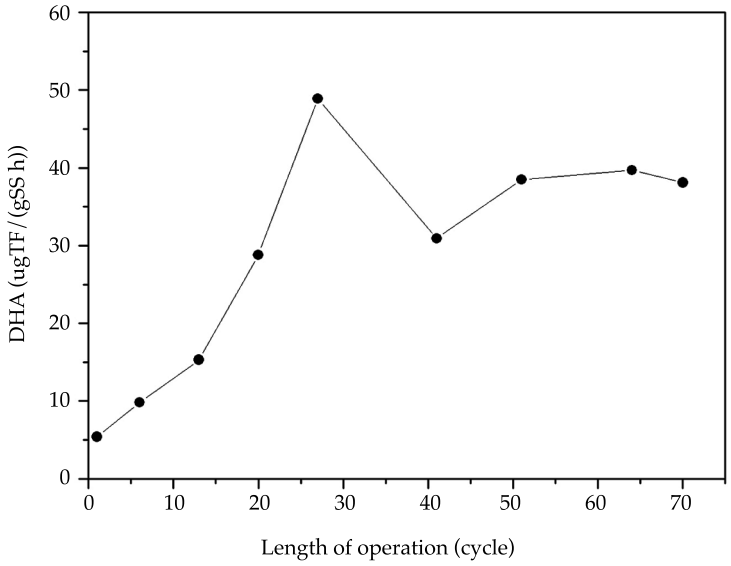

Figure 3. Variation of dehydrogenase activity (DHA) during reactivation.

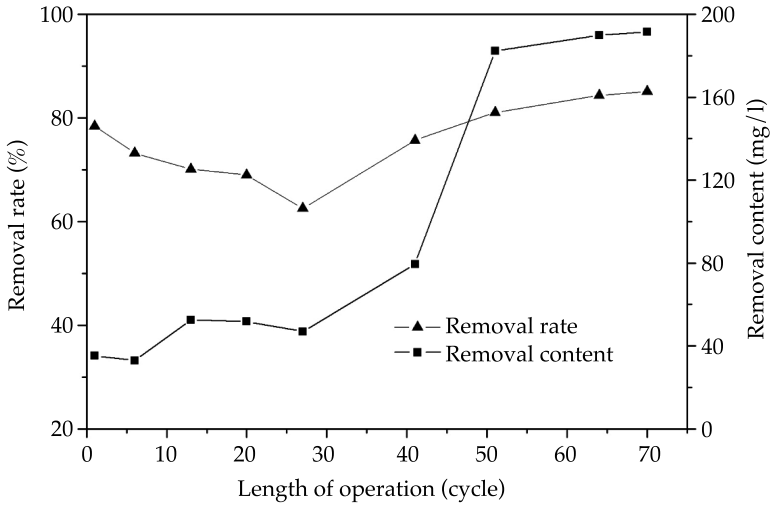

Figure 4. Variation of ammonia (NH_4^+-N) removal during reactivation.

During the initial recovery operation period (phase I), granules experiencing low temperature storage still presented in a good nitrification characteristics, and removal efficiency of NH_4^+-N can reach to 78% at 45 mg l^{-1} of influent concentration. It was analyzed that nitrifying bacteria, which were autotrophic microbes, were less affected by the lack of nutrients during storing. Once the temperature and DO of reactor were appropriate, growth activity of nitrifying bacteria can be recovered quickly. However, with reactivation continuing, nitrifying characteristic

decreased a little, which can be explained by the fact that sufficient substrate concentration promoted microbial energy metabolism process to recover growth activity of heterotrophs with the increase of organic loading. It should be indicated in particular that filamentous gradually become dominant bacteria during recovery, resulting in growth of nitrifiers restrained eventually. Meanwhile, nitrifying bacteria were washed out of the system with broken granules because of the deterioration of granules settling performance, and then resulted in the decrease of NH_4^+-N removal rate gradually. The removal efficiency of NH_4^+-N decreased to the lowest, only 62.58%, when influent ammonia nitrogen concentration was 75 mg l^{-1}. With filamentous bacteria effectively controlled, particle size of aerobic granules increased and compacted gradually with nitrifiers constantly fixing in all parts of the granule interior, and finally resulted in presenting different metabolic function of aerobic granules and forming a distinctive structural features. Thereafter, removal efficiency of NH_4^+-N increased constantly with the continued increase of influent organic and ammonia nitrogen loading. On cycle 64, removal rate of NH_4^+-N reached to 84.35%, and this time aerobic granules in SBR had reached the treating loading before storage. The final ammonia removal rate was stable at about 85% at 225 mg l^{-1} of influent concentration. Result demonstrates that nitrifying property of hypersaline aerobic granules has been recovered.

Conclusions

The apparent structure of granules basically remained an initial shape after storage, while the colors had turn to gray white or light yellow and structure had translated to loose. The stored aerobic granules experienced a process of particle disintegration, fragmentary particles, filamentous bacteria-like particles, and dense granules during more than one month recovery, and finally developed smooth and compact granules during reactivation. Meanwhile, settling performance of granules experienced a process of expansion and recovery. Some effective strategies had been adopted in this study, such as properly adding influent water alkalinity, increasing aeration rate, shortening settling time and others, and then decentralized growth pattern of granules was availably controlled in the following operation phase, resulting in the recovery of settling property of granules. SVI was finally stable at 34 mg l^{-1} and MSV was high to 3.83 m h^{-1}. Experiencing more than one-month re-cultivated, activity of hypersaline aerobic granules were completely recovered. DHA of stored granules was relatively low and only 1/8 of initial level, while nitrifying characteristic can resume in a short time. After one-week operation, DHA gradually improved to the maximum of 48.9 ugTF g^{-1}SS h^{-1} with the dispersive growth of granules, whereas nitrifying bacteria were continuously washed out from the system due to sludge bulking, resulting in a gradual drop of nitrification performance. When filamentous was controlled effectively during the following re-cultivated, nitrifying bacteria bred to strength the nitrification characteristic to a certain extent, and removal rate of NH_4^+-N was finally stable at about 85%. At the same time, DHA declined a little and maintained around 38 ugTF g^{-1}SS h^{-1}.

Acknowledgment

The research was supported by Scientifical & Technological Research Project of Chongqing Education Commission (No. KJ110403), Research Plan of National Engineering Research Center for Inland Waterway Regulation (No. NERC2014B06) and Chinese Scholarship Council (CSC) (Grant No. 201508505098).

References

Adav, S. S., Lee, D. J., & Tay, J. H. (2007). Activity and structure of stored aerobic granules. *Environ. Technol.*, 28, 1227-1235.

Adav, S. S., Lee, D. J., Show, K. Y., & Tay, J. H. (2008). Aerobic granular sludge: Recent advances. *Biotech. Adv.*, *26*(5), 411-423.

APHA (2005). *Standard methods for the examination of water and wastewater* (21st ed.). Washington, DC: American Public Health Association.

Chen, Y., Yang, B. L., & Yu, G. (2013). Granulation process and mechanism of hypersaline aerobic granular sludge. *China Water & Wastewater*, *29*(23), 8-13.

De Kreuk, M. K., Pronk, M., & Van Loosdrecht, M. C. M. (2005). Formation of aerobic granules and conversion processes in an aerobic granular sludge reactor at moderate and low temperatures. *Water Res*., 39, 4476-4484.

Gao, D. W., Yuan, X. J., & Liang, H. (2012). Reactivation performance of aerobic granules under different storage strategies. *Water Res*., 46, 3315-3322.

Gaval, G., & Pernell, J. J. (2003). Impact of the repetition of oxygen deficiencies on the filamentous bacteria proliferation in activated sludge. *Water Res*., 37, 1991-2000.

Kishida, N., Kim, J., Tsuneda, S., & Sudo, R. (2006). Anaerobic/oxic/anoxic granular sludge process as an effective nutrient removal process utilizing denitrifying polyphosphate-accumulating organisms. *Water Res*., *40*(12), 2303-2310.

Lee, D. J., Chen, Y. Y., Show, K. Y., Whiteley, C. G., & Tay, J. H. (2010). Advances in aerobic granule formation and granule stability in the course of storage and reactor operation. *Biotech. Adv*., 28, 919-934.

Liu, Q. S., Tay, J. H., & Liu, Y. (2003). Substrate concentration-independent aerobic granulation in sequential aerobic sludge blanket reactor. *Environ. Technol*., 24, 1235-1242.

Liu, Y. Q., Liu, Y., & Tay, J. H. (2004). The effects of extracellular polymeric substances on the formation and stability of biogranules. *Appl. Microbiol. Biotechnol*., 65, 143-148.

Liu, Y., & Tay, J. H. (2004). State of the art of biogranulation technology for wastewater treatment. *Biotechnol. Adv*., *22*(7), 533-563.

Liu, Y., & Liu, Q. S. (2006). Causes and control of filamentous growth in aerobic granular sludge sequencing batch reactors. *Biotech. Adv*., 24, 115-127.

Liu, H. B., Yang, C. Z., Pu, W. H., Liu, Y. S., & Lan, D. (2009). Effect of ammonia concentration on the characteristic of aerobic granular sludge. *Environmental Science*, *30*(7), 2030-2034.

Lv, Y., Wan, C. L., Liu, X., Zhang, Y., Lee, D. J., & Tay, J. H. (2013). Freezing of aerobic granules for storage and subsequent recovery. *J. Taiwan Inst. Chem. E*., *44*(5), 770-773.

Morales, N., Figueroa, M., Mosquera-Corral, A., Campos, J. L., & Méndez, R. (2012). Aerobic granular-type biomass development in a continuous stirred tank reactor. *Sep. Purif. Technol*., *89*(3), 199-205.

Moussavi, G., Barikbin, B., & Mahmoudi, M. (2010). The removal of high concentrations of phenol from saline wastewater using aerobic granular SBR. *Chem. Eng. J*., *158*(3), 498-504.

Rosman, N. H., Anuar, A. N., Chelliapan, S., Md Din, M. F., & Ujang, Z. (2014). Characteristics and performance of aerobic granular sludge treating rubber wastewater at different hydraulic retention time. *Bioresource Technol*., 161, 155-161.

Taheria, E., Khiadani, M. H., Amina, M. M., Nikaeen, M., & Hassanzadeh, A. (2012). Treatment of saline wastewater by a sequencing batch reactor with emphasis on aerobic granule formation. *Bioresource Technol*., 111, 21-26.

Tay, J. H., Liu, Q. S., & Liu, Y. (2001). The effects of shear force on the formation, structure and metabolism of aerobic granules. *Appl. Microbiol. Biot*., *57*(1-2), 27-33.

Wang, Y. D., Li, Z. H., & Wang, X. C. (2008). Growth model of aerobic granule under different salinities. *Environmental Science*, *29*(10), 2804-2808.

Wang, J. L., Zhang, Z. J., & Wu, W. W. (2009). Research advances in aerobic granular sludge. *Acta Scientiae Circumstantiae*, *29*(3), 449-473.

Zhang, D. H., Yue, Q. Y., Wang, S. G., Jiang, D., Sun, F. Y., & Li, J. Y. (2006). Characterization of aerobic granular sludge in sequencing batch reactor. *China Water & Wastewater*, *22*(1), 80-83.

Zhao, Y. G., Huang, J., Zhao, H., & Yang, H. (2013). Microbial community and N removal of aerobic granular sludge at high COD and N loading rates. *Bioresour. Technol*., 143, 439-446.

Author´s institutional address

Yao Chen

Chongqing Jiaotong University
Key Laboratory of Hydraulic & Waterway Engineering of the Ministry of Education
School of River and Ocean Engineering
Chongqing 400074, PR China

Cooperative Research Centres (CRC) for Water Sensitive Cities
Melbourne VIC 3800, Australia

Monash University
Moansh Sustainability Institute
Department of Civil Engineering
Melbourne VIC 3800, Australia
cycquc8163.com
Jia-Yue Zhu
Zhi-Min Zhang

Chongqing Jiaotong University
School of River and Ocean Engineering
Chongqing 700074, PR China

Yu Qin
Shao-Chun Yuan

Chongqing Jiaotong University
Key Laboratory of Hydraulic & Waterway Engineering of
the Ministry of Education
School of River and Ocean Engineering
Chongqing 400074, PR China
qinyu54001@163.com

cycquc@163.com

Haga clic aquí para escribir al autor

• ISSN 2007-2422

Improvement of the vertical "scatter degree" method and its application in evaluating water environmental carrying capacity

• Zhi-Hong Zheng* • Yan-Xu Yu •
North China University of Water Resources and Electric Power
*Corresponding author

Abstract

Zheng, Z. H., & Yu, Y. X. (March-April, 2017). Improvement of the vertical "scatter degree" method and its application in evaluating water environmental carrying capacity. *Water Technology and Sciences* (in Spanish), 8(2), 71-76.

The "scatter degree" method is an objective evaluation method based on a "difference drive*". However, it is currently perceived as incapable of properly reflecting the subjective information of the evaluator. In order to reflect the objective law of raw data and assist decision-makers to control major factors of the water environmental carrying capacity (WECC), this paper proposes a method to process the weight of the indicator by combining the analytic hierarchy process (AHP) and the vertical "scatter degree" method. The computing results of this improved method are virtually identical to those of the old method, but the former is more scientific and reliable.

Keywords: Water environmental carrying capacity; analytic hierarchy process; processing weight; improved vertical "scatter degree" method.

Resumen

Zheng, Z. H., & Yu, Y. X. (marzo-abril, 2017). Mejoramiento del método de "grado de dispersión" vertical y su aplicación en la evaluación de la capacidad de carga ecológica del agua. Tecnología y Ciencias del Agua, *8(2), 71-76.*

El "grado de dispersión" vertical es un método de evaluación objetiva; sin embargo, actualmente se percibe como incapaz de reflejar de forma adecuada la información subjetiva del evaluador. Con el fin de reflejar la ley objetiva de datos brutos y ayudar a los tomadores de decisiones a controlar los principales factores de la capacidad de carga ecológica del agua (WECC), este trabajo propone un método para procesar la ponderación del indicador, al combinar el proceso de jerarquía analítica (AHP) y el método de "grado de dispersión" vertical. Los resultados de este método mejorado son prácticamente idénticos a los obtenidos con el antiguo método, pero el primero es más científico y confiable.

Palabras clave: *capacidad de carga ecológica del agua, proceso de jerarquía analítica, ponderación, método de "grado de dispersión" vertical mejorado.*

Received: 28/04/2016
Approved: 22/09/2016

Introduction

Water is the primary nature resource for human survival and social development. The water environment is the synthesis of water bodies, and it is closely related to various kinds of natural factors and social factors. WECC (Water Environmental Carrying Capacity) is based on the relationship between sustainable development and water environment, and its size determines the scale and speed of development of human society. Many scholars, both domestic and overseas, have researched WECC and its significance to humans (Long & Jiang, 2003). Various methods have been used for its evaluation, such as the system dynamics model (Han, 2005), the vector norm method (Huang & Song, 2013), the fuzzy comprehensive evaluation method (Fang, 2014), the multi-objective model (Wang, Zhou, & Yu, 2015), the artificial neural network model (Wang, Sun, Li, & Hou, 2007), the radial basis function (RBF) artificial neural network model (Hu, Xu, Xu, & Fu, 2015), and the catastrophe progression method (Wu, Wang, Cao, Wang, & Zhao, 2015), and so on. The evaluation of the water environmental carrying capacity involves hydrology in

addition to analysis of social, environmental, and ecological factors. These factors can be multi-layered, dubious and complex. Because of this complexity, this paper combines the analytic hierarchy process (AHP) and the vertical "scatter degree" method, which considers objective and subjective information fully in its evaluation. Through the comparison with the vertical "scatter degree" method, this method is determined to be more reasonable. In addition, it can provide technical support for improving regional WECC.

Improvement of "scatter degree" method

The theory of the "scatter degree" method (Guo, 2012)

The synthetic function is the linear function of greatest-type indicators (x_1, x_2,…, x_m):

$$y = \omega_1 x_1 + \omega_2 x_2 + \cdots + \omega_m x_m = \omega^T x \quad (1)$$

where $\omega = (\omega_1, \omega_2 \ldots \omega_m)^T$ is an m-dimensional pending positive vector.

Inserting the standard observed values (x_{i1}, x_{i2},…, x_{im}) of evaluation object S_i into Eq. (1), Eq. (2) is acquired:

$$y = \omega_1 x_{i1} + \omega_2 x_{i2} + \cdots + \omega_m x_{im} = \sum_{j=1}^{m} \omega_j x_{ij} \quad (2)$$

If and, Eq. (2) is converted to Eq. (3):

$$y = A\omega \quad (3)$$

The variance of evaluation objects $y = \omega^T x$:

$$s_2 = \frac{1}{n}\sum_{i=1}^{n}(y_i - \bar{y})^2 = \frac{y^T y}{n} - \bar{y}^2 \quad (4)$$

The principle of determining the weight coefficient of the "scatter degree" method is getting the linear function $\omega^T x$ of index vector x and making the variance of the evaluated object's values as high as possible; $y = A\omega$ is substituted into Eq. (4). When $\bar{y} = 0$, the new formula is as follows:

$$ns^2 = \omega^T A^T A\omega = \omega^T H\omega \quad (5)$$

where $H = A^T A$ is a real symmetric matrix.

When ω is unlimited, formula (5) can be an arbitrarily large value. Here, $\omega^T\omega = 1$, and the maximum value of formula (5) is acquired. Namely, the value ω is acquired to meet the constraints:

$$\max \omega^T H\omega$$
$$s.t.\begin{cases}\omega^T\omega = 1\\ \omega > 0\end{cases} \quad (6)$$

For formula (5), when ω is standard feature vector of the largest eigenvalues of H, $\omega^T H\omega$ achieves its maximum value. The weight coefficient vector $(\omega_1, \omega_2, \ldots \omega_m)^T$ is obtained by normalizing ω, and . The comprehensive values y_i of the evaluation object are obtained by using Eq. (2).

The improvement of the "scatter degree" method

The "scatter degree" method emphasizes that the method should highlight the differences among the evaluation objects as a whole, and it runs under the premise of the same importance of the evaluation target to every evaluation indicator. In fact, the degree of the importance is not same. The "function drive" theory provides the weighting coefficient $r_j (j = 1,2, \ldots, m)$ of each indicator x_j. On this basis, each indicator is weighted by the following formula:

$$x_{ij}^* = r_j x_{ij}, j = 1,2,\ldots,m; i = 1,2,\ldots,n \quad (7)$$

where x_{ij} are the standard observed values. The mean value and mean square deviation of x_{ij}^* are 0 and r_j^2, respectively. The weighting coefficient of weighted data $\{x_{ij}^*\}$ is acquired by using the "scatter degree" method. Then, the comprehensive evaluation values can be obtained.

• ISSN 2007-2422

Analytic Hierarchy Process (Deng, Li, Zeng, Chen, & Zhao, 2012)

In this article, the Analytic Hierarchy Process (AHP) is used to confirm the weighting coefficients r_j of each indicator.

AHP was discovered by Satty while performing operational research in the 1970's. The indicators are classified into several levels of objective, criterion, and index. This method is based on both quantitative and qualitative approaches.

The steps of AHP include building a hierarchical model, building a matrix of each level, performing a consistent check, and verifying the total arrangement of each hierarchy with a consistent check.

The process and results of the evaluation

The evaluating data and its standards

Reference data was adopted from (Geng, 2012). All the nine indicators are classified into positive and negative classes, and need to be standardized to remove the influence of inverse indices and different dimensions.

For the positive index:

$$x_{ij}^{*}=\frac{x_{ij}-m_j}{M_j-m_j}=\left(i=1,2,\ldots,n;j=1,2,\ldots,m\right) \quad (8)$$

For the negative index:

$$x_{ij}^{*}=\frac{M_j-x_{ij}}{M_j-m_j}=\left(i=1,2,\ldots,n;j=1,2,\ldots,m\right) \quad (9)$$

where $M_j=\max_i\left\{x_{ij}\right\}$ and $m_j=\min_i\left\{x_{ij}\right\}$

Matrix A is calculated based on the raw data as well as Eqs. (8) and (9). The results shown as follows:

$$A=\begin{bmatrix}1.000 & 0.000 & 0.000 & 0.000 & 0.785 & 0.000 & 0.832 & 0.436 & 0.604\\ 0.000 & 0.137 & 0.256 & 0.293 & 1.000 & 0.247 & 1.000 & 0.000 & 1.000\\ 0.448 & 0.360 & 0.587 & 0.698 & 0.981 & 0.258 & 0.000 & 0.876 & 0.328\\ 0.069 & 0.801 & 0.877 & 0.788 & 0.238 & 0.852 & 0.857 & 1.000 & 0.000\\ 0.552 & 1.000 & 1.000 & 1.000 & 0.000 & 1.000 & 0.814 & 0.907 & 0.029\end{bmatrix}$$

The application of vertical "scatter degree"

Symmetric matrix H is calculated by using the formula $H=A^TA$.

$$H=\begin{bmatrix}1.5101 & 0.7685 & 0.8753 & 0.9191 & 1.2414 & 0.7261 & 1.3404 & 1.3987 & 0.7675\\ 0.7685 & 1.7898 & 1.9485 & 1.9230 & 0.6820 & 1.8091 & 1.6378 & 2.0239 & 0.2852\\ 0.8753 & 1.9485 & 2.1783 & 2.1757 & 1.0404 & 1.9615 & 1.8212 & 2.2984 & 0.4777\\ 0.9191 & 1.9230 & 2.1757 & 2.1946 & 1.1658 & 1.9241 & 1.7826 & 2.3076 & 0.5514\\ 1.2414 & 0.6820 & 1.0404 & 1.1658 & 2.6361 & 0.7035 & 1.8573 & 1.4407 & 1.7966\\ 0.7261 & 1.8091 & 1.9615 & 1.9241 & 0.7035 & 1.8536 & 1.7918 & 1.9855 & 0.3614\\ 1.3404 & 1.6378 & 1.8212 & 1.7826 & 1.8573 & 1.7918 & 3.0896 & 1.9588 & 1.5265\\ 1.3987 & 2.0239 & 2.2984 & 2.3076 & 1.4407 & 1.9855 & 1.9588 & 2.7817 & 0.5780\\ 0.7675 & 0.2852 & 0.4777 & 0.5514 & 1.7966 & 0.3614 & 1.5265 & 0.5780 & 1.4737\end{bmatrix}$$

The maximal eigenvalue and eigenvector of matrix H' is calculated by using MATLAB: $\lambda_{max}(H)=13.9332$, $\omega(H)=(0.0768, 0.1124, 0.1280, 0.1287, 0.0980, 0.1144, 0.1391, 0.1436, 0.0591)^T$.

The values of WECC in the years of 2005 and 2009 are calculated by plugging $x_j(t_k)$ and w_j into Eq. (2).The results are shown in table 1.

The application of AHP-Vertical "scatter degree"

Calculation of the weight using AHP

1. A system of evaluation is established according to the reference, which is as follows: 1) Level of objective: WECC; 2) Level of indicators: ratio of water resource to utilization and exploitation X_1, gross regional output per capita X_2, water consumption of GDP X_3, water consumption of industrial output X_4, discharged volume of wastewater of industrial output X_5, discharged chemical oxygen demand of industrial output X_6, repeated utilization rate of industrial wastewater X_7, attainment rate of the industrial wastewater X_8, daily water consumption per capita X_9.
2. The weight of the index: The relative importance of all indicators was determined with

ISSN 2007-2422

reference to the literature. Then, matrix B is acquired as follows:

$$B=\begin{bmatrix} & X_1 & X_2 & X_3 & X_4 & X_5 & X_6 & X_7 & X_8 & X_9 \\ X_1 & 1.00 & 1.00 & 0.33 & 0.25 & 0.33 & 0.33 & 0.50 & 0.50 & 0.25 \\ X_2 & 1.00 & 1.00 & 0.33 & 0.25 & 0.33 & 0.33 & 0.50 & 0.50 & 0.25 \\ X_3 & 3.00 & 3.00 & 1.00 & 0.50 & 1.00 & 1.00 & 2.00 & 2.00 & 0.50 \\ X_4 & 4.00 & 4.00 & 2.00 & 1.00 & 2.00 & 2.00 & 3.00 & 3.00 & 1.00 \\ X_5 & 3.00 & 3.00 & 1.00 & 2.00 & 1.00 & 1.00 & 2.00 & 2.00 & 0.50 \\ X_6 & 3.00 & 3.00 & 1.00 & 0.50 & 1.00 & 1.00 & 2.00 & 2.00 & 0.50 \\ X_7 & 2.00 & 2.00 & 0.50 & 0.33 & 0.50 & 0.50 & 1.00 & 1.00 & 3.00 \\ X_8 & 2.00 & 2.00 & 0.50 & 0.33 & 0.50 & 0.50 & 1.00 & 1.00 & 3.00 \\ X_9 & 4.00 & 4.00 & 2.00 & 1.00 & 2.00 & 2.00 & 0.33 & 0.33 & 1.00 \end{bmatrix}$$

Then, the weight of the indicator is obtained by using MATLAB: $\lambda_{max} = 9.886$, $r = (0.043, 0.043, 0.127, 0.217, 0.127, 0.127, 0.092, 0.092, 0.133)^T$.

3. Consistency check: 1) consistency index: $CI = \frac{\lambda_{max} - n}{n-1}$, where n is the number of indicators, and $CI = 0.11075$; 2) consistency ratio: $CR = \frac{CI}{RI}$, where RI is the mean random consistency index, and when $n = 9$, $RI = 1.46$. So, $CR = 0.07586 < 0.10$, and the judgment matrix is consistent.

The WECC of AHP-Vertical "scatter degree". The matrix X' is acquired using Eq. (7).

$$X'=\begin{bmatrix} 0.430 & 0.000 & 0.000 & 0.000 & 0.997 & 0.000 & 0.765 & 0.401 & 0.803 \\ 0.000 & 0.059 & 0.325 & 0.635 & 1.270 & 0.314 & 0.920 & 0.000 & 1.330 \\ 0.193 & 0.155 & 0.745 & 1.515 & 1.246 & 0.328 & 0.000 & 0.806 & 0.437 \\ 0.030 & 0.344 & 1.113 & 1.711 & 0.303 & 1.082 & 0.788 & 0.920 & 0.000 \\ 0.237 & 0.430 & 1.270 & 2.170 & 0.000 & 1.270 & 0.749 & 0.835 & 0.039 \end{bmatrix}$$

A symmetric matrix H' is derived from the formula: $H' = X'^T X'$

$$H'=\begin{bmatrix} 0.2792 & 0.1421 & 0.4780 & 0.8576 & 0.6779 & 0.3965 & 0.5303 & 0.5533 & 0.4389 \\ 0.1421 & 0.3309 & 1.0641 & 1.7944 & 0.3724 & 0.9879 & 0.6479 & 0.8007 & 0.1631 \\ 0.4780 & 1.0641 & 3.5134 & 5.9959 & 1.6781 & 3.1638 & 2.1279 & 2.6855 & 0.8069 \\ 0.8576 & 1.7944 & 5.9959 & 10.3342 & 3.2128 & 5.3027 & 3.5588 & 4.6069 & 1.5915 \\ 0.6779 & 0.3724 & 1.6781 & 3.2128 & 4.2517 & 1.1347 & 2.1701 & 1.6833 & 3.0346 \\ 0.3965 & 0.9879 & 3.1638 & 5.3027 & 1.1347 & 2.9897 & 2.0935 & 2.3199 & 0.6104 \\ 0.5303 & 0.6479 & 2.1279 & 3.5588 & 2.1701 & 2.0935 & 2.6150 & 1.6580 & 1.8678 \\ 0.5533 & 0.8007 & 2.6855 & 4.6069 & 1.6833 & 2.1399 & 1.6580 & 2.3544 & 0.7072 \\ 0.4389 & 0.1631 & 0.8069 & 1.5919 & 3.0346 & 0.6104 & 1.8678 & 0.7072 & 2.6068 \end{bmatrix}$$

The maximal eigenvalue and eigenvector of matrix H' is calculated using MATLAB: $\lambda_{max}'(H') = 22.22$, $\omega'(H') = (0.0260, 0.0442, 0.1490, 0.2570, 0.1046, 0.1322, 0.1066, 0.1177, 0.0627)^T$.

The values of WECC in the years of 2005 and 2009 were calculated by putting $x_j(t_k)$ and w_j' into Eq. (2). The results are shown in table 1.

From the table and figures, it is clear that the results of the evaluation are basically consistent.

Conclusions

By comparing the results of the two methods, the conclusions are as follows: (1) The trend of the two methods' calculation of the WECC is the same; namely, the WECC is enhanced. This enhancement in WECC is closely related to the strengthening of the environmental governance, upgrading of production equipment, and the improvement of water-saving and environmental awareness; (2) As the two groups of data were calculated and compared, the WECC of 2005 was found to be 0.3677 or 0.2947 with the two models, respectively. From this data, it shows that the WECC of 2006 increased 11.59% and 93.45% relative to the WECC of 2005 by vertical "scatter degree" method and AHP-vertical "scatter degree" method. Based on the original data of the reference, there were eight indicators' data of 2006 higher than them of 2005, and their increasing rates were mostly greater than

Table 1. The results of WECC by two different methods.

Year	2005	2006	2007	2008	2009
Vertical "scatter degree" method	0.3677	0.4103	0.5108	0.6925	0.7712
AHP-Vertical "scatter degree" method	0.2947	0.5701	0.8083	0.9886	1.1206

• ISSN 2007-2422

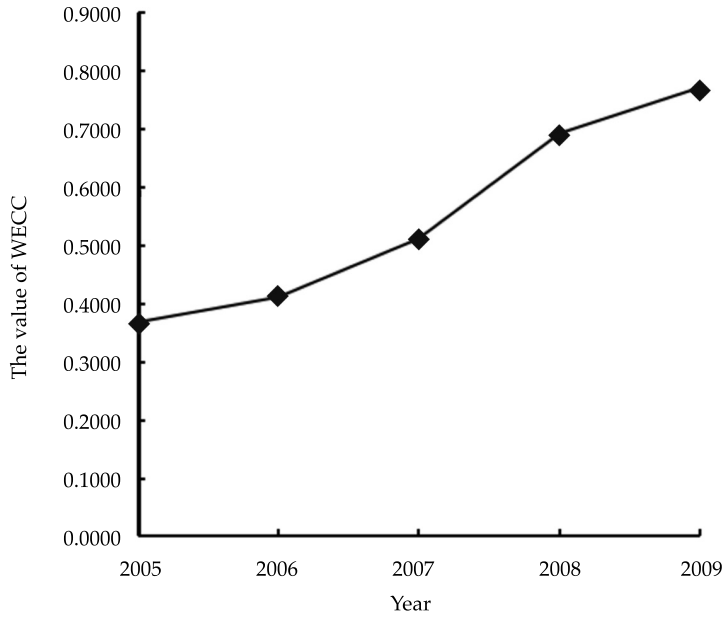

Figure 1. Water environmental carrying capacity of Shanxi Province spots (vertical "scatter degree" method).

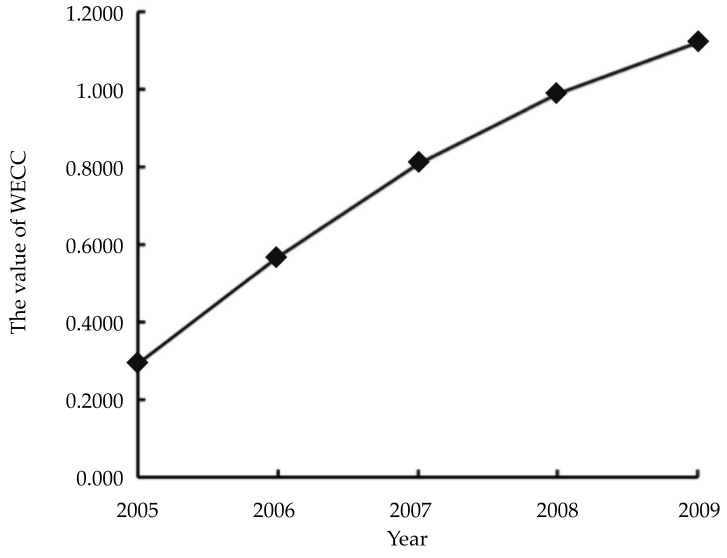

Figure 2. Water environmental carrying capacity of Shanxi Province spots (AHP-vertical "scatter degree" method).

10%. This indicated a clear increase in WECC from 2005 to 2006. Therefore, the result of the AHP-vertical "scatter degree" method is more reasonable. The other groups of the data in the table 1 had the same features.

Overall, the results show that the AHP-Vertical "scatter degree" method is more scientific and reasonable than the original method. It overcomes the weaknesses of the vertical scatter degree method which the subjective information

from the evaluators cannot be reflected. By combining the subjective weighting and subjective weighting methods, the twice-weighted process not only expresses the degree of important for each of the indicators but also highlights the difference of every evaluating object. It has the advantage of remedying the single use of the subjective weighting method and the objective weighting method.

Acknowledgements

The Key Science and Technology Project of Henan Province "Integration and Demonstration of Domestic Sewage Treatment Technology in Typical Villages and Towns in Henan Province" financially supported this work (Project number: 161100310700).

References

Deng, X., Li, J. M., Zeng, H. J., Chen, J. Y., & Zhao, J. F. (2012). Research on computation methods of AHP wight vector and its application. *J. Mathematics in Practice and Theory*, *47*(2), 93-100.

Fang, R. (2014). Calculating system build of Manas River Basin water environmental carrying capacity. *J. Ground Water*, *36*(6), 105-107.

Geng, Y. N. (2012). Water environmental carrying capacity in Shanxi Province based on improved fuzzy optimization process. *J. Journal of Water Resources & Water Engineering*, *23*(3), 65-70.

Guo, Y. J. (2012). *Theories, methods and expansion of comprehensive evaluation* (p. 37). Beijing: Beijing Science Press.

Han, N. N. (2005). *The Research onWater Environment Carrying Capacity of Sanggan River in Shanxi D.* Xi'an, China: Xi'an University of Technology.

Hu, X. G., Xu, R. H., Xu, H. B., & Fu, Y. C. (2015). River water environmental bearing capacity evaluation study in the city. *J. Journal of Water Resources Water Engineering*, *26*(3), 106-109.

Huang, T. Z., & Song, S. B. (2013). Evaluation of water environment carrying capacity in Huaihe River Basin. *J. China Rural Water and Hydropower*, 4, 45-49.

Long, T. G., & Jiang, C. Y. (2003). Advancement in research on carrying of water resource (environment) *J. Advances in Water Science*, *14*(2), 249-253.

Wang, J., Sun, T. H., Li, P. J., & Hou, W. (2007). Evaluation model of regional water environmental carrying capacity based on artificial neural network and its application in Liaoning Province. *J. Chinese Journal of Ecology*, *26*(1), 139-144.

Wu, Y. C., Wang, Z., Cao, L., Wang, X. J., & Zhao, Y. W. (2015). Evaluation on water environment carrying of Xuzhou City in recent 10 years based on catastrophe progression method. *J. Bulletin of Soil and Water Conservation*, *35*(2), 231-235.

Wang, Y. F., Zhou, B. H., & Yu, L. (2015). Analysis of Jinan's Water Environmental Carrying Capacity Index System. *J. Water Conservancy Planning and Design*, 4, 4-7.

Author´s institutional address

Zhi-Hong Zheng
Yan-Xu Yu

North China University of Water Resources and Electric Power
School of Environmental & Municipal Engineering
Zhengzhou 450045, PR China
Telephone: +13 (623) 823 982
zzh@ncwu.edu.cn
1656392474@qq.com

Haga clic aquí para escribir al autor

The runoff variation characteristics of Dongting Lake, China

• Dehua Mao* • Chang Feng •
Hunan Normal University, China
*Corresponding author

• Hui Zhou •
Hunan Normal University/Hydrology and Water Resources Survey Bureau of Hunan Province, China

• Guangwei Hu •
Hunan Industry University

• Zhengzui Li •
Hydrology and Water Resources Survey Bureau of Hunan Province, China

• Ruizhi Guo •
Hunan Normal University, China

Abstract

Mao, D., Feng, C., Zhou, H., Hu, G., Li, Z., & Guo, R. (March-April, 2017). The runoff variation characteristics of Dongting Lake, China. *Water Technology and Sciences* (in Spanish), *8*(2), 77-91.

The runoff variation characteristics of Dongting Lake were analyzed by applying the methods of concentration degree, concentration period, Mann-Kendall trend test, and variation coefficient. The analysis showed that: 1) The runoff concentration period of Dongting Lake occurs mainly between June and July of each year, with the peak time in late June–early July, and the composite vector directions in concentration period range from 103.2° to 190.2°; 2) The runoff variation coefficient ranges from 0.194 to 0.761, which indicates the instability of runoff. Extreme ratios of inflow and outflow are over 0.6 with an obvious attenuation; 3) The alternating pattern between wet years and dry years showed that the water distribution of the four rivers is relatively equal, while Ouchikou from three bayous is more violent, accounting for 32.79% of wet years and 57.38% of dry years respectively. The drastic change of annual water allocation is adverse to rational utilization of water resources.

Keywords: Runoff variation characteristics, annual variation, concentration degree and period, interannual variation, trend analysis, Dongting Lake.

Resumen

Mao, D., Feng, C., Zhou, H., Hu, G., Li, Z., & Guo, R. (marzo-abril, 2017). Características de la variación de escurrimiento del lago Dongting, China. Tecnología y Ciencias del Agua, *8(2), 77-91.*

Se analizaron las características de la variación de escurrimiento del lago Dongting mediante la aplicación de los métodos de grado de concentración, periodo de concentración, análisis de tendencias de Mann-Kendall y coeficiente de variación. El análisis mostró que 1) el periodo de concentración de escurrimiento del lago Dongting ocurre principalmente entre junio y julio de cada año, presentándose el tiempo máximo entre finales de junio y principios de julio, y las direcciones de los vectores compuestos en el periodo de concentración van de 103.2 a 190.2°; 2) el coeficiente de variación del escurrimiento oscila entre 0.194 y 0.761, lo cual indica la inestabilidad del escurrimiento; las proporciones extremas del flujo de entrada y el flujo de salida son superiores a 0.6, con una obvia atenuación; 3) el patrón alternante entre los años húmedos y los años secos mostró que la distribución de agua de los cuatro ríos es relativamente igual, mientras que en Ouchikou de tres canales pantanosos es más violento, representando 32.79% de los años húmedos y 57.38% de los años secos, respectivamente. El drástico cambio de asignación anual de agua es adverso a la explotación racional de los recursos hídricos.

***Palabras clave**: características de variación de escurrimiento, variación anual, grado y periodo de concentración, variación interanual, análisis de tendencias, lago Dongting.*

Received: 09/04/2016
Approved: 22/09/2016

Over view of the study area

Located in the northeast of Hunan Province and on the south bank of Jingjiang River, a stem stream of Yangtze River, Dongting Lake lies across Hunan and Hubei Province and has a close relationship with middle reaches of Yangtze River. Dongting Lake is the second largest freshwater lake in China, which has surface area 2 625 km^2 and plays an important role in flood water storage. The inflow contains four big rivers of Hunan (Xiang River, Zi River, Yuan River, Li River), three bayous of Yangtze River (Songzikou, Ouchikou, Taipingkou) and several small rivers (Miluo River, Xingqiang River, etc.). Those flows inject into Dongting Lake, stored, and then discharges into Yangtze River at Chenglingji. The details of the schematic diagram are presented in (figure 1).

Temporal distribution of precipitation is uneven in Dongting Lake Region.The wet season which from April to September provides about 65% of annual precipitation, which increases the risk for regional flood disaster. Because of the unevenness of inter-annual rainfall, drought and flood possibility is very high, what's worse, even in the flood years, the extreme weather like drought would possibly happen in Dongting Lake Region. Flood and drought disasters are the most severe disasters in Dongting Lake Region. According to the statistics, the annual average direct economic loss caused by flood is up to 1.858 billion in agriculture (Li, Zheng, & Gao, 2000). During last 60 years, the most terrible floods occurred in 1954, 1996 and 1998 (Mao, 1998; Mao, 2000) while in 1960, 1963 and 1968 occurred serious droughts. During time period from1970 to 2005, the extreme droughts occurred 5 times.1998 and 2002 are extreme flood year and 1969, 1973, 1980, 1993, 1995 and 1999 flood years (Zhang, Zhang, & Li, 2009). In 21 century, the drought situation is getting worse; 2003, 2006 and 2011 were sustained drought years in Dongting Lake region. Water shortage threatened inhabitants' water security and water supply in agriculture and industry around the lake, which has caused great attention from scholars. Researchers focus on the analysis of hydrology and sediment transport process, evaporation, precipitation, climate etc. The main aim of this study is an investigation of the relationship between runoff (three bayous

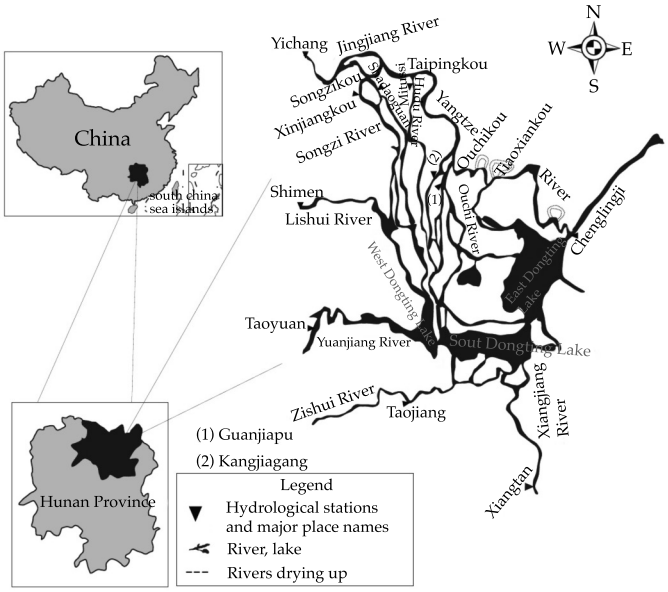

Figure 1. Schematic diagram of study area.

• ISSN 2007-2422

and four rivers) variation and drought and flood disasters based on the hydrological database.

Data and methodology

Data

Hydrological database from 1951 to 2011 has been used in this study which was collected from hydrological stations on the following rivers: Songzikou (Xinjiangkou and Shadaoguan), Taipingkou (Mituosi), Ouchikou (Kangjiagang and Guanjiangpu), Xiang River (Xiangtan), Zi River (Taojiang), Yuan River (Taoyuan), Li River (Shimen), Chenglingji (Qilishan). Monthly data series were used to analysis annual characteristics. All these data were obtained from Hunan Hydrology Bureau and *Bulletin of the Yangtze River Sediment* during 2000 and 2011.

Methodology

Mann-Kendall trend test method

Mann-Kendall (M-K) trend test method is usually used for identification the mutation characteristic of a long time series data (Wang, Zhou, & Tang, 2011; Zhang, Chen, & Jiang, 2008). M-K trend test method is widely recognized which does not require the original data obeying certain probability distribution and require only submitted random independence. Set the time sequence $x_1, x_2, x_{3,\ldots}, x_n$, m_i represent the cumulative amount that the i sample x_i is greater than $x_j (1 \le j \le i)$. Defined the statistical magnitude:

$$dk = \sum_{i}^{k} m_i \quad (2 \le k \le n) \tag{1}$$

If the original sequence is random and independent, the mean and variance of dk respectively are, $E[dk] = k(k-1)/4$, $\mathrm{var}[dk] = k(k-1)(2k+5)/72$ $(2 \le k \le n)$. Further standardization of dk, defined statistic $UF_k = (dk - E[dk])/\sqrt{\mathrm{var}[dk]}$ $(k = 1, 2, 3, \ldots, n)$. If $k > 10$, UF_k converges to the standard normal distribution. Adopt bilateral trend test, given a certain significant level a $(a = 0.05)$. Check the critical value of $U_{a/2}$ in the normal distribution table, If $|UF_k| < U_{a/2}$, it indicate that the tendency is not obvious; If $UF_k | > U_{a/2}$, it indicated that there is a significant trend change. If the UF_k value is positive, the long series shows increasing trend and vice versa. Make the inverse time series of x repeated computation according to the above process, at the same time make $UB_k = -UF_k$ $(k = n, n-1, \ldots, 1)$. The two curves of UB_k and UF_k cross at one point, and the cross point is mutation point. If the mutation point is located between the given confidence level of 95%, it means mutation time is significant in statistics.

Concentration degree and concentration period method

The calculation principle of concentration degree and concentration period method follows (Liu, Li, & Su, 2007): to add the monthly runoff value up in terms of the vector sum in a year. The ratio of the modulus of resultant vector and annual runoff is the annual runoff concentration degree (R_d). The annual runoff concentration period (R_p) is the direction of the resultant vector.

Set a monthly runoff for $r_i (I = 1, 2, 3,.., 12)$. The vector r_i is divided into horizontal and vertical direction vector; horizontal vector $r_{ix} = r_i \cos\theta_i$; vertical vector $r_{iy} = r_i \sin\theta_i$; the vector angle of the i monthly runoff is θ_i. Calculation formula:

$$R_x = \sum_{i=1}^{12} r_{ix} = \sum_{i=1}^{12} r_i \cos\theta_i \quad R_y = \sum_{i=1}^{12} r_{iy} = \sum_{i=1}^{12} r_i \sin\theta_i \tag{2}$$

$$R = \left(R_x^2 + R_y^2\right)^{1/2} = \left[\left(\sum_{i=1}^{12} r_i \cos\theta_i\right)^2 + \left(\sum_{i=1}^{12} r_i \sin\theta_i\right)^2\right]^{1/2}$$

$$W = \sum_{i=1}^{12} r_i \tag{3}$$

$$R_d = \frac{R}{W} \times 100\% \quad R_p = \arctan\left(\frac{R_y}{R_x}\right) \tag{4}$$

R stands for monthly runoff synthetic vector norm; R_x and R_y represent the horizontal

ISSN 2007-2422

and vertical component of the synthetic vector respectively; W is the annual runoff.

Annual distribution uniformity coefficient

Annual distribution uniformity coefficient reflects annual runoff distribution uneven degree in a watershed (Li, Li, & Wang, 2002; Yao, Guan, & Gao, 2003; Huang, 2003). Calculation formula:

$$C_v = \sigma / \overline{R} \tag{5}$$

$$\sigma = \left[\sum_{i=1}^{n}\left(R_i - \overline{R}_i\right)^2\right]^{1/2} \quad \overline{R} = \frac{1}{n}\sum_{i=1}^{n} R_i \quad (i = 1, 2, \ldots, 12) \tag{6}$$

C_v represents annual distribution uniformity coefficient; $\overline{R}$ represents average monthly runoff; R_i represents monthly runoff.

The mean difference T test

Defined mutation index of a sample sequence:

$$AI_j = \frac{\overline{x}_1 - \overline{x}_2}{s_1 + s_2} \tag{7}$$

$\overline{x}_1$, s_2 stand for the mean value and standard deviation before the base year m respectively; $\overline{x}_2$, s_2 stand for the mean value and standard deviation after the base year m respectively.

Defined the statistics:

$$t = \frac{\overline{x}_1 - \overline{x}_2}{s_p\left(\frac{1}{m_1} + \frac{1}{m_2}\right)^{1/2}} \tag{8}$$

m_1, m_2 represent the sample length of the two sequence before and after base year m respectively; s_p stands for joint sample variance:

$$s_p^2 = \frac{(m_1 - 1)s_1^2 + (m_2 - 1)s_2^2}{m_1 + m_2 - 2} \tag{9}$$

Given a certain significant level a ($a = 0.05$), when $t > t_a$, the mean value of m_1 and m_2 on both sides of the reference point has a significant difference, namely a mutation happen in the reference point.

Anomaly percentage

Calculation formula:

$$K_i = \frac{x_i - \overline{x}}{\overline{x}} \times 100\% \quad ; \quad \overline{x} = \frac{1}{n}\sum_{i=1}^{n} x_i \tag{10}$$

K_i represents the anomaly percentage of the i year; x_i represents the runoff of the i year; $\overline{x}$ stands for mathematical expectation of n annual runoff, $i = 1, 2, 3, \ldots, n$; n represents the total number of samples.

Runoff characteristics of Dongting Lake

Essential characteristics of Dongting Lake's inflow and outflow

The complicated flood combination of Dongting Lake's inflow is composed of three bayous and four rivers. The flood of three bayous is similar to Yangtze River whose flood peaks are obesity and last long. The distribution of three bayous' runoff is uneven, water in flood season (May to October) accounts for over 90% of the total. Four rivers' flood peak is sharp, thin and last shorter. Floods in flood season contribute 65% to the total. According to the measured hydrological data from 1951 to 2011, incoming water from three bayous and four rivers is 2 567 × $10^8 m^3/a$, and outflow was 2 862 × $10^8 m^3/a$. water came from three bayous of Yangtze Rivers was 912 × $10^8 m^3/a$, accounts for 31.9% of the total outflow. Four rivers contribute 1 655 × $10^8 m^3/a$ in the discharge which is 57.8% of the total. The rest local inflow is 295 × $10^8 m^3/a$, occupying 10.3% of the portion.

Annual runoff variation characteristics

Concentration degree and Concentration period is a vector approach which was first applied to the analysis of meteorological factors. In 1982, Tang introduced this method to identified the

• ISSN 2007-2422

distribution of monthly runoff annually and discovered water distribution characteristics of rivers in China (Tang, Cheng, & Li, 1982). Then, this method was adopted in other different basins (Zhang & Qian, 2003; Ding, Xu, & Pan, 2010; Zhang & Lu, 2011; Bai, Chin, & Ma, 2012). Concentration degree reflects the non-uniform distribution characteristics while concentration period informs the runoff concentrated period (monthly). The results are shown in table 1.

Table 1 illustrates the heterogeneity distribution of inflow and outflow. Distribution of three bayous' annual runoff is uneven for its concentration degree is between 66.9 and 85.2%. The maximum is in Kangjiagang and the minimum is in Xinjiangkou. Four rivers' concentration degree is between 32.2 and 43.7% and Chenglingji is 37.8% which is the smallest. Concentration period of three bayous and Chenglingji is July and that of four rivers is May-July. Their concentration period's synthesis vector direction is between 103.2° and 190.2. Statistic results and measured reality are in phase. Judging from the runoff variation amplitude, Ouchikou is the largest and Taojiang is the smallest. Absolute variation amplitude difference lies in each river. Maximum variation is 402.5 × $10^8 m^3$ of Chenglingji outflow and Kangjiagang is the smallest of 7.3 × $10^8 m^3$. Of the four rivers, absolute runoff change of Xiangtan and Taojiang are generally inconsistent, while that of Taojiang and Shimen are with the same trend. This consistency has a close relationship with their catchment area. The Bigger area corresponds with the larger change rate of runoff.

Figure 2 gives an overall good consistency of annual runoff variation from four rivers and three bayous. From April to May, four rivers begin their rain period and runoff increase rapidly and peak in late May-early June, in the form of a single symmetrical peak.

Among all, Xiangtan and Taoyuan have larger peaks. Three bayous step into flood season in May-June. Their runoff peak out in July. Among them, the west branch of Songzikou and Ouchikou have larger peaks. The outflow at Chenglingji is alternately affected by flood peaks from three bayous and four rivers, experiencing a relatively longer flood period. It enters into flood period from April to May and then experiences a larger flow period from June-August. Flood peaks appear in late June-early July. The flood peak times is between that of three bayous and four rivers and disappears by the end of August. After a linear decrease, Dongting Lake enters into the dry season.

Concentration period of runoff in Dongting Lake is June-July of each year and the maximum runoff occurs in late June-early July. Flood happens in late July mostly. Zeng *et al.* analyzed

Table 1. Statistic characteristics of annual runoff in Dongting Lake's inflow and outflow.

Hydrological Station	Time scale (year)	Concentration Degree (%)	Synthesis vector Direction (°)	Month	Relative change	Absolute change ($10^8 m^3$)
Xingjiangkou	1955-2011	66.9	175.4	July	166.8	70.0
Shadaoguan	1955-2011	75.1	181.1	July	639.9	28.6
Mituosi	1955-2011	69.3	179.6	July	362.0	36.9
Kangjiagang	1955-2011	85.2	190.2	July	/	7.3
Guanjiapu	1955-2011	75.3	178.9	July	2626.3	80.4
Xiangtan	1956-2011	38.2	106.5	May	5.0	91.1
Taojiang	1956-2011	32.2	103.2	May	3.8	25.8
Taoyuan	1956-2011	41.0	145.3	June	6.1	94.8
Shimen	1956-2011	43.7	180.4	July	8.9	24.5
Chenglingji	1951-2011	37.8	170.1	July	6.7	402.5

Tecnología y Ciencias del Agua, vol. VIII, núm. 2, marzo-abril de 2017, pp. 77-91
ISSN 2007-2422

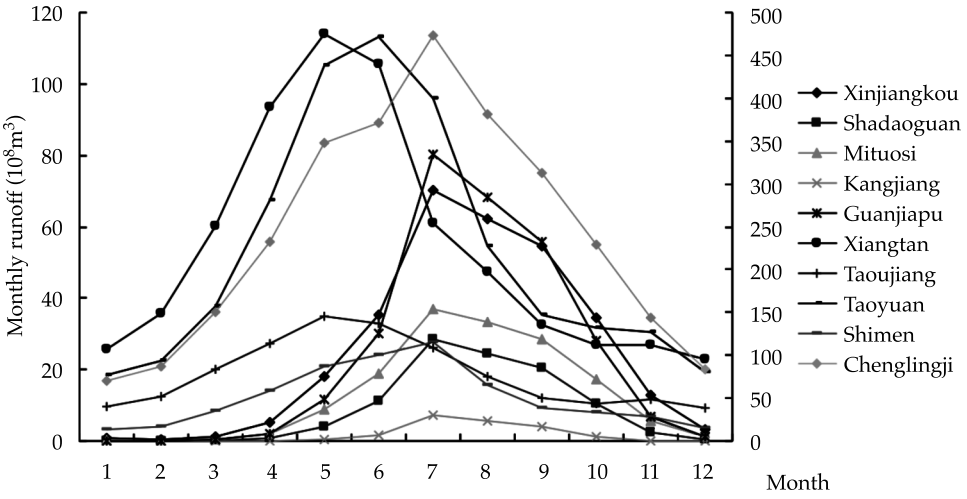

Figure 2. Monthly distribution characteristics of main rivers' runoff in Dongting Lake.

the flood-inducing system of Dongting Lake and then made a conclusion as follows (Zeng, Hao, & Liu, 2004): The meteorology system in the upper reach leads to the flood. Watersheds of four rivers were in the same monsoon zone whose rain season is from May to August. Rain belt moved from upper reach to downstream or even cover the whole watershed. When four river's flood arrived at the bank of Dongting Lake, it was experiencing its rainy period. The internal and external floods coincided to form severe disasters. The most typical examples are floods of Taojiang and Taoyuan in 1995 and 1996.

Inter annual runoff variability

Inter annual runoff variations are commonly calculated by variation coefficient (C_v) and inter annual extreme ratio. C_v is the ratio of the standard deviation and arithmetic mean of the sample sequence. It is an important indicator to reflect the evenness of inter annual runoff. Results are in table 2. According to calculation results, the C_v of inflow and outflow is between 0.194-0.761, among which three bayous' C_v are larger than others'. Results demonstrate the variability and unstable status of inter annual runoff. C_v of three bayous is different from that

Table 2. Average and variation coefficient of rivers in Dongting Lake basin.

Hydrological station	Statistic years	Annual mean	Maximum	Year	Minimum	Year	*Cv*	Extreme ratio
Xiangtan	1951-2011	654	1 035	1994	281	1963	0.251	0.73
Taojiang	1951-2011	227	372	1954	103	1956	0.229	0.72
Taoyuan	1951-2011	636	1 030	1954	379	2011	0.194	0.63
Shimen	1951-2011	146	264	1954	83	1992	0.277	0.69
Songzikou	1951-2011	409	750	1954	119	2006	0.272	0.84
Taipinkou	1951-2011	155	270	1954	34	2006	0.333	0.87
Ouchikou	1951-2011	333	1 156	1954	29.12	2006	0.761	0.97

• ISSN 2007-2422

of four rivers. The maximum C_v of three bayous is 0.761 in Ouchikou and that of four rivers is 0.277 in Shimen.

Runoff trend analysis

There are many methods to diagnose the continuous hydrological sequence. The most widely used and simple intuitive ways are moving average method and Mann-Kendall (marked by M-K) trend test method. This paper analyzes Dongting Lake's inflow and outflow with M-K trend test method which is widely accepted by a hydrologist. This method does not assume the distribution form for the data under investigation, only provided it is random independent with its time. The statistical significance of the trend was assessed at the 5% in this paper.

Figure 3(a) shows four crosses of UF and UB within the confidential interval. Based on the statistical significance of M-K mutation test, 1995, 1980, 1983 and 1987 were possible runoff mutation time of Xiangtan. From 1957 to 1994, UF curve was below the zero line within the confidential thresholds which explained a downward but not obvious trend in its runoff. In fig. 3(b), UF statistic curve and UB statistic curve for 5 times within the confidential intervals; 1955, 1962, 1967, 1972 and 1978 were potential mutation time for Zi River. From 1956 to 1993, Taojiang's runoff performed downward but not significant trend while in the rest of the time it was on the rise. Taoyuan's UF and UB have seven crossover points within the confidential intervals. The abscissa value of these points was likely to appear during mutation moments. An unobvious descent trend occurred from 1956 to 1967, 1985 to 1995 and 2007 to 2011. In figure 3 (d), Shimen's runoff trend was more complex than others. UF and UB coincided a lot in the confidential intervals and fluctuated. Its runoff went upward in 1951-1975 and declined in 1976-2011.But the trend was not significant for its crossovers were located in the confidential intervals.

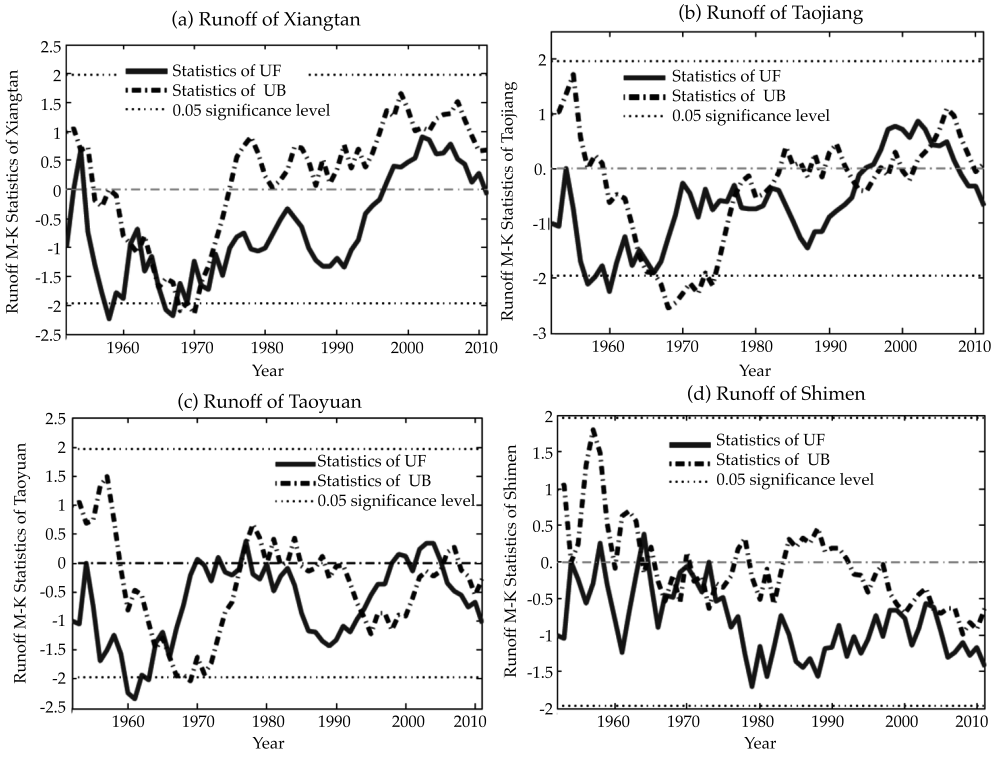

Figure 3. The M-K trend analysis of runoff of Four Water basin in Hunan.

ISSN 2007-2422 •

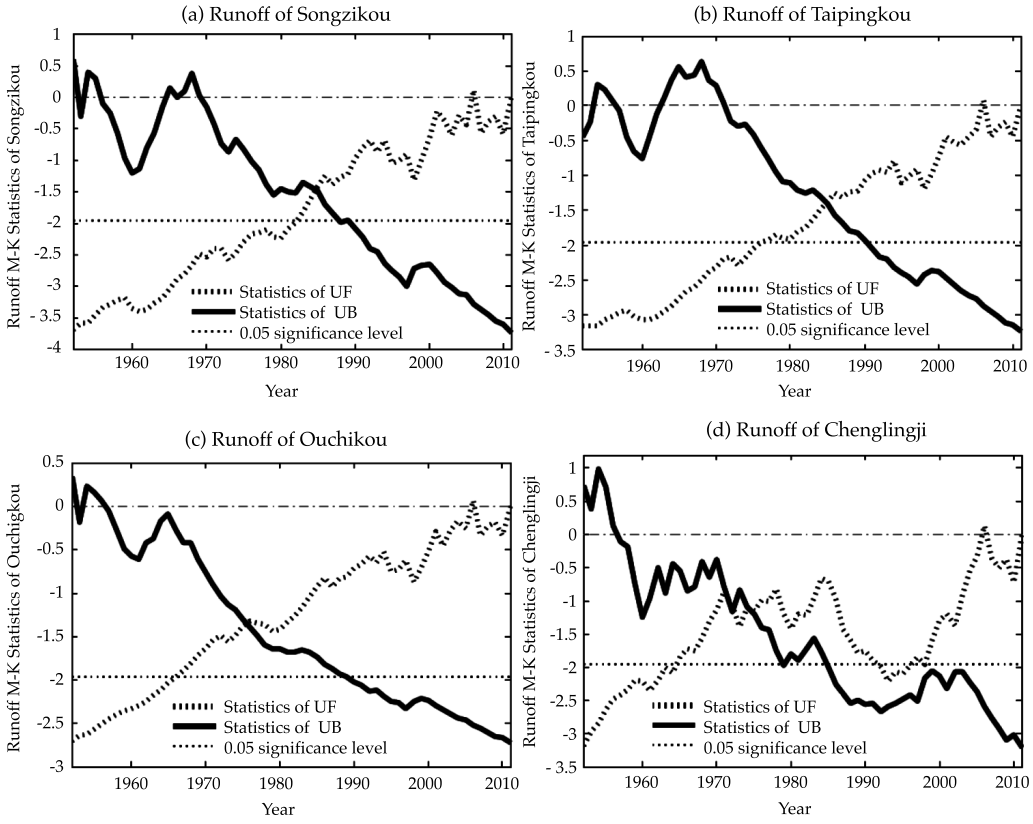

Figure 4. The M-K trend analysis of runoff of three outflows and Chenglingji.

Songzikou's runoff in figure 4(a) presents that UF and UB intersected in 1985 within the confidential intervals. After the mutation, UF overcame the confidential threshold to form a significant change. It demonstrated that after continuous descending, its runoff experienced an obvious and sudden change in the vicinity of 1985 which was exactly the 4th year after the completion of Gezhou Water Control Project. The discharge kept on decaying after the mutation point. Taipingkou's runoff in figure 4 (b) mutated at the same time with that of Songzikou and broke the confidential threshold in 1990 downwardly. The mutation time of Ouchikou's runoff was earlier and it's UF and UB met between 1975 and 1976 within the confidential zone. Its UF breaks the confidential zone and exhibited a significant attenuation trend in 1989. Ouchikou's runoff was affected by the lower-Jingjiang River's channel straightening project from 1967 to 1972. Figure 4 (d) shows outflow of Dongting Lake mutated between 1974 and 1975, after which the outflow revealed a continuous and downward oscillation and intersected with the confidential line in 1985 showing a significant attenuation.

In order to identify the accuracy of M-K mutation test, this paper uses the mean-difference T-test to verify the accuracy of the mutation year. The results are shown in table 3.

According to results from mean-difference T-test, statistic t value of three bayous and Chenglingji is 6.533, 7.660, 10.156 and 4.366, respectively. All have passed the significant test (significant level $\alpha = 0.01$, the critical value is 2.704). Four rivers' runoff did not mutate which means they have failed to pass the significant test.

• ISSN 2007-2422

Table 3. Mean-difference T-test statistic of annual runoff of three outflows, four rivers, and Chenglingji.

Station	M_j	Mutation index (A_{ij})	Statistic (t)	Significant level (a)	Thresholds (ta)	Station	M_j	Mutation index (A_{ij})	Statistic (t)	Significant level (a)	Thresholds (ta)
Songzikou	35	0.847	6.533	0.01	2.704		14	0.02	0.143	0.01	2.704
Taipingkou	35	1.015	7.660	0.01	2.704		16	0.02	-0.148	0.01	2.704
Ouchikou	25	1.372	10.156	0.01	2.704		26	0.115	0.893	0.01	2.704
Chenglingji	25	0.559	4.366	0.01	2.704	**Taoyuan**	27	0.175	1.366	0.01	2.704
Xiangtan	5	0.242	1.032	0.01	2.704		30	0.15	1.165	0.01	2.704
	30	0.085	-0.664	0.01	2.704		44	0.039	0.272	0.01	2.704
	33	0.012	-0.096	0.01	2.704		55	0.498	2.180	0.01	2.704
	38	0.127	-0.958	0.01	2.704		27	0.104	0.799	0.01	2.704
Taojiang	5	0.525	2.571	0.01	2.704		37	0.099	0.750	0.01	2.704
	12	0.052	0.366	0.01	2.704		42	0.078	0.559	0.01	2.704
	17	0.050	-0.376	0.01	2.704	**Shimen**	47	0.103	0.674	0.01	2.704
	22	0.006	-0.047	0.01	2.704		49	0.201	1.211	0.01	2.704
	28	0.001	0.012	0.01	2.704		53	0.346	1.576	0.01	2.704
							57	0.195	0.649	0.01	2.704

Dry period and wet period of inter annual runoff series

To identify wet period and dry period of inter annual runoff series, this paper follow *the hydrology forecasting manual* established by the information center of the water resources ministry to define the runoff classification. The annual runoff anomalies (in percentages) K_i is defined into 5 levels: $K_i < -20\%$ is dry year, $-20\% \le K_i < -10\%$is semidry year, $-10\% \le K_I \le 10\%$ is normal flow year, $10\% < K_i \le 20\%$ is semi wet year, $K_i > 20\%$is wet year.

According to annual K_i of four rivers in Hunan in figure 5 and table 4, we can find that wet years alternate with dry years. The percentage of normal flow year in Xiangtan, Taojiang, Taoyuan and Shimen are 22.95, 40.98, 36.07 and 27.87%, respectively. From wet to dry, percentages in each classification of Xiangtan are 22.95, 11.48, 22.95, 18.03 and 4.59%. These data listed above indicates a small inter annual runoff change and relatively equal wet and dry years in the last 61 years. The normal flow percentage of Taojiang is 40.98% which means very few floods and droughts in Zi River Basin. Wet years, dry years and normal flow years are of the same percentage in Shimen of Li river basin. It suggests a great even of inter annual runoff which is beneficial for the exploration of water resources. On the other hand, four rivers' normal flow year percentage is the maximum followed by wet years' and dry years'. Each level does not last long. Therefore, the flow of four rivers is neither wet nor dry sustainable. In other words, the water allocation is relatively average yields the likelihood of drought and flood is small.

The statistical anomalies of three bayous' runoff describe its variation characteristics (figure 5, table 4). The portions of Songzikou's normal flow years, wet year and dry year accounts for 32.79, 21.31 and 24.59% of the total. That is a fairly large inter annual change. The 5 ratios from wet to dry of Taipingkou is 24.59, 9.84, 22.95, 18.03 and 24.59% which is evener. In Ouchikou, the dry years account for 57.38% of all while the wet years occupies 32.79%.The dramatic inter annual water change is unfavorable for rational utilization of water resources. Figure 5 displays the runoff characteristic of three bayous. From 1951 to 1968, three bayous sustained in a wet period. During the period between 1969 and 1985, wet years alternated

ISSN 2007-2422

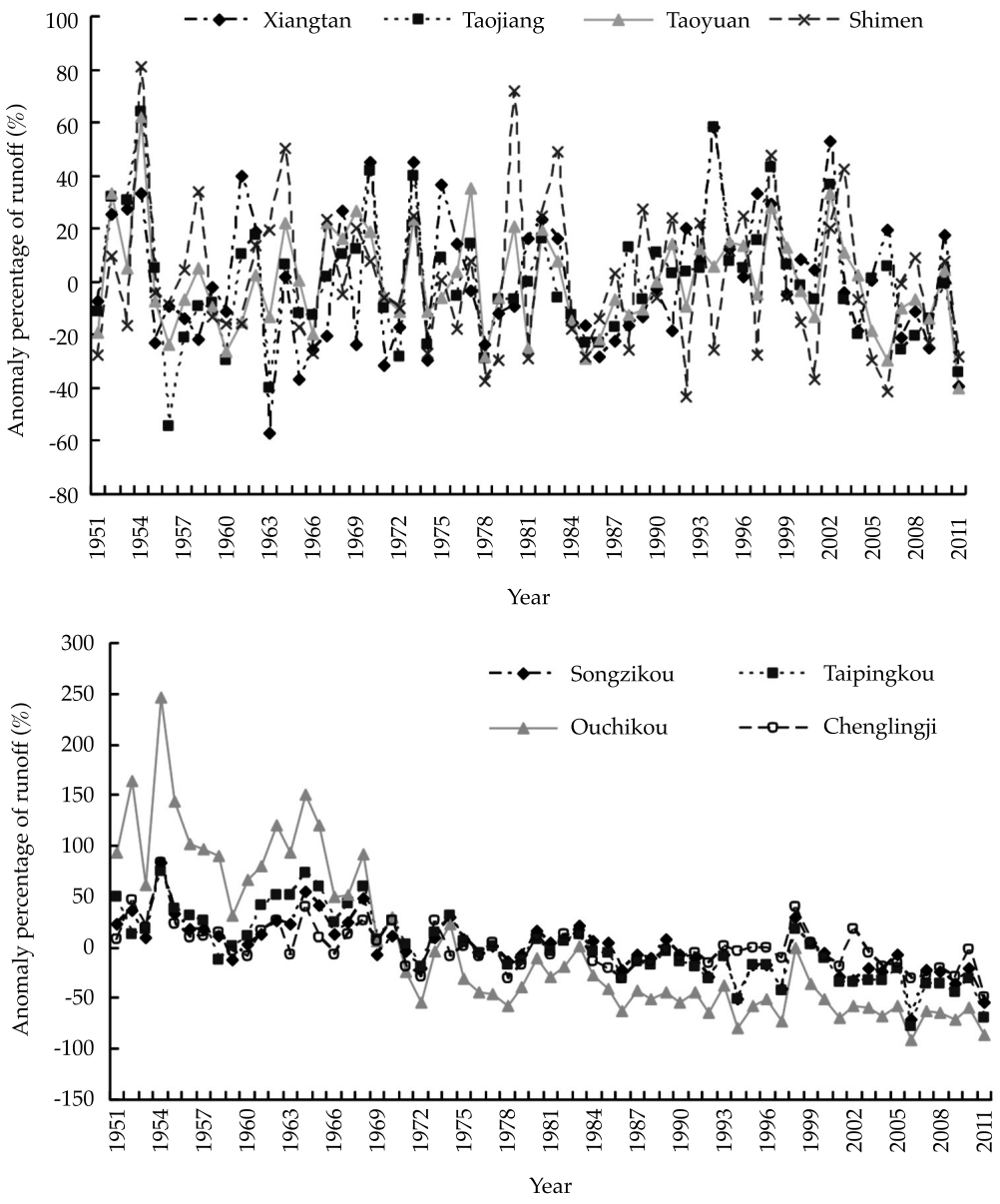

Figure 5. Percentage of runoff anomaly in Dongting Lake.

Table 4. Runoff classified statistics of Dongting Lake.

Hydrological station	Wet year	Semi wet year	Normal flow year	Semidry year	Dry year	Hydrological station	Wet year	Semi wet wet year	Normal flow year	Semidry year	Dry year
Songzikou	13	7	20	6	15	Xiangtan	14	7	14	11	15
Taipingkou	15	6	14	11	15	Taojiang	8	9	25	6	13
Ouchikou	20	0	4	2	35	Taoyuan	10	9	22	12	8
Chenglingji	9	10	23	10	9	Shimen	16	3	17	9	16

• ISSN 2007-2422

with dry years. From 1986 on, its runoff was low and exhibited an obvious duration till 2011. Ouchikou, in particular, with the maximum dry percentage, faces the severe risk of shrinking up. The increasing percentage of dry years of three bayous has posed a threat to the water utilization in the lake. At the same period, the outflow runoff in Chenlingji is evenly distributed. Its normal flow percentage is 37.7%, semi-wet and semi-dry portion are both 16.39%, wet and dry ratio are both 14.74%, which demonstrate the stability of outflow.

To further identify the characteristics of inflow and outflow, this paper curves Dongting Lake's runoff by calculating its annual anomalies.

As can be seen from figure 6, since 21 century, four rivers have entered into a low flow period. The anomaly percentage of that period is the lowest in the past 61 years. Four rivers annual average discharge is 594 × $10^8 m^3$, 198 × $10^8 m^3$, 548 × $10^8 m^3$, 139 × $10^8 m^3$, respectively. Judging from the descending slope of that stage, the absolute value of 4 stations indicated a consistent

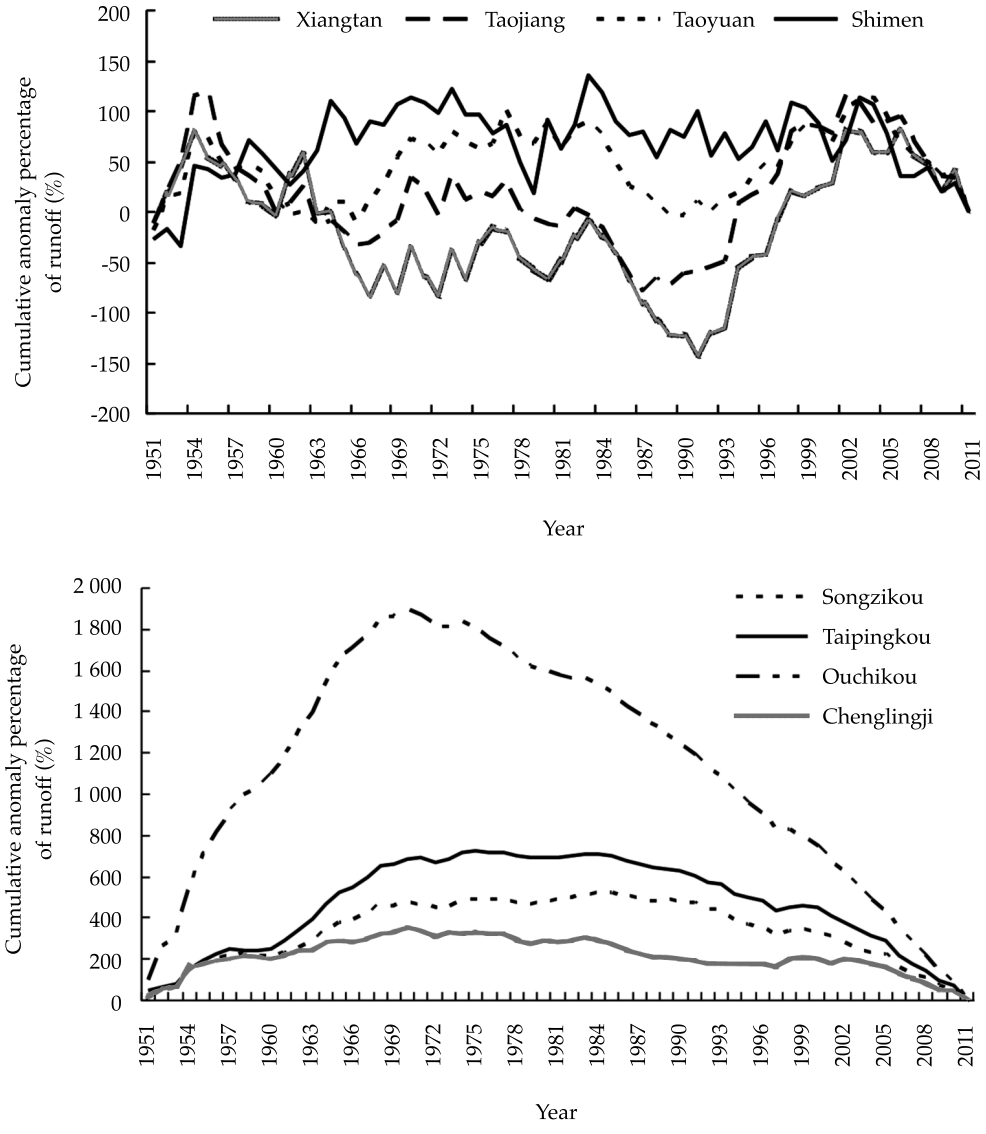

Figure 6. Percentage of runoff cumulative anomaly in Dongting Lake.

ISSN 2007-2422 •

reducing rate. Xiangtan station's runoff from 1951 to 2011 can be divided into four stages: 1951-1955 and 1988-2002 were a wet period, 1956-1987 and 2003-2011 were dry periods. Taoyuan station's runoff can be divided into 6 stages: 1951-1954, 1964-1983 and 1991-2003 were wet periods, 1955-1963, 1984-1990 and 2004-2011 were dry periods. Shimen station's runoff can be divided into four stages: 1951-1973 and 1980-1983 were wet years; 1974-1979 and 1984-2011 were dry periods.

According to three bayous' runoff cumulative anomalies (figure 6), Songzikou, Taipingkou, and Ouchikou stepped into the dry stage from the 1970s and 1980s, among which, Ouchikou's flow reduced most early in 1971 and got worse after the 21 century so that its slope ratio reached the sharpest. Songzikou and Taipingkou began to reduce at 1986 and 1978, but their curve slope ratio is flatter so the inter annual change was less velocity. Based on the periodical statistics data of three bayous, their runoff can be divided into two stages. The wet periods of Songzikou, Taipingkou was and Ouchikou is 1951-1985, 1951-1977 and 1951-1970, while the dry stages are 1986-2011, 1978-2011 and 1971-2011.

The stage runoff changes are the result of comprehensive functions of nature factors and human activities. Based on existing research, the climate is the main factor that leads to the runoff change (Zhai, Ren, & Zhang, 1999); Liu, Ji, & Wu, 2006); Wang, Wang, & Zhao, 1999) water and soil erosion and hydraulic engineering constructions also accelerate the change to some extent (Li, 1998). The author used wavelet analysis to study the period of inflow and outflow of Dongting Lake. The conclusion is as follows: Xiangtan station's runoff is characterized with multi-temporal periodicity, among which the period of 30-40a is the most distinct. Meanwhile, the first period of Taojiang station's runoff is 30-40a, the most stable period of Taoyuan's is 8-15a and the most obvious period in Shimen station is 20-27a. Those periods are identical with our stage analysis conclusion. The wavelet analysis of three bayous' runoff is 25-40 (Songzikou), 22-40 (Taipingkou) and 25-40 (Ouchikou), which is also in accordance with this paper's research. The conclusion means that three bayous will stay in a dry period now and move into another cycle in the next stage.

Conclusions and discussion

River runoff can reflect water quantity supplied from precipitation, as well as the hydrological phenomena such as watershed closure, soil infiltration, evaporation etc. Watershed storage change results from the comprehensive effects of climate change, hydraulic engineering construction, human activity and soil underlying surface parameters.

Concentration period of Dongting Lake's runoff focuses on June-July each year. The maximum runoff appears in the late June-early July. Due to the time of combined flood peaks coming from three bayous and four rivers, floods are usually in late July, The catchments of four rivers come into the raining season from April to May, after which their discharge increases rapidly and reaches a peak in the late May and early June with a single symmetrical. The peak shape is approximately symmetric single. However, three bayous' runoff starts their wet period in May and June and gets their peaks in July. The flood peaks superimpose in the lake and raise the water level. Meanwhile, the stage of Yangtze River rises, resulting in the flood jacking on the outflow of Dongting Lake and increasing the lake's flood hazard. In summary, 1996 and 1998 extraordinary floods were the typical examples of floods superposition.

The variation coefficient of outflow and inflow is between 0.194 and 0.761 which is pretty significant, especially that of three bayous. It can explain the instability of runoff and inter annual variation. All branches' extreme ratio is bigger than 0.6, particularly that of three bayous, indicating the significant inter annual reduction. The water reduction of three bayous is the main reason of seasonal water shortage which aggravates the drought disaster and threatens water supply around the lake.

• ISSN 2007-2422

Wet years alternate with dry years regularly in four rivers' regions. The normal flow percentages in Xiang River, Zi River, Yuan River and Li River are 22.95, 40.98, 36.07 and 27.87%, respectively, which accounts for the maximum possibilities of five classes. Percentages of normal years are followed by that of wet years and dry years who always appear in a short time which shows the water distribution is well allocated in four rivers. According to three bayous' wet and dry period, Songzikou's inter annual runoff is variable while Taipingkou's is evener. The wet year percentage and the dry year percentage of Ouchikou are 32.79 and 57.38%. The dramatic inter annual change doesn't make for the rational development of water resources. Three bayous' drought possibility increases, with the dry percentage of Ouchikou the maximum, which indicates a higher risk of drying up and ultimately threatens the water utilization. The lake's discharge is related to the atmospheric circulation, precipitation change, ENSO and solar activity.

According to M-K test results, four rivers' runoff within the statistical time were mutated, the annual runoff trends fluctuate up and down, but did not break the confidence intervals. Thus the change is not significant. As can be seen, the hydraulic engineering constructions, water and soil conservation and other measures in four watersheds play significant ecological effects. Songzikou's flow mutation occurred in 1985, after that, runoff showed significant attenuation changes, which may be one of the effects of the completion of the Gezhou dam in 1981. Taipingkou's mutation time happened in 1985 which is consistent with that of Songzikou and a breakthrough confidential threshold in 1990 showed significant attenuation trend. Ouchikou broke the confidential threshold in 1989 then exhibited a significant attenuation trend afterward. From 1967 to 1972, after Jingjiang channel straightening, Ouchikou's flow was greatly affected and decayed sharply.

The stage changes in runoff are affected by human activities and nature factors. Climate change takes the main responsibility for the runoff stage evolution, meanwhile, water and soil erosion, hydraulic engineering constructions and human activities accelerate the change progress. In climate respect, four rivers' flood peak encounters with that of three bayous' is the main cause of lake's flood disaster. Since the 1990s, the Yangtze River basin has experienced several large precipitation progress, a flood from four rivers and three bayous superimposed on each other and lead substantial water to the lake. At the same time, the water level of outflow was very high. As a result, abundant income and flood water jacking yielded a high water level of the lake and caused severe flood disasters. Floods in 1954 and 1998 are such typical examples. Human activities don't affect four rivers significantly for their water amount is large and inter annual fluctuation is small. But channel straightening, constructions of Three Gorge and Gezhou dam have changed the natural law between Dongting Lake and Yangtze River. Three bayous' runoff attenuation has resulted in the seasonal drought of Dongting Lake. In conclusion, the appearance of Lake Flood is the result of floods superimposition by the flood from three bayous and four rivers. In the long-term, climatic is the dominant factor causes runoff change, while human activities such as building dam intensify the procedure.

The runoff variation of Dongting Lake are caused by the comprehensive impact of climate change and human activities, but how many the contribution rate of the two kind factors to runoff variation at inflows, outflow and totality respectively, what are the drive mechanism causing the difference of the contribution rate et al. These will be researched in future.

Acknowledgments

This study was supported by the Key Research Project of Hunan Provincial Education Department (grant no. 15A113), the Construct Program of the Key Discipline in Hunan Province of China (2011001) and the Key Research Project of Hunan Provincial Water Resources Department (grant no. [2015]13-22).

ISSN 2007-2422

References

Bai, H., Chin, H., & Ma, X. (2012). Hydrological characteristics and their response to precipitation changes in Jinqian River Basin of Qinling over last 50 years. *Geographical Sciences*, *32*(10), 1230-1235.

Ding, J., Xu, Y., & Pan, G. (2010). Urban development impacts on precipitation of Jiaxing-Huzhou area. *Geographical Sciences*, *30*(6), 886-891.

Huang, Z. (2003). *Hydrological statistics* (pp. 108-125). Nanjing, China: Hohai University Press.

Li, J. (1998). A Study on the features and causes of the flood disasters in Dongting Lake Plain in 1996. *Acta Geographica Sinica*, *53*(2), 166-173.

Li, J., Zheng, Y., & Gao, H. (2000). A discussion on the geographical regularity of flood and drought in Hunan Province. *Journal of Natural Disasters*, *9*(4), 115-120.

Li, L., Li, H., & Wang, J. (2002). Hydrology and water environment characteristics and temporal differentiation of launching river. *Geographical Science*, *22*(1), 49-56.

Liu, X., Ji, Z., & Wu, H. (2006). The extreme differences distribution in temperature and precipitation of China for nearly 40 years. *Journal of Tropical Meteorology*, *22*(6), 618-624.

Liu, X., Li, J., & Su, Q. (2007). Inter annual runoff distribution based on degree and period of concentration for rivers. *Geographical Science*, *27*(6), 791-795.

Mao, D. (1998). Analysis of flood characteristics in Dongting Lake Region from 1471 to 1996. *Lake Science*, *10*(2), 85-91.

Mao, D. (2000). Assessment and analysis of flood-waterlogging disaster condition in Dongting Lake Region. *Journal of Natural Disasters*, *9*(3), 46-53.

Tang, Q., Cheng, T., & Li, X. (1982). Preliminary study of concentration and centralization of China's monthly runoff river. *Acta Geographica Sinica*, *37*(4), 383-393.

Wang, H., Wang, Q., & Zhao, Y. (1999). Characteristics of precipitation anomaly over the middle-lower reaches of the Yangtze River related to precipitation and temperature anomalies of China. *Journal of Nanjing Meteorology University*, *22*(4), 685-691.

Wang, C., Zhou, S., & Tang, X. (2011). Spatial and temporal distribution of precipitation in the past 48 years of Tibetan plateau. *Geographical Science*, *31*(4), 471-477.

Yao, Z., Guan, Y., & Gao, Y. (2003). Analysis of distribution regulation of annual runoff and affection to annual runoff by human activity in the Chaobaihe River. *Progress in Geography*, *22*(6), 599-607.

Zeng, T., Hao, Z., & Liu, X. (2004). Dongting Lake flood and its solving. *Advances in Water Resources and Hydropower Science*, *24*(1), 7-14, 69.

Zhai, P., Ren, F., & Zhang, Q. (1999). China extreme precipitation trend detection. *Meteorology*, *57*(2), 208-216.

Zhang, L., & Qian, Y. (2003). Annual distribution features of the yearly precipitation in China and their inter annual variations. *Acta Meteorological Sinica*, *17*(2), 146-163.

Zhang, Q., Chen, G., & Jiang, T. (2008). Water and sediment trends of Yangtze River and possible influence factors. *Resources and Environment in the Yangtze Basin*, *17*(2), 257-263.

Zhang, Q., & Lu, Z. (2011). Research on information decay with a distance of travel site. *Geographical Sciences*, *37*(7), 886-890.

Zhang, J., Zhang, X., & Li, Z. (2009). Dry and wet climate change in the Dongting Lake area. *Yunnan Geographic Environment Research*, *21*(5), 56-62.

Author´s institutional address

Ph.D. Dehua Mao

Hunan Normal University, China
College of Resources and Environmental Science
No. 36, Lushan Road, Changsha, Hunan Province,
PA 410081, PR China
Telephone: +86 18684953186
850276407@qq.com

M.S. Chang Feng

Hunan Normal University
College of Resources and Environmental Science,
No. 36, Lushan Road, Changsha, Hunan Province,
PA 410081, PR China
Telephone: +86 13974906206
35909538@qq.com

Ph.D. Hui Zhou

[1] Hunan Normal University, China
College of Resources and Environmental ScienceNo. 36,
Lushan Road, Changsha, Hunan Province,
PA 410081, PR China,
[2] Hydrology and Water Resources Survey Bureau of
Hunan Province, PR China
No. 370, Shaoshan Road, Changsha, Hunan Province,
PA 410081, PR China
Telephone: +86 13787107935
27402239@qq.com

Ph.D. Guangwei Hu

Hunan Industry University
College of Architecture and Urban and Rural Plan,
No. 88, Taishanxi Road, Zhuzhou, Hunan Province,
PA 412007, PR China
Telephone: +86 18692622407
280452570@qq.com

• ISSN 2007-2422

Ph.D. Zhengzui Li

Hydrology and Water Resources Survey Bureau of Hunan Province
No. 370, Shaoshan Road, Changsha, Hunan Province, PA 410081, PR China
Telephone: +86 15874137848
hn_lzz@163.com

Ph.D. Ruizhi Guo

Hunan Normal University
College of Mathematics and Computer Science
No. 36, Lushan Road, Changsha, Hunan Province, PA 410081, PR China
Telephone: 86-18974955343
471738824@qq.com

Haga clic aquí para escribir al autor

Tecnología y Ciencias del Agua, vol. VIII, núm. 2, marzo-abril de 2017, pp. 77-91
ISSN 2007-2422 •

Región Administrativa Especial de Hong Kong de la República Popular China.

Foto: Fernando Leyva Calvillo.

Kinetics and influential factors of nanoscale iron-facilitated nitrate nitrogen removal

• Yujia Song* •
Changchun University of Science and Technology, China
Corresponding author

• Shoufa Song •
Northeast Coal Industry Institute of Environmental Protection, China

Abstract

Song, Y. & Song, S. (March-April, 2017). Kinetics and influential factors of nanoscale iron-facilitated nitrate nitrogen removal. *Water Technology and Sciences* (in Spanish), *8*(2), 93-103.

In this paper, a new nanoscale iron adsorbent was prepared using the liquid phase reduction method. The effects of the initial nitrate nitrogen concentration, pH, and reaction temperature on the nitrate nitrogen removal efficiency of the nanoscale iron were investigated. The experimental results indicated that the initial nitrate nitrogen concentration significantly affected the reaction rate, but not the removal efficiency of the nanoscale iron. In addition, the optimal pH for the removal of nitrate nitrogen was 2.0. As the temperature increased, the nitrate nitrogen removal rate increased. A pseudo-second-order kinetic equation, in which the nitrate nitrogen concentration at reaction time *t* was used as the initial concentration, was developed in order to determine the reaction rate constant *k* at different temperatures. According to the results, the maximum value of *k* (0.014 mg/(l/min)) was observed at 50°C. The reaction activation energy *Ea* was approximately 17.18 kJ/mol. The reaction was primarily influenced by the mass transfer. In a neutral solution, in this case water, the reduction product of the nitrate nitrogen was ammonia nitrogen.

Keywords: Nitrate nitrogen, water pollution, reaction kinetics, nanometer, adsorption.

Resumen

Song, Y. & Song, S. (marzo-abril, 2017). Cinética y factores de influencia en la remoción de nitrógeno nítrico facilitada por hierro a escala nanométrica. Tecnología y Ciencias del Agua, *8(2), 93-103.*

En el presente trabajo se preparó un nuevo adsorbente de hierro a escala nanométrica empleando el método de reducción en fase líquida. Se investigaron los efectos de la concentración inicial de nitrógeno nítrico, el pH y la temperatura de reacción en la eficacia de remoción de nitrógeno nítrico del hierro a escala nanométrica. Los resultados experimentales indicaron que la concentración inicial del nitrógeno nítrico afectó significativamente el índice de reacción, pero no la eficacia de remoción del hierro a escala nanométrica. Además, el pH óptimo para la remoción del nitrógeno nítrico fue de 2.0. Conforme se incrementó la temperatura aumentó el índice de remoción de nitrógeno nítrico. Se desarrolló una ecuación cinética de pseudo segundo orden, en la que la concentración de nitrógeno nítrico en el tiempo de reacción t *se usó como la concentración inicial, con el fin de determinar la constante del índice de reacción* k *a diferentes temperaturas. Según los resultados, el valor máximo de* k *(0.014 mg/ml(l/min)) se observó a 50 °C. La energía de activación de reacción* Ea *fue aproximadamente de 17.8 kJ/mol. La reacción estuvo influenciada principalmente por la transferencia de la masa. En una solución neutral, en este caso agua, el producto de la reducción del nitrógeno nítrico fue nitrógeno amoniacal.*

***Palabras clave**: nitrógeno nítrico, contaminación del agua, cinética química, nanómetro, adsorción.*

Received: 31/10/2015
Approved: 07/04/2016

Introduction

Groundwater has become increasingly polluted with nitrate nitrogen as a result of rapid industrial and agricultural development. Nitrate pollution increases the concentration of nitrogen in water, resulting in eutrophication. In the human body, nitrate is converted to nitrite, which is highly toxic (Fan, Qu, Liu, & Meng, 2000; Kapoor & Viraraghavan, 1997; Chew & Zhang, 1998; Michael & Michellem, 2002). Therefore, the removal of nitrate from water is of great practical significance. The methods currently used to remove NO_3^- from surface water primarily include ion exchange,

reverse osmosis, biological treatment, and chemical reduction. The repeated regeneration processes that occur during ion exchange and reverse osmosis produce secondary pollution. Likewise, biological treatment entails numerous operation and management requirements, including a sufficient carbon source. Compared to ion exchange, reverse osmosis, and biological treatment, the chemical reduction has many advantages, such as rapid reaction rates. In addition, the chemical reduction does not cause secondary pollution, is not difficult to perform and is suitable for the treatment of small and distributed areas (Chen & Wu, 2009; Fan, Guan, Ma, & Ai, 2009). Kinetics and corrosion products of aqueous nitrate reduction by iron powder without reaction conditions control (*Journal of Environmental Sciences*, 2009, 21, 1028-1035).

Since the 1990s, numerous studies concerning the removal of nitrate-nitrogen pollution from surface water using nanoscale iron as an adsorbent and reductant have been conducted (Song & Song, 2015; Chen & Wu, 2009; Fan *et al*., 2009; Cheng, Muftikian, Fernando, & Korte, 1997; Huang, Wang, & Chiu, 1998; Choe, Chang, Hwang, & Khim, 2000; Lien & Zhang, 2001; Ponder, Darab, & Mallouk, 2000). Nanoscale iron has a large surface area (Liou, Lo, & Lin, 2005; Philips & Laura, 1992; Siantar, Schreier, Chou, & Reinhard, 1996; Wang & Zhang, 1997; Kanel, Manning, Charlet, & Choi, 2005; Yuan & Lien, 2006; Lien, Jhuo, & Chen, 2007; Tratnyek, Johnson, & Scherer, 1996), good surface adsorption, and strong reduction capabilities (Murphy, 1991). Previous studies have shown that 4 g/L of nanoscale iron can efficiently and effectively remove 30-120 mg/l of nitrate nitrogen. In one study, Seunghee Choe (Seunghee, Howard, & Li, 2004) investigated the effects of pH on the reaction rate of nitrate nitrogen in a nanoscale iron removal solution. The results indicated that nitrate nitrogen can be removed entirely under acidic conditions. In another study, Liou (Liou *et al*., 2005) studied the effects of temperature on the reaction rate of nitrate nitrogen as well as the nitrate removal efficiency of nanoscale iron. Furthermore, Chunming (Chunm & Robert, 2004) investigated the influential factors and reaction products of nanoscale iron-facilitated nitrate-nitrogen removal in different acidic solutions. In all of these studies, the influential factors and nitrate-nitrogen removal efficiency of nanoscale iron were investigated using relatively large amounts of nanoscale iron. In this study, the influential factors and nitrate-nitrogen removal efficiency of small amounts of nanoscale iron are analyzed in order to facilitate the efficiency of nitrate removal in practical applications. In addition, the reaction kinetics of the removal process were studied in order to develop a kinetic equation that effectively describes the reaction rate and activation energy of nanoscale iron-facilitated nitrate-nitrogen removal and, thereby, provides a theoretical basis for the application of nanoscale iron technology to the treatment of wastewater.

Materials and methods

Instruments and reagents

The reagents used for the purposes of this study included KNO_3 (analytical reagent grade, A.R.), $FeSO_4 \cdot 7H_2O$ (A.R.), NaOH (A.R.), KBH_4 (A.R.), absolute ethyl alcohol (A.R.), polyethylene glycol (A.R.), and reduced iron powder (200 mesh).

In addition, the D/MAX-2500 X-ray diffractometer (Japan), Philips EM400ST transmission electron microscope, 752N UV-Vis spectrophotometer, DJIC-100 electric mixer, Formal1025 anaerobic operation box, THZ-82B air bath constant-temperature-oscillator, JW-04 nitrogen adsorption surface area tester, and Delta-320 pH meter were used to conduct the experiments (Song & Song, 2015).

All of the glassware was immersed in 10% (volume fraction) HNO3 for 48 hours and then rinsed with tap water and deionized water several times before use.

Preparation and characterization of the nanoscale iron

At room temperature, a 1.6 mol/l $NaBH_4$ solution was added drop by drop to the same

• ISSN 2007-2422

volume of 1.0 mol/l $FeCl_3$ solution; during this process, a magnetic stirrer was used to stir the mixture. Then after ten minutes of reaction, we obtained the nanoscale iron particles needed for the experiment. According to reaction equation (1), this process resulted in the reduction of Fe^{3+} to nanoscale iron (Zhang, Wang, & Lien, 1998):

$$4Fe^{3+} + 3BH_4^- + 9H_2O \rightarrow 4Fe^0 \downarrow + 3H_2BO_3^- + 12H^+ + 6H_2 \uparrow \quad (1)$$

The black iron grains obtained via the above method have washed a minimum of three times with de-ionized water and absolute alcohol and then dried for 4 hours at 100-105 °C. The samples were then preserved in the dry container. All of these processes were conducted under nitrogen protection conditions.

The specific surface area and porosity analyzer were used to measure the specific surface area of the nanoscale iron particles via the nitrogen adsorption method. The X-ray diffractometer was used to perform a phase analysis of the nanometer particles with Cu as the target, Ka as the ray, and 100 mA as the current flow rate. The scanning transmission electron microscope was used to observe the features of the particles, and the nitrogen adsorption surface area tester was used to determine the specific surface areas of the particles.

Water sample analysis method

The methods adopted in the water sample analysis experiments included the nitrate nitrogen test method (UV spectrophotometry), the sub-nitrate nitrogen test method (N-(1-naphthyl)-ethylenediamine photometry), and the ammonia nitrogen test method (Nessler reagent spectrophotometry).

Nitrate nitrogen removal method

First, 5 ml of nitrate nitrogen solution with a known concentration and nanoscale iron were added to a 250-ml conical flask and allowed to react in the water-bathing constant temperature vibrator at a rotation speed of 150 rpm. The water-bathing constant temperature vibrator was used to control the reaction temperature. Next, after time sampling, each sample was filtered using a 0.45-μm membrane. Then, the concentration of each sample was measured.

Results and discussion

Characterization analysis results

According to the results, the diameter of the nano-iron particles ranged from 20 nm to 60 nm. In addition, the synthesized particles primarily existed in the granular and linear states with numerous gaps, indicating that the absolute alcohol controlled the accumulation of the nanoscale iron parcels during the synthesis process. Therefore, the absolute alcohol significantly increased the specific surface area of the nanoscale iron particles (Wang, Jin, Li, Zhang, & Gao, 2006). The average specific surface area of the synthesized nanoscale iron parcels was approximately 41.16 m^2/g, 1 to 2 orders of magnitude higher than that of the micro iron particles available for purchase. The results obtained via the X-ray diffractometer (figure 1) indicated that when the scanned diffraction angle (2θ) ranged from 30° to 100°, the synthesized nanoscale iron exhibited diffraction peaks at 44.58, 64.03, 81, and 89°, corresponding to the diffraction peaks of the body-centered cubic a-Fe (110). Furthermore, diffraction peaks approximate to those of the body-centered cubic a-Fe (200) and a-Fe (211) were observed (figure 1), indicating that the particles prepared through these experiments were comprised of iron rather than iron oxide.

Influence of the initial nitrate nitrogen concentration on the removal efficiency

At a constant temperature of 25 °C, 0.5 g of nanoscale iron was added to water containing 10, 50, and 100 mg/l of nitrate nitrogen. Then, the nitrate nitrogen concentrations at different reactions were measured with the spectrophotometer. The reaction time was used as the

ISSN 2007-2422

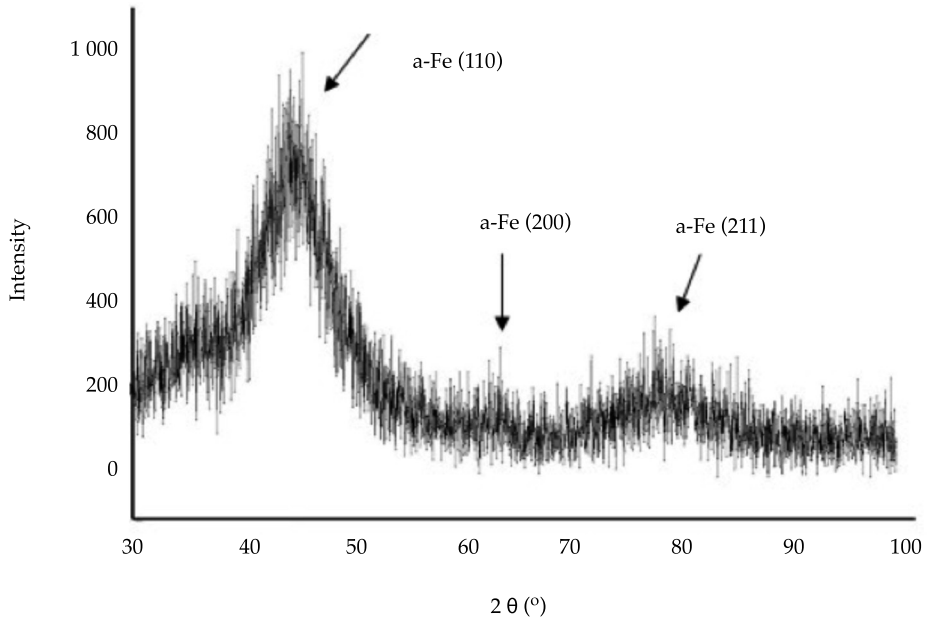

Figure 1. XRD spectrogram of the particle samples (the X-ray diffractometer was used to perform a phase analysis of the nanometer particles with Cu as the target, *Ka* as the ray, and 100 mA as the current flow rate).

abscissa and the nitrate removal efficiency was used as the ordinate. The effects of the initial nitrate nitrogen concentration on the removal efficiency were investigated, as shown in figure 2. As shown in this figure, as the initial concentration decreased, the removal rate increased and the ratio of the final concentration to the initial concentration decreased, with ratios of 0.69, 0.67, and 0.64. The removal rate was highest when the nitrate nitrogen concentration was 10 mg/l. In addition, the reaction rate became constant after 30 minutes regardless of the initial nitrate-nitrogen concentration. The experimental results indicated that the initial nitrate nitrogen concentration affected the reaction rate, but not the removal rate. In nanoscale iron-facilitated nitrate-nitrogen removal, the nanoscale iron first absorbs the nitrate nitrogen. Then, the nitrate nitrogen is converted into nitrite nitrogen, ammonia, and trace amounts of nitrogen via chemical reactions on the surface of the nanoscale iron (Zhang, Jin, Han, & Qin, 2006). The adsorption and response capacities of nanoscale iron are constants. As a result, the nanoscale iron content was relatively excessive when the nitrate nitrogen concentration was low, resulting in complete adsorption and conversion. Likewise, the nanoscale iron content was relatively inadequate when the nitrate nitrogen content was high, resulting in incomplete absorption and conversion.

Influence of pH on the removal efficiency

Iron forms ions easily in acidic solutions and combines with hydroxide ions to form precipitates in alkaline solutions. Therefore, the effects of pH on the nitrate-nitrogen removal efficiency were also investigated. In the experiment, 0.5 g of nanoscale iron was added to water containing 50 mg/l of nitrate nitrogen at a constant temperature of 25 °C. Next, dilute HCl and NaOH were used to adjust the pH of the solution to values of 2.0, 4.0, 6.0, 7.0, 8.0, and 10.0. The nitrate nitrogen concentration was then measured after different reaction times.

The results are shown in figure 3. As shown in this figure, the ratio of the final nitrate

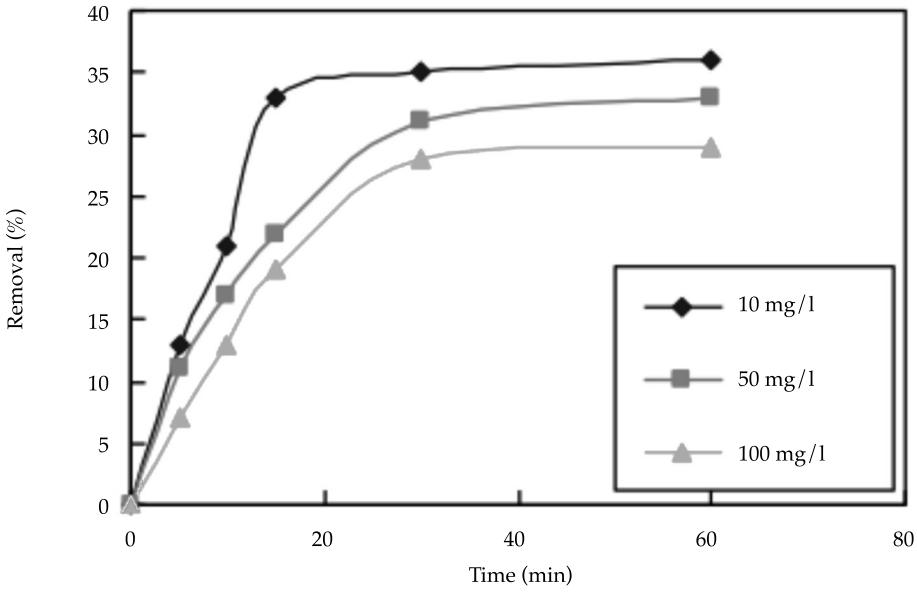

Figure 2. Influence of different initial concentrations on removal efficiency (at a constant temperature of 25 °C, 0.5 g o f nanoscale iron was added to water containing 10, 50 and 100 mg/l of nitrate-nitrogen).

nitrogen concentration (C) to the initial nitrate nitrogen concentration (C_0) of the solution increased gradually as the pH increased. In addition, the maximum removal efficiency occurred when the pH of the solution was 2.0. As the pH increased, the removal rate also gradually increased. After achieving equilibrium, the highest nitrate-nitrogen removal rate was only approximately 20%. This was attributed to the conversion of zero-valent iron to iron ions. The reaction equation can be expressed as:

$$Fe^0 + 2H_2O \rightarrow Fe^{2+} + H_2 + 2OH^- \quad (2)$$

As shown in the following equation, the zero-valent iron also reacted with the nitrate nitrogen:

$$5Fe^0 + 2NO_3^- + 6H_2O \rightarrow 5Fe^{2+} + N_2 + 12OH^- \quad (3)$$

Furthermore, under acidic conditions, the zero-valent iron reduced the nitrate nitrogen according to the following reaction equation:

$$Fe^0 + NO_3^- + 2H^+ \rightarrow Fe^{2+} + H_2O + NO_2^- \quad (4)$$

In an alkaline environment, Fe^0 is easily converted into $Fe(OH)_2$, $Fe(OH)_3$, and several ferrous hydroxide complexions, such as $[Fe(OH)]^+$, $[Fe(OH)_3]^-$, $[Fe(OH)_4]^{2-}$, and $[Fe(OH)_4]^{2+}$. These changes significantly reduce the ability of iron to absorb nitrate nitrogen (Martin *et al*., 2008; Yang & Lee, 2005). Due to the dual role of adsorption and reduction during nanoscale iron-facilitated nitrate-nitrogen removal, the pH of the solution significantly impacted the reactions. Since the acidity of water in practical engineering applications varies, adjusting the pH of water could allow for improved nitrate-nitrogen removal.

Influence of temperature and kinetic analysis of the removal of nitrate-nitrogen

In the experiment, 0.5 g of nanoscale iron was added to water containing 50 mg/l of nitrate-nitrogen. Then, the nitrate nitrogen content was measured at 25, 30, 35, 40, 45, and 50 °C. The

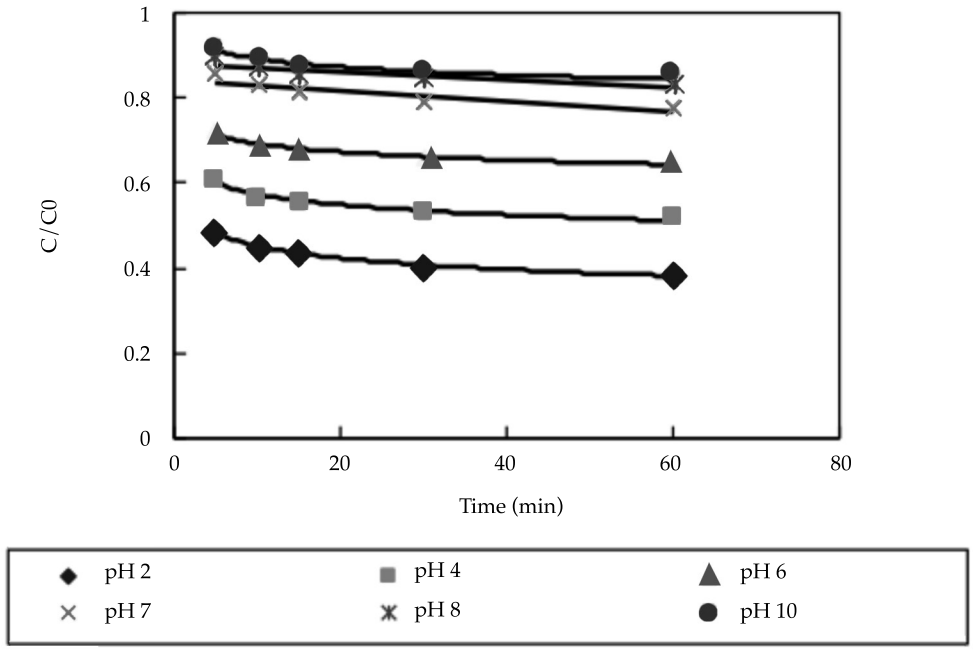

Figure 3. Influence of different pH values on removal efficiency (in the experiment, 0.5 g of nanoscale iron was added to water containing 50 mg/l of nitrate nitrogen at a constant temperature of 25 °C).

results are shown in figure 4. As shown in this figure, the nitrate nitrogen content varied at different temperatures, with nitrate removal rates of 50 and 60% at 25 °C and 50 °C, respectively. Thus, as the temperature increased, the amount of nitrate nitrogen removed by the nanoscale iron increased. However, these effects were not significant. Thus, efficient nitrate-nitrogen removal can be achieved at various temperatures in practical engineering applications. Figure 4 also shows that the reaction rate decreased gradually over time, but became constant after approximately 10 minutes. Therefore, the reaction that occurred between the nanoscale iron and nitrate nitrogen cannot be determined with this information alone. However, the products of the reaction between the nanoscale iron and water as well as the conditions of the aqueous solution determined the products of nitrate reduction. Thus, the reaction that occurred between the nanoscale iron and nitrate nitrogen under different conditions can be described by the following equation:

$$NO_3^- + 6H_2O + 8\,e^- \rightarrow NH_3 + 9OH^- \qquad (5)$$

Since the removal of nitrate-nitrogen occurs via adsorption and reduction facilitated by both the large specific surface area and high activity of nanoscale iron, the reaction between nitrate nitrogen and nanoscale iron cannot be effectively described by an adsorption reaction equation alone. Previous studies concerning the kinetics of nanoscale iron-facilitated nitrate-nitrogen removal have yielded varying results. Liou (Liou *et al*., 2005) reported that the reaction between nanoscale iron and nitrate nitrogen can be described with a pseudo-first-order kinetic equation. In contrast, Gordon (Molly *et al*., 2003) claimed that this reaction cannot be described by a pseudo-first-order kinetic equation or first-order kinetic equation. Since the effects of adsorption and reduction and interrelationships on nanoscale iron-facilitated nitrate-nitrogen removal cannot be determined, the products and reactant concentrations are assumed to be influenced by the conditions under which the

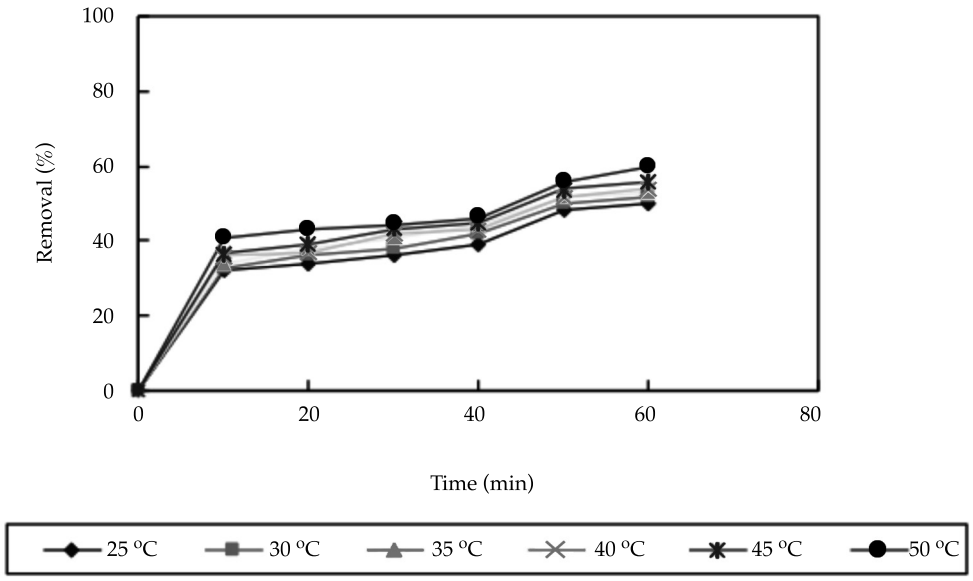

Figure 4. Influence of different temperature on removal efficiency (in the experiment, 0.5 g of nanoscale iron was added to water containing 50 mg/l of nitrate-nitrogen).

reaction occurs. Thus, there is no universally accepted kinetic equation for the reaction between nanoscale iron and nitrate nitrogen. In this paper, a pseudo-second-order kinetic equation was developed in order to determine the value of the reaction rate constant at different temperatures. Since the nitrate removal rate in this study ranged from 50 to 60%, not appropriate to research its kinetics equation from the half-life point of view. The data also indicated that the reaction became constant after 10 minutes due to the increased concentration of reacted nitrate nitrogen and resulting decrease in the reaction rate. The following pseudo-second-order kinetic equation was used to describe the reaction between the nitrate nitrogen and nanoscale iron:

$$dC_i / dt = k (C_a - C_i)^2 \quad (6)$$

In this equation, C_i represents the difference between the initial nitrate concentration C_0 and the nitrate concentration at time t C_t (mg/l), C_a represents the difference between the initial nitrate concentration C_0 and the stable nitrate concentration C_e (mg/l), and k is the reaction rate constant (mg/(l·min). This equation was integrated and simplified as:

$$C_t = C_0 - k_t C^2_a / 1 + k_t C_a \quad (7)$$

Equation (7) was used to calculate the value of k. Then, the appropriate value of k was selected based on the statistical error between the fitted value and experimental data. The results are shown in figure 5 and table 1.

Temperature also affects the reaction rate. According to the Arrhenius equation:

$$\ln k = Ea / RT + \ln A \quad (8)$$

An lnk 1/T relationship diagram was constructed in order to determine the activation energy, as shown in figure 6. According to the data presented in figure 6, the activation energy Ea of the reaction was approximately 17.18 kJ/mol. First, the nitrate nitrogen was absorbed by the nanoscale iron. Next, the nitrate nitrogen reacted with the surface of the nanoscale iron. Then, a fraction of the zero-valent nanoscale iron was converted into divalent iron ions. Therefore,

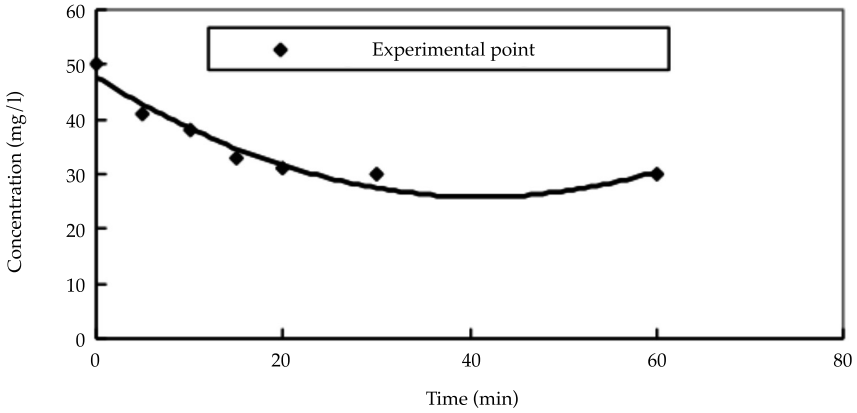

Figure 5. Kinetics analysis of experimental data according to pseudo-second-order at 25 °C (the following pseudo-second-order kinetic equation was used to describe the reaction between the nitrate nitrogen and nanoscale iron: $C_t = C_0 - k_t C_a^2 / 1 + k_t C_a$).

Table 1. Reaction rate constant at different temperatures.

Temperature (°C)	k (mg/(l·min))	Correlation coefficient (*r*)	Mean square error (MSE)	Mean absolute error (MAE)
25	0.008	0.9901	3.0532	1.2078
30	0.009	0.9894	1.7475	1.5564
35	0.010	0.9849	2.7315	1.4972
40	0.011	0.9818	3.2267	1.6060
45	0.012	0.9861	3.0446	1.4689
50	0.014	0.9966	0.7865	0.7078

the *Ea* included the total amount of reduced nitrate and oxidized nanoscale iron. Since the activation energy of the reaction, which was primarily influenced by the mass transfer of the aqueous solution, was limited to 10-20 kJ/mol, the factor that primarily influenced the reaction was the mass transfer of the solution rather than the chemical reactions (Liou *et al*., 2005). These results corresponded with those reported by Liou, who used a nanoscale iron to remove nitrate-nitrogen at 10-60 °C (Liou *et al*., 2005).

Product analysis of the nitrate-nitrogen removal process

At a constant temperature and pH of 25 °C and 7.0, respectively, 0.5 g of nanoscale iron was added to water containing 50 mg/l of nitrate nitrogen in order to determine the nitrate nitrogen, nitrite nitrogen, and ammonia concentrations of the solution after different reaction times. The results are shown in figure 7. As shown in figure 7, chemical reactions occurred during the nanoscale iron-facilitated removal of the nitrate-nitrogen. The nitrite content was very low. According to the curves of the three nitrogenous compounds, the reactant concentration decreased from the initial concentration of 50 to 45 mg/l, indicating that a portion of the nitrate nitrogen was converted into nitrogen and then released.

According to the experimental results, during the reaction between the nitrate nitrogen and nanoscale iron, most of the nitrate

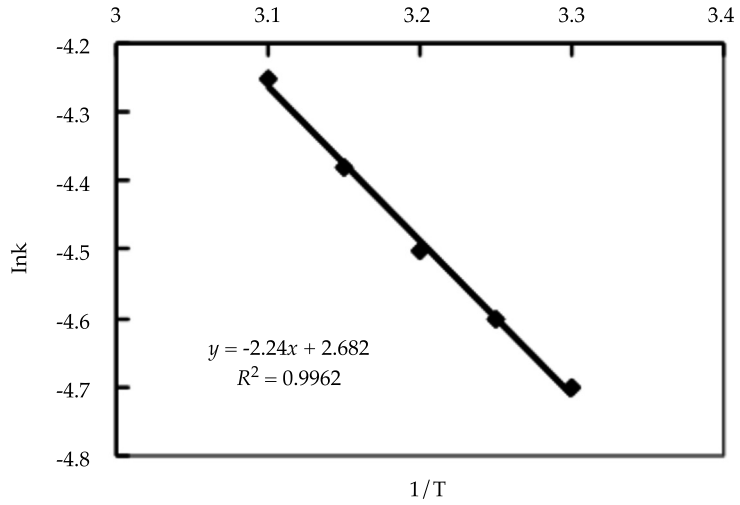

Figure 6. Analysis of the activation energy required to initiate nitrate-nitrogen removal by nanoscale iron.

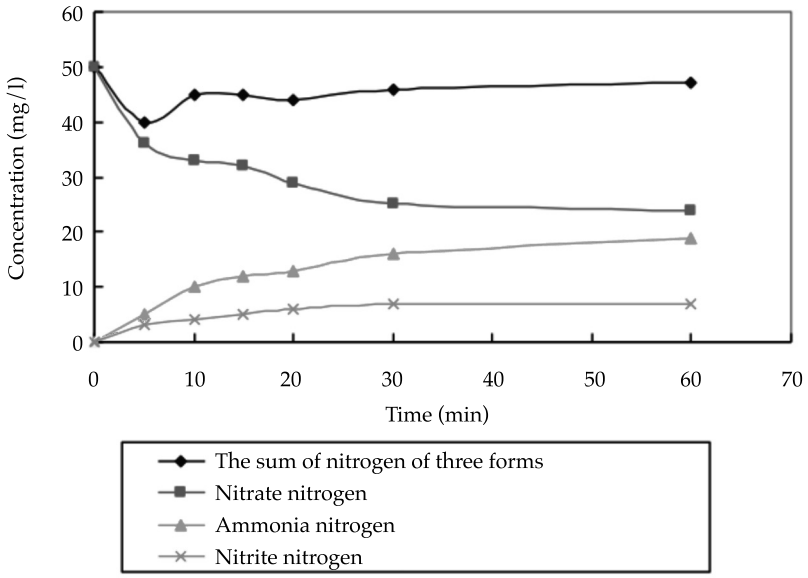

Figure 7. Production of nitrate´s deoxidization by nanoscale iron (at a constant temperature and pH of 25 °C and 7.0.).

nitrogen was converted to ammonia and nitrite nitrogen, which were later removed. As shown in equations (5) and (6), under the neutral reaction conditions, most of the nitrate nitrogen was converted to ammonia. Thus, the nitrate nitrogen was primarily reduced to ammonia. The standard electrode potential of the Fe^0 and its oxidation-reduction reaction with Fe^{2+} within the liquid solution (Fe^0/Fe^{2+}) was approximate -0.440 V, indicating that Fe^0

is a strong reducing agent of substances that can be easily reduced, such as H^+, CO_3^{2-}, SO_4^{2-}, NO_3^-, and O_2 (Schlieker *et al*., 2000). In the Fe–NO_3^- system, Fe^0 acts as the reductant and loses electrons, while NO_3^- acts as the oxidant and gains electrons. The NO_3^- gains electrons released by the Fe^0 as well as the oxidation products of the Fe, including Fe^{2+} and H_2. According to thermodynamics, Fe^0 could be converted into Fe^{2+} after losing electrons, and NO_3^- is reduced to N_2. Therefore, Fe^0 can completely reduce NO_3^-, but the reduction products of NO_3^- are determined by the reaction conditions (Agrawal & Tratnyek, 1996).

Conclusions

1. When nitrate-nitrogen removal was performed with different concentrations of nanoscale iron, lower nitrate nitrogen concentrations were associated with increased removal. This was primarily influenced by the adsorption site of the nanoscale iron.
2. Under acidic conditions, the nanoscale iron exhibited the highest adsorption ability and maximum nitrate-nitrogen removal when the pH of the solution was 2.0.
3. The temperature of the solution influenced the reaction rate. The kinetic equation $C_t = C_0 - k_t C^2_a / 1 + k_t C_a$ was developed based on the experimental data. According to the equation, the reaction rate constant k was highest with a value of 0.014 mg/(l/min) at 50 °C.
4. By calculating the value of the reaction rate constant k at different temperatures, the reaction activation energy *Ea* was determined to be approximately 17.18 kJ/mol. The results indicated that the reaction was primarily affected by the mass transfer of the solution.
5. Under neutral conditions, the reaction product of the nitrate nitrogen solution was ammonia.

Acknowledgments

This project was supported by the National Natural Science Foundation of China (40871005). This project was supported by the "Simulation and regulation of nitrogen and phosphorus transfer in small drainage basins on the periphery of urban areas" research program, which is funded by the Thirteenth Five-Year Scientific Research Program of the Jilin Province Department of Education. This project was funded by the Scientific Research Foundation of the Changchun University of Science and Technology.

References

Agrawal, A., & Tratnyek, P. G. (1996). Reduction of nitroaromatic compounds by zero-valent iron metal. *Environmental Science and Technology*, 30, 153-160.

Chen, S. Y., & Wu, X. F. (2009). Summarization on the remediation technologies of nitrate-contaminated groundwater. *Journal of Irrigation and Drainage*, 28, 124-127.

Cheng, I. F., Muftikian, R., Fernando, Q., & Korte, N. (1997). Reduction of nitrate to ammonia by zero-valent iron. *Chemosphere*, 35, 2689-2695.

Chew, C. F., & Zhang, T. C. (1998). In situ remediation of nitrate-contaminated groundwater by electrokinetics/iron wall process. *Water Science and Technology*, 38, 135-146.

Choe, S., Chang, Y. Y., Hwang, K. Y., & Khim, J. (2000). Kinetics of reductive denitrification by nanoscale zero-valent iron. *Chemosphere*, 41, 1307-1311.

Chunm, S., & Robert, W. P. (2004). Nitrate reduction by zero-valent iron effects of formate, oxalate, citrate, chloride, sulfate, borate, and phosphate. *Environmental Science and Technology*, 38, 2715-2720.

Fan, B., Qu, J. H., Liu, S. X., & Meng, G. H. (2000). Removal of nitrate in drinking water. *Techniques and Equipments for Environmental Pollution Control*, 1, 44-50.

Fan, X. M., Guan, X. H., Ma, J., & Ai, H. (2009). Kinetics and corrosion products of aqueous nitrate reduction by iron powder without reaction conditions control. *Journal of Environmental Sciences*, 21, 1028-1035.

Huang, C. P., Wang, H. W., & Chiu, P. C. (1998). Nitrate reduction by metallic iron. *Water Research*, 32, 2257-2264.

Kapoor, A., & Viraraghavan, T. (1997). Nitrate removal from drinking water review. *Journal of Environmental Engineering and Science*, 123, 371-380.

Kanel, S. R., Manning, B., Charlet, L., & Choi, H. (2005). Removal of arsenic (III) from groundwater by nanoscale aero-valent iron. *Environmental Science and Technology*, 39, 1291-1298.

Lien, H. L., & Zhang, W. X. (2001). Nanoscale iron particles for complete reduction of chlorinated ethenes. *Colloids and Surfaces A*., 191, 97-105.

Lien, H. L., Jhuo, Y. S., & Chen, L. H. (2007). Effect of heavy metals on dechlorinating of carbon tetrachloride by iron

• ISSN 2007-2422

nanoparticles. *Environmental Engineering Science*, 24, 21-29.

Liou, Y. H., Lo, S. L., & Lin, C. J. (2005). Chemical reduction of an unbuffered nitrate solution using catalyzed and uncatalyzed nanoscale iron particles. *Journal of Hazardous Materials* B., 127, 102-110.

Martin, J. E., Herzing, A. A., Yan, W. L., Li, X. Q., Koet, B. E., Kiely, C. J., & Zhang, W. X. (2008). Determination of the oxide layer thickness in core-shell zero-valent iron nanoparticles. *Langmuir*, 24, 4329-4334.

Michael, J. A., & Michellem, S. (2002). Kinetics of nitrate-nitrite and Cr (VI) reduction by iron metal. *Environmental Science and Technology*, 36, 299-306.

Molly, M. M., Daniel, L. C., Peter, J. V., Tamar, K., Adam, C. G., & Laura, A. L. (2003). Applications of surface analysis in the environmental sciences: Dehalogenation of chlorocarbons with zero-valent iron and iron-containing mineral surfaces. *Analytica Chimica Acta*, 496, 301-313.

Murphy, A. P. (1991). Chemical removal of nitrate from water. *Nature*, *350*, 223-225.

Philips, B., & Laura, G. (1992). Science at the atomic scale. *Nature*, 355, 760-761.

Ponder, S. M., Darab, J. G., & Mallouk, T. E. (2000). Remediation of Cr (VI) and Pb (II) aqueous solutions using supported nanoscale zero-valent iron. *Environmental Science and Technology*, 34, 2564-2569.

Schlieker, O., Ebert, M., Fruth, M., Weidner, M., Wust, W., & Dahmke, A. (2000). Degradation of TCE with iron: The role of competing for chromate and nitrate reduction. *Ground Water*, 38, 403-409.

Seunghee, C., Howard, M., & Li, L. (2004). Nitrate reduction by zero-valent iron under different pH regimes. *Applied Geochemistry*, 19, 335-342.

Siantar, D., Schreier, C. G., Chou, C. S., & Reinhard, M. (1996). Treatment of 1, 2-dibromo-3-chloroproprane and nitrate contaminated water with zero-valent iron or hydrogen/palladium catalysts. *Water Research*, 30, 2315-2322.

Song, Y. J., & Song, S. F. (2015). Preparation, characterization, and kinetics of nanoscale iron in nitrate nitrogegen removal from polluted water. *Toxicological & Environmental Chemistry*, 97, 379-387.

Tratnyek, P. G., Johnson, T. L., & Scherer, M. M. (1996). Kinetics of halogenated organic compound degradation by iron metal. *Environmental Science and Technology*, 30, 2634-2640.

Wang, C. B., & Zhang, W. X. (1997). Nanoscale metal particles for dechlorination of TCE and PCBs. *Environmental Science and Technology*, 31, 2154-2156.

Wang, W., Jin, Z. H., Li, T. L., Zhang, H., & Gao, S. (2006). Preparation of spherical iron nanoclusters in ethanol-water solution for nitrate removal. *Chemosphere*, 65, 1396-1404.

Yuan, C., & Lien, H.L. (2006). Removal of arsenate from aqueous solution using nanoscale iron particles. *Water Quality Research Journal of Canada*, 41, 210-215.

Yang, G. C., & Lee, H. L. (2005). Chemical reduction of nitrate by nanosized iron: Kinetics and pathways. *Water Research*, 39, 884-894.

Zhang, W. X., Wang, C. B., & Lien, H. L. (1998). Treatment of chlorinated organic contaminants with nanoscale bimetallic particles. *Catalysis Today*, 40, 387-395.

Zhang, H., Jin, Z. H., Han, L., & Qin, C. H. (2006). Synthesis of nanoscale zero-valent iron supported on exfoliated graphite for removal of nitrate. *Transactions of Nonferrous Metals Society of China*, 16, 345-349.

Author´s institutional address

Ph.D. Yujia Song

Changchun University of Science and Technology
Department of Environmental Engineering
Changchun, PR China
No. 156C-2-402, Huxi Road,
Changchun City, PR China
Telephone: +86 13596171347
jlsongyujia@126.com

Professor Shoufa Song

Northeast Coal Industry Institute of Environmental Protection
Changchun, PR China
No. 1566, Boxue Road, Changchun, City,
PR China
ccssf0431@163.com

Haga clic aquí para escribir al autor

ISSN 2007-2422

Feria de artesanías en Beijing, China.

Foto: Fernando Leyva Calvillo.

Research on the hydrologic cycle characteristics using stable isotopes of oxygen and hydrogen in the Jinxiuchuan Basin

• Tong Wang • Zhenghe Xu* •
University of Jinan, China
*Corresponding author

• Shengdong Zhang •
Beijing Zhongshui Runke Certification Co., Ltd., China

• Lizhi Zhang • Zhiqiang Zhao •
University of Jinan, China

Abstract

Wang, T., Xu, Z., Zhang, S., Zhang, L., & Zhao, Z. (March-April, 2017). Research on the hydrologic cycle characteristics using stable isotopes of oxygen and hydrogen in the Jinxiuchuan Basin. *Water Technology and Sciences* (in Spanish), 8(2), 105-115

Stable isotopes of oxygen ($\delta^{18}O$) and hydrogen (δD) in water were used as important indicators to research the hydrologic cycle or processes. To study the hydrologic cycle characteristics of the Jinxiuchuan basin, the isotope labelling and the industrial salt tracing method were used in this research. Sixty-seven samples of different water bodies were collected at different sampling sites from July 2011 to July 2012. The stable hydrogen and oxygen isotopes in water samples were measured by using Liquid Water Isotope Analyzer (LWIA-24d) to study the conversion relationship among precipitation, river water, soil water, and groundwater of the Jinxiuchuan basin in Jinan. The results show that δD and $\delta^{18}O$ varied from 35.6‰ to 128.3‰ and from 5.3‰ to 17.5‰, respectively. A meteoric water line of $\delta D = 7.16\delta^{18}O + 4.35$‰, which was in accordance with the global meteoric water line and the meteoric water line of China, was established in the Jinxiuchuan basin. The deuterium excess values vary with time and space, ranging from 5.1 to 22.3‰, and increase gradually from the southeast to the northwest. In addition, the exchange of different water bodies was determined preliminarily, the rates of precipitation transforming into river water, soil water, and groundwater are 43.76 21.91 and 6.84‰, and the remaining is 27.49‰ returned to the atmosphere. The results indicated the hydrologic cycle characteristics in the Jinxiuchuan basin. It may provide the references for precipitation isotopes research in semi-humid regions.

Keywords: Stable isotopes of hydrogen and oxygen; precipitation; deuterium excess; Jinxiuchuan basin.

Resumen

Wang, T., Xu, Z., Zhang, S., Zhang, L., & Zhao, Z. (marzo-abril, 2017). Estudio de las características del ciclo hidrológico empleando isótopos estables de oxígeno e hidrógeno en la cuenca de Jinxiuchuan. Tecnología y Ciencias del Agua, 8(2), *105-115.*

Se emplearon isótopos estables de oxígeno ($\delta^{18}O$) e hidrógeno (δD) en agua como indicadores importantes para comprender el ciclo hidrológico o sus procesos. Para comprender las características del ciclo hidrológico en la cuenca de Jinxiuchuan, en este estudio se empleó el método de marcaje isotópico y la técnica de trazabilidad de sal industrial. Se tomaron 67 muestras de distintos cuerpos de agua en diferentes sitios de muestreo de julio de 2011 a julio de 2012. Se midieron los isótopos estables de hidrógeno y oxígeno en las muestras de agua mediante el uso del Analizador de Isótopos en Agua Líquida (LWIA-24-d) para examinar el vínculo entre la precipitación, el agua de río, el agua de suelo y el agua subterránea de la cuenca de Jinxiuchuan, en Jinan. Los resultados muestran que δD y $\delta^{18}O$ variaron de 35.6 a 128.3 5‰ y de 5.3 a 17.5‰, respectivamente. La línea de agua meteórica se estableció en la cuenca de Jinxiuchuan, por ejemplo $\delta D = 7.16\delta^{18}O + 4.35$‰, lo cual concordó con la línea de agua meteórica global y la línea de agua meteórica de China. Los valores de exceso de deuterio varían en el tiempo y el espacio entre 5.1 y 22‰, y se incrementan gradualmente del sudeste al noroeste. Asimismo, se determinó preliminarmente el intercambio de distintos cuerpos de agua; los índices de precipitación que se transformaron en agua de río, agua de suelo y agua subterránea son de 43.76, 21.91 y 6.84‰, y el restante 27.49‰ regresó a la atmósfera. Los resultados indicaron las características del ciclo hidrológico en la cuenca de Jinxiuchuan, las cuales tienen valor de referencia para la investigación de isótopos en la precipitación en regiones semihúmedas.

Palabras clave: *isótopos estables de hidrógeno y oxígeno, precipitación, exceso de deuterio, cuenca de Jinxiuchuan.*

Received: 27/03/2016
Approved: 26/10/2016

Introduction

The hydrogen and oxygen stable isotopes in water are widely used as tracers in meteorology, hydrology, and hydrogeology (Bosilovich & Schubert, 2002; Wang & Xu, 2011). The stable isotopes fractionation run through the entire hydrologic cycle in large scale, and the environment change as well as the mixing of different water make the content of δD and $\delta^{18}O$ different from other water bodies (Zhang, Wu, & Wen, 2006; He *et al*., 2006). The isotopic ratios of hydrogen and oxygen in precipitation are closely related with meteorological processes and moisture sources. The δD and $\delta^{18}O$, particularly in the small-sized basin, are not only controlled by the climate change (Wu, Wan, & Lin, 2011; Wu, Yang, & Ding, 2011; Pan, Ping, & Gleixner, 2011), but also affected by the local meteorological and geographical conditions that make them change regularly with time and space (Price & Swart, 2008). In view of the composition of stable isotopes in precipitation, the main issues in this research field have focused on the temporal and spatial variation, the meteoric water line, deuterium excess, isotope effect and theoretical relations, and so on (Li, Zhang, & Ma, 2012). The research on hydrogen and oxygen studied in China had started in 1966, and observation stations of stable isotope were built up collect rainfall samples in large and medium-sized cities of China (Song, Liu, & Sun, 2007). Zhang and Wu (2007) analyzed the change of $\delta^{18}O$ in precipitation based on the rainfall samples and meteorological data, the results showed that $\delta^{18}O$ was affected by season, altitude, rainfall and temperature effects. Liu, Tian and Yao (2009) analyzed the relationships of $\delta^{18}O$ in precipitation with latitude and altitude, and established a quantitative relationship.

The data of stable isotopes in precipitation presented a seasonal distribution in the semi-arid and semi-humid region in China (Tian & Yao, 2004). However, the research on the stable isotopes of atmospheric precipitation in monsoon climate mountain area was relatively less than others so far. In view of the current status of the research in this field, this paper aimed to the following parts: (1) the variation of stable isotopes in atmospheric precipitation; (2) the establishment of local meteoric water line equation, and (3) the conversion rates of precipitation into surface water, groundwater, and soil water. Meanwhile, some insights to the water cycle mechanism in the semi-humid region will be added in this research. This paper may provide technical support for the establishment of the eco-hydrologic model and the sustainable management of water resources.

Material and methods

Site description

The study area is located in the southern mountainous area of Jinan, Shandong Province. The area of the drainage basin is 528.2 km^2 with a total river length of 41.63 km (figure1). There are two reservoirs, Jinxiuchuan Reservoir and Wohushan Reservoir, in the study area. The Jinxiuchuan Reservoir is located in the midstream, and the other one in the downstream. The total storage capacity is 0.6 billion m^3. They are not only the main drinking water sources of the resident population but also the recharge area of rivers, lakes, and springs of Jinan.

The climate is of the semi-humid warm temperate continental monsoon type with annual average precipitation of 703.1 mm. According to the survey, there are few historical precipitation of spring (April) and autumn (October) in Jinxiuchuan Basin, and maximum precipitation is 0.8 mm occasionally. Summer is generally from late May to early September. The average temperature is about 25.1 °C and the extreme maximum temperature is more than 40 °C. The average rainfall is about 380 mm that over 83% of the annual rainfall due to the warm moist air flow from the sea. Winter is generally from late November to early March of the following year. Due to the continental polar air masses, the average temperature of the region in winter is about 2 °C, and rainfall is about 6 to 15 mm, which occupies only 6-11% of the annual

• ISSN 2007-2422

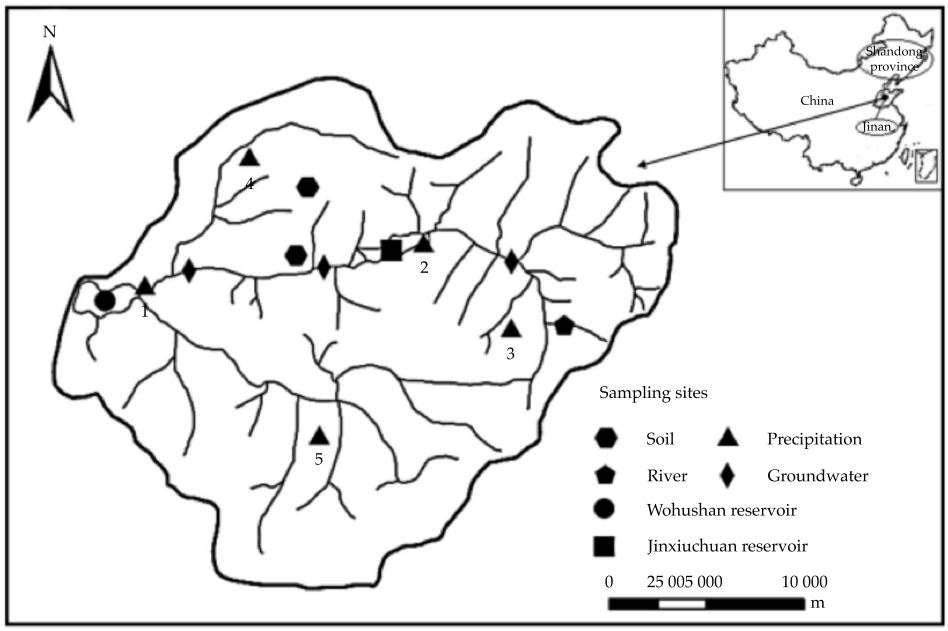

Figure 1. The map of the study area and sampling sites (1 Zhonggong; 2 Jinxiuchuan watershed; 3 Ouchi; 4 Zhengjia; 5 Liubu).

rainfall. The transitional seasons of spring and autumn are both less than two months. The Jinxiuchuan Basin's climate is characterized by spring the dry multi-winds, the winter snow.

The Jinxiuchuan basin basement is Archean Taishan Group metamorphic rock, which terrain slopes downward from the south to the north. The rock stratum is monoclinic occurrence without obvious folds. The basin mainly includes Cambrian and Ordovician, which are limestone. The surface dissolution is well developed with karren, slot, dissolving fissure, and so on. It has good connectivity, which can be propitious to recharge groundwater in the Jinxiuchuan basin.

Sample collection and analysis method

Sampling methods

Water samples of precipitation, river water, soil and groundwater, as show in figure 1, were collected from July 2011 to July 2012. After each precipitation event, rainfall samples in all sites were collected, which were obtained by rainwater tanks. In order to avoid isotope fractionation, each rainfall sample was stocked in a 150 ml sealed brown vial and placed in the dark at a lower temperature.

To ensure the accuracy of water samples of river and groundwater, the implementation of sampling must strictly enforce according to Assurance Manual of Environmental Water Monitoring Quantity (China National Environmental Monitoring Centre Assurance, 2010). Water specimens were collected by using polyethylene bottle of acid-washed. During sampling procedure, firstly, the bottles were washed three times by using raw water, then samples were collected at the sampling sites. To avoid the isotopic fractionation of the sample, firstly, samples were collected below the surface, then the air in the bottle was vented, and the samples were stored in an airtight; finally, the samples were sent to a laboratory to analyze under refrigerated conditions.

According to characteristics of topsoil in the Jinxiuchuan Basin, the soil samples were collected from five different depths (0-10 cm,

10-20 cm, 20-25 cm, 25-30 cm, 30-35 cm). The collect private collector of soil was employed to store it, to avoid isotope fractionation, the samples were sealed in a cool place. In the end, 67 samples of different water bodies were collected for analyzing the composition of hydrogen and oxygen stable isotopes.

Analysis method

Water samples were analyzed by using Liquid Water Isotope Analyzer (LWIA-24d, Los Gatos Research, USA) at the Key Laboratory for Yellow River Delta Ecological Environment of Shandong Province. Based on the international V-SMOW standard, isotope value was marked by δ (‰). δ refers to thousand points of difference between the ratios of the two measured stable isotopes and the standard (Craig, 1961), as the following Eq. (1):

$$\delta‰ = \frac{R_{\text{sample}} - R_{\text{standard}}}{R_{\text{standard}}} \times 10^3 \quad (1)$$

Where R is the isotope ratio (D/H or $^{18}O/^{16}O$), the positive and negative value of δ indicated that the sample is richer in the heavy isotope and light isotope than the standard, respectively. The precision of the D/H is within ± 0.6‰, and $^{18}O/^{16}O$ within ± 0.2‰.

The calculation of weighted average is showed in the following. As a starting point, suppose that there are X samples, and they are X_1, X_2,…, X_i (I = 1, 2, 3… n). Every sample (X_i) contains a certain amount of Y_i. The weighted average of Y is called Y', and the formula as follow:

$$Y' = \frac{\sum_{i=1}^{n}(X_i * Y_i)}{\sum_{i=1}^{n}(X_i)} \quad (i = 1, 2, 3\ldots n) \quad (2)$$

Water retention and renewal time is an important link in the transformation process of water in the phreatic water aquifer. The two end-member isotope mixing model is used to part water sources. Given that mixed water (sample) comprises well mixed M and N water samples, the proportions of M and N in the sample can be derived from a conventional two end-member mass-balance equation in terms of δ values:

$$Q_{\text{sample}}\delta_{\text{sample}} = Q_M\delta_M + Q_N\delta_N \quad (3)$$

$$Q_{\text{sample}} = Q_M + Q_N \quad (4)$$

$$X_M = \frac{Q_M}{Q_{\text{sample}}} \quad (5)$$

Where X_M and X_N are the fractions of M and N in the sample, respectively.

The solution for X_M is:

$$X_M = \frac{\delta_{\text{sample}} - \delta_N}{\delta_M - \delta_N} \quad (6)$$

Results and discussion

Variations of δD and $\delta^{18}O$ of the Jinxiuchuan Basin

From July 2011 to July 2012, the basic information of precipitation, temperature and relative humidity was measured and showed in figure 2. The results showed that: precipitation and temperature have obvious seasonal variations. The average monthly relative humidity gradually decreases from February. The lowest value is about 36% in April or May, the maximum value of 89% in August. However, the value of relative humidity in September decreases again, and the difference between maximum and minimum value is 53% in figure 2.

The data of stable isotopes in precipitation was employed to research its change in the local region. The characteristic values of isotopiciso-topic included the weighted average value of δD, $\delta^{18}O$ and deuterium excess in each sampling

• ISSN 2007-2422

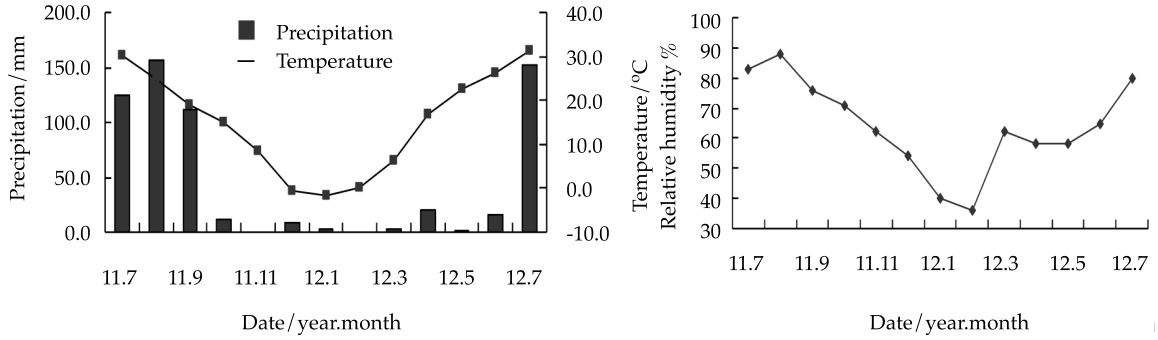

Figure 2. The monthly rainfall, temperature and relative humidity from 2011.7 to 2012.7.

Table 1. Atmospheric precipitation details in the Jinxiuchuan Basin.

Sampling points	Location	Height (m)	Time	Average monthly Temperature (°C)	Relative humidity (%)	Average monthly rainfall (m)	Weighted average value (‰)		*d*-excess (*d*) (‰)
							δD	$\delta^{18}O$	
1	117.01°E	127	Summer	26	78	76	-61.5	-8.9	9.7
	36.49°N		Winter	1	54	8	-109.3	-15.6	15.5
2	117.17°E	240	Summer	27	82	124.2	-54.4	-7.9	8.8
	36.51°N		Winter	2	50	19	-87.8	-12.8	14.6
3	117.22°E	360	Summer	27	86	156.1	-44.9	-6.4	6.3
	36.47°N		Winter	2.5	55	26	-92.9	-13.6	15.9
4	117.07°E	285	Summer	26	66	69	-63.1	-9.1	9.7
	36.55°N		Winter	0	43	21	-113.8	-16.3	16.6
5	117.11°E	261	Summer	27	74	51	-62.7	-9	9.3
	36.42°N		Winter	1	41	2	-116.6	-15.8	9.8

site (Wu *et al.*, 2011a y b; Zhai, Wang, & Teng, 2011), as shown in table 1. Summer precipitation is from June to September, and the winter precipitation is from November through the following March. April, May, and October are the major time of transmission for water vapor. The local evaporation is relatively slow with low surface temperature, and cannot form effective precipitation. In order to avoid replication of the season samples, the precipitation data of these three months are not used for comparison.

According to the isotope data, δD in atmospheric precipitation is within the limits of -128.3 to -35.6‰, averaging -79.8‰, while $\delta^{18}O$ range from -17.5‰ to -5.3‰, with the average of -11.3‰. Comparing the two isotope values, the change of $\delta^{18}O$ is smaller than δD. The reason is mainly that the fractionation effect of hydrogen isotope is much better than oxygen isotope. Zheng, Hou and Ni (1983) reported that δD range from -210‰ to 20‰, and $\delta^{18}O$ from -24‰ to 2.0‰ in precipitation of China. In the study area, the stable isotopes content belong to the ranges of China and the global atmospheric precipitation, and the average values are smaller than both of them.

The weighted average values of δD and $\delta^{18}O$ in precipitation were obtained by the precipitation-weighted method, to get the seasonal variation law of the isotope values, as shown in

ISSN 2007-2422

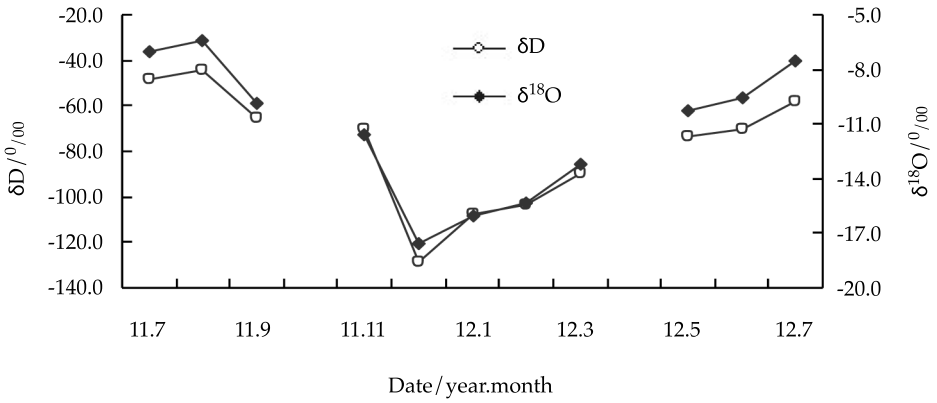

Figure 3. Changes of δD and δ18O in precipitation with time from 2011.7 to 2012.7.

figure 3. The results indicated that δD and $\delta^{18}O$ have an obvious change with the season, and the maximum values of δD and $\delta^{18}O$ occurred in July and August (wet season) were -35.6‰ and 5.3‰, respectively; and their average values were -43.8‰ and -7.6‰, respectively. The minimum δD and $\delta^{18}O$ occurred in November and December (the dry season) were -128.3‰ and -17.5‰, respectively, and the average were -122.6‰ and -15.3‰, respectively.

The isotope values shown in figure 3 has great difference between summer and winter, and it indicated the precipitation was controlled by different water sources. The basin has a typical monsoon climate and is affected by the warm moist air flows from the sea, and the rainy days and precipitation amount are mainly concentrated in summer. It results in the enrichment of heavier isotopes, therefore, the values of δD and $\delta^{18}O$ become larger. However, the polar continental air mass is prevailing in winter, and the weather is dry and wintry. As the vapor pressure of isotope is inversely proportional to the mass number, heavy isotopes were condensed preferentially with transported of water vapor, and it led to δD and $\delta^{18}O$ dilution in precipitation. The reason eventually made δD and $\delta^{18}O$ decrescent in winter precipitation. Precipitation was invalid in April and October for analyzing isotopes. In history, the rainfall amount of April and October is little in the Jinxiuchuan Basin. Results from figure 3 indicated that sampling sites are the most representative.

Meteoric water line of the Jinxiuchuan Basin

The relationship between δD and $\delta^{18}O$ of precipitation is generally referred to the meteoric water line (MWL), which is of great significance to study the isotope changes in the water cycle (Li, Li, & Shen, 2010). Craig (1961) initially put forward for the global meteoric water line (GMWL) equation: $\delta D = 8\delta^{18}O + 10‰$, the average value of GMWL is 10‰. When the values are less than 10‰, the imbalanced degree of the gas and liquid isotopic fractionation has a big impact on the formation of clouds. If it is less than 10‰, the evaporation plays a significant role during the precipitation process. According to the 107 rainfall samples of isotopes, Zheng Shuhui et al. (1983) obtained the meteoric water line in China(CMWL): $\delta(D) = 7.9\delta^{18}O + 8.2‰$. The local meteoric water line (LMWL) equation is as follows: $\delta D = 7.16\delta^{18}O + 4.35‰$, $R^2 = 0.92$.

The LMWL of the Jinxiuchuan Basin is close to GMWL and CMWL, as shown in figure 4. But the slope and intercept of the former line are lower than those of the latter, due to the impact of evaporation. The δD and $\delta^{18}O$ values of

• ISSN 2007-2422

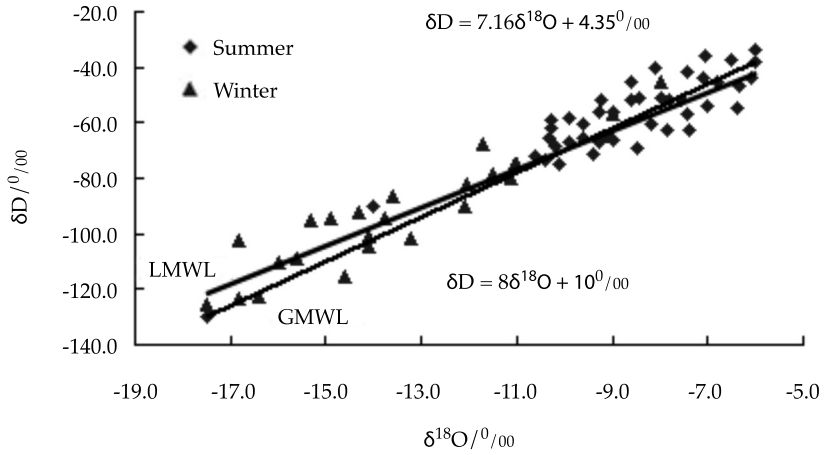

Figure 4. The relationship between δD and δ18O in precipitation.

precipitation are mainly distributed in -90‰ ~ -30‰ and -11‰ ~ -5‰ in summer, respectively. The variation ranges of δD and $\delta^{18}O$ of precipitation are -130‰ ~ -70‰ and -17.5‰ ~ -12.8‰ in winter respectively, influenced by evaporation. Most of the isotope values are higher in summer than those in winter from the figure 4.

Deuterium excess analysis (d-*excess*)

Deuterium excess (*d*-excess), referred to as *d* value, is put forward by Dansgaard (1964), the formula for $d = \delta D - 8\delta^{18}O$. Different values reflect the disparate unbalanced degree of evaporation and condensation process in the region intuitively. It also shows the relationship between d and evaporation rate in the region of the moisture source. In other words, the higher evaporation, the greater the value of *d*. It is actually an important comprehensive environmental index of atmospheric precipitation (Wang, Chen, & Wang, 2009). According to the linear relationship between *d* values and isotopes, the former is considerably affected by temperature, humidity, rainfall and secondary evaporation within the region. Generally, global average *d* value is 10‰. The process of the water cycle is mainly affected by evaporation in one region, and *d* value is greater than 10‰ in general.

In the study area, vapor sources of precipitation have different sources in summer and winter due to the monsoon, which led to higher *d* value in winter than summer. In addition, the *d* values of different sampling sites along the direction of the clouds movement are different. There is little precipitation at Zhonggong and Liubu sampling sites, therefore it is not discussed. The changes of *d* value at Zhengjia, Jinxiuchuan Reservoir, and Ouchi sampling sites from July 2011 to July 2012 are shown in figure 5. The *d* values vary from 5.1 to 22.3‰ throughout the year. It ranges from 5.1 to 10‰ in summer (from June to September), the average is 7.9‰, and the maximum is less than 10‰. The results indicated that the area is mainly controlled by marine air masses in summer. However, *d* values are higher in winter (from December to March), with the range 12.8 to 22.3‰, and an average of 14.0‰, which is higher than summer. It showed that the *d* value is mainly affected by polar air masses in winter.

Due to the monsoon climate, the ocean warm air masses firstly move to the Jinxiuchuan Basin in summer, and then pass the Ouchi sampling site located in the southeast. The isotope data of Ouchi represent the initial summer precipitation data, the *d* value of 5.1‰; *d* values tends to increase from southeastern

ISSN 2007-2422

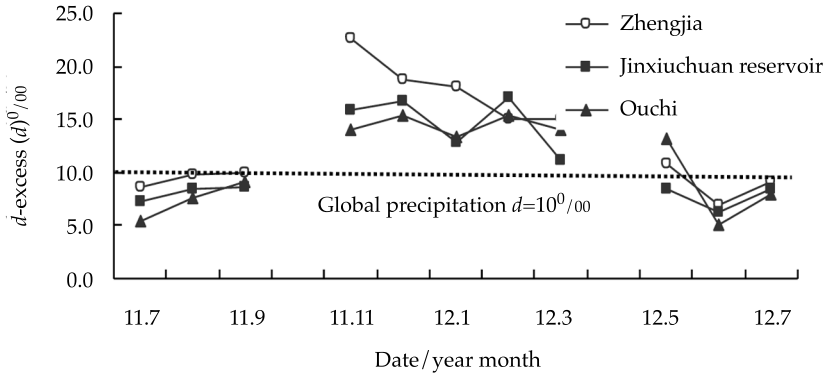

Figure 5. Change curve of deuterium excess from 2011.7 to 2012.7.

(Ouchi) to northwestern (Zhengjia), range from 5.1 to 7.0‰. In winter, the polar continental air masses first reach to Zhengjia rainfall station located in the northwest and the isotope data can represent the initial winter precipitation data, *d* value is 22.3‰; *d* values tends to decrease from Zhengjia to Ouchi, range from 22.3 to 12.8‰.

Analysis of conversion relationship among different water

Hydrogen and oxygen isotopes are used to mark atmospheric precipitation, river water, Spring water (groundwater) and soil water. According to the representative sample data of 37 groups, the isotope compositions in different water were compared, and the transforming relationships were determined.

As showed in figure 6, $\delta^{18}O$ values of river water are near the atmospheric precipitation line with a small deviation, and these points scatter between the values of precipitation and groundwater of the Jinxiuchuan Basin. It indicated that supply components for the river are consistent with the river components. The study area belongs to mountain and hilly area, whose area is small so that atmospheric precipitation mainly transforms into surface water and groundwater. Those are the main supply source of the river.

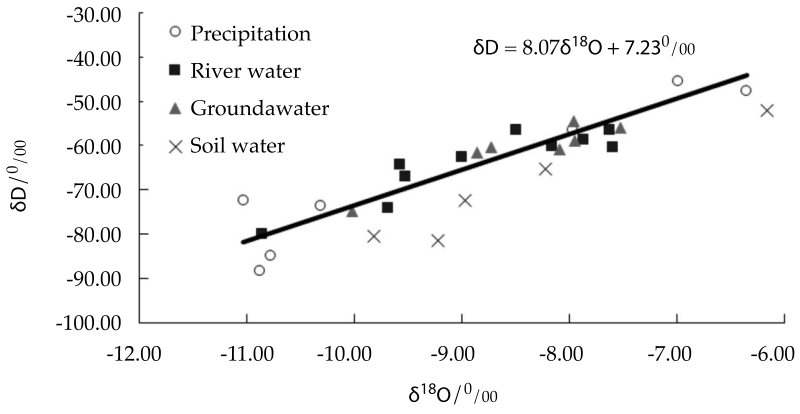

Figure 6. Analysis of isotope composition in different water.

• ISSN 2007-2422

The $\delta^{18}O$ values of groundwater and river water have a high degree of fitting, and the $\delta^{18}O$ values of groundwater are mainly distributed among the $\delta^{18}O$ values of precipitation, as shown in figure 6. The results showed that there are close relationships in different water bodies. The soil thickness is small and the average of about 20 cm, and a rigid top slab of the impermeable floor. However, karren, slot, dissolving fissure develop extraordinary in the Jinxiuchuan Basin, so as to the more frequent hydraulic contact between groundwater and precipitation.

In the Jinxiuchuan Basin, the river is supplied by precipitation in the form of overland flow, and soil water and groundwater from infiltration of precipitation. Groundwater exposes on the surface and supplies river by spring. River evaporates in the process of flow and then returns into the atmosphere. The water cycle is completed between different water bodies finally. According to equation (6) and take $\delta^{18}O$ for example, δ_M is the value of precipitation, $\delta^{18}O$ = -7.9713‰; δ_N is the value of groundwater, $\delta^{18}O$ = -8.8895‰; δ_{sample} is the value of river water, $\delta^{18}O$ = -8.4877‰. After calculation, precipitation accounts for 43.76% in river water. In the same way, precipitation accounts for 21.91% in soil water and 6.84% in groundwater, as shown in table 2. The δD and $\delta^{18}O$ of river water increase from valley to outlet because of the weak evaporation, and the river is supplied by groundwater. It is confirmed by field investigation that three springs expose to supply surface water, which makes groundwater convert into surface water. So the proportion of river water transformed by soil water and groundwater is 28.75%. The total supply ratio is 72.51%, and the remaining is 27.49%. The remaining water consumed by surface evaporation and plants intercept, which can be understand as the soil water and river water reverse supplemental atmospheric water.

Based on the relevant data of the Jinan's hydrological bureau, the above conclusions are verified by the water balance method. Taking precipitation and river as an example, the conversion relationship between rainfall and river water are analyzed based on the precipitation of August 25, 2011. There are five precipitation monitoring sites, and the average precipitation is 55.2 mm. The watershed total rainfall is calculated by the Thiessen polygon method, and the value is $2976.66\times10^4 m^3$. River runoff is calculated based on the data of river level before and after this precipitation, and it is $1254.36\times10^4 m^3$. The river section is downstream in the Jinxiuchuan Basin. The ratio of between rainfall and river water is 42.14%. The results showed that the precipitation accounts for 42.14% in river water, and the results obtained from two methods are close to each other. Meanwhile, it indicated that the previous conclusion which obtained from the stable isotopes method is scientific and rational.

Atmospheric precipitation is absorbed or becomes surface runoff, which gradually flows into rivers. Surface water partly evaporates and infiltrates into the soil to recharge groundwater. The atmospheric precipitation converts into surface runoff and underground runoff eventually through a series of processes, and groundwater changes into surface water. From table 2, the conversion rate of groundwater is high in the slope runoff area of the Jinxiuchuan Basin. The study area has strong ability to intercept and store water, because it has higher vegetation coverage. Karren, slot and dissolving fissure well developed, which leads to increase the number of infiltration recharge to groundwater in the slope zone.

Table 2. Supply ratio of atmospheric precipitation.

Water type	δ value		Supply ratio
	δD/‰	$\delta^{18}O$/‰	of atmospheric precipitation /%
Soil water	-72.3637	-8.9569	21.91
Groundwater	-74.9468	-8.8895	6.84
River	-56.5361	-8.4877	43.76

ISSN 2007-2422

Conclusions

Rainfall samples were collected examined from July 2011 to July 2012 in the Jinxiuchuan Basin. The results showed that composition of hydrogen and oxygen stable isotopes within the range of δD and $\delta^{18}O$ in China and global atmospheric precipitation; δD in precipitation is within the limit of -128.3 to -35.6‰, and the average is -79.8‰; $\delta^{18}O$ ranges from -17.5 to -5.3‰, and the average is -11.3‰. The local meteoric water line is $\delta D = 7.16\delta^{18}O + 4.35‰$ (R^2 = 0.92), which slope and intercept are both less than the global meteoric water line due to the impact of evaporation in the Jinxiuchuan Basin. Values of d-excess vary with time and space. On the one hand, *d* values are higher in winter than summer due to the impact of different air masses. From here, the following are divided into the second paragraph. The conversion relationships and rates of different water bodies are determined preliminarily in water cycle process of the Jinxiuchuan Basin. Results as follows: the rates of precipitation transforming into river water, soil water and groundwater are 43.76, 21.91 and 6.84%, respectively. The rates of groundwater transforming into river water is 28.75%, and 27.49% of the surface water supplies the atmosphere by evaporation. Based on the the analytic result, the conversion relationships and rates of different water body of the hydrologic cycle in the Jinxiuchuan Basin are initially determined.

Acknowledgments

Research funding was provided by the National Sci-Tech Support Plan (grant no. 2012BAD08B05 and 2015BAD20B02), the Shandong Province Water Conservancy Research and Technology Promotion Projects (grant no. SDSLKY201410), the Graduate Innovation Foundation of University of Jinan (grant no. GIFUJN). Many thanks to Teacher YongSen Wang at the University of Jinan for assistance with statistical analysis, and the editors and anonymous reviewers who provided essential guidance on previous versions of this manuscript.

References

Bosilovich, M. G., & Schubert, S. D. (2002). Water vapor tracers as diagnostics of the regional hydrologic cycle. *Journal of Hydrometeorology*, 3, 149-165.

China National Environmental Monitoring Centre Assurance (2010). *Manual of Environmental Water Monitoring Quantity Writing Group 2010. Assurance Manual of Environmental Water Monitoring Quantity*. Beijing: Chemical Industry Press.

Craig, H. (1961). Standards for reporting concentrations of deuterium and oxygen-18 in natural waters. *Science*, 133, 1833-1834.

Dansgaard, W. (1964). Stable isotopes in precipitation. *Tellus*, 16, 436-468.

He, Y. Q., Pang, H. X., Theakstone, W. H. *et al*. (2006). Isotopic variations in precipitation at Bangkok and their climatological significance. *Hydrological Process*, 20, 2873-2884.

Li, Y. Y., Li, H. C., & Shen, C. Z. (2010). Study on the δD and $\delta^{18}O$ characteristics of meteoric precipitation during 2006-2008 in Chongqing China. *Advances in Water Science*, 21, 757-764.

Li, X. F., Zhang, M. J., & Ma, Q. (2012). Characteristics of stable isotopes in precipitation over northeast China and its water vapor sources. *Environmental Science*, 33, 2924-2931.

Liu, Z. F., Tian, L. D., & Yao, T. D. (2009). Spatial distribution of $\delta^{18}O$ in precipitation over China, *Chinese Science Bulletin*, 54, 804-811.

Pan, L., Ping, A. P., & Gleixner, G. (2011). The empirical relationship between leaf wax n-alkane δD and altitude in the Wuyi, Shennongjia and Tianshan Mountains China. *Implications for Pale Altimetry Earth and Planetary Science Letters*, 301, 285-296.

Price, R. M., & Swart, P. K. (2008). Seasonal and spatial variation in the stable isotopic composition ($\delta^{18}O$ and δD) of precipitation in south Florida. *Journal of Hydrology*, 358, 193-205.

Song, X. F., Liu, J. R., & Sun, X. M. (2007). Establishment of Chinese network of isotopes in precipitation (CHNIP) based on CERN. *Advances in Earth Science*, 22, 738-747.

Tian, L. D., & Yao, T. D. (2004). A study of hydrogen isotope in precipitation in west China. *Glaciology and Geocryology*, 20, 75-79.

Wang, Y. S., Chen, J. S., & Wang, J. Y. (2009). Theoretical research on the relationship between deuterium and oxygen-18 in precipitation. *Advances in Water Science*, 20, 204-208.

Wang, Y. S., & Xu, Z. H. (2011). The study on the precipitation isotope characteristic and effect factor for the water cycle. *Water Resource and Environmental Protection*, 3, 2165-2167.

Wu, Y. Z., Wan, J. W., & Lin, Y. (2011a). Characteristics of hydrogen and oxygen isotopes for precipitation in Xiling Gorge Region of Yichang, Hubei Province, China. *Geological Science and Technology Information*, 30, 93-97.

Wu, J. K., Yang, Q. Y., & Ding, Y. J. (2011b). Variations and simulation of stable isotopes in precipitation in the Heihe River Basin, China. *Environmental Science*, 32, 1858-1866.

Zhai, Y. Z., Wang, J. S., & Teng, Y. G. (2011). Variations of δD and $\delta^{18}O$ in water in Beijing and their implications for the local water cycle. *Resources Science*, 33, 92-97.

Zhang, Y. H., Wu, Y. Q., & Wen, X. H. (2006). Application of environmental isotopes in the water cycle. *Advances in Water Science*, 17, 738-747.

Zhang, Y. H., & Wu, Y. Q. (2007). Characteristics of the $\delta^{18}O$ in precipitation in the upper and middle reaches of Heihe River. *Glaciology and Geocryology*, 29, 440-445.

Zheng, S. H., Hou, F. G., & Ni, B. L. (1983). Research of stable isotope in precipitation in China. *Chinese Science Bulletin*, 28, 801-806.

Author´s institutional address

M. Tong Wang
Ph.D. Zhenghe Xu
M. Lizhi Zhang
M. Zhiqiang Zhao

University of Jinan
School of Resources and Environment Jinan
No. 336 Nanxinzhuang Road, Shizhong District, Jinan City, Shandong Province, PR China
Telephones: +86 18766125036 / 0531-82769235 / 18764468590 / 15153128935
18766125036@163.com
xu4045@126.com
965778591@qq.com
1299324237@qq.com

M. Shengdong Zhang

Beijing Zhongshui Runke Certification Co., Ltd.
No. A1 Fuxing Road, Haidian District, Beijing, PR China
Telephone: +86 15698005533
409879082@qq.com

Haga clic aquí para escribir al autor

Calles de Beijing, China.

Foto: Fernando Leyva Calvillo.

Simulation for non-point source pollution based on QUAL2E in the Jinghe River, Shaanxi Province, China

• Jucui Wang •
Chang'an University/Key Laboratory of Subsurface Hydrology and Ecological Effect in Arid Region of Ministry of Education, China

• Aidi Huo* • Anyan Hu • Xuezhen Zhang •
Chang'an University, China
*Corresponding author

• Yanqing Wu •
Shanghai Jiaotong University, China

Abstract

Wang, J., Huo, A., Hu, A., Zhang, X., & Wu, Y. (March-April, 2017). Simulation for non-point source pollution based on QUAL2E in the Jinghe River, Shaanxi Province, China. *Water Technology and Sciences* (in Spanish), *8*(2), 117-126.

Water pollution in river basins is significantly influenced by point-source and non-point-source pollutants. Compared with point-source pollutants, the identification and quantification of non-point-source pollutants are critical but difficult issues in water environmental pollution studies. The Jinghe River is one of the main tributaries of the Weihe River. However, the non-point-source pollution of this river is not well understood. In order to analyze the sources of point- and non-point loads to river water, the river water quality model QUAL2E and Principal Component Analysis (PCA) & Factor Analysis (FA) were applied simultaneously to calculate the point- and non-point-source loads of ammonia nitrogen and nitrate nitrogen, respectively, in dry and wet seasons from 2002 to 2007. The results show that NO_3^--N can be associated with point-source pollution, such as domestic sewage in dry seasons, but non-point-source pollution generated by precipitation in wet seasons. NH_4^+-N can be associated with point-source pollution throughout the year. The methods applied in this research provide reliable results on non-point-source pollution caused by storm runoff.

Keywords: QUAL2E, degradation coefficient, source/sink term, non-point-source pollution.

Resumen

Wang, J., Huo, A., Hu, A., Zhang, X., & Wu, Y. (marzo-abril, 2017). Simulación de contaminación difusa mediante el modelo QUAL2E en el río Jinghe, provincia de Shaanxi, China. Tecnología y Ciencias del Agua, *8(2), 117-126.*

La contaminación del agua en cuencas hidrológicas tiene una fuerte influencia de contaminantes puntuales y difusos. En comparación con los contaminantes puntuales, la identificación y cuantificación de los contaminantes difusos es un tema de gran importancia, pero difícil, en los estudios de contaminación ambiental del agua. El río Jinghe es uno de los principales tributarios del río Weihe; sin embargo, la contaminación difusa de este río no se ha dilucidado del todo. Con el fin de analizar las fuentes de cargas puntuales y difusas hacia el agua del río se aplicaron simultáneamente el modelo QUAL2E, el Análisis de Componente Principal (PCA) y el Análisis de Factores (FA) para calcular las cargas puntuales y difusas de nitrógeno amoniacal y de nitrógeno nítrico, respectivamente, en las temporadas seca y húmeda de 2002 a 2007. Los resultados muestran que el NO_3N puede estar asociado con contaminación puntual, como la producida por aguas residuales domésticas en la temporada seca, pero con la contaminación difusa generada por la precipitación en las temporadas húmedas. El NH_4^+N puede estar asociado con la contaminación puntual durante todo el año. Los métodos aplicados en este estudio proporcionan resultados confiables en la contaminación difusa ocasionada por escurrimientos pluviales.

Palabras clave: *QUAL2E, coeficiente de degradación, término fuente/sumidero, contaminación difusa.*

Received: 01/03/2016
Approved: 26/10/2016

Introduction

The extensive expansion of agriculture, rapid urbanization, and large-scale industrialization in China over the past three decades were accompanied with inevitable side effects, including water pollution, which is getting more severe each year. Moreover, anthropogenic activities associated with the revival and development of the Silk Road can further aggravate the water pollution crisis (Li, Qian, & Wu, 2014; Li, Qian, Howard, & Wu, 2015). Noteworthy is that surface water pollution has two main sources: (a) point source pollutants, such as industrial wastes and domestic sewage, and (b) non-point source pollutants, such as pesticides, herbicides, and fertilizers from agricultural activities. In addition, pollutants may originate from recharge of poor-quality groundwater and deposition of atmospheric pollutants. Once entering the aquatic environment, these pollutants may alter the composition and functions of ecosystems, thereby leading to a series of irreversible ecological changes (Huo *et al.*, 2014). While the point source pollution can be monitored by routine procedures and techniques, the non-point source one is difficult to control because it comes from the everyday activities of many different people, such as fertilizing a lawn, using a pesticide, or constructing a road or building. The fact that non-point source pollution is dynamic and complex process, which usually covers extensive areas, makes it quite problematic to provide an accurate quantification of its spatial location, extent, and discharge volume (Chowdary, Rao, & Sarma, 2005).

In order to face this challenge, numerous researchers developed various models of the agricultural non-point source pollution, most of which are based on different land use patterns (Whitehead, Johnes, & Butterfield, 2002; Polyakov, Fares, Kubo, Jacobi, & Smith, 2007; Munafo, Cecchi, Baiocco, & Mancini, 2005). Although these models are clearly mechanistic, they require a large number of input data, and it is difficult to directly monitor some of the processes for which data are required. Pollutant mobilization processes and transport to the river network vary by region and river; studies that report model simulations at a range of spatial and temporal scales are also very scarce, so wide-spread application is constrained by both the variability in the landscape and lack of experience (Azzellino, Salvetti, Vismara, & Bonomo, 2006). We have made progress in non-point source pollution research in China by using software combined with remote sensing (RS) and Geographical Information Systems (GIS) (Feier, Huanchun, Yingxu, & Dong, 2003; Guihong & Jiangyong, 2007; Gao, Zhu, Zhou, Zhi, & Tang, 2008). However, these above methods are prone to large discrepancies when there are unique geographical features, complex landscape types, and diverse land use patterns in loess regions, which may, to a certain degree, bias the large-scale simulation results.

In this study, we used the River and Stream Water Quality Model (QUAL2E) developed by the United States Environmental Protection Agency (USEPA, 1992). We also used multivariate statistics principal component analysis (PCA) and factor analysis (FA) (Melching & Yoon, 1996; Wu, Li, Qian, Duan, & Zhang, 2014) to examine the sources of non-point pollution and to highlight the impacts of point and non-point source pollution on river water quality. The object of this study was the Shaanxi Reach of the Jinghe River in Shaanxi province of China. To provide a robust scientific basis for reducing water pollution in this area, the point source and non-point source loads of ammonia nitrogen and nitrate nitrogen between Jingcun and Zhangjiashan in dry and wet seasons are assessed.

Materials and methods

Study area

The Jinghe River originates in the eastern foothills of the Liupan Mountain, Jingyuan County, Ningxia Hui Autonomous Region. It enters

• ISSN 2007-2422

Shaanxi Province in Tangqu in Changwu County and merges with the Weihe River in Chenjiatan Village, Gaoling County. The Jinghe River is about 272.5 km long and it drains an area of 9 210 km^2 in Shaanxi Province (figure 1). In the Zhangjiashan section, the Jinghe Basin is mainly composed of a loess plateau and hilly gullies. The loess plateau region has a flat surface and is the agricultural center of the area, while the hilly-gully one is subjected to significant soil erosion promoted by high runoff rates and the relatively poor vegetation coverage. There are also small areas of stony soil and mountain forest in the Jinghe Basin. The area downstream from Zhangjiashan is dominated by river terraces. The average precipitation is 556 mm, but there is significant inter- and intra-annual variations in precipitation. Precipitation in the four months from July to October accounts for 56% of the annual precipitation. The industry is yet underdeveloped in this agricultural region, which is the main grain and cotton producer of Shaanxi province. However, in recent years, water quality has been steadily deteriorating in Shaanxi province because of the on-going industrial and agricultural developments.

River water quality model

Three main processes occur when pollutants enter a river, namely, flow migration, random diffusion at pollutant points, and transformation of pollutants (Beck, 1987). It is very difficult to find a solution for a non-steady multidimensional model, and furthermore, the analytical formula is very complex. However, recent studies have shown that one-dimensional steady models can solve the actual problems in many rivers. We used QUAL2E, the updated and improved version of the QUAL-I and II developed by the USEPA in the 1970s, for the simulation. It is based on the stream dispersion mass transfer equation that describes spatial and temporal changes in any water quality variable. In this equation, the source and sink caused by chemical, physical, and biological effects (including the impacts of the branch and discharge outlet) are included along with terms to describe flow migration and dispersion (Reckhow, 1999), as follows:

$$\frac{\partial(Ac)}{\partial t} = \frac{\partial}{\partial x}\left(D_x A \frac{\partial c}{\partial x}\right) - \frac{\partial(Qc)}{\partial x} \pm S^{\alpha} \qquad (1)$$

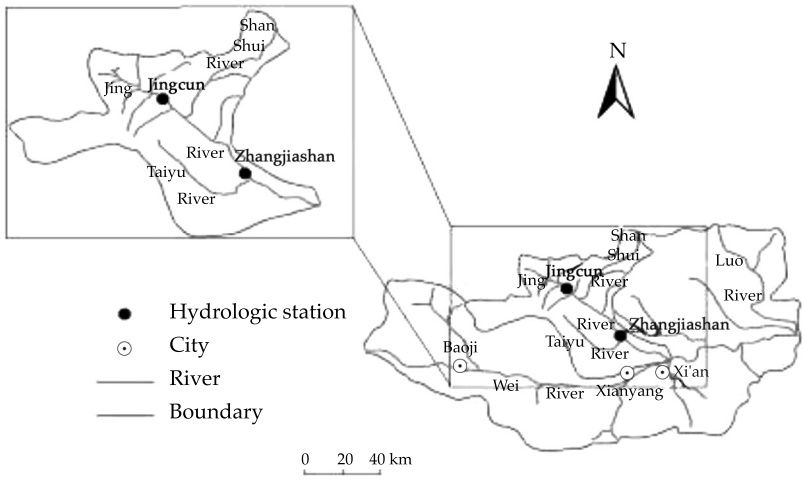

Figure 1. Jinghe River basin, Shaanxi province, China.

ISSN 2007-2422

where c is the average concentration of pollutants in the section of river (mg/l); Q is the average flow of the section (m^3/s); D_x is the longitudinal dispersion coefficient (m^2/s); A is cross-sectional area (m^2); S^{α} is the source-sink term; x is the distance between the monitoring point and the pollution source (m), and t is the time at the monitoring point (s).

If the flow (flux) is steady, then $\frac{\partial Q}{\partial t}=0$ and $\frac{\partial A}{\partial t}=0$. Equation (1) then becomes:

$$\frac{\partial c}{\partial t}=\frac{\partial}{A\partial x}\left(D_x A\frac{\partial c}{\partial x}\right)-\frac{\partial(Qc)}{A\partial x}+\frac{S_{int}}{A}+\frac{S_{ext}}{A} \quad (2)$$

where S_{int} is the internal source and sink of the water quality variable (*i.e.*, chemical reaction, etc.) (kg/(s.m)), and S_{ext} is the external source and sink (*i.e.*, branch impact, etc.) (kg/(s.m)).

To apply a steady model, the sections of the river must be even, the hydrological conditions should be stable, the current velocity and the dispersion coefficient should not change with time, and the source-sink term should be constant, namely $\frac{\partial c}{\partial t}=0$. Equation (2) can be simplified into:

$$D_x\frac{\partial^2 c}{\partial x^2}-u\frac{\partial c}{\partial x}-kc+S=0 \quad (3)$$

where u is the average current velocity through the river section (m/s); k is the degradation coefficient of the pollutant (1/d), and S is the external source from the branch (mg/l.d).

As commonly occurs in non-tidal rivers, more pollutants are removed by flow migration than by the dispersion effect. Under steady state conditions, the dispersion effect can be ignored, and we obtain:

$$u\frac{\partial c}{\partial x}=-kc+S \quad (4)$$

If the initial condition is: $x=0$, $c(x=0)=c_0$, equation (4) is solved within the interval from $x=0$ to $x=x$, and the analytical solution to the one-dimensional water quality model is:

$$c=c_0\exp\left(-\frac{k}{u}x\right)+\frac{S}{k} \quad (5)$$

The diffuse source pollution between the Jingcun and Zhangjiashan sections is ascribed to the confluent pollutants introduced by the tributaries in the wet season (including the discharge from point sources in the dry season) and can be obtained by subtracting the confluent pollutants from the tributaries in the dry season from those in the wet season.

When the water quality model is applied, the confluent pollutants from the branches between the two sections are the source-sink term distributed evenly between the two sections. The space between the two sections is subdivided into several uniformly-spaced small cells to improve the accuracy, as is shown in figure 2.

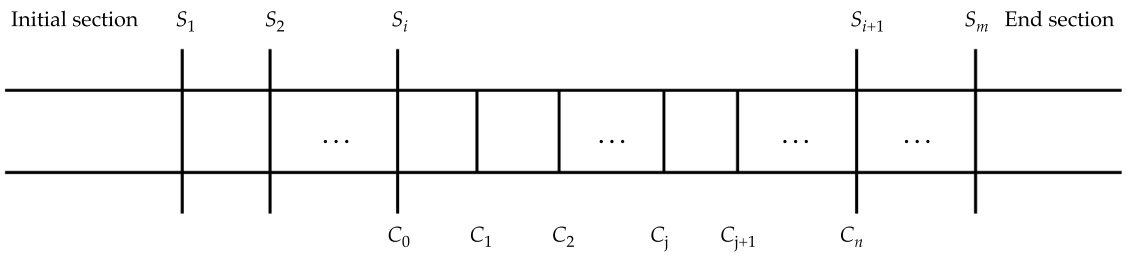

Figure 2. One-dimensional diagram of the river sections.

• ISSN 2007-2422

Where S_1, S_2,… S_i,… S_m are sections in the basin; c_0 is the concentration of section S_i; c_n is the concentration of section S_{i+l}; the basin is divided into n parts uniformly spaced between S_i and S_{i+l}; c_1, c_2,… c_j,…, c_n are the concentrations of all the sections. The precision is higher for higher values of n. The concentration of the j^{th} section is taken as the initial concentration of the $j + 1^{st}$ section. When calculated with equation (5), then:

$$c_1 = c_0 \exp\left(-\frac{k}{u}x\right) + \frac{S}{k} \tag{6}$$

$$c_2 = c_0 \exp\left(-\frac{2k}{u}x\right) + \frac{S}{k}\left[1 + \exp\left(-\frac{k}{u}x\right)\right] \tag{7}$$

$$c_3 = c_0 \exp\left(-\frac{3k}{u}x\right) + \frac{S}{k}\left[1 + \exp\left(-\frac{k}{u}x\right) + \exp\left(-\frac{2k}{u}x\right)\right] \tag{8}$$

$$c_{j+1} = c_0 \exp\left(-\frac{(j+1)k}{u}x\right) + \frac{S}{k}\sum_{\lambda=0}^{j}\exp\left(-\frac{\lambda k}{u}x\right) \tag{9}$$

Similarly,

$$c_n = c_0 \exp\left(-\frac{nk}{u}x\right) + \frac{S}{k}\sum_{j=0}^{n-1}\left(-\frac{jk}{u}x\right) \tag{10}$$

Then

$$S = \frac{c_n - c_0 \exp\left(-\frac{nk}{u}x\right)}{1 - \exp\left(-\frac{nk}{u}x\right)}\left[1 - \exp\left(-\frac{k}{u}x\right)\right]\cdot k \tag{11}$$

where the water quality and hydrological values of the conventional sections can be acquired by monitoring, and only the degradation coefficient (k) is unknown. Usually, the degradation coefficient is temperature- dependent, and is calculated using equation (12):

$$k = k_{(20°C)}1.008^{(T-20)} \tag{12}$$

where $k_{(20\,°C)}$ is the degradation coefficient of the water quality parameter at a temperature of 20 °C (1/d), and T is the water temperature (°C).

The degradation coefficient of different water quality parameters is determined by different methods. For the water quality parameter BOD_5, the methods include the laboratory method, slope method, two-point method, multi-point method, and others. Nitrogen is involved a very complex circulation process in the water environment, comprising nitrifying and denitrifying processes. Since, in general the inorganic nitrogen concentrations in rivers are quite low, the basic reactions are reduced to nitrification and denitrification. In this study, we used the two-point method to calculate the degradation coefficient between S_i and S_{i+1} at 20 °C using the following equation:

$$k = \frac{86400u}{l}\ln\left(\frac{c_{up}}{c_{down}}\right) \tag{13}$$

where k is the degradation coefficient (1/d); u is the average current velocity between sections (m/s); l is the distance between sections (m); c_{up} is the upstream concentration of the water quality parameter (mg/l), and c_{down} is the concentration of the water quality parameter downstream (mg/l).

Equation (11) is applied to calculate the source-sink term of the water quality parameter in wet and dry seasons of a hydrological year, respectively; the difference between the source-sink term in wet season and that in dry season is the diffuse source pollution for the water quality parameters between S_i and S_{i+1} in the current hydrological year. The diffuse source pollution from all the adjacent sections in the basin during the hydrological year is calculated, and the total sum being the diffuse pollution load of the basin for the hydrological year.

There are two monitoring sections on the Jinghe River in Shaanxi province, namely the Jingcun and Zhangjiashan sections, with no point source discharges in-between, except for such tributaries as the Taiyu River and Sanshui River. The area between these two sections is the

ISSN 2007-2422 •

study area, and two water quality parameters, ammonia nitrogen (NH_4^+-N) and nitrate nitrogen (NO_3^--N), were chosen as nitrogen nutrient indices to calculate the diffuse source pollution load in this study by combining the results of PCA for the water quality variables.

The water quality data from the Water Environment Monitoring Center of Shaanxi Provincial Hydrologic Bureau indicated that the average water temperature of the two monitoring stations in June each year was approximately 20 °C (lower than 20 °C for Jingcun and higher than 20 °C for Zhangjiashan, with the temperature difference between them not exceeding 1 °C). Concentrations of nitrite nitrogen were very low in both sections, therefore nitrifying reactions of nitrite nitrogen were disregarded, but only the denitrifying effect of NO_3^--N was taken into account. Equation (13) was used to calculate the degradation coefficients of NH_4^+-N and NO_3^--N, based on the values for the year when the precipitation in June was low and on the average values for many years at 20 °C. To account for the impact of temperature on water quality parameters, the degradation coefficients for each month of each year were calculated using equation (12).

Principal component analysis (PCA) and factor analysis (FA)

River pollution is a complex process comprised of several water quality parameters that may interact with each other. This implies that it may not be possible to obtain accurate results because of colinearity between the parameters. PCA groups the original parameters into a few mutually-independent comprehensive indices by a linear transformation to simplify the data and improve the reliability of the analysis results (Wu *et al.*, 2014; Xiaohua, Ruiming, & Yong, 2008). PCA has been applied in recent years to assess surface water quality in combination with other multivariate statistical analysis, such as cluster analysis (CA), factor analysis (FA), and discriminant analysis (DA) (Li, Wu, & Qian, 2013a; Li, Qian, Wu, Zhang, & Zhang, 2013b; Ouyang, 2005; Ouyang, Nkedi-Kizza, Wu, Shinde, & Huang, 2006; Shrestha & Kazama, 2007); it has also been used in non-point source load forecasting along with multiple regression analysis (Geladi & Kowalski, 1986). In particular, FA has been integrated with a water quality model to study the distribution of point and non-point sources of nutrients in surface water (Azzellino *et al.*, 2006). To highlight spatial and temporal changes in water quality in different periods of a year, the SPSS software (version 16.0) was used for PCA and FA of water quality parameters in dry and wet seasons. The analysis involved the following five main steps, as follows (Li *et al.*, 2013a; Li *et al.*, 2013b; Wu *et al.*, 2014):

1. An original data matrix was set up ($M_{ij}(I = 1, 2,\ldots, n; j = 1, 2,\ldots, p)$) with n samples and p indices, which were standardized to ensure that they all had equal weights in the analysis.
2. The covariance matrix R_{jk} was calculated.
3. The eigenvalues ($\lambda_k (k = 1, 2,\ldots, p)$) and corresponding eigenvectors ($L_k(k = 1, 2,\ldots, p)$) were derived.
4. The variance contribution rate $T_k = \lambda_k \Big/ \sum_{i=1}^{p} \lambda_k$ and the cumulative variance contribution rate $D_k = \sum_{i=1}^{k} T_i$ were calculated, and the principal components that corresponded to the eigenvalues $\lambda_1, \lambda_2,\ldots, \lambda_m (m < p)$ were selected for $Dk \geq 85\%$.
5. The factor loading matrix was developed and a $vari_{max}$ rotation was performed on the factor loading matrix to infer the principal parameters. In this study, only those factors that had an eigenvalue greater than one were retained.

Data sources

In this study, 16 sets of monitoring data from the Jingcun and Zhangjiashan sections in the Shaanxi Reach of the Jinghe River were selected for the analysis. We used data from Nov 2001

to Oct 2007; the period from Nov to Feb of the following year represented dry seasons while the period from July to Oct represented wet seasons. The average values of the current velocity and the flow rate from 2002 and 2007 for the two sections were selected. The river reaches from the Jingcun section to Zhangjiashan section is 120 km long.

Results and analysis

PCA was conducted for the 16 sets of water quality data for dry seasons in the Jingcun section and for dry and wet seasons in the Zhangjiashan section from Nov 2004 to Oct 2007. The rotated factor loadings matrixes obtained for the different periods are give elsewhere (Wang *et al.*, 2012). Six factors with eigenvalues greater than 1 extracted from the Jingcun section contributed to 87.737% (> 85%) of the variance in dry seasons, and three and four factors extracted from the Zhangjiashan section corresponded to 87.253 and 92.865% (> 85%) of the variance in dry and wet seasons, respectively. The most meaningful parameters within each component can be identified by investigating the factor loadings matrix. It can be reasonably assumed that parameters of the same component share the same origin.

The main pollutants in the Jingcun section during dry season were salt indices (VF1, including chloride, conductivity, NO_x, and salinity) and organic pollution indices (VF2, including volatile phenol and ammonia nitrogen), whereas those of the Zhangjiashan section in dry seasons were organism indices (VF1, including sulfate, COD_{Mn}, NH_4^+-N, NO_x, and BOD_5) and salt indices (VF2, including salinity, electrical conductivity, and chloride). In dry seasons, the river water was recharged by the groundwater, and NO_x and chloride in the Jingcun section were closely associated on VF1, which suggests an exchange of water from the groundwater to surface water system. In the Zhangjiashan section, NO_x was loaded on VF1 and was thus associated with point source discharges of domestic sewage, and similar other discharges. In dry seasons, ammonia nitrogen and volatile phenol in the Jingcun section were loaded on VF2, the source of which was waste water discharged from papermaking enterprises in the upper reaches of the Jinghe River; in the Zhangjiashan section, ammonia nitrogen and NO_x, which came from point source discharges of domestic sewage and similar, were on VF1. In wet seasons, the main pollutants in the Zhangjiashan section were non-point source pollution indices (VF1, including nitrogen nutrient indices (NO_x and total nitrogen) and sulfate) and organic pollution indices (VF2, including volatile phenol, ammonia nitrogen, and salinity).

The above analysis shows that, regardless of dry or wet seasons, the water environment between the Jingcun and Zhangjiashan sections was mainly polluted by nitrogen nutrient and organic pollution indices.

The source-sink terms of NH_4^+-N and NO_3^--N in wet and dry seasons from 2002 to 2007, respectively, were calculated using equation (11) and tabulated in table 1.

There was a slight variation in the source-sink terms of NO_3^--N in dry seasons of the years (table 1), showing that the point source discharges of domestic sewage and similar were stable; the terms varied considerably in wet seasons, and the values in 2003 and 2007 were much higher than in those the other years. The precipitation and runoff values were large in the wet seasons of 2003 and 2007, so the non-point source pollution loads were also quite large. Examination of the annual precipitation and corresponding non-point source load of NO_3^--N (figure 3) shows that, when the precipitation was between 400 and 500 mm, the non-point source load did not change significantly, but as the precipitation increased, the load also increased rapidly, because the increased amount of runoff carried more pollutants. However, with further increases in precipitation, the non-point source load gradually dropped down, which may be attributed to the smaller amount of fertilizers in the soil. Even though 2006 was a normal year, the non-point source load of NO_3^--N was less

ISSN 2007-2422

Table 1. NPS loads of NO_3^--N and NH_4^+-N from 2002 to 2007.

Year	Source-sink terms of NO_3^--N (t)		Non-point load (t)	Source-sink terms of NH_4^+-N (t)		Non-point load (t)
	Wet season	Dry season		Wet season	Dry season	
2002	558.433	303.387	255.047	75.642	69.739	6.390
2003	1 012.816	175.820	836.996	152.163	80.829	71.333
2004	–	–	–	37.489	18.973	18.555
2005	506.638	297.984	208.653	56.418	51.117	5.302
2006	286.242	209.878	76.364	37.466	29.140	8.327
2007	1 297.502	147.330	1 150.958	26.037	6.231	19.806
Annual average	732.301	226.880	505.604	64.203	42.672	21.619

Note: There is no monitoring value of NO_3^--N in 2004.

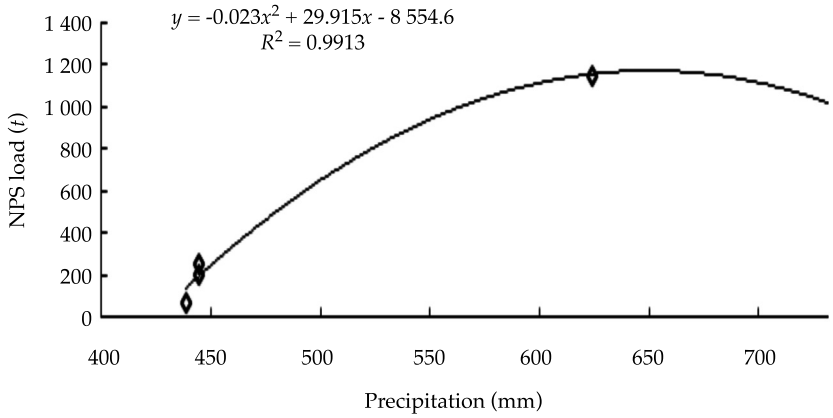

Figure 3. Fitted curve chart of annual precipitation and NPS loads of NO_3^-N from 2002 to 2007.

than in the other normal years, due to lower monthly precipitation from July to October in 2006, as compared to those of other normal years. In 2006, the maximum monthly precipitation occurred in June.

There is a wide variation of the source-sink terms of NH_4^+-N in dry and wet seasons, indicating the instability of point and non-point source discharges, due to different sources of NH_4^+-N in dry and wet seasons. PCA analysis shows that NH_4^+-N, COD_{Mn}, and BOD_5 were loaded on factor VF1 in dry seasons, which indicates that they were from domestic sewage and organic waste water discharged by juice factories. NH_4^+-N, volatile phenol and salinity were loaded on factor VF2 in wet seasons, showing that the main sources were industrial waste water discharged by papermaking enterprises in the upper reaches of the Jinghe River and NH_4^+-N adsorbed to eroded non-point source soil particles that were transported in runoff. Because the waste water discharges were different in these years, the source-sink terms of NH_4^+-N were different in dry and wet seasons. The non-point source load of NH_4^+-N was 71.3328 tons in 2003, which was higher than those observed in other years. Since 2003 was an unusually wet year, runoff transported large amounts of NH_4^+-N associated with eroded soil particles to the river channel, whereas in other

• ISSN 2007-2422

years, NH_4^+-N in the river mainly came from point source discharges such as domestic sewage and organic waste water.

The above method yielded quite expected results for such non-point source pollutants, as NO_3^--N, and somewhat contradictory ones on such point source pollutants, as NH_4^+- N.

Conclusion

In this study, we proposed the combined application of QUAL2E, a river water quality model, and PCA and FA to study the source apportionment of point and non-point pollutant loads to surface water. PCA and FA were used to evaluate pollutant sources in different river sections in dry and wet seasons, and then the amount of point source and non-point source pollution was calculated by using QUAL2E.

The results of PCA and FA show that the water pollution in the lower reaches of the Jinghe River mainly involved nitrogen and organisms. NH_4^+-N and NO_3^--N, as the nitrogen nutrient indices, were taken as the objects, and the QUAL2E model equation was adopted to calculate their source-sink terms in dry and wet seasons, respectively; the difference between the terms in wet and dry seasons were the non-point source loads. The calculation results for NO_3^--N were reasonable, while those of NH_4^+-N were somewhat unexpected, but consistent with the results of PCA and FA. NO_3^--N comes from point source discharges of domestic sewage and similar in dry seasons and from non-point source pollution generated by precipitation in wet seasons, whereas NH_4^+-N was mainly discharged from point sources throughout the year. The instability of the point source discharges caused the above deviation of the calculation results. It is shown that application of the QUAL2E river water quality model provides reliable results for non-point source pollution caused by storm runoff, but unreliable results for point source pollution. Therefore, further model refinement or application of newer version QUAL2K (https://www.epa.gov, http://www.qual2k.com/) may be expedient. In contrast to QUAL2E, which segments the system into river reaches comprised of equally spaced elements. QUAL2K uses unequally-spaced reaches. In addition, multiple loadings and abstractions can be input to any reach, which may be quite instrumental for more accurate account of the local specific features.

Acknowledgements

We would like to thank the Project of Science and Technology of Social Development in Shaanxi Province [grant number 2016SF-411]. We would also like to express our thanks to all helpers from the Water Environment Monitoring Center and Reconnaissance Office of Shaanxi Provincial Hydrologic Bureau, China for providing *in situ* survey data, without whom this study would not be possible.

References

Azzellino, A., Salvetti, R., Vismara, R., & Bonomo, L. (2006). Combined use of the EPA-QUAL2E simulation model and factor analysis to assess the source apportionment of point and nonpoint loads of nutrients to surface waters. *Science of the Total Environment*, *371*(1), 214-222.

Beck, M. B. (1987). Water quality modeling: A review of the analysis of uncertainty. *Water Resources Research*, *23*(8), 1393-1442.

Chowdary, V., Rao, N., & Sarma, P. (2005). Decision support framework for the assessment of non-point-source pollution of groundwater in large irrigation projects. *Agricultural Water Management*, *75*(3), 194-225.

Feier, W., Huanchun, L., Yingxu, C., & Dong, W. (2003). Prediction of output loading of nitrogen and phosphorus from Qiandao Lake watershed based on AnnAGNPS Model. *Transactions of the Chinese Society of Agricultural Engineering*, *19*(6), 281-284.

Gao, Y., Zhu, B., Zhou, P., Zhi, Y., & Tang, J. (2008). Study on the application AnnAGNPS and SWAT to non-point resource pollution research: A case of Yanting agro-ecological experimental station. Chinese Academy of Sciences. *Journal of Shanghai Jiaotong University (Agricultural Science)*, *6*(6), 567-572.

Geladi, P., & Kowalski, B. R. (1986). Partial least-squares regression: A tutorial. *Analytica Chimica Acta*, 185, 1-17.

Guihong, Z., & Jiangyong, C. (2007). Simulation of agricultural non-point pollution based on AnnAGNPS model. *Transactions of the Chinese Society of Agricultural Engineering*, *23*(12), 11-17.

Huo, A., Zhang, J., Qiao, C., Li, C., Xie, J., Wang, J., & Zhang, X. (2014). Multispectral remote sensing inversion for city landscape water eutrophication based on genetic algorithm-support vector machine. *Water Quality Research Journal of Canada*, *49*(3), 285-293.

Li, P., Wu, J., & Qian, H. (2013a). Assessment of groundwater quality for irrigation purposes and identification of hydrogeochemical evolution mechanisms in Pengyang County, China. *Environmental Earth Sciences*, *69*(7), 2211-2225, DOI: 10.1007/s12665-012-2049-5.

Li, P., Qian, H., Wu, J., Zhang, Y., & Zhang, H. (2013b). Major ion chemistry of shallow groundwater in the Dongsheng Coalfield, Ordos Basin, China. *Mine Water and the Environment*, *32*(3), 195-206, DOI: 10.1007/s10230-013-0234-8.

Li, P., Qian, H., & Wu, J. (2014). Accelerate research on land creation. *Nature*, *510*(7503), 29-31, DOI: 10.1038/510029a.

Li, P., Qian, H., Howard, K. W. F., & Wu, J. (2015). Building a new and sustainable "Silk road economic belt". *Environmental Earth Sciences*, *74*(10), 7267-7270, DOI: 10.1007/s12665-015-4739-2.

Melching, C. S., & Yoon, C. G. (1996). Key sources of uncertainty in QUAL2E model of Passaic River. *Journal of Water Resources Planning and Management*, *122*(2), 105-113.

Munafo, M., Cecchi, G., Baiocco, F., & Mancini, L. (2005). River pollution from non-point sources: A new simplified method of assessment. *Journal of Environmental Management*, *77*(2), 93-98.

Ouyang, Y. (2005). Application of principal component and factor analysis to evaluate surface water quality monitoring network. *Water Research*, *39*(20), 2621-2635.

Ouyang, Y., Nkedi-Kizza, P., Wu, Q., Shinde, D., & Huang, C. (2006). Assessment of seasonal variations in surface water quality. *Water Research*, *40*(20), 3800-3810.

Polyakov, V., Fares, A., Kubo, D., Jacobi, J., & Smith, C. (2007). Evaluation of a non-point source pollution model, AnnAGNPS, in a tropical watershed. *Environmental Modelling & Software*, *22* (11), 1617-1627.

Reckhow, K. H. (1999). Water quality prediction and probability network models. Canadian *Journal of Fisheries and Aquatic Sciences*, *56*(7), 1150-1158.

Shrestha, S., & Kazama, F. (2007). Assessment of surface water quality using multivariate statistical techniques: A case study of the Fuji river basin, Japan. *Environmental Modelling & Software*, *22*(4), 464-475.

Wang, J., Wu, Y. Q., Dang, B. L., Xu, Z. R., Hu, A. Y., & Zhang, X. Z. (2012). Spatial and temporal distribution of surface water quality using multivariate statistical analysis in Jinghe River of Shaanxi Province, China. *Journal of Natural Resources*, *27*(4), 674-685.

Whitehead, P., Johnes, P., & Butterfield, D. (2002). Steady state and dynamic modelling of nitrogen in the River Kennet: Impacts of land use change since the 1930s. *Science of the Total Environment*, 282, 417-434.

Wu, J., Li, P., Qian, H., Duan, Z., & Zhang, X. (2014). Using correlation and multivariate statistical analysis to identify hydrogeochemical processes affecting the major ion chemistry of waters: Case study in *Laoheba phosphorite* mine in Sichuan, China. *Arabian Journal of Geosciences*, *7*(10), 3973-3982, DOI: 10.1007/s12517-013-1057-4.

Xiaohua, Y., Ruiming, L., & Yong, Z. (2008). *Environment statistics analysis* (in Chinese, with English abstract) (pp. 164-169). Beijing: Beijing Normal University Press.

Author´s institutional address

Ph.D. Jucui Wang

Chang'an University
College of Environmental Science and Engineering
Xi'an 710054, PR China

Xi'an University of Technology
College of Water Conservancy and Hydropower
Xi'an 710048, PR China
Yanta south road No. 126, Xi'an City,
Shaanxi Province, PR China
Telephone: +86 (029) 8233 9952
wjvcuisw@sina.com

Ph.D. Aidi Huo
Ph.D. Anyan Hu
Ph.D. Xuezhen Zhang

Chang'an University
College of Environmental Science and Engineering
Xi'an 710054, PR China
Yanta south road No. 126, Xi'an City,
Shaanxi Province, PR China
Telephone: +86 (029) 8233 9952
huoaidi@163.com
huanyan97@163.com
346628478@qq.com

Ph.D. Yanqing Wu

Shanghai Jiaotong University
College of Environmental Science and Engineering
Shanghai 200240, PR China
Dongchuan Road No.800, Shanghai City, PR China
Telephone: +86 (021) 3420 3731
wuyanqing@sjtu.edu.cn

Haga clic aquí para escribir al autor

Improved online sequential extreme learning machine for simulation of daily reference evapotranspiration

• Yubin Zhang • Zhengying Wei* • Lei Zhang • Qinyin Lin • Jun Du •
Xian Jiaotong University, China
*Corresponding author

Abstract

Yubin, Z., Zhengying, W., Lei, Z., Qinyin, L., & Jun, D. (March-April, 2017). Improved online sequential extreme learning machine for simulation of daily reference evapotranspiration. *Water Technology and Sciences* (in Spanish), *8*(2), 127-140.

The traditional extreme learning machine has significant disadvantages, including slow training, difficulty in selecting parameters, and difficulty in setting the singularity and the data sample. A prediction model of an improved Online Sequential Extreme Learning Machine (IOS-ELM) of daily reference crop evapotranspiration is therefore examined in this paper. The different manipulation of the inverse of the matrix is made according to the optimal solution and using a regularization factor at the same time in the model. The flexibility of the IOS-ELM in ET0 modeling was assessed using the original meteorological data (*T*max, *Tm*, *T*min, *n*, *Uh*, *RHm*, ϕ, *Z*) of the years 1971-2014 in Yulin, Ankang, Hanzhong, and Xi'an of Shaanxi, China. Those eight parameters were used as the input, while the reference evapotranspiration values were the output. In addition, the ELM, LSSVM, Hargreaves, Priestley-Taylor, Mc Cloud and IOS-ELM models were tested against the FAO-56 PM model by the performance criteria. The experimental results demonstrate that the performance of IOS-ELM was better than the ELM and LSSVM and significantly better than the other empirical models. Furthermore, when the total ET0 estimation of the models was compared by the relative error, the results of the intelligent algorithms were better than empirical models at rates lower than 5%, but the gross ET0 empirical models mainly had 12% to 64.60% relative error. This research could provide a reference to accurate ET0 estimation by meteorological data and give accurate predictions of crop water requirements, resulting in intelligent irrigation decisions in Shaanxi.

Keywords: Daily reference evapotranspiration, extreme learning machine, online learning, matrix singularity.

Resumen

Yubin, Z., Zhengying, W., Lei, Z., Qinyin, L.,& Jun, D. (marzo-abril, 2017). Máquina de aprendizaje extremo secuencial en línea mejorada para la simulación de la evapotranspiración de referencia diaria. Tecnología y Ciencias del Agua, *8(2), 127-140.*

*La máquina de aprendizaje extremo tradicional tiene desventajas significativas, como entrenamiento lento, dificultad en la selección de parámetros y dificultad en establecer la singularidad y la muestra de datos. Por lo tanto, en el presente artículo se examina un modelo de predicción de una máquina de aprendizaje extremo secuencial en línea mejorada (IOS-ELM) de la evapotranspiración de referencia diaria de cultivos. La diferente manipulación de la inversa de la matriz se hace de acuerdo con la solución óptima y utilizando un factor de regularización al mismo tiempo en el modelo. La flexibilidad de la IOS-ELM en la modelación de la ET0 se evaluó empleando los datos meteorológicos originales (*T*max,* Tm, *T*min,* n, Uh, RHm, ϕ, *Z) de los años 1971-2014 en Yulin, Ankang, Hanzhong, y Xi'an en Shaanxi, China. Estos ocho parámetros se usaron como insumos o datos de entrada, mientras que los valores de la evapotranspiración de referencia fueron los datos de salida o el producto. Asimismo, se probaron los modelos ELM, LSSVM, Hargreaves, Priestley-Taylor, Mc Cloud y IOS-ELM contra el modelo FAO-56 PM mediante los criterios de desempeño. Los resultados experimentales demuestran que el desempeño de IOS-ELM fue mejor que el de ELM y LSSVM y significativamente mejor que los demás modelos empíricos. Más aún, al comparar la estimación total de ET0 de los modelos mediante el error relativo, los resultados de los algoritmos inteligentes fueron mejores que los modelos empíricos a índices inferiores a 5%, pero los modelos empíricos de ET0 bruta tuvieron un error relativo de 12 a 64.60%. Esta investigación podría proporcionar una referencia para la estimación precisa de ET0 mediante datos meteorológicos y proporcionar predicciones precisas de los requerimientos de agua de los cultivos, lo cual resultaría en decisiones de riego inteligentes en Shaanxi.*

***Palabras clave**: evapotranspiración de referencia diaria, máquina de aprendizaje extremo, aprendizaje en línea, singularidad de la matriz.*

Received: 30/04/2016
Approved: 26/102016

Introduction

The calculation of reference crop evapotranspiration is a key to intelligent irrigation systems. Therefore, accurate estimation of *ET*0 becomes important in irrigation schedules for planning and optimizing the agriculture area. Numerous methods have been put forward to estimate *ET*0. Of these, the Penman-Monteith 56 (PM) model has given the best results; it was officially recommended by the Food and Agriculture Organization of the United Nations (FAO) in 1998 (Allen *et al*., 1998). FAO selected the PM model as the standard equation for *ET*0 estimation because it can provide the most accurate results in the world. *ET*0 is also a key parameter in the design of intelligent irrigation for field crops. Engineers need to know the irrigation water consumption requirements for each crop so that they can calculate or estimate the remaining components of the water balance. Also, agriculturists need to obtain the specific water requirements of a crop so that they can generate a satisfactory yield. It is also necessary to know whether these specific requirements are being met with ordinary irrigation.

As described by Kisi (2008) and (Yubin *et al*., 2014), about 50 measures have been proposed for estimating evapotranspiration, which can be sorted into four types: radiation, temperature, synthetic and evaporating dish. FAO assumed the ET definition given by Smith, Allen and Pereira (1997), and adopted the FAO-56 PM as the sole equation for estimation of *ET*0.

However, the PM model requires a lot of meteorological data as input, and the calculation process involves complex and nonlinear regression among these factors. So, a simpler and more accurate simulation model needs to seek *ET*0 in the case of lack of meteorological data. Thus, artificial intelligence algorithms (*e.g*., neural networks) for reference evapotranspiration (*ET*0) modeling have been given more attention in recent decades. Feng and Cui (2015) found that an ELM model gave better results than empirical models in the area of central Sichuan. Kisi (2007) estimated daily ET0 using the ANN method and compared their calculation results with the other models. Ozgur Kisiet (2013) proposed a reference evapotranspiration model by LSSVM. Kisi (2011a) considered daily *ET*0 using wavelet regression model and compared this model to other empirical models. Kisi (2011b) modeled *ET*0 using evolutionary feed-forward neural networks. Marti, Gonzalez-Altozano and Gasque (2011) used ANN to estimate daily *ET*0 without local climatic data. Kumar, Raghuwanshi and Singh (2011) researched the application of ANN in estimating evapotranspiration modeling. Shiri *et al*. (2012) established an *ET*0 simulation model using GEP (gene expression programming) for Spanish Basque, and found that the GEP model performed better than the ANFIS, Hargreaves and Priestley-Taylor models. Wang, Traore and Kerh (2008), and Traore, Wang and Kerh (2010) estimated daily *ET*0 using BP-ANN. However, BP-ANN has major disadvantages, such as its slow speed of training and difficulty in selecting parameters. In recent years, new intelligent algorithms have appeared in the industrial field, such as extreme learning machines (ELM) and support vector machine, among others.

In the present study, ELM is proposed as an alternative to other models for predictive control. It can randomly choose hidden nodes and analytically determine the output weights of SLFNs. However, ELM cannot confirm the singularity of the output matrix of the hidden layer, and it also cannot make fine tuning according to the characteristics of the data set, which will affect its efficiency and stability.

The main purpose of this paper is to optimize the ELM approach in the modeling of daily *ET*0 using the original meteorological data. All previous studies have indicated that intelligent models can input the factors of FAO-56 PM as they estimate *ET*0. In fact, these factors will be another complex computing project by meteorological raw data, to avoid creating more severe error during multistage formula calculation. Also, the manipulation of the inverse of the

• ISSN 2007-2422

matrix is adjusted with reference to the optimal solution and the regularization factor at the same time, which is motivated by the online learning method. In summary, an improved online sequential extreme learning machine (IOS-ELM) is designed, and the new algorithm can produce good generalization performance in a model of daily *ET*0 in an irrigation system.

Materials and case study

The study was conducted in Yulin (38.27° N, 109.78° E), Ankang (32.72° N, 109.03° E), Hanzhong (33.07°N, 107.7°E) and Xi'an (34.3° N, 108.9° E) in Shaanxi province in China, shown in Fig. 1. The area has a hot and dry climate for the greater part of the year.

Daily meteorological data used for this study was from the years 1971–2014. The following observed eight meteorological variables with daily temporal resolution were used: wind speed at 10m above the ground (*Uh*), mean temperature (*T*), mean relative humidity (*RH*), minimum temperature (*T*min), maximum temperature (*T*max), actual Sunshine duration (*n*), latitude (ϕ) and elevation (*Z*), which were downloaded from China meteorological data sharing service system (http://cdc.nmic.cn/home.do). Data from the first 29 years (1971-1999) was used to train the models. Data from the next ten years (2000-2009) was used for the test. The data from the remaining years was used for validation. It must be noted, however, that missing data was replaced by the average of the data from the day before and the day before. The regional climate characteristics are given in table 1.

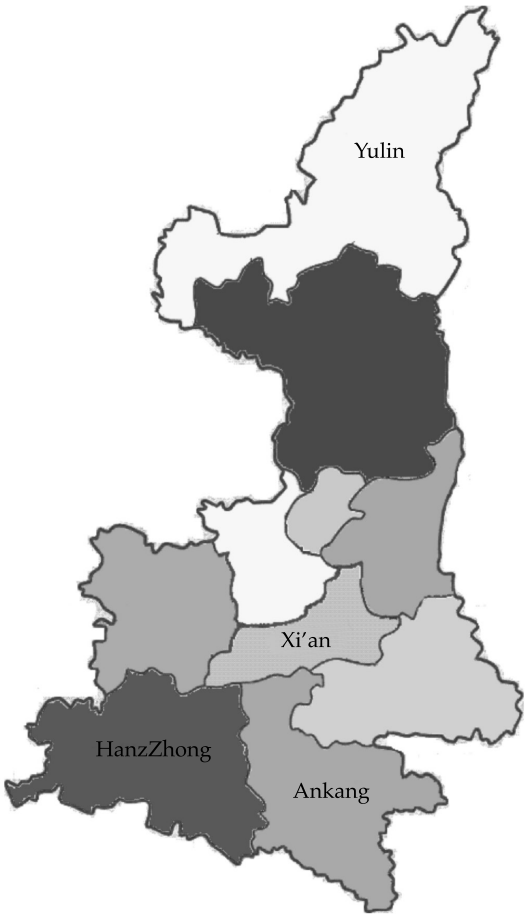

Figure 1. The location of the cities.

Methodology

Calculation models of reference crop evapotranspiration

The study focused on the comparison of the proposed IOS-ELM model with the ELM, LSSVM,

Table 1. Means of main variables.

	Uh	*T*	*RH*	*T* min	*T* max	*n*	ϕ	*Z*
Yulin	2.14	9.2	53.5	3.1	16.2	7.32	0.67	1157
An kang	1.35	15.9	74.1	12.1	21.4	4.58	0.57	290.8
Han zhong	1.15	15.1	78.5	11.5	19.8	4.03	0.58	509.5
Xi'an	1.60	14.6	64.3	9.7	19.6	4.54	0.60	397.5

Tecnología y Ciencias del Agua, vol. VIII, núm. 2, marzo-abril de 2017, pp. 127-140
ISSN 2007-2422

Hargreaves, Mc-Cloud, and Priestley-Taylor models. First, the *ET*0 values of four cities were calculated using the FAO-56 PM. Then, the standard formula evapotranspiration calculation for all empirical models is shown.

(1) FAO-56 Penman-Monteith:

$$ET0 = \frac{0.418\Delta\left(R_s - G\right) + \gamma \frac{900}{T + \gamma 273} u_2 \left(e_s - e_a\right)}{\Delta + \gamma\left(1 + 0.34u_2\right)} \quad (1)$$

The original meteorological data of T_{max}, T, T_{min}, n, Uh, RH_m, ϕ and Z were used in the model:

(2) Hargreaves:

$$ET0 = \frac{0.0023 \times R_a \left(T + 17.8\right)\left(T_{max} - T_{min}\right)^{\frac{1}{2}}}{\lambda} \quad (2)$$

T_{max}, T, T_{min}, n and ϕ were used in the model:

(3) Mc-Cloud:

$$ET0 = 0.254 \times 1.07^{(1.8T)} \quad (3)$$

Only T was referred to in the model:

(4) Priestley-Taylor

$$ET0 = 1.26 \frac{\Delta}{\Delta + \gamma} \cdot \frac{\left(R_n - G\right)}{\lambda} \quad (4)$$

T_{max}, T, T_{min}, n and ϕ were used.

However, these variables are obtained directly or indirectly from the meteorological raw data (*Uh*, *T*, *RH*, *T*min, *T*max, *n*, ϕ and *Z*). Furthermore, the calculation formula for them did not have a precise formula by estimation or experience.

Therefore, the inputs *Uh*, *T*, *RH*, *T*min, *T*max, *n*, ϕ and *Z*, the *ET*0 output were calculated by the FAO-56 PM method and used for the calibration of the IOS-ELM models. The mean absolute error (MAE), the root mean square error (RMSE), effectiveness index of the model (EF) and self-correlation coefficient (R^2) statistics were used for the assessment criteria of the models in this study. EF model efficiency mainly depends on the Nash coefficient EF values; as the values approach one, the efficiency of the model increases. The study adopted the calculation model of the validity index for EF by Nash and Sutcliffe.

Extreme learning machine (ELM)

For N random distinct samples (x_i, t_i) where $x_i = [x_{i1}, x_{i2},..., x_{in}]^T \in R^n$, $t_i = [t_{i1}, t_{i2},..., t_{in}]^T \in R^m$ and for the standard SLFNs ($\tilde{N}$ hidden nodes), the activation function $g(x)$ is expressed as:

$$\sum_{i=1}^{\tilde{N}} \beta_i g_i\left(x_i\right) = \sum_{i=1}^{\tilde{N}} \beta_i g\left(w_i \cdot x_j + b_i\right) = 0_j \quad j = 1,...,N \quad (5)$$

where $w_i = [w_{i1}, w_{i2},..., w_{in}]^T$ is the weight vector connecting the ith hidden node and the input nodes, $\beta_i = [\beta_{i1}, \beta_{i2},..., \beta_{in}]^T$ is the weight vector connecting the ith hidden node and the output nodes and b_i is the threshold of the ith hidden node.

$$\sum_{i=1}^{\tilde{N}} \beta_i g\left(w_i \cdot x_j + b_i\right) = t_j \quad j = 1,...,N \quad (6)$$

The above N equations can be written compactly as

$$H\beta = T \quad (7)$$

where

$$H\left(w, b, x\right) = \begin{bmatrix} g\left(w_1 \cdot x_1 + b_1\right) & \text{L} & g\left(w_{\tilde{N}} \cdot x_1 + b_{\tilde{N}}\right) \\ \text{M} & \text{L} & \text{M} \\ g\left(w_1 \cdot x_N + b_1\right) & \text{L} & g\left(w_{\tilde{N}} \cdot x_N + b_{\tilde{N}}\right) \end{bmatrix}_{N \times \tilde{N}} \quad (8)$$

$$\beta = \begin{bmatrix} \beta_1^T \\ \text{M} \\ \beta_{\tilde{N}}^T \end{bmatrix}_{\tilde{N} \times m}, \; T = \begin{bmatrix} t_1^T \\ \text{M} \\ t_N^T \end{bmatrix}_{N \times m} \quad (9)$$

• ISSN 2007-2422

where H is called the hidden layer output matrix in the neural network, and the ith column of H is the ith hidden node output toward inputs $x_1, x_2, ..., x_N$.

The aim is to solve the above issues and put forward an extreme learning machine for SLFNs.

A training set was provided as:

$\aleph = \left\{ \left(x_i, t_i \right) \middle| x_i \in R^n, t_i \in R^m \right\}_{i=1}^{N}$, the activation function $g(x)$, and hidden node number $\tilde{N}$.

Step 1: Randomly allocate input weight w_i and bias b_i, $i = 1, 2, ..., \tilde{N}$.

Step 2: Calculate the hidden layer output matrix H.

Step 3: Calculate the output weight β.

$$\hat{\beta} = H^{+}T \tag{10}$$

where $T = [t_1, ..., t_N]^T$, H^+ is a generalized inverse of MP.

Online sequential ELM (OS-ELM)

ELM is a relatively effective and simple algorithm that is also able to learn quickly and generalize well. However, meteorological data are difficult to collect and the data set is large, which may cause a decline in the performance of the *ET*0 model. Thus, the online sequential extreme learning machine (OS-ELM) by Liang (2006) was referenced in the previous research.

The output weight matrix $\hat{\beta} = H^{+}T$ is a least-squares solution of (7). Meanwhile, the matter where $rank(H) = \tilde{N}$ the number of hidden nodes (Ao, Xiao, & Mao, 2009) is considered. So, $H^+$of (10) is given as:

$$H^{+} = \left(H^T H \right)^{-1} H^T \tag{11}$$

If $H^T H$ tends to become fantastic, it can also be made nonsingular by increasing the number of data or choosing a smaller network size. Substituting (11) into (10) gives:

$$\hat{\beta} = \left(H^T H \right)^{-1} H^T T \tag{12}$$

Equation (12) is called the least-squares solution to $H\beta = T$. Sequential implementation of the least-squares solution of (12) gives the OS-ELM. However, the OS-ELM may have some deficiencies, especially the fact that solving the generalized inverse matrix MP of H may cost a huge amount of time in the training process. The general method of singular value decomposition is used to solve matrix H, but its computational complexity is $O(4N\tilde{N}^2 + 8\tilde{N}^3)$ (Brown, 2009).

Improved algorithm of OS-ELM (IOS-ELM)

This paper proposes an improved OS - ELM called IOS-ELM. This new model was developed by modifying and improving the singularity of the matrix. First, Equation $H\beta = T$ will be replaced by $H^T H\beta = H^T T$, which has at least one optimization solution. This reduces the computational complexity of solving the inverse, which results in a reduction of the training time. Second, the regular factor $1/\lambda$ is joined when calculating the output weights. Last, the subsequent online learning stage is added. In theory, this algorithm can provide good generalization performance at an extremely fast learning speed.

Step (1): Allocate random input weights w_i and bias b_i, initialize network and calculate the initially hidden layer output matrix H_0.

Step (2): Set $r = rank(H)$, if $r = N_0$, then calculate the initial weight matrix $\beta^0 = P_1 H_0^T T_0$.If $r = N$ then calculate the initial weight $\beta^0 = H_0^T P_2 T_0$.

Where $P_1 = \left(\frac{1}{\lambda} + H_0 H_0^T \right)^{-1}$, $P_2 = \left(\frac{1}{\lambda} + H_0^T H_0 \right)^{-1}$.

If $r \neq N_0$ and $r \neq \tilde{N}$, to solve the two optimization models:

$$\min_{B \in g^*} \left\| M - B \right\| \quad \text{and} \quad \min_{B \in R^{N0}} \left\| B^* \beta^0 - c \right\|$$

Then, the optimization solution B^* and β^0 can be obtained.

ISSN 2007-2422

Where $c = H_0^T T_0$, $M = H_0^T H_0$, $g^+ = \{g \in R^{N_0 \times N_0}\}$, g is a positive definite symmetric matrix.

Step (3) Set $K = 0$; then, present the $(K + 1)$th chunk of new observations:

$$\aleph_{K+1} = \left\{\left(x_i, t_i\right)\right\}_{i=\left(\sum_{j=1}^{K} N_j\right)}^{\sum_{j=1}^{K+1} N_j}$$

where N_{K+1} is the number of observations in the $(K + 1)$th chunk.

Step (4) Calculate the partially hidden layer output matrix H_{K+1} for the $(K + 1)$th chunk of data $\aleph_{K+1}$, as shown in (17):

$$H_{K+1} = \begin{bmatrix} g\left(w_1 \cdot x_1 + b_1\right) & \cdots & g\left(w_{\tilde{N}} \cdot x_1 + b_{\tilde{N}}\right) \\ \vdots & \cdots & \vdots \\ g\left(w_1 \cdot x_{N_{K+1}} + b_1\right) & \cdots & g\left(w_{\tilde{N}} \cdot x_N + b_{\tilde{N}}\right) \end{bmatrix}_{N_{K+1} \times \tilde{N}} \quad (13)$$

Step (5) According to step (1), calculate the output weight β^{K+1}.

Step (6) Set $k = k + 1$. Go to Step (3).

Application and results

IOS -ELM model under lack of data

The original eight meteorological parameters chose and combined with a different pattern in this section, which was taken as input values. Meanwhile, the calculation of FAO 56 Penman-Montieth was put as the output value. By this method, the IOS-ELM model is established. However, it needs to further consider the effectiveness of the combination pattern among the eight meteorological data. Therefore, the correlation between *ET*0 and the data was analyzed. In this way, ISO-ELM can choose reasonable meteorological parameters to complete the forecast even if there is a lack of meteorological data. This is shown in table 4.

It can be clearly seen from table 2 that the *ET*0 outperformed all eight meteorological parameters in terms of correlation. Although the data set is not similar for different cities, the correlation behaved in the same way. T_{max} is closely correlated with evapotranspiration for each city, followed by the average temperature, minimum temperature, the actual sunshine time and wind speed. The influence of the latitude and altitude were so small that they were negligible. Finally, the humidity is negative.

The simulation accuracy of the IOS-ELM model was discussed by referring to table 2 under lack of meteorological data. It should be noted that the latitude and altitude were eliminated because they had virtually no effect on the results. Taking Yulin city as an example, the first 10-year (1971-1999) span of data was used to train the models. Then, using different combinations, the error was analyzed, as well as the correlation coefficient and effectiveness of the prediction. This is shown in table 3.

The ISO-ELM model was applied by comparing the different parameters shown in table 3. It is immediately noticeable that the prediction results were the same for eight-parameter and six-parameter inputs. That is because the latitude and altitude almost have no effect on the prediction for the same station. Secondly, the temperature had the largest influence on the prediction, particularly the maximum temperature. As long as the temperature is one of

Table 2. Correlation of data and *ET*0.

	Uh	*T*	RH_m	T_{min}	T_{max}	*n*	ϕ	*Z*
Yulin	0.20	0.88	-0.36	0.79	0.92	0.50	-2e-15	NaN
Ankang	0.15	0.85	-0.34	0.71	0.93	0.70	-7e-16	
Hanzhong	0.21	0.85	-0.48	0.73	0.93	0.69	4e-15	
Xi'an	0.30	0.80	-0.43	0.72	0.85	0.66	1e-16	

• ISSN 2007-2422

Table 3. Influence of different meteorological data combinations on *ET*0.

Model inputs	RMSE	R^2	EF%
All	**0.4132**	**0.9696**	**95.72**
T_{max}, T, T_{min}, n, Uh, RH	**0.4132**	**0.9696**	**95.72**
T_{max}, T, T_{min}, n, Uh	0.7865	0.9625	92.3
T_{max}, T, T_{min}, n, RH	**0.6737**	**0.9619**	**94.3**
T_{max}, T, T_{min}, Uh, RH	0.7868	0.9620	92.2
T_{max}, T, n, Uh, RH	0.9021	0.9496	89.8
T_{max}, T_{min}, n, Uh, RH	0.9135	0.9490	89.6
T, T_{min}, n, Uh, RH	0.9666	0.9423	88.3
T_{max}, T, T_{min}, n	0.8270	0.9591	91.4
T_{max}, T, T_{min}, Uh	0.7338	0.9673	93.2
T_{max}, T, T_{min}, RH	**0.6368**	**0.9651**	**94.9**
T_{min}, n, Uh, RH	1.2321	0.9060	81.1
T, n, Uh, RH	1.0048	0.9377	87.4
T_{max}, n, Uh, RH	0.8428	0.9560	91.1
T_{max}, T, T_{min}	0.8505	0.9566	90.9
n, Uh, RH	2.2612	0.6222	36.3
T_{max}, T, RH	0.6480	0.9753	94.7
T_{max}, T_{min}, n	0.8580	0.9548	90.8
T_{max}, T_{min}, Uh	0.7942	0.9616	92.1
T_{max}, Uh, RH	0.7436	0.9668	93.1
T_{max}, n, RH	**0.6298**	**0.9664**	**95.06**
T_{max}, n, Uh	0.8786	0.9513	90.3
T_{max}, T	0.9464	0.9432	88.8
T, T_{min}	0.9119	0.9502	89.64
T_{max}, RH	**0.6258**	**0.9670**	**95.12**
T_{max}, n	0.9012	0.9483	89.89
T_{max}, Uh	0.9999	93.59	87.55
n, RH	2.1127	0.6694	44.42
n, Uh	2.1611	0.6543	41.85
Uh, RH	2.6964	0.3395	9.47

the parameters, the model is accurate. Thirdly, when only two temperatures were used as the inputs, it still performed better than RMSE, EF and R^2 statistics. So, properly reducing some variables and adopting reasonable combinations of variables can improve the accuracy of prediction.

Comparison with other calculation formulas

The IOS-ELM model was compared with the ELM and LSSVM, as well as conventional models including Hargreaves, Mc-Cloud and Priestley-Taylor methods in respect of RMSE and MAE statistics in different cities in tables 4-5. There are six parameters as input variables in the model.

Tables 4-5 show that IOS-ELM outperformed all other models by all performance criteria. Compared with the intelligent and empirical models, the ISO-ELM performed the best value of RMSE<0.46 and MAE<0.41, and the ELM and LSSVM models performed better than the others. A few differences appeared among the Mc Cloud and Priestley-Taylor models. It was

ISSN 2007-2422

Table 4. RMSE of the models in the test period.

Models	RMSE (mm/day)			
	Yulin	A kang	Hanzhong	Xi'an
IOS-ELM	041	0.45	0.45	0.41
ELM	0.86	0.72	0.88	0.78
LSSVM	0.96	1.38	1.30	1.05
Hargreaves	2.18	1.38	1.27	0.79
Mc Cloud	3.53	2.20	1.98	1.70
Priestley-Taylor	2.43	1.73	1.59	0.71

Table 5. MAE of the models in the test period.

Models	MAE (mm/day)			
	Yulin	Ankang	Hanzhong	Xi'an
IOS-ELM	0.40	0.35	0.33	0.31
ELM	0.52	0.68	0.62	0.55
LSSVM	0.77	1.20	1.13	0.93
Hargreaves	1.97	1.25	1.19	0.58
Mc Cloud	3.15	1.86	1.66	1.36
Priestley-Taylor	2.13	1.56	1.40	0.51

also discovered that the Hargreaves method provided better accuracy than other methods among the empirical models.

Although IOS-ELM, ELM and LSSVM models had better simulation effects, the running time is distinguishing, as shown in table 6.

It is clear from table 6 that the IOS-ELM model runs faster than ELM and LSSVM in the process of calculating by at least 24.8%.

In order to consider the portability and error causes of the IOS - ELM model, the estimates of each model for four cities are shown in figures 2-5 in the form of scatter plots in the validation period. It is generally clear from the scatter plots that the six input ISO-ELM estimates are closer to the corresponding FAO-56 PM *ET*0 values than other models. The fit line equations $y = ax + b$ and R^2 values indicate that the ISO-ELM model performed with better accuracy. Meanwhile, the a and b coefficients of the six-input ISO-ELM model were closer to 1 and 0, respectively, with a higher R^2 value than those of the other models.

For Yulin, ISO-ELM and ELM estimates were closer to the FAO-56 PM *ET*0 values than those of the other models ($R^2 > 0.96$). A slight difference exists between LSSVM, and Hargreaves was better than the surplus models. The Mc Cloud estimate had the least accuracy. It can be concluded that the ISO-ELM and ELM models are the best methods to use for daily *ET*0 estimation in Yulin.

Table 6. Running time of different models.

Model	Running time (S)			
	Yulin	Ankang	Hangzhong	Xi'an
IOS-ELM	16.5	17.9	13.8	17.1
ELM	28.8	23.8	21.2	25.8
LSSVM	22.4	30.5	19.9	36.5

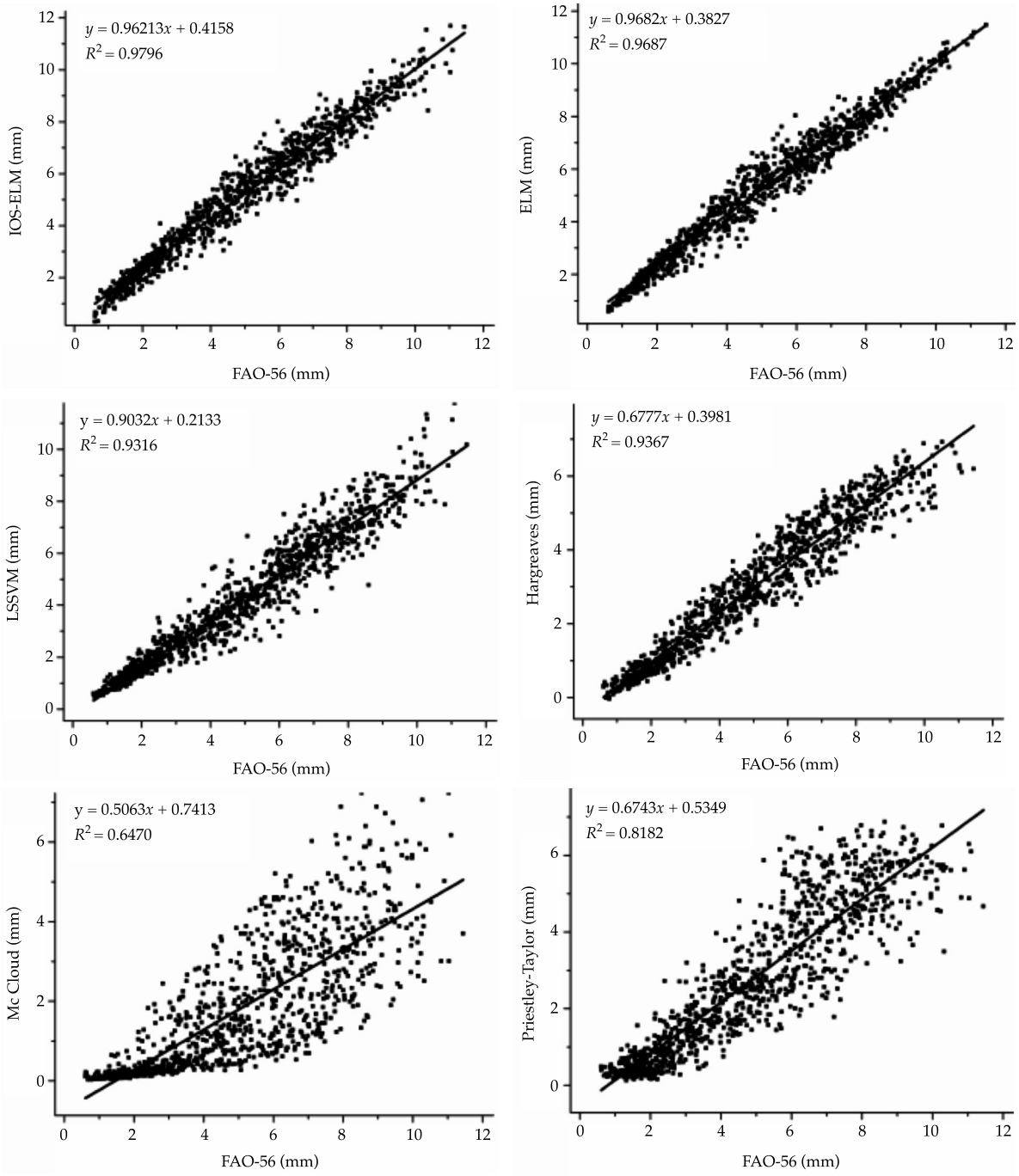

Figure 2. The FAO-56 PM *ET*0 and estimated ET0 values of Yulin.

For Ankang, ISO-ELM and Hargreaves were closer to the FAO-56 PM *ET*0 values, a slight difference exists between LSSVM, and ELM was better than the Mc Cloud model. In this city, the Mc Cloud estimate was also the least accurate ($R^2 = 0.6141$). This leads to the conclusion that in this city, the ISO-ELM and empirical Hargreaves models were the best.

ISSN 2007-2422 •

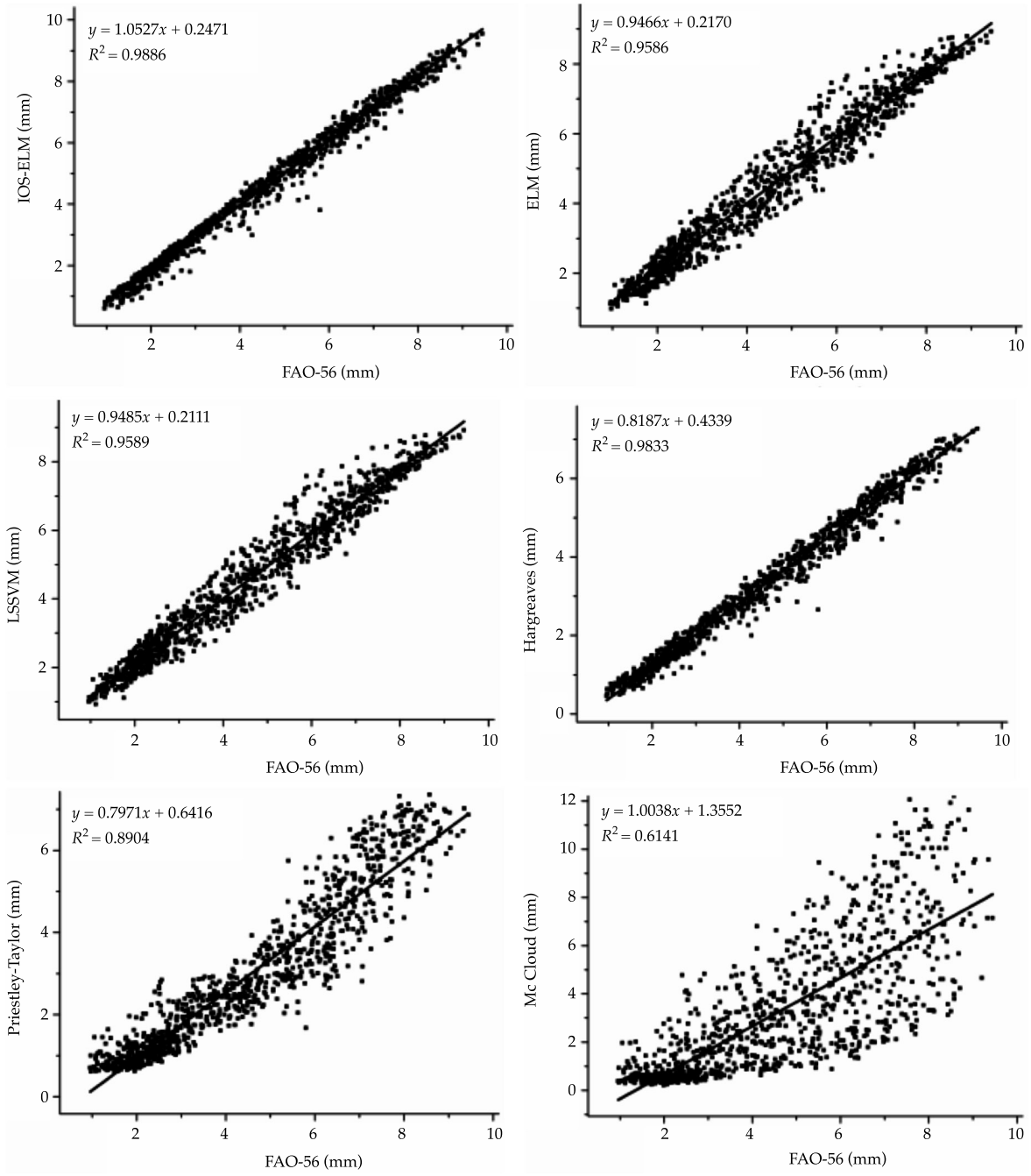

Figure 3. The FAO-56 PM *ET*0 and estimated ET0 values of Ankang.

For Hanzhong, ISO-ELM was closer to the FAO-56 PM *ET*0 of $R^2 = 0.9911$, followed by the Hargreaves, ELM, and LSSVM models. The Mc Cloud and Priestley-Taylor estimates were the least accurate.

For Hanzhong, ISO-ELM was closer to the FAO-56 PM *ET*0 with $R^2 = 0.9905$, followed by the ELM, LSSVM, Priestley-Taylor, Hargreaves and Mc Cloud models, which had R^2 values of 0.9547, 0.9488, 0.8804, 0.8335 and 0.5577, respectively.

• ISSN 2007-2422

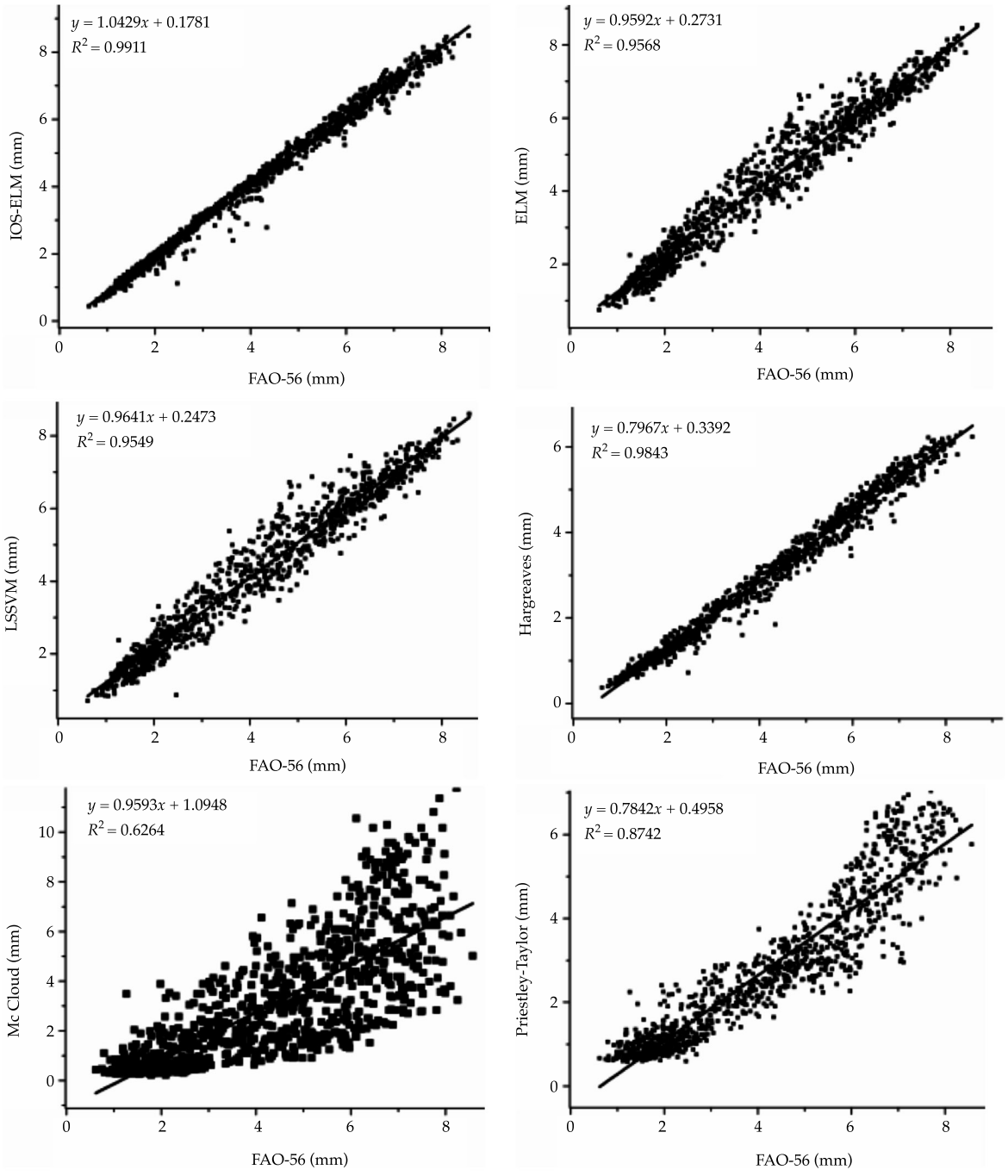

Figure 4. The FAO-56 PM ET0 and estimated *ET*0 values of Hanzhong.

The total *ET*0 estimation of every model is compared in table 7 because of its importance in irrigation management. The ISO-ELM clearly performed better than the other models from the relative error, which was 4.76, 0.23, 0.02 and 0.54%, respectively. In four of the cities, it gave the closest estimate to the total FAO-56 PM *ET*0 during the validation period.

For Yulin, the ELM and LSSVM had the same accuracy, which was the second best, and

ISSN 2007-2422 •

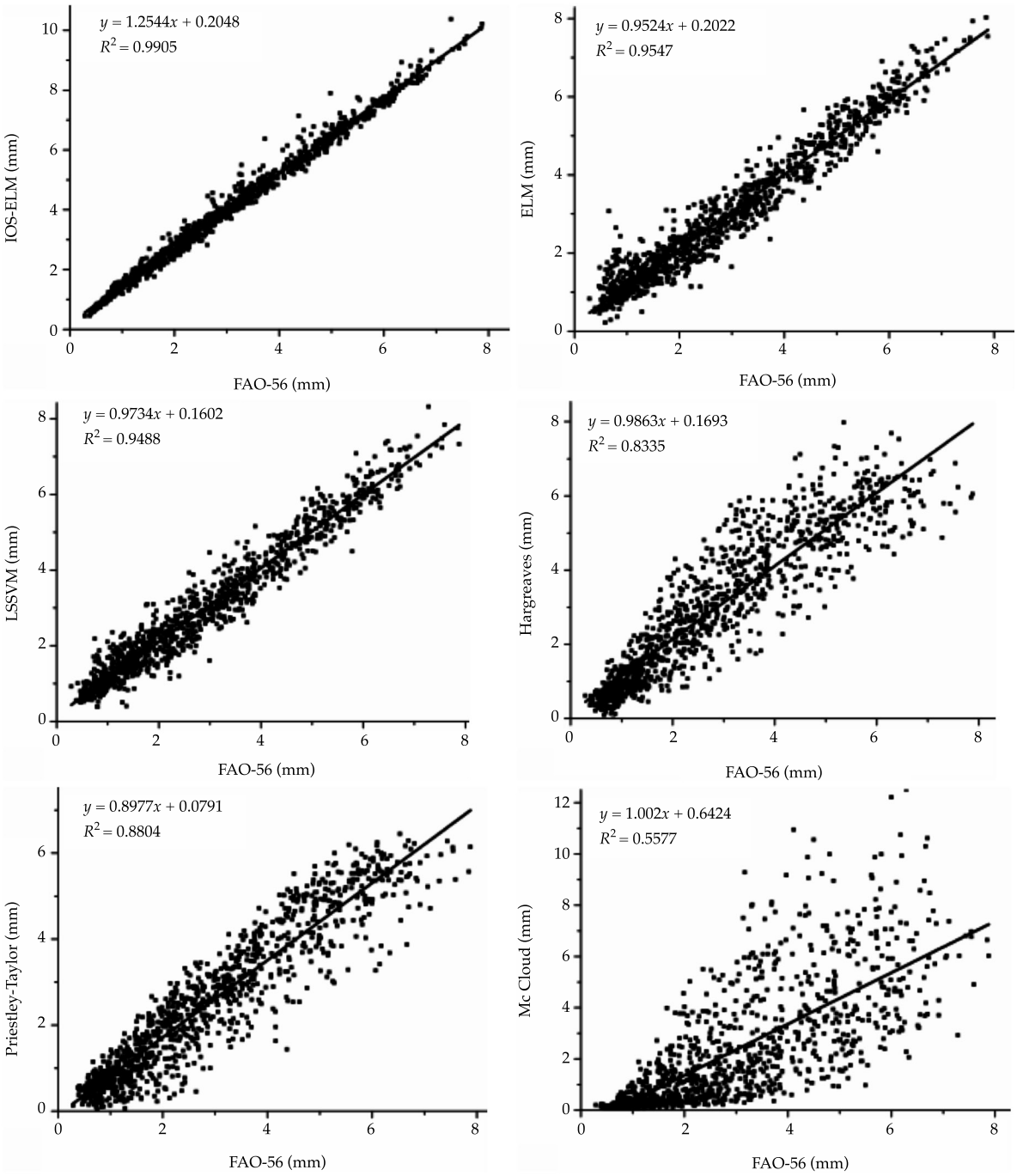

Figure 5. The FAO-56 PM ET0 and estimated *ET*0 values of Xi'an.

had 5274 and 5488 estimates lower than the 10% error, respectively. They were followed by Hargreaves, Priestley-Taylor and, lastly, McCloud (1955), which had the highest error at 64.60%. For Ankang, the LSSVM was ranked as the second best, followed by the ELM, Mc Cloud, Hargreaves and, finally, Priestley-Taylor. For Hangzhong, the LSSVM was ranked as the second best, followed by ELM, Hargreaves, Mc Cloud, and Priestley-Taylor, which had 28.49,

Table 7. Performance statistics of the models in the validation period.

Models	Total ET0(mm)				Relative error (%)			
	Yulin	Ankang	Hanzhong	Xi'an	Yulin	Ankang	Hanzhong	Xi'an
Observed	5 039	4 661	4 307	3 134	-	-	-	-
ISO-ELM	5 279	4 650	4 306	3 117	4.76	0.23	0.02	0.54
ELM	5 274	4 636	4 413	3 207	4.66	0.54	2.46	2.33
LSSVM	5 488	4 639	4 408	3 226	8.91	0.47	2.35	2.94
Hargreaves	3 003	3 362	3 080	3 276	40.40	27.87	28.49	4.53
Mc Cloud	1 784	3 672	2 999	2 436	64.60	21.22	30.37	22.27
Priestley-Taylor	2 844	3 051	2 864	2 727	43.56	34.54	33.50	12.99

30.37 and 33.50% error, respectively. For Xi'an, the ELM, LSSVM, and Hargreaves were ranked the second best, followed Priestley-Taylor and, finally, Mc Cloud.

In short, for the different cities, the ISO-ELM performed better than the other models, and the other models had different degrees to adapt to the application.

Conclusion

The improved sequential extreme learning machine (IOS-ELM) is designed and applied for simulation of daily reference evapotranspiration through different manipulation of the inverse of the matrix and using the regularization factor and online learning method at the same time Experimental results demonstrated that the IOS-ELM can learn faster and achieve better performance than traditional ELM.

First, the IOS-ELM model effectively overcomes the defects of traditional ELM, such as slow training speed, difficult parameter decisions, difficulty in setting the singularity and effect of data samples.

Second, the potential of the ISO-ELM technique for the estimation of reference evapotranspiration was investigated for four areas in Shaanxi of China; particularly, eight meteorological data were used as inputs.

Third, it was demonstrated that intelligent algorithm models (IOS-ELM, ELM, and LSSVM) are widely applicable to different areas, but empirical models were limited to specific regions and required modification.

Fourth, in the different meteorological data combinations for *ET*0 estimation, as long as there was a temperature-related parameter calculation, the calculation accuracy of *ET*0 was over 94%, and *T*max was especially effective. These accurate calculations can be a valuable reference for the development of intelligent irrigation in water decision-making systems.

Acknowledgments

This work was supported by the National High Technology Research and Development Program of China (863 Program) under Grant Nos. 2011AA100509-01.

Notation

The following symbols are used in this paper:

$ET0$ = reference evapotranspiration (mm day^{-1}).
Δ = slope of the saturation vapor pressure function (kPaC^{-1}).
Rn = net radiation (MJ m^{-2} day^{-1}).
G = soil heat flux density (MJ m^{-2} day^{-1}).
c = psychometric constant (kPa C^{-1}).
T = mean air temperature (°C).
U2 = average24-h wind speed at 2 m height (ms^{-1}).
Rs = solar radiation (MJ m^{-2} day^{-1}).
es = the saturation vapor pressure (kPa).
ea = the actual vapor pressure (kPa).

ISSN 2007-2422

References

Allen, R. G., Pereiral, L. S., Raes, D. *et al*. (1998). *Crop evapotranspiration: Guidelines for computing crop water requirements* (pp. 56). Rome: FAO Irrigation and Drainage.

Ao, T., Xiao, D., & Mao, Z. (2009). Batch-to-batch iterative learning control of a batch polymerization process based on online sequential extreme learning machine. *Industrial & Engineering Chemistry Research*, *48*(24), 11108-11114.

Feng, Y., & Cui, N. (2015). Prediction model of reference crop evapotranspiration based on extreme learning machine. *Transactions of the Chinese Society of Agricultural Engineering*, *31*(1), 153-158.

Kumar, M., Raghuwanshi, N. S., & Singh, R. (2011). Artificial neural networks approach in evapotranspiration modeling: A review. *Irrigation Science*, 29, 11-25.

Kisi O. (2007). Evapotranspiration modelling from climatic data using a neural computing technique. *Hydrol Process* 21:1925–1934.

Kisi O. (2008). The potential of different ANN techniques in evapotranspiration modelling. *Hydrol Process* 22:1449–2460

Kisi, O. (2011a). Evapotranspiration modeling using a wavelet regression model. *Irrigation Science*, *29*(3), 241-252.

Kisi, O. (2011b). Modeling reference evapotranspiration using evolutionary neural networks. *Journal of Irrigation and Drain Engineering*, *137*(10), 636-643.

McCloud, D. E. (1955). Water requirement of field crops in Florida as influenced by climate. *Proc. Soil Soc. Fla*., 15, 165-172.

Marti, P., Gonzalez-Altozano, P., & Gasque, M. (2011). Reference evapotranspiration estimation without local climatic data. *Irrig. Sci*., 29, 479-495.

Ozgur, K. (2013). Least squares support vector machine for modeling daily reference evapotranspiration. *Irrigation Science*, 31, 611-619.

Shiri, J., Kisi, O., Landeras, G. *et al*. (2012). Daily reference evapotranspiration modeling by using genetic programming approach in the Basque Country (Northern Spain). *Journal of Hydrology*, 414/415, 302-316.

Smith, M., Allen, R., & Pereira, L. (1997). *Revised FAO methodology for crop water requirements*. Rome: Land and Water Development Division, FAO.

Traore, S., Wang, Y. M., & Kerh, T. (2010). Artificial neural network for modeling reference evapotranspiration complex process in Sudano-Sahelian zone. *Agricultural Water Management*, *97*(5), 707-714.

Wang, Y. M., Traore, S., & Kerh, T. (2008). Neural network approach for estimating reference evapotranspiration from limited climatic data in Burkina Faso. *WSEAS Transactions on Computers*, *7*(6), 704-713.

Yubin, Z., Zhengying, W. *et al*. (2014). Calculation methods of crop reference evapotranspiration on the extreme weather. *Journal of China Rural Water and Hydropower*, 12, 64-71.

Author´s institutional address

Ph.D. Yubin Zhang
Prof. Zhengying Wei
Ph.D. Lei Zhang
Qinyin Lin
Ph.D. Jun Du

Xian Jiaotong University
School of Mechanical Engineering
State Key Laboratory of Manufacturing System Engineering
Department of Irrigation No. 28, Xianning West Road,
Xi'an, Shaan xi
Xi'an 710054, PR China
Telephone: +86 (181) 9270 5570
lzlgdx08-2@163.com
zywei@xjtu.edu.cn
403766645@qq.com
363370595@qq.com
99079477@qq.com

Haga clic aquí para escribir al autor

• ISSN 2007-2422

Comparison on nitrosation and anaerobic ammonium oxidation between activated sludge and biofilm from an autotrophic nitrogen removal SBBR

• Yu Qin* •
Chongqing Jiaotong University, China
*Corresponding author

• Jinsong Guo • Fang Fang •
Chongqing University, China

Abstract

Qin, Y., Guo, J., & Fang, F. (March-April, 2017). Comparison on nitrosation and anaerobic ammonium oxidation between activated sludge and biofilm from an autotrophic nitrogen removal SBBR. *Water Technology and Sciences* (in Spanish), *8*(2), 141-149.

Activated sludge and biofilm from a Sequencing Biofilm Batch Reactor (SBBR) were studied to analyze their different roles in autotrophic nitrogen removal process. Results showed that under aerobic conditions, the ammonia oxidation rate of activated sludge was 100% and the maximum rate was 0.23 mgN $mgVSS^{-1}$ d^{-1} during a 48 h test cycle. Under the same conditions, the ammonia oxidation rate of the biofilm was 72% and the maximum rate was 0.08 mgN $mgVSS^{-1}$ d^{-1}. The population of AOB (ammonium oxidizing bacteria) in activated sludge was 1.88×10^{11} cells/g, 10 times that in biofilm. The TN (total nitrogen) removal rate of activated sludge and biofilm under anaerobic conditions were 37% and 83%, respectively. The rate of anaerobic ammonium oxidation by activated sludge was 0.09 mgN $mgVSS^{-1}$ d^{-1} and that of biofilm was 0.22 mgN $mgVSS^{-1}$ d^{-1}. ANAMMOX (anaerobic ammonium oxidizing bacteria) were the dominant bacteria in terms of cell number in this system, with 2.66×10^{12} cells/g in biofilm, 2.6 times more than in activated sludge. TN was removed mainly by anaerobic ammonium oxidation.

Keywords: Autotrophic nitrogen removal, biofilm, activated sludge, AOB, ANAMMOX.

Resumen

Qin, Y., Guo, J., & Fang, F. (marzo-abril, 2017). Comparación de la nitrosación y la oxidación anaerobia de amonio entre lodo activado y biopelícula de un reactor biológico secuencial por lotes para la remoción autotrófica de nitrógeno. Tecnología y Ciencias del Agua, *8(2), 141-149.*

Se estudió el lodo activado y la biopelícula de un reactor biológico secuencial por lotes (SBBR) para analizar sus diferentes papeles en el proceso de remoción autotrófica de nitrógeno. Los resultados muestran que bajo condiciones aerobias, la velocidad de oxidación del amoníaco del lodo activado fue del 100% y la velocidad máxima fue de 0.23 mgN $mgVSS^{-1}$ d^{-1} durante un ciclo de pruebas de 48 horas. Bajo las mismas condiciones, la velocidad de oxidación del amoníaco de la biopelícula fue de 72% y la velocidad máxima fue de 0.08 mgN $mgVSS^{-1}$ d^{-1}. La población de BOA (bacterias oxidantes del amonio) en el lodo activado fue de 1.88×10^{11} células/g, diez veces más que en la biopelícula. La tasa de remoción del NT (nitrógeno total) del lodo activado y de la biopelícula bajo condiciones anaerobias fue del 37 y 83%, respectivamente. La velocidad de oxidación anaerobia del amonio por el lodo activado fue de 0.09 mgN $mgVSS^{-1}$ d^{-1} y la de la biopelícula fue de 0.22 mgN $mgVSS^{-1}$ d^{-1}. Las bacterias anaerobias oxidantes de amonio (ANAMMOX) fueron las bacterias dominantes en términos del número de células en este sistema, con 2.66×10^{12} células/g en la biopelícula, 2.6 veces más que en el lodo activado. El NT fue removido principalmente mediante la oxidación anaerobia del amonio.

Palabras clave: *remoción autotrófica de nitrógeno, biopelícula, lodo activado, BOA, ANAMMOX.*

Received: 24/05/2016
Approved: 26/10/2016

Introduction

Traditional nitrogen removal biotechnologies take a long process. But some researchers show that autotrophic denitrification can be performed by a Sequence Batch Biofilm Reactor (SBBR). Because this is done in a single reactor, rapidly, and using simple techniques, it has become a subject

of great interest in the field of biological nitrogen removal (Ahn, 2006; Jetten *et al*., 2005). The prevailing view holds that the main functional bacteria in this process are ammonia oxidizing bacteria (AOB), nitrite oxidizing bacteria (NOB) and anaerobic ammonium oxidizing bacteria (ANAMMOX) (Dong & Tollner, 2003; Sliekers *et al*., 2002; Third, Sliekers, Kuenen, & Jetten, 2001). Ammonium is partially oxidized by AOB to nitrite, which is subsequently consumed by ANAMMOX together with the remaining ammonium. However, AOB and NOB are aerobic bacteria while ANAMMOX are obligate anaerobes, which do not tolerate dissolved oxygen (DO) (Strousm, Vanger, Kuenen, & Jetten, 1997). Therefore, the key to one-step autotrophic denitrification in a single reactor is to balance the supply and demand of dissolved oxygen (Qin, Guo, Fang, & Yang, 2009; Hippen, Rosenwinkel, Baumgarten, & Seyfried, 1997; Galluzzo, Ducato, Bartolozzi, & Picciotto, 2001) and how to make them coexist in one reactor.

In this study, autotrophic nitrogen removal was conducted in an SBBR (Guo, Qin, Fang, & Yang, 2008). Previous research has shown that autotrophic nitrogen removal process has been set up and microbial community structure exerts significant influence on the performance of this system (Fang, Qin, Guo, Jia, & Yang, 2010). Microbes are at the core of the reactor, and the denitrification effect of activated sludge and biofilm is directly determined by the composition of the microbial community. This is a comparative study of activated sludge and biofilm in an SBBR, with quantitative analysis of functional bacterial populations as well as nitrogen transfer pathways. This study is to analyze the different roles between activated sludge and biofilm in autotrophic nitrogen process.

Materials and methods

Experimental apparatus

A schematic view of the SBBR autotrophic denitrification reactor is shown in figure 1. The reactor was filled with hollow balls fillers and soft combination packing. Under the condition of 30 °C and pH of 8.0, artificial synthetic ammonia nitrogen wastewater was added in. The concentration of NH_4HCO_3 was 160 mg/l without organic carbon sources. According to the optimal operation condition about 2h: 2h aeration/non-aeration ratio and DO 2.0 (aeration) mg/l /0.4 (non-aeration) mg/l, after half year domestication, autotrophic nitrogen removal system was set up successfully. TN removal rate reached to 80% while ammonia conversion rate reached to 100%.

Nitrosation and anaerobic ammonium oxidation were tested separately in both activated sludge and biofilm samples in the SBBR. Other tests were done in conical flasks (figure 2), which were sealed with rubber plugs to maintain a stable DO concentration. Artificial wastewaters with different NH_4^+-N or NO_2^--N concentrations were added.

Experimental apparatus

(1) Quantitative analysis of functional bacteria

DNA was extracted using a Shanghai Biocolors BioScience and Technology Company K717 environment genomic DNA extraction kit. Quantitative real-time PCR was carried out using SYBR Green Real-time PCR Master Mix Kit (Bio-Rad) in an iCycler IQ® Multiplex Real-Time PCR DNA System (Bio-Rad). A melting curve analysis was performed for each sample after PCR amplification to ensure that a single product with the expected melting curve characteristics had been obtained. The recombinant plasmid vectors were constructed by standard procedures.

(2) Nitrosation rate

Activated sludge and biofilm samples were taken from an SBBR which was performing effective and stable autotrophic nitrogen removal. The samples were diluted with distilled water and then inoculated into two 250 ml flasks, into which had already been added 100 ml of artificial wastewater. The initial concentration of NH_4HCO_3 was 70 mg/l, and pH was adjusted to 8.0 (± 0.2) by the addition of $NaHCO_3$. The nutrient solution with trace elements such as Fe, Mg

• ISSN 2007-2422

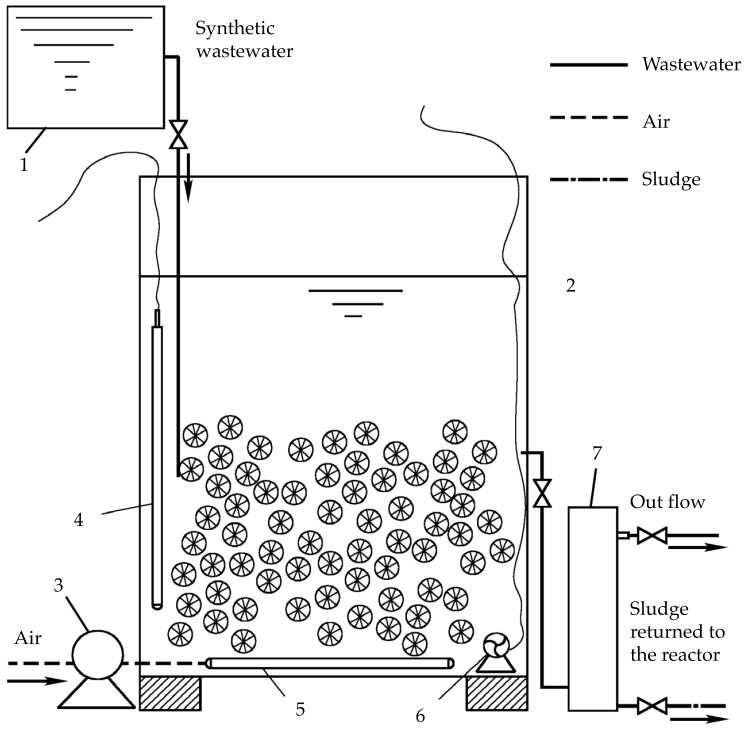

Figure 1. Schematic representation of the reactor and workflow. 1. Wastewater tank; 2. SBBR reactor; 3. Air pump; 4. Calorstat; 5. Aerating stick; 6. Stirrer; 7. Effluent tank.

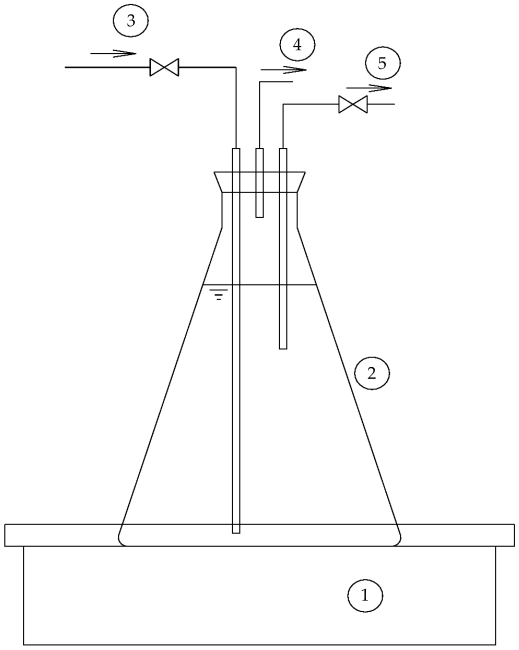

Figure 2. Schematic representation of the flask-shaking experiment. 1. Incubator; 2. Conical flask; 3. Aeration tube; 4. Exhaust tube; 5. Sampling tube.

ISSN 2007-2422

Table 1. Primers and parameters used in real-time PCR.

	Primers	Reaction parameters	Reference
AOB	5′-GGAGRAAAGCAGGGGATGG-3′ 5′-CGTCCTCTCAGACCARCTACTG-3′	95 °C × 5 min; 95 °C × 15 s, 60 °C × 45 s; 45 cycles	Li, Liu, Zhang, Du, & Chen, 2007
NOB	5′-CCTGCTTTCAGTTGCTACCG-3′ 5′-GTTTGCAGCGCTTTGTACCG-3′	95 °C × 5 min; 95 °C × 1 min; 60 °C × 1 min; 72 °C × 2 min; 35 cycles	Dionisi *et al.*, 2002
ANAMMOX	5′-ATGGGCACTMRGTAGAGGGGTTT-3′ 5′-AACGTCTCACGACACGAGCTG-3′	50 °C × 2 min; 94 °C × 10 min; 94 °C × 15 s; 60 °C × 1 min; 40 cycles	Ikuo, Tomonori, & Satoshi, 2007

was also added (EDTA 5.0 g/l, $CoCl_2{\cdot}6H_2O$ 1.6 g/l, $ZnSO_4{\cdot}7H_2O$ 2.2 g/l, $MnCl_2{\cdot}4H_2O$ 5.1 g/l, $CuSO_4{\cdot}5H_2O$ 1.6 g/l $(NH_4)_6Mo_7O_{24}{\cdot}4H_2O$ 1.1 g/l, $CaCl_2{\cdot}2H_2O$ 5.5 g/l, $FeSO_4{\cdot}7H_2O$ 5.0 g/l). The flasks were maintained at a temperature of 30 °C using a heated magnetic stirrer. DO concentration was controlled to 2.0 mg/l by aerating with a mixture of O_2 and Ar. The flasks were placed in a constant temperature shaking reactor at 30 °C and shaken at 150 revs/min.

Concentrations of NH_4^+, NO_2^-, NO_3^- and TN were measured at intervals during each 48 h test to obtain concentration curves. The maximum reaction rate Vmax was calculated from the maximum slope of each concentration curve. At the end of each test, activated sludge or biofilm samples were taken out of the flask by brushing with a sterile brush and rinsing with distilled water, and volatile suspended solids (VSS) were measured:

$$V_{max} = \frac{k_{max}(\text{mgN}/d)}{\text{VSS}(\text{mgVSS})}$$

(3) Anaerobic ammonium oxidation rate

The experimental procedure and analysis was similar to the study of nitrosation rate, except for the components of artificial wastewater and DO concentration. NH_4HCO_3 and $NaNO_2$ concentrations in the artificial liquid were both 70 mg/l. The liquid was sparged with Ar gas for 30 min to remove DO to below the detection limit (0.01 mg/l) of an LDO™ HQ10 dissolved oxygen meter.

Results and discussion

Identification of recombinant plasmid

The recombinant plasmids sequences were analyzed using a GenBank BLAST search. As shown in table 2, conservative regions of 16S rDNA of functional bacteria were obtained. These recombinant plasmids were suitable for quantitative analysis of AOB, NOB, and ANAMMOX in real-time PCR experiments.

Quantitative analysis of AOB, NOB, and ANAMMOX

Quantitative real-time PCR results are shown in table 3. The populations of the three main functional bacteria (ammonia oxidizing bacteria AOB, nitrite oxidizing bacteria NOB and anaerobic ammonium oxidizing bacteria ANAMMOX) in activated sludge and biofilm samples were

Table 2. A partial result of recombinant sequence alignment with genes in GenBank.

Sample	Length	Number	Similarity	Blast result
I	117bp	FJ445022	CP000450 (98%)	*Nitrosomonas*
II	151bp	FJ490152	AJ224046 (100%)	*Nitrospira*
III	275bp	FJ490144	AF375995 (99%)	*Candidatus kuenenia stuttgartiensis*

• ISSN 2007-2422

Table 3. Bacterial population in different samples (cells/g VSS).

Sample	AOB	NOB	ANAMMOX
Activated sludge	1.88×10^{11}	1.19×10^{9}	1.04×10^{12}
Biofilm	1.90×10^{10}	7.62×10^{8}	2.66×10^{12}

significantly different. That is to say that in this autotrophic nitrogen removal system, activated sludge and biofilm contained different communities of functional bacteria. This suggests that activated sludge and biofilm play different roles in the overall nitrogen removal procedure.

AOB

In the first step in the nitrogen removal process, ammonium was oxidized to nitrite by AOB. The population of AOB in the activated sludge sample was 1.88×10^{11} cells/g, almost nine times higher than the 1.90×10^{10} cells/g found in the biofilm. AOB are typically aerobic bacteria which thrive under high DO. Activated sludge was suspended in the reactor and was in intimate contact with DO. However, poor mass transfer of DO, into the biofilm meant that the interior layer of biofilm was anaerobic or at least had low DO concentration. Therefore AOB tended to be found in activated sludge or the exterior layer of biofilm.

NOB

NOB numbers were 2 to 4 orders of magnitude less than AOB and ANAMMOX in both activated sludge and biofilm samples. NOBs were not the dominant bacteria in terms of cell number in this SBBR reactor although they multiplied faster than AOB under normal conditions (5-20 °C) (Hellinga, Schellen, Mulder, & Heijnen, 1998). Other studies have also shown that at higher temperatures (> 20 °C), the degradation rate of AOB can be higher than that of NOB (Hellinga *et al*., 1998). During the start-up period of this study, the temperature was kept around 30 °C so that NOB was depleted and AOB became be the dominant group to accomplish one-step autotrophic nitrogen removal and prevent nitrite from being oxidized to nitrate.

ANAMMOX

The population of ANAMMOX was 5.5 times that of AOB and 874 times that of NOB in activated sludge samples. These differences were more pronounced in biofilm samples, at 140 times and 3491 times, respectively. Jetten *et al.* (2001) reported that anaerobic ammonia oxidation was achieved only when the ANAMMOX population was higher than 10^{10}–10^{11} cells/ml. Therefore, although ANAMMOX cells were the most abundant one among three functional bacteria in this study, they did not dominate the metabolic functionality. AOB and NOB are an aerobic bacteria, but ANAMMOX are anaerobic and are sensitive to DO. They can not survive even at 0.5–2.0% air saturation. The low rate of mass transfer of DO in biofilm and depletion by AOB and NOB in the outer layer made the interior of the biofilm an ideal condition for ANAMMOX. As a result, the population of ANAMMOX in biofilm was 2.66×10^{12} cells/g, which was 2.6 times that in activated sludge.

Nitrosation of activated sludge and biofilm

Transformation of nitrogen in activated sludge and biofilm samples in a cycle of nitrosation are shown in figures 3a and 3b.

Figure 3a shows that ammonia can be fully oxidized by activated sludge in a single 48 h cycle, with the ammonia oxidation rate reaching 100%. The maximum rate occurred between the 6 and 20 h with a maximum ammonia oxidation rate of 0.23 mgN mgVSS^{-1} d^{-1}. 85% of the oxidized ammonia was present as NO_2^--N and 9% as NO_3^--N. There was the limited removal of

ISSN 2007-2422

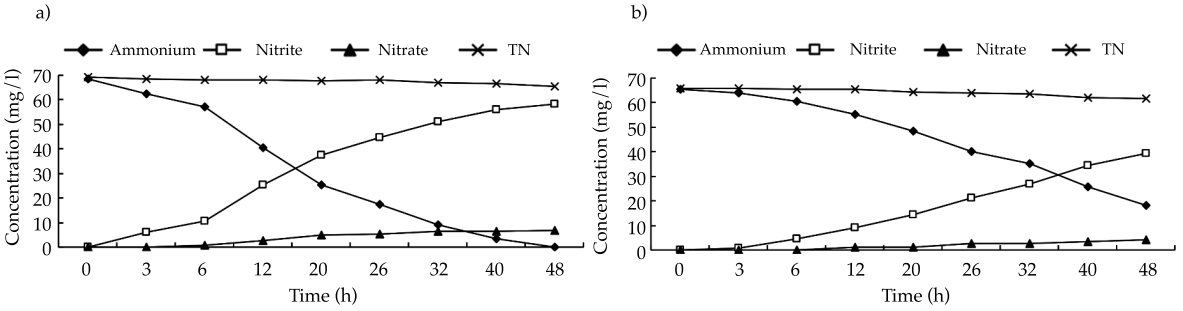

Figure 3a. Nitrosation by activated sludge. Figure 3b. Nitrosation by biofilm.

TN. The activated sludge in this system showed good ammonia oxidation activity under aerobic conditions. Nitrogen transformation by biofilm during a 48 h cycle is shown in figure 3b. The ammonia oxidation rate was 72%. Compared with nitrosation by activated sludge, there was no obvious inflection point on the ammonia concentration curve with biofilm. The maximum rate of ammonia oxidation rate by biofilm was 0.08 mgN mgVSS^{-1} d^{-1}. The nitrosation activity of activated sludge was about 2.89 times that of the biofilm. Ammonia was mainly oxidized to NO_2^--N and the maximum concentration of NO_3^--N was only 4 mg/l at the end of the reaction cycle. The TN removal rate was 6.7%.

Both activated sludge and biofilm showed high nitrosation activities and there was little NO_3^--N accumulation in either system because they were acclimated to nitrosating conditions at the start of the experiment. NOB had been depleted and so most of the oxidized ammonia existed as nitrite. There were 158 times as many AOB as NOB cells in activated sludge samples while the ratio was 25 times in the biofilm sample. Accordingly, the aerobic ammonia oxidation rate of biofilm was less than that of activated sludge. This also led to a difference in nitrosation capacity between the two samples. This experiment used real-time PCR technology for bacterial quantification. Results showed that the populations of AOB were 1.88×10^{11} cells/g in the activated sludge samples and 1.90×10^{10} cells/g in biofilm samples. Cell counts in the sludge sample were about ten times those in the biofilm. AOB, which were responsible for aerobic ammonia oxidization, were mainly found in activated sludge in this SBBR autotrophic nitrogen removal reactor.

Studies have shown that there might be denitrification under aerobic conditions by aerobic denitrifiers (Robertson & Kuenen, 1990; Chen, Xia, & Ju, 2003; Hung, Mitsuyo, & Makoto, 2005). However, in this study, aerobic TN removal rates of activated sludge or biofilm samples were both low. After 48 h, the TN removal rates of sludge and biofilm samples were only 6.7 and 5.3% respectively. The NH_4^+ to NO_2^- conversion rates of sludge and biofilm samples were 85 and 83%, respectively. The concentration of NO_3^- was low, with the highest concentrations seen at the end of the 48 h experiment cycle of just 6.7 and 4.0 mg/l. Little aerobic denitrification was seen in the SBBR autotrophic nitrogen removal process. ANAMMOX activity was limited by continuous aeration to maintain a DO concentration of 2.0 mg/l, but ANAMMOX which survived in the activated sludge flocs and the interior of biofilm might provide the system with some anaerobic nitrogen removal capability.

Anaerobic ammonium oxidation of activated sludge and biofilm

Figures 4a and 4b show the anaerobic ammonium oxidation activities of activated sludge and

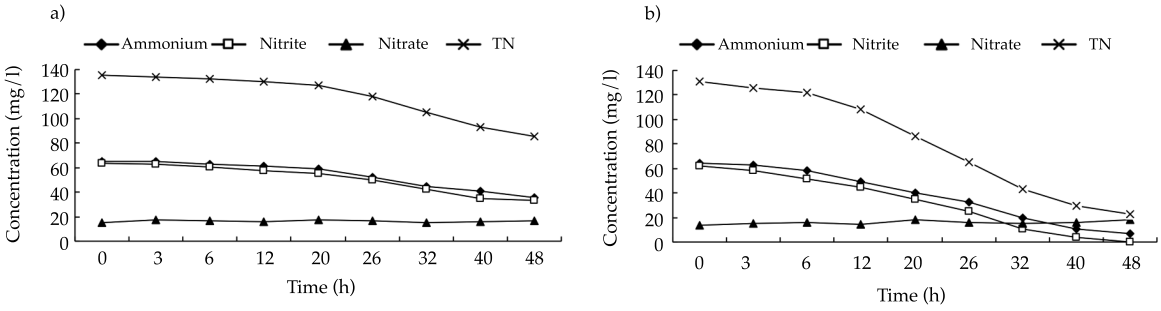

Figure 4a. Anaerobic oxidation of ammonium. Figure 4b. Anaerobic oxidation of ammonium by activated sludge by biofilm.

biofilm samples. Initial concentrations of NH_4^+ and NO_2^- in the artificial wastewater were both 70 mg/l. TN concentrations in both samples declined over the 48h experimental period. TN removal rates were 37% by activated sludge and 83% by biofilm. In contrast with nitrosation activity, it was confirmed that TN was removed mainly by anaerobic ammonium oxidation in this reactor. The reaction rate of anaerobic ammonium oxidation by activated sludge was 0.09 mgN mgVSS^{-1} d^{-1}. This was just 41% of the rate seen in biofilm, which was 0.22 mgN mgVSS^{-1} d^{-1}.

The concentration of NO_3^- in the activated sludge treatment varied between 15.0 and 17.4 mg/l, and in the biofilm treatment, the range was 13.8 to 18.0 mg/l, though no NO_3^--N was added to the artificial wastewater. The initial concentrations of NO_3^- in activated sludge and biofilm treatments were 15.0 and 13.8 mg/l, respectively. One possibility is that $NaNO_2^-$ was unstable and was partially oxidized to $NaNO_3$, which provided the initial NO_3^-. Figures 4a and 4b show that the concentrations of NO_3^- did not vary greatly over the course of the experiments. The small fluctuations that were observed may have been caused by measurement error. Van de Graaf *et al*. (1995) concluded that ANAMMOX could utilize both NO_3^- and NO_2^- in the anaerobic ammonium oxidation reaction because both can function as electronic receptors to convert the remaining NH_4^+ into N_2. When the substrate contained both NO_3^- and NO_2^-, it was the NO_2^- that acted as the main electronic receptor for ANAMMOX. In this study, the removal efficiency of TN was high and the largest consumption rates of NH_4^+ and NO_2^- in activated sludge were 0.05 and 0.06 mgN mgVSS^{-1} d^{-1}, respectively while for biofilm the values were 0.12 and 0.14 mgN mgVSS^{-1} d^{-1}. The concentration of NO_3^- in the system was more-or-less constant, which suggests that NO_2^- was the main electronic receptor in anaerobic ammonium oxidation in this SBBR system. This was in accordance with Van de Graaf's findings.

Conclusions

Activated sludge and biofilm played different roles in autotrophic nitrogen removal process.

Both activated sludge and biofilm samples exhibited nitrosation activity in the SBBR autotrophic denitrification system, the maximum ammonia oxidation rates of activated sludge and biofilm were 0.23 and 0.08 mgN mgVSS^{-1} d^{-1}, respectively. The nitrosation activity of activated sludge was about 2.89 times that of the biofilm. The populations of AOB in activated sludge and biofilm were 1.88×10^{11} and 1.90×10^{10} cells/g, respectively.

The maximum anaerobic ammonia oxidation rate of activated sludge was 0.09 mgN mgVSS^{-1} d^{-1}, just 41% of the maximum rate of biofilm, which was 0.22 mgN mgVSS^{-1} d^{-1}. Anaerobic ammonia oxidation occurred mainly in the biofilm, with ANAMMOX being the dominant

ISSN 2007-2422

bacteria in this process. The populations of ANAMMOX were 1.04×10^{12} cells/g in activated sludge and 2.66×10^{12} cells/g.

TN removal rates of sludge and biofilm samples were just 6.7 and 5.3%, respectively, under aerobic conditions with both NO_2^- and NO_3^- present. No significant aerobic denitrification was seen in this SBBR autotrophic nitrogen removal system. TN removal in this study was performed mainly by ANAMMOX under anaerobic condition.

Acknowledgments

This work was supported by the National Natural Science Foundation Project of China (51609026).

References

Ahn, Y. H. (2006). Sustainable nitrogen elimination biotechnologies: A view. Process Biochemistry, 41(8), 1709-1721.

Chen, F., Xia, Q., & Ju, L. K. (2003). Aerobic denitrification of Pseudomonas aeruginosa monitored by online NAD(p)H fluorescence. Applied & Environmental Microbiology, 69(11), 6715-6722.

Dionisi, H. M., Layton, A. C., Harms, G., Gregory, I. R., Robinson, K. G., & Sayler, G. S. (2002). Quantification of Nitrosomonas oligotropha-like ammonia-oxidizing bacteria and Nitrospira spp. from full-scale wastewater treatment plants by competitive PCR. Applied and Environmental Microbiology, 68(1), 245-253.

Dong, X., & Tollner, E. W. (2003). Evaluation of anammox and denitrification during anaerobic digestion of poultry manure. Bioresource Technology, 86(2), 139-145.

Fang, F., Qin, Y., Guo, J. S., Jia, L., & Yang, G. H. (2010). The relationship between performance and microbial community structure of SBBR autotrophic nitrogen removal process. Journal of Civil, Architectural & Environmental Engineering, 32(3), 113-118.

Galluzzo, M., Ducato, R., Bartolozzi, V., & Picciotto, A. (2001). Expert control of DO in the aerobic reactor of an activated sludge process. Computers & Chemical Engineering, 25, 619-625.

Guo, J. S., Qin, Y., Fang, F. & Yang, G. H. (2008). Characterization of the start-up period of single-step autotrophic nitrogen removal in a sequencing batch reactor. Journal of Chongqing University (English edition), 7(1), 17-22.

Hippen, A., Rosenwinkel, K. H., Baumgarten, G., & Seyfried, C. F. (1997). Aerobic deammonification: A new experience in the treatment of wastewater. Water Science and Technology, 35(10), 111-120.

Hellinga, C., Schellen, A. A. J. C., Mulder, J. W., & Heijnen, J. J. (1998). The Sharon process: An innovative method for nitrogen removal from ammonium rich wastewater. Water Science and Technology, 37(9), 135-142.

Hung, S. J., Mitsuyo, H., & Makoto, S. (2005). Characteristics of ammonium removal by heterotrophic nitrification-aerobic denitrification. Bioscience and Bioengineering, 100(2), 184-191.

Ikuo, T., Tomonori, K., & Satoshi, O. (2007). Quantification of anaerobic ammonium-oxidizing bacteria in enrichment cultures by real-time PCR. Water Research, 41(4), 785-794.

Jetten, M. S. M., Cripus, I., Kartal, B., Van Niftrik, L., Van de Pas-Schoonen, K. T., Sliekers, O., Haaijer, S., Van der Star, W., Schmid, M., Van de Vossenberg, J., Schmidt, I., Harhangi, H., Van Loosdrecht, M., Gijs Kuenen, J., Op den Camp, H., & Strous, M. (2005). 1994-2004: 10 year of research on the anaerobic oxidation of ammonium. Biochemical Society Transactions, 33(1), 119-123, DOI: 10.1042/BST0330119.

Jetten, M. S., Wagner, M., Fuerst, J., Van Loosdrecht, M., Kuenen, G., & Strous, M. (2001). Microbiology and application of the anaerobic ammonium oxidation (anammox) process. Curr. Opin. Biotechnol., 12(3), 283-288.

Li, G. W., Liu, H., Zhang, F., Du, G. C., & Chen, J. (2007). Real-time PCR quantification of ammonia-oxidizing bacteria in aerobic granular sludge and activated sludge influenced by pentachlorophenol. Acta Microbiologica Sinica, 47(1), 136-140.

Qin, Y., Guo, J. S., Fang, F. & Yang, G. H. (2009). Effect of DO and aeration/non-aeration ratio on the microbial community structure in one-step SBBR completely autotrophic nitrogen removal process. Environmental Science, 30(2), 191-196.

Robertson, L. A., & Kuenen, J. G. (1990). Combined heterotrophic nitrification and aerobic denitrification in Nitrosomonas oligotropha and other bacteria. Antonie Van Leeuwenhoek, 57, 139-152.

Sliekers, A. O., Derworth, N., Gomez, J. L. C. Strous, M., Kuenen, J. G., & Jetten, M. S. (2002). Completely autotrophic nitrogen removal over nitrite in one single reactor. Water Research, 36(10), 2475-2482.

Strousm, M., Vanger, V., Kuenen, J. G., & Jetten, M. (1997). Effects of aerobic and microaerobic conditions on anaerobic ammonium-oxidizing (Anammox) sludge. Applied and Environmental Microbiology, 63(6), 2446-2448.

Third, K. A., Sliekers, A. O., Kuenen, J. G., & Jetten, M. S. (2001). The CANON (completely autotrophic nitrogen removal over nitrite) under ammonium limitation: interaction and competition between three groups of bacteria. Systematic and Applied Microbiology, 24(4), 588-596.

Van de Graaf, A. A., Mulder, A., De Bruijn, P., Jetten, M. S., Robertson, L. A., & Kuenen, J. G. (1995). Anaerobic oxidation of ammonium is a biologically mediated process. Applied and Environmental Microbiology, 61(4), 1246-1255.

Author´s institutional address

Ph.D. Yu Qin

Chongqing Jiaotong University
Key laboratory of Hydraulic and Waterway Engineering of the Ministry of Education, Chongqing Jiaotong University
No. 66 Xuefu Road, Nanan district, Chongqing, 400074, PR China
Telephone: +86 (138) 8365 6798
qinyu54001@163.com

Ph.D. Jinsong Guo
Ph.D. Fang Fang

Chongqing University
Faculty of Urban Construction and Environmental Engineering
No. 174 Shazheng Road, Shapingba district, Chongqing, 400045, PR China
Telephone: +86 (139) 0836 1681 / (133) 2028 5392
guo0768@cqu.edu.cn
fangfangcq@cqu.edu.cn

Haga clic aquí para escribir al autor

Plaza de Tiananmén, Beijing, China.

Foto: Fernando Leyva Calvillo.

Water table response to a pumping test in the hinterland core area of the Taklimakan Desert, China

• Yaping Wei •
Xinjiang Institute of Ecology and Geography Chinese Academy of Sciences/ University of Chinese Academy of Sciences

• Jinglong Fan* • Xinwen Xu • Jiaqiang Lei •
Xinjiang Institute of Ecology and Geography Chinese Academy of Sciences
*Corresponding author

Abstract

Wei, Y., Fan, J., Xu, X., & Lei, J. (March-April, 2017). Water table response to a pumping test in the hinterland core area of the Taklimakan Desert, China. *Water Technology and Sciences* (in Spanish), *8*(2), 151-158.

In this article, hydrogeological parameters were determined by a single well pumping test. Over the course of the study, BETCO was used to eliminate the effects of atmospheric pressure changes on water level based on the regression deconvolution method. The aquifer test was used to analyze data and to calculate hydrogeological parameters. Finally, from the three unconfined aquifer models, though the Boulton model cannot successfully gain well-fitting results, the Theis model with Jacob correction and the Neuman model results obtained hydrogeological parameters by curve-fitting. Additionally, permeability coefficient of the two models is in good agreement with previous research, which can provide a reference for further study in the hinterland of the desert, especially for the construction of hydrological modeling research.

Keywords: Pumping test, aquifer test, pressure correction, hydrogeological parameters.

Resumen

Wei, Y., Fan, J., Xu, X., & Lei, J. (marzo-abril, 2017). Respuesta de la capa freática a una prueba de bombeo en el área interior central del desierto de Taklimakan, China. Tecnología y Ciencias del Agua, *8*(2), *151-158.*

En el presente artículo se determinaron los parámetros hidrogeológicos mediante una prueba de bombeo de un solo pozo. Durante el estudio se utilizó BETCO para eliminar los efectos de los cambios de presión atmosférica en el nivel del agua con base en el método de regresión-deconvolución. Se utilizó la prueba de acuíferos para analizar los datos y calcular los parámetros hidrogeológicos. Finalmente, de los tres modelos de acuíferos confinados, aunque el modelo Boulton no puede arrojar resultados bien ajustados, el modelo Theis con corrección de Jacob y el modelo Neuman obtuvieron resultados de parámetros hidrogeológicos mediante ajuste de curvas. Además, el coeficiente de permeabilidad de los dos modelos concuerda bien con investigaciones anteriores, las cuales pueden servir de referencia para estudios posteriores en el interior del desierto, especialmente para la investigación de modelos hidrológicos.

Palabras clave: *prueba de bombeo, prueba de acuíferos, corrección de presión, parámetros hidrogeológicos.*

Received: 15/06/2016
Approved: 26/10/2016

Introduction

A comprehensive and accurate understanding of aquifer hydraulic properties is the basis for efficient management of groundwater resources, which can be developed by pumping test determining aquifer hydrological parameters for groundwater modeling, aquifer vulnerability assessment, among others (Wen, Wu, Yeh, & Tseng, 2010; Li, Qian, & Wu, 2014; Criollo, Velasco, Vázquez-Suñé, & García-Gil, 2016). The accuracy of data derived from pumping test is of concern to parameters calculation, which fluctuating along with the variety of barometric pressure, sea tides and so on (Guo & Jiao, 2008; Guo, Jiao, & Weeks, 2008). In the process of

studying, hydrogeologists devoted themselves to theoretical and practical work on pumping tests, it was found the influence of barometric pressure on water level cannot be ignored, that pressure efficiency is expressed by a simple linear equation at first (Jacob, 1940). After long time duration of studying, for the pumping test process, it was found that the groundwater level (especially the deep well water level) response is not linear, but rather a complex nonlinear response, which makes it inappropriate to use a linear regression method for the pressure correction (Quilty & Roeloffs, 1991; Seo, 2001). Among lots of researchers, Rasmussen and Crawford (1997) used a regression deconvolution method to determine pressure correction and achieved good results.

The hinterland of the Taklimakan Desert, which belongs to a sedimentary area in the southern section of the Tarim Basin, is an ancient alluvial flood plain that formed from many rivers in the northern slope of the Kunlun Mountains. Precipitation and condensed water supply no recharge to groundwater basically (Yu, 1992), which is mainly affected by the Kunlun Mountain piedmont plain groundwater lateral runoff recharge. There are rich oils and natural gas resources, but the climate is extremely dry, and the precipitation is below 50 mm with an annual evaporation of 3 000 mm, no surface water exists generally (Xu, Li, Zhou, & Zhou, 2001). Therefore, the water used for production and living comes entirely from the exploitation of groundwater, unconfined water, particularly, which is formed by river infiltration and lateral groundwater infiltration belonging to pore water stored in Quaternary deposits, whose main hydrochemical types are Na-Mg-Cl-SO_4 and Na-Cl-SO_4 (Wei, Fan, Xu, Jin, & Zhou, 2016), and salinity is 3-10 g/l. The depth of groundwater between longitudinal dune usually is 1-5 m, and over 20 m at top of ones. It was found that when the groundwater depth is less than 1.5 m, the groundwater is affected by strong evaporation (Fan *et al*., 2010), coincide with the terrain trend, the water table is relatively flat, with a flow velocity measured between 21 m/year and 205 m/year (Lei, Li, Jin, & Xu, 2008).

In this paper, a single-well pumping test established at the core area of pumping in the hinterland of the Taklimakan Desert was used to calculate the hydrogeological parameters, in order to provide a reference of the future groundwater research, especially the construction of hydrological modeling.

Methods and experiments

We observed the water level of the whole year and conducted single-well pumping test from 2009 Jul. 27th to Aug. 12th day in the core area of water supplying in the oil field with observation time interval was every 30 min. The pumping well is located in the hinterland of the Taklimakan Desert (38º 58′ 20.77″, 83° 39′ 39.60″) (figure 1), with the observation well (38° 58′ 21.78″, 83° 39′ 37.35″) logging in the northwest at a distance of r = 58.6 m (figure 2). The elevation of pumping well is 1 104.9 m. The thickness and effective thickness of unconfined aquifer are 66.00 and 40 m, respectively in the study area where the depth of groundwater is 6m, the formation is single fine sand of Quaternary. The casing pipe of the partial penetrating observation well is hard PVC material and depth was measured by Solinst Levelogger Model 3001. In the experiment, discharge rate was set as 32 m^3/h and it was regarded as having achieved stable state when the fluctuation of the drawdown was not more than 1% (Wang *et al*., 2013). The regression deconvolution was performed in order to adjust the groundwater level using BETCO from Sandia Labs (USA). The hydrogeological parameters were calculated by Aquifer Test 2011.1 designed by Waterloo Hydrogeologic Inc. (incorporated into Schlumberger Water Services since 2005) to provide a reference for the construction of hydrological modeling.

Barometric pressure correction

In measuring groundwater level, many natural forces have important theoretical and practical significance to the borehole water level (Guo & Jiao, 2008). In particular, when the impact of

• ISSN 2007-2422

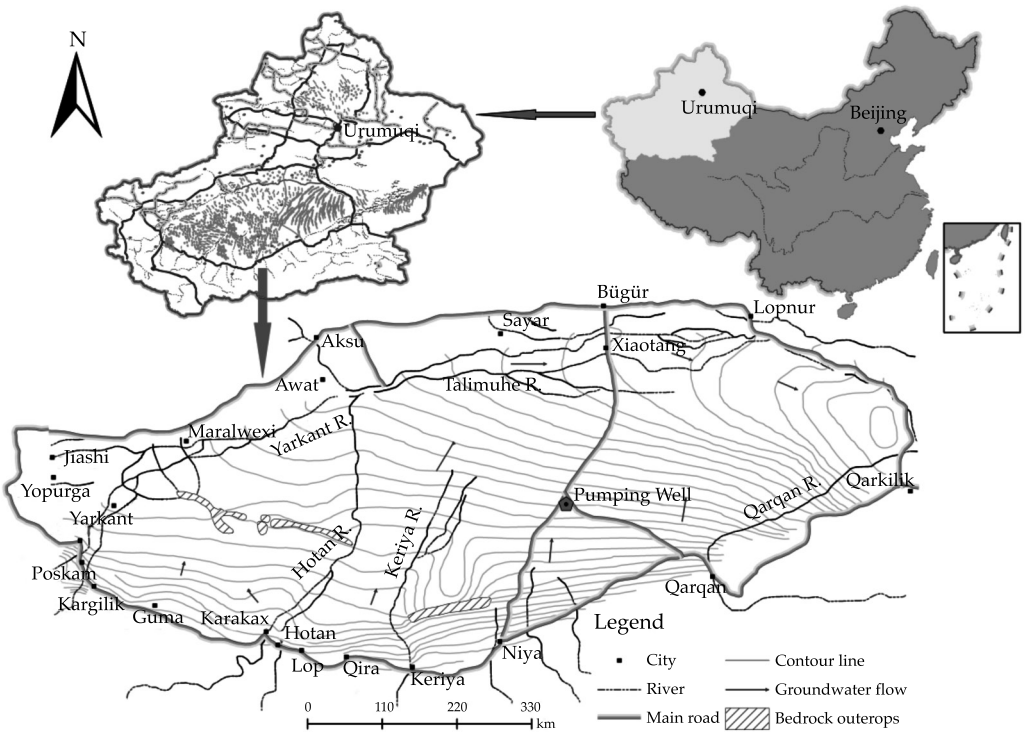

Figure 1. The location of Pumping Well in the Taklimakan Desert.

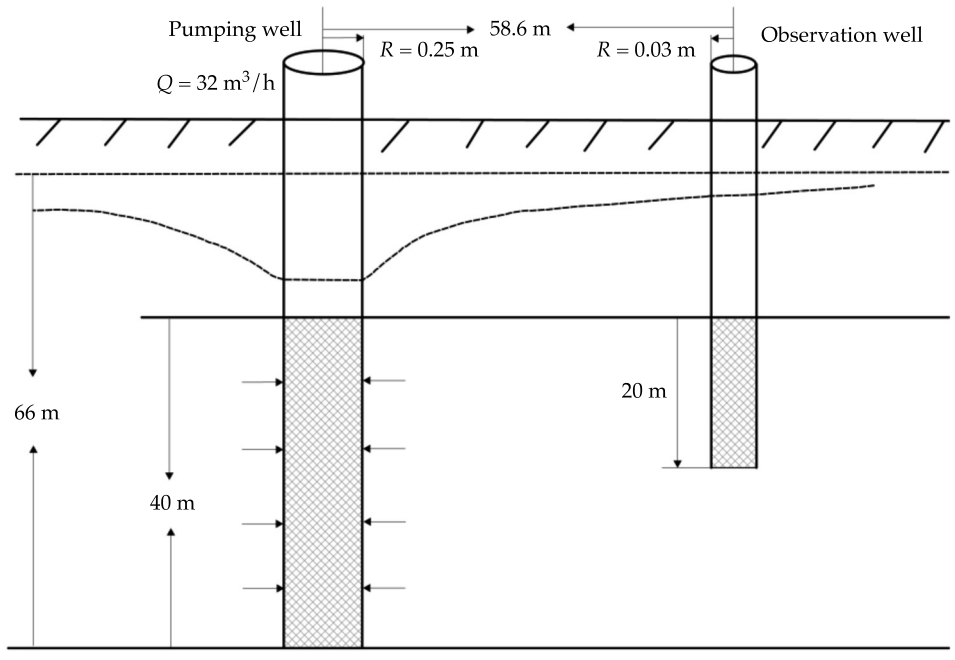

Figure 2. The geometry of the pumping and observation wells.

ISSN 2007-2422

barometric pressure on the water level cannot be ignored compared to the larger circumstances (such as the late period pumping test), it is important to perform barometric pressure calculations in order to obtain accurate aquifer parameters (Wang *et al.*, 2012). During an extended period of pumping test processes, the delayed response, due to the transmission of the barometric pressure perturbation through the unsaturated zone and borehole storage or skin effects, causes a water level difference between the aquifer and the pumping well. Rasmussen and Crawford proposed the regression deconvolution method could be used to correct the groundwater level in order to eliminate the influence of barometric pressure (Rasmussen & Crawford, 1997). After the response function $\delta(i)$ to a barometric pressure pulse is obtained by using ordinary least square method linear regression, the step response $\alpha(j)$ can be found by summing the impulse responses:

$$\alpha(j) = \sum_{i=0}^{j} \delta(i) \tag{1}$$

Then, it was following correction variables of the water levels that being found (Toll & Rasmussen, 2005):

$$\begin{bmatrix} W_m^* \\ W_{m+1}^* \\ W_{m+2}^* \\ \dots \\ W_n^* \end{bmatrix} = \begin{bmatrix} \Delta B_1 & \Delta B_2 & \Delta B_3 & \dots & \Delta B_m \\ \Delta B_2 & \Delta B_3 & \Delta B_4 & \dots & \Delta B_{m+1} \\ \Delta B_3 & \Delta B_4 & \Delta B_5 & \dots & \Delta B_{m+2} \\ \dots & \dots & \dots & \dots & \dots \\ \Delta B_{n-m+1} & \Delta B_{n-m+2} & \Delta B_{n-m+3} & \dots & \Delta B_n \end{bmatrix} \begin{bmatrix} \alpha_1 \\ \alpha_2 \\ \alpha_2 \\ \dots \\ \alpha_m \end{bmatrix} \tag{2}$$

where W^* is the corrected variable for each observation within time t from m to n; ΔB_t is the change in the barometric pressure at time t; m is the maximum lag selected by the user, and n is the total number of observations in the dataset.

To gain more accurate data of the water level, we corrected the observed pumping test data by BETCO, which is the application of the regression deconvolution (Toll *et al.*, 2005).

Calculation of hydrogeological parameters

In Aquifer Test, methods for unconfined aquifer analysis usually are either Neuman or Boulton. Theis with Jacob correction can also be used for late-time of the pumping test. Due to unsteady flow within the pumping tests by the artificial control of water stability, we need to determine the water level changes with time in order to obtain hydrogeological parameters in an unconfined aquifer of unstable movement. In this paper, the Neuman model, the Boulton model, and the Theis model with the Jacob correction (Theis with Jacob) for unconfined aquifer are used to fit the water level variation curve of the pumping process.

Jacob (1940) proposed the following correction:

$$s_{cor} = s - (s^2/2D) \tag{3}$$

Where s_{cor} is the corrected drawdown, s is the measured drawdown, and D is the original saturated aquifer thickness. There are no additional type curve parameters for this solution method.

The equation developed by Neuman representing drawdown in an unconfined aquifer is given by (Neuman, 1975):

$$s = \frac{Q}{4\pi T} W\left(u_A, u_B, \beta\right) \tag{4}$$

Where $W(\mu_A . \mu_B . \beta)$ is known as the unconfined well function; $\mu_A = r^2 s/4Tt$ is the Type A curve for early time steps; $\mu_B = r^2 S_y/4Tt$ is the Type B curve for later time steps; $\beta = r^2 K_v/K_H$, K_V, K_H: vertical and/or horizontal permeability; r is the distance to the observation well; S is storativity; S_y is *specific* yield, usable probe volume; T is transmissivity.

The method developed by Boulton (1963) can be performed as follows:

$$s_D = \frac{2\pi T(H - D)}{Q} \tag{5}$$

Where H is defined as the average head along the saturated thickness, and other parameters defined as mentioned above.

• ISSN 2007-2422

Results and discussions

Barometric pressure correction results

From the figure 3, we can conclude that, at the period of Jan. 1st to Feb. 21st and Sep. 23rd to Dec. 31st, the water level was roughly stable, which is consistent with the main water use period of the project from March to November. Though the pumping well was performed in a production well, the test was started after the water level reaching stable judged by long time observation of recovery period.

The previous researchers have done so many about barometric pressure correction (Spane, 2002; Dong, Shimada, Kagabu, & Yang, 2015) and hydrogeological parameters' calculation (Lubczynski & Roy, 2005; Samuel & Jha, 2014), But for the combination of the two methods, relevant research is relatively small (Allen, 2008; Vilhelmsen, Christensen, Behroozmand, & Søltoft, 2014), and most of them used barometric efficiency (Acworth & Brain, 2008; Delcourt-Honorez & Scholz, 2014) to correct the influence of barometric pressure, which didn't consider the delay effect to vadose zone soil layer. The delay effect is considered in BETCO software, and the result of pressure correction is more accurate.

The regression deconvolution method is used to correct the deviation that barometric pressure variation causes the measured groundwater level, and the results seem to be good. And it is easy concluded that barometric pressure correction is crucial to the accuracy of groundwater level in pumping tests, which is of great concern to delay factor. In the BETCO, though we conduct that maximum response time as 12, it can be noticed that at the preliminary stage of observation, there are still exits the phenomenon of delaying. After the correction for barometric pressure, the annual water depth has been changed; the maximum of the initial water depth was 8.518, though, with the correction, it was 8.491.

It is important to note that other natural conditions, such as tidal, meteorological, and hydrological factors will also affect the water

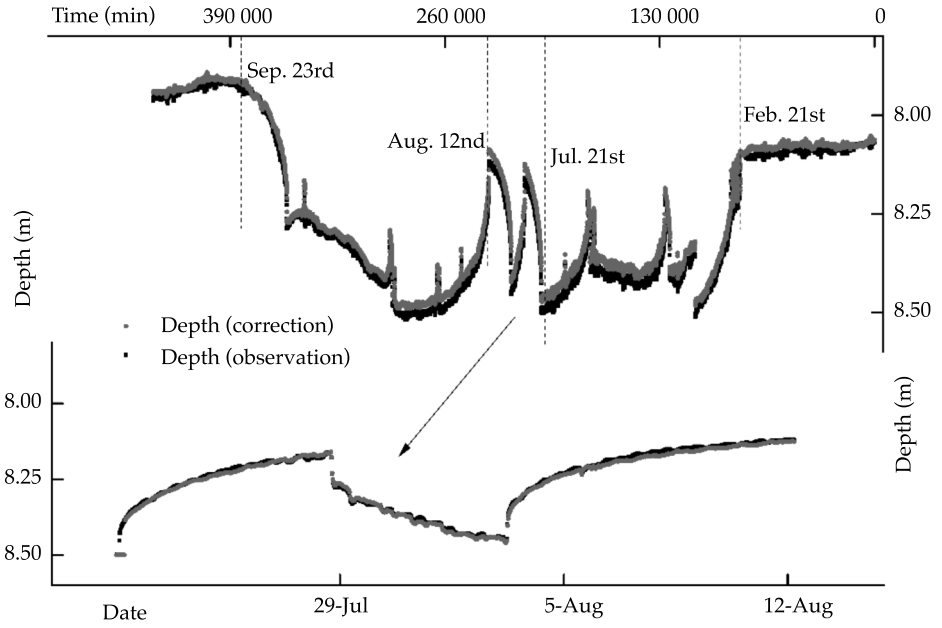

Figure 3. The comparison of the water depth with data reconciliation.

Tecnología y Ciencias del Agua, vol. VIII, núm. 2, marzo-abril de 2017, pp. 151-158
ISSN 2007-2422

level fluctuation. If these effects are taken into consideration for correction, we can determine a more accurate water level correction.

The upper graph is the observation water depth of whole year, and the inferior graph is the depth during the pumping test.

Hydrogeological parameters

The Boulton model does not achieve fitting results. The remaining two models are more successful and achieve the results shown in figure 4.

Through curve fitting, the hydrogeological parameters of the Theis model with the Jacob correction are as follows:

$$T = 8.96E2(\text{unit:m}^2/d) \quad (6)$$

$$S = 6.11E-2 \quad (7)$$

And the hydrogeological parameters of the Neuman model are as follows:

$$T = 8.76E2(\text{unit:m}^2/d) \quad (8)$$

$$S_y = 5.00E-1,\ K_v/K_H = 1.12E-3,\ S_y/S = 1.00E1 \quad (9)$$

The permeability coefficient of the two models calculated is 13.6 m/d and 13.3 m/d, which is good agreement with previous $K = 12.85$ m/d (Fan *et al.*, 2010) and $K = 13.32$ m/d (Fan, Jin, Lei, Xu, & Zhou, 2013). These hydrogeological parameters are calculated using the water level process curve model fitting based on the pumping test, and the results are useful for the construction of the hydrological model.

Conclusions

In this paper, for the unsteady flow pumping test in an unconfined aquifer, three kinds of

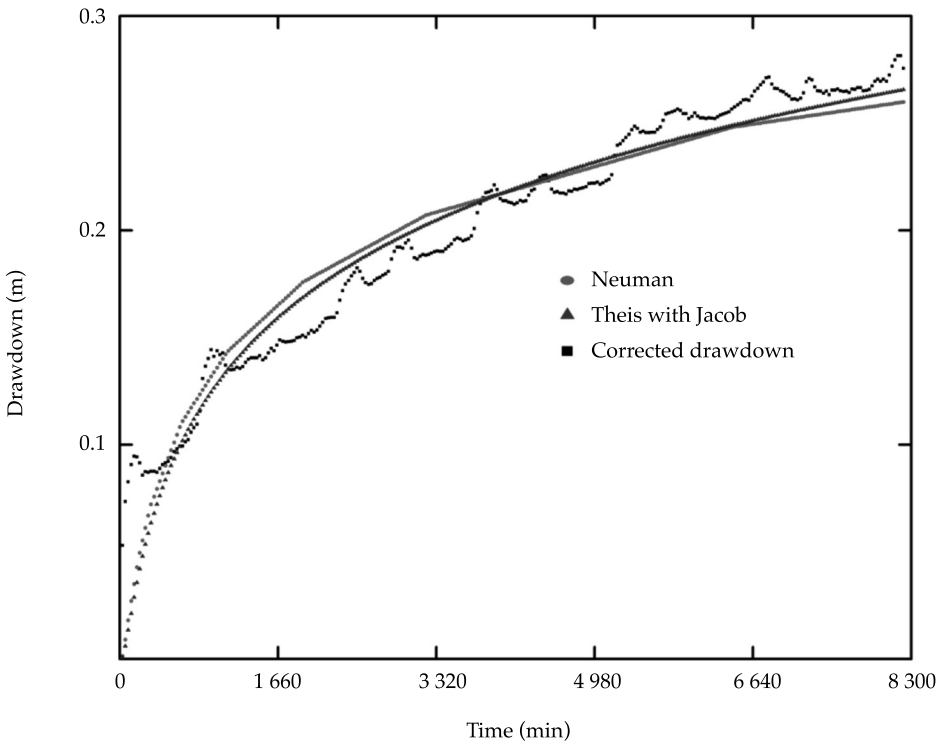

Figure 4. Groundwater level fitting of the Theis with Jacob correction and Neuman Models during pumping.

• ISSN 2007-2422

unconfined models were used to calculate hydrogeological parameters. Boulton cannot successfully gain the results, the parameters that Theis with Jacob calculated are T = 8.96 E2 m²/d, S = 6.11 E -2 and those calculated by Neuman are T = 8.76 E2 m²/d, S_y = 5.00 E-1, K_v/K_H = 1.12 E-3, S_y/S = 1 .00 E1, the permeability coefficient calculated by two models is 13.6m/d and 13.3 m/d. From the calibration results in this paper, considering the unsaturated zone delay effect, the results are closer to the true value. But in the pumping test, the study area is used as a homogeneous isotropic field. The calculated permeability coefficient is one of the point values of the region, which can't reflect the heterogeneity of the scale. However, these parameters results provide a certain reference value to further study on hydrogeological conditions in the study area and the methods used in this paper can provide solutions to the problems that may be encountered in similar projects.

Acknowledgements

This study is supported by National Natural Science Foundation of China (Grant No. 41301038, 31300449, 41471222, 41571498), and the Research Projects of the Tarim Branch of Petro China Company Limited (Grant No. 971014060006).

References

Acworth, R. I., & Brain, T. (2008). Calculation of barometric efficiency in shallow piezometers using water levels, atmospheric and earth tide data. *Hydrogeology Journal*, *16*(8), 1469-1481.

Allen, F. (2008). Analytical and numerical analyses of an unconfined aquifer test considering unsaturated zone characteristic. *Water Resources Research*, *44*(6), 88-88.

Boulton, N. S. (1963). Analysis of data from non-equilibrium pumping tests allowing for delayed yield from storage. *Ice Proceedings*, *26*(3), 469-482.

Criollo, R., Velasco, V., Vázquez-Suñé, E., & García-Gil, A. (2016). An integrated GIS-based tool for aquifer test analysis. *Environmental Earth Sciences*, *75*(5), 1-11.

Delcourt-Honorez, M., & Scholz, E. (2014). Earth tidal and barometric responses observed in the Callovo-Oxfordian clay Formation at Andra Meuse/Haute-Marne Underground Research Laboratory. *Geological Society London Special Publications*, *400*(1), 53-62.

Dong, L., Shimada, J., Kagabu, M., & Yang, H. (2015). Barometric and tidal-induced aquifer water level fluctuation near the Ariake Sea. *Environmental Monitoring & Assessment*, *187*(1), 1-16.

Fan, J. L., Xu, X. W., Li, S. Y., Zhao, J. F., & Zhou, H. H. (2010). Ground-water tables' changes with water pumping of a single well in the hinterland Taklimakan Desert. *Arid Land Geography*. Arid Land Geography (in Chinese), *33*(1), 16-22.

Fan, J., Jin, X., Lei, J., Xu, X., & Zhou, H. (2013). Responses of ground water level to pumping water from the Tarim Desert highway shelterbelt project. *Chinese Agricultural Science Bulletin* (in Chinese), *29*(2), 114-119.

Guo, H.-P., & Jiao, J. J. (2008). Numerical study of airflow in the unsaturated zone induced by sea tides. *Water Resources Research*, *44*(6), 128-134.

Guo, H., Jiao, J. J., & Weeks, E. P. (2008). Rain-induced subsurface airflow and Lisse effect. *Water Resources Research*, *44*(7), 767-768.

Jacob, C. E. (1940). On the flow of water in an elastic artesian aquifer. *Eos Transactions American Geophysical Union*, *21*(2), 574-586.

Lei, J., Li, S., Jin, Z., & Xu, B. (2008). Comprehensive eco-environmental effects of the shelter-forest ecological engineering along the Tarim Desert Highway. *Chinese Science Bulletin*, *53*(S2), 190-202.

Li, P., Qian, H., & Wu, J. (2014). Comparison of three methods of hydrogeological parameter estimation in leaky aquifers using transient flow pumping tests. *Hydrological Processes*, *28*(4), 2293-2301.

Lubczynski, M., & J. Roy (2005). MRS contribution to hydrogeological system parametrization. *Near Surface Geophysics*, *3*(3), 131-139.

Neuman, S. P. (1975). Analysis of pumping test data from anisotropic unconfined aquifers considering delayed gravity response. *Water Resources Research*, 11(11), 329–342.

Quilty, E. G., & Roeloffs, E. A. (1991). Removal of barometric pressure response from water level data. *Journal of Geophysical Research Atmospheres*, *961*(B6), 10209-10218.

Rasmussen, T. C., & Crawford, L. A. (1997). Identifying and removing barometric pressure effects in confined and unconfined aquifers. *Ground Water*, *35*(3), 502-511.

Samuel, M. P., & Jha, M. K. (2014). Estimation of aquifer parameters from pumping test data by genetic algorithm optimization technique. *Journal of Irrigation & Drainage Engineering*, *129*(5), 348-359.

Seo, H. (2001). Modeling the influence of changes in barometric pressure on groundwater levels in wells. *Environmental Geology*, *41*(1): 155-166.

Spane, F. A. (2002). Considering barometric pressure in groundwater flow investigations. *Water Resources Research*, *38*(6): 14-18.

Toll, N., & Rasmussen, T. C. (2005). BETCO: A computer program for the removal of barometric and earth tide

effects from water levels. *AGU Fall Meeting Abstracts*. AGU Fall Meeting Abstracts.

Toll, N. J., & Rasmussen, T. C. (2005). Removal of barometric pressure effects and earth tides from observed water levels. *Ground Water*, 45(1), 101-105.

Vilhelmsen, T. N., Christensen, S., Behroozmand, A., & Søltoft, T. H. (2014). Joint inversion of aquifer test, MRS, and TEM data. *Water Resources Research*, *50*(5), 3956-3975.

Wang, L. Y., Guo, H. P., Wen-Peng, L. I., Fan, S. S., Zhu, J. Y., & Feng, W. (2012). Impact of atmospheric loading on the water level in a well and methods for calibrating it. *Hydrogeology & Engineering Geology* (in Chinese), *39*(6), 29-34.

Wang, J., Wu, Y., Zhang, X., Liu, Y., Yang, T., & Feng, B. (2013). Field experiments and numerical simulations of whirlpool foundation pit dewatering. *Environmental Earth Sciences*, *71*(7), 3245-3257.

Wei, Y., Fan, J., Xu, X., Jin, X., & Zhou, H. (2016). Hydrogeochemical modelling of groundwater chemical evolution from southern margin to hinterland of the Taklamakan Desert. *Journal of Desert Research* (in Chinese), *36*(3), 798-804.

Wen, J. C., Wu, C. M., Yeh, T. C. J., & Tseng, C. M. (2010). Estimation of effective aquifer hydraulic properties from an aquifer test with multi-well observations (Taiwan). *Hydrogeology Journal*, *18*(5), 1143-1155.

Xu, X. W., Li, B. W., Zhou, Z. B., & Zhou, H. W. (2001). Demonstration of bio-control technology for desert expansion to protect the oil road in the hinterland of Takilamakan Desert —Study on saline water drop irrigation system. *Chinese Journal of Soil Science* (in Chinese), *32*(s1): 112-114.

Yu, Q. H. (1992). Preliminary study on soil coagulation water at Qongkol Region in northeastern fringe of Tarim Basin Xinjiang. *Arid Land Geography* (in Chinese), 3, 77-84.

Author´s institutional address

Yaping Wei

Postgraduate student
University of Chinese Academy of Sciences Beijing
100049, PR China
Telephone: +86 09917823142
weiypingya@163.com

Xinjiang Institute of Ecology and Geography Chinese Academy of Sciences Urumqi 830011, PR China
818 South Beijing Road, Urumqi, Xinjiang, PR China

Ph.D. Jinglong Fan

University of Chinese Academy of Sciences Beijing
100049, PR China
818 South Beijing Road, Urumqi, Xinjiang, PR China
Telephone:+86 09917823146
fanjl@ms.xjb.ac.cn

BSc. Xinwen Xu

University of Chinese Academy of Sciences Beijing
100049, PR China
818 South Beijing Road, Urumqi, Xinjiang, PR China
Telephone:+86 09917823139
sms@ms.xjb.ac.cn

Ph.D. Jiaqiang Lei

University of Chinese Academy of Sciences Beijing
100049, PR China
818 South Beijing Road, Urumqi, Xinjiang, PR China
Telephone:+86 09917885345
leijq@ms.xjb.ac.cn

Haga clic aquí para escribir al autor

Discusión

Las notas o artículos técnicos se encuentran abiertos a discusión de acuerdo con los siguientes lineamientos:

- La discusión se escribirá en tercera persona.
- El redactor de la discusión deberá usar el término polemista cuando se refiera a él mismo y el término autor cuando se trate del responsable de la nota o artículo técnicos.
- La discusión deberá remitirse durante los doce meses posteriores al último día del trimestre en que se publicó el artículo o la nota técnicos.
- El periodo de discusión puede ser extendido mediante la solicitud por escrito del polemista.
- La discusión se presentará conforme a la *Guía para colaboradores* publicada en esta misma revista (se hará caso omiso de los datos referentes a la extensión, resumen y *abstract*). Además, contará con la cita bibliográfica de las notas o artículos técnicos aludidos.
- La extensión de la discusión ocupará como máximo cuatro páginas de la revista (aproximadamente diez cuartillas, incluyendo figuras y cuadros).
- Las figuras y los cuadros presentados por el polemista deberán marcarse progresivamente con números romanos y cuando se citen los realizados por el autor se habrá de respetar la numeración original.
- Los editores suprimirán los datos ajenos al objeto de la discusión.
- La discusión se rechazará si contiene temas tratados en otras fuentes, promueve intereses personales, está descuidadamente preparada, pone en controversia hechos ya establecidos, es puramente especulativa o es ajena a los propósitos de la revista.
- La discusión se publicará junto con los comentarios del autor o autores aludidos.
- La discusión se dirigirá al editor en jefe.

Símbolo de felicidad, China.

Foto: Fernando Leyva Calvillo.

Guía para colaboradores

La revista ***Tecnología y Ciencias del Agua*** invita a los especialistas a colaborar con artículos o notas técnicas **inéditos, relacionados con el agua, derivados de una investigación, que brinden aportaciones originales** y se desarrollen dentro de la hidrología, hidráulica, gestión del agua, agua y energía, calidad del agua, ciencias físicas, biológicas y químicas, así como ciencias políticas y sociales, entre otras disciplinas, conforme a las normas que se enunciarán a continuación.

PREPARACIÓN DEL ARTÍCULO

FORMATO

Tipo de letra: Palatino en todo el documento (cuerpo del texto, cuadros e ilustraciones).

tamaño de letra: el documento se presentará en ocho, nueve, diez y veinte puntos de acuerdo con el siguiente cuadro:

8 puntos (Palatino)	9 puntos (Palatino)
• Cuadros. • Figuras. • Agradecimientos.	• Nombre de los autores. • Institución de los autores. • Resumen. • *Abstract* y *keywords*. • Dirección institucional de los autores.
10 puntos (Palatino)	**20 puntos versales (Palatino)**
• Cuerpo del texto. • Título del trabajo en inglés.	• Título del trabajo en español.

interlineado: doble espacio.

numeración de páginas: todas las páginas deben ir numeradas.

Extensión
***Artículo técnico*:** **treinta páginas** (numeradas), incluyendo figuras y cuadros.
***Nota técnica*:** **diez páginas** (numeradas), incluyendo figuras y cuadros.

CONTENIDO

Contenido
El artículo deberá presentar aportes significativos al conocimiento científico y tecnológico dentro de la especialidad; se basará en trabajos terminados o que hayan cumplido un ciclo en su desarrollo; mostrará resultados de una serie de experiencias de un año o más de investigación y estará respaldado por una revisión bibliográfica adecuada. **La estructura básica del texto deberá contener una introducción, el desarrollo y las conclusiones**. De preferencia, seguir el esquema clásico: resumen (abstract), introducción, metodología, resultados, discusión, conclusiones y referencias.

Título
El título, **redactado en español e inglés**, deberá ser informativo, sin que exceda de 12 palabras.

Resumen
El resumen, **redactado en español e inglés** (*abstract*), deberá ser conciso y proporcionar un amplio panorama de la investigación (objetivo, método, resultados y conclusiones), sin que sobrepase las 250 palabras.

Palabras clave
Se debe proporcionar una relación de ocho palabras o frases clave (máximo) redactadas **en español e inglés** (*keywords*), que faciliten la recuperación de la información.

Pies de página
No se admiten. Deberán incorporarse al texto.

Agradecimientos
Se incluirán después del texto y antes de las referencias.

Cuadros
- Deberá usarse una página para cada cuadro.
- Después de las referencias se presentará la lista de todos los cuadros que se citen.

Figuras
- Deberá usarse una página para cada figura.
- Todos los nombres de las figuras deberán incluirse después de los cuadros.
- Deberán tener alta resolución (300 dpi).

Nota: cuando el artículo se apruebe para publicación, el autor deberá remitir cada figura en archivo JPG, en alta resolución (300 dpi).

Referencias
- Toda la bibliografía debe estar referenciada en el cuerpo principal del documento.
- En el caso del abordaje de temas del dominio común en el ámbito científico y tecnológico, deberán citarse trabajos que denoten el conocimiento de los autores sobre el estado del arte.
- En la medida de lo posible, evitar las autocitas.
- Se tomará como base el formato APA de citación.

Algunos ejemplos con base en el formato APA:

Libros completos

Apellido, A. A. (Año). Título del trabajo. Ciudad de edición: Editorial.
Apellido, A. A. (Año). Título del trabajo. Recuperado de http://www.xxxxx
Apellido, A. A. (Año). Título del trabajo. doi:xxxxx
Apellido, A. A. (Ed.). (año). Ciudad de edición: Editorial.

Capítulos de libros

Apellido, A. A., & Apellido, B. B. (Año). Título del capítulo o entrada. En A. Apellido, B. Apellido & C. Apellido (Eds.), Título del libro (pp. xxx-xxx). Lugar: Editorial.
Apellido, A. A., & Apellido, B. B. (Año). Título del capítulo o entrada. En A. Editor & B. Editor (Eds.), Título del libro (pp. xxx-xxx). Recuperado de http://www.xxxxxxx

Artículo o nota de publicación periódica recuperado de la web

Apellido, A. A., & Apellido, B. B. (Año). Título del artículo. Título de la publicación, volumen(número), pp. Recuperado de http:// www.xxxxxxx

Esto es: Apellido, A. A., & Apellido, B. B. (Año). Título del artículo. Título de la publicación, 1(2), 5-17. Recuperado de http:// www.xxxxxxx

Artículo o nota de publicación periódica impresa

Apellido, A. A., & Apellido, B. B. (Año). Título del artículo. Título de la publicación, 8(1), 73-82.

Artículo de publicación periódica con DOI

Apellido, A. A., Apellido, B. B., & Apellido, C. C. (Año). Título del artículo. Título de la publicación, 8(1), 73-82, doi:xxxxxx

Congresos y simposia

Colaborador, A. A., Colaborador, B. B., Colaborador, C. C., & Colaborador, D. D. (Mes, año). Título de la colaboración. En E. E. Presidente (Presidencia), Título del simposio. Simposio llevado a cabo en la conferencia de Nombre de la Organización, Lugar.

Idioma

Español o inglés.

Separación de números y uso de punto decimal

En *Tecnología y Ciencias del Agua* se marcará la división entre millares con un espacio en blanco; mientras que para separar los números enteros de sus fracciones, cuando las haya, se usará el punto.

Al respecto, se retoma lo que indica el *Diccionario panhispánico de dudas*, editado por la Real Academia Española y la Asociación de Academias de la Lengua Española, en 2005, sobre las expresiones numéricas: "**se acepta el uso anglosajón del punto, normal en algunos países hispanoamericanos…: π = 3.1416.".**

Envío del artículo

Enviar el artículo en *Word* con nombre de autores y dirección institucional a **revista.tyca@gmail.com**, con copia a la licenciada Elizabeth Peña Montiel, elipena@tlaloc.imta.mx.

Información general

Una vez recibido el material, comenzará un proceso de revisión, durante el cual es posible que el manuscrito se rechace; si el texto es susceptible de ser dictaminado, pues cumple a cabalidad con la Política Editorial y así lo considera el Consejo Editorial, pasará a la etapa de arbitraje.

De acuerdo con el proceso de arbitraje, el texto puede ser aceptado sin cambios, con cambios menores, cambios mayores o ser rechazado.

Al ser publicado un trabajo, el autor principal tiene derecho, en forma gratuita a dos revistas y diez sobretiros.

En caso de cualquier duda, escribir a la licenciada Helena Rivas López, hrivas@tlaloc.imta.mx o a la licenciada Elizabeth Peña Montiel, elipena@tlaloc.imta.mx.

Citas dentro del cuerpo del texto

Tipo de cita	Primera cita en el texto	Citas subsecuentes en el texto	Formato entre paréntesis, primera cita en el texto	Formato entre paréntesis, citas subsecuentes en el texto
Un trabajo por un solo autor	Apellido (Año)	Apellido (Año)	(Apellido, año)	(Apellido, año)
Un trabajo por dos autores	Apellido y Apellido (Año)	Apellido y Apellido (Año)	(Apellido & Apellido, Año)	(Apellido & Apellido, Año)
Un trabajo por tres autores	Apellido, Apellido y Apellido (Año)	Apellido *et al*. (Año)	(Apellido, Apellido, & Apellido, año)	(Apellido del primer autor *et al*., año)
Un trabajo por cuatro autores	Apellido, Apellido, Apellido y Apellido (Año)	Apellido *et al*. (Año)	(Apellido, Apellido, Apellido, & Apellido, año)	(Apellido del primer autor *et al*., año)
Un trabajo por cinco autores	Apellido, Apellido, Apellido, Apellido y Apellido (Año)	Apellido *et al*. (Año)	(Apellido, Apellido, Apellido, Apellido, & Apellido , año)	(Apellido del primer autor *et al*., 2008)
Una obra por seis o más autores	Apellido del primer autor *et al*. (Año)	Apellido del primer autor *et al*. (Año)	(Apellido del primer autor *et al*., Año)	(Apellido del primer autor *et al*., año)
Grupos (identificados fácilmente a través de abreviaturas) como autores	Nombre completo de la institución (Siglas, año)	Siglas (Año)	(Nombre completo de la institución [siglas], año)	(Institución, año)
Grupos (sin abreviaturas) como autores	Nombre completo de la institución (año)	Nombre completo de la institución (año)	(Nombre completo de la institución, año)	

Política Editorial

Misión

Difundir el conocimiento y los avances científicos y tecnológicos en materia de agua, a través de la publicación de artículos y notas técnicas inéditas, que brinden aportaciones originales.

Nuestros principios

- Imparcialidad.
- Objetividad.
- Honestidad.

Nuestros valores

- Conocimiento.
- Experiencia.
- Autoridad temática.

Contenido

Interdisciplinario, conformado por aportaciones plasmadas en artículos y notas inéditos, relacionados con el agua, derivados de una investigación, que brinden aportaciones o innovaciones científicas y tecnológicas originales, que se desarrollen dentro del campo del conocimiento de diversas disciplinas.

Cobertura temática

Interdisciplinaria, relacionada con agua, con prioridad temática en los siguientes ámbitos del conocimiento:

- Agua y energía.
- Calidad del agua.
- Ciencias físicas, biológicas y químicas.
- Ciencias hidroagrícolas.
- Ciencias políticas y sociales.
- Desarrollo e innovación científica y tecnológica.
- Gestión del agua.
- Hidrología.
- Hidráulica.

Tipo de contribuciones

Artículo: documento científico que trata y comunica por primera vez los resultados de una investigación o innovación exitosa, cuyas contribuciones aportan e incrementan el conocimiento actual en materia hídrica.

Nota: texto inédito que trata avances principalmente en el campo de la ingeniería hidráulica y de la práctica profesional en materia de agua.

Algunos trabajos sometidos al proceso de arbitraje como artículo pueden terminar publicándose como notas o viceversa. Esto se hará bajo propuesta y un proceso de mutuo acuerdo entre los autores y el editor por tema responsable. Ambas contribuciones tienen prácticamente la misma estructura (resumen, introducción, metodología, resultados, discusión, conclusiones, referencias).

Proceso de arbitraje

La revista se rige por un riguroso proceso de arbitraje, el cual establece que cada trabajo debe ser analizado separadamente por tres revisores, quienes recomiendan su aceptación, su aceptación con cambios menores, su aceptación con cambios mayores, su rechazo o su aceptación como nota técnica con los cambios necesarios. Con base en estas recomendaciones, el editor temático responsable emite el dictamen final.

Se buscará que al menos uno de los revisores sea de alguna institución del extranjero.

Los revisores no podrán pertenecer a la misma institución de los autores que proponen el artículo o nota para publicación.

Cuando los dictámenes se contrapongan o resulten poco consistentes, el editor temático correspondiente podrá dictaminar, o solicitar la intervención de otros revisores o de algún miembro(s) del Consejo Editorial.

En los casos que lo amerite, el editor temático podrá decidir sobre la aprobación o no de un artículo o nota con el dictamen de dos revisores, más su propia opinión como editor por tema correspondiente, o la del editor en jefe.

Todo artículo o nota rechazado no se admitirá para un nuevo proceso de revisión.

El proceso de arbitraje se desarrollará bajo la modalidad de arbitraje "doble ciego", de tal manera que tanto los autores como los revisores no conozcan el nombre de su contraparte, a fin de mantener la imparcialidad del proceso.

Toda documentación asociada con el proceso de arbitraje se clasifica como confidencial; esto incluye nombre de los árbitros, dictámenes, para mantener la imparcialidad del proceso, y de los datos personales, a fin de cumplir con las leyes de la materia.

El proceso de arbitraje lo llevan a cabo especialistas y expertos de alto nivel, de reconocido prestigio nacional e internacional en su ámbito profesional, con la capacidad para evaluar, de manera confiable y expedita, tanto la calidad como las aportaciones originales como el grado de innovación científica y tecnológica del material que se somete a dictamen para posible publicación.

Esta participación se considera una contribución profesional, que es realizada de manera honorífica.

Para la elaboración de su dictamen, los árbitros cuentan con la "Guía para el revisor".

Dictamen final

El dictamen que se emita, derivado del proceso de arbitraje, es inapelable.

Autores

Se publican trabajos de autores de cualquier nacionalidad, que presenten sus contribuciones en español o inglés.

A fin de promover la diversidad de autores y su procedencia, un mismo autor o coautor no podrá publicar en la revista ***Tecnología y Ciencias del Agua*** más de dos trabajos al año, con excepción de artículos o notas publicadas en ediciones especiales y números extraordinarios.

Una vez que se acepta un artículo o nota para ser publicado, los autores firman un permiso para publicar, en donde ceden los derechos patrimoniales en exclusiva al Instituto Mexicano de Tecnología del Agua, titular de la revista ***Tecnología y Ciencias del Agua***.

Responsabilidad de los autores

La propuesta de un trabajo compromete al autor o autores a no someterlo simultáneamente a la consideración de otras publicaciones. En caso de que el artículo o nota sea entregado a otro medio para su eventual publicación, los autores se comprometen a hacerlo del conocimiento de la Coordinación Editorial, que suspenderá el proceso de arbitraje e informará al Consejo Editorial sobre la decisión tomada por los autores; esta misma suspensión tendrá efecto si la revista ***Tecnología y Ciencias del Agua*** identifica y corrobora una situación similar.

La responsabilidad del contenido, originalidad y autenticidad de los artículos o notas corresponde a los autores.

Los autores son responsables de la calidad del español e inglés que utilicen. Si su redacción es deficiente, se rechazará su contribución. La revista ***Tecnología y Ciencias del Agua*** sólo se hará cargo del cuidado editorial.

Los autores se comprometen a realizar los ajustes que sean señalados por el editor temático en el tiempo fijado por éste; en caso de incumplimiento, el artículo o nota será retirado del proceso de dictaminación y será calificado como rechazado.

Los autores deberán estar atentos para resolver las dudas y propuestas que presenten el editor y el coordinador editorial.

Los autores deberán aprobar las pruebas finales de imprenta de sus textos.

Los autores de la revista aceptan formar parte del grupo de árbitros de la revista ***Tecnología y Ciencias del Agua***, con la responsabilidad que ello implica.

Los autores deben basarse en la "Guía para colaboradores" para remitir sus artículos o notas.

Una vez que reciban la carta de aceptación para publicar su artículo o nota, los autores no podrán incluir a ningún otro autor.

Los autores sólo podrán eliminar a un autor del artículo o nota en proceso mediante oficio dirigido a la revista ***Tecnología y Ciencias del Agua***. Dicho oficio debe ir firmado (en papel) tanto por el autor principal como por el autor a quien se pretende eliminar y quien da su consentimiento expreso.

El porcentaje de autocitas en un artículo no podrá ser superior al 20%.

Lectores

Académicos, investigadores, especialistas y profesionales interesados en el análisis, investigación y búsqueda del conocimiento y soluciones de problemas relacionados con el agua.

Recepción de trabajos

La recepción de artículos y notas es permanente.

Periodicidad

Edición bimestral.

Se tendrá una versión *preprint* de los artículos y notas aprobados para ser publicados; esto, sin esperar a integrar un número completo.

Suscripción y distribución

La revista se distribuye por medio de suscripciones pagadas y honorarias.

Acceso abierto

La revista ***Tecnología y Ciencias del Agua*** permite consultar en su versión digital todo el material publicado sin costo, incluyendo el de las revistas que la precedieron: *Irrigación en México*; *Ingeniería hidráulica en México*, primera época; *Recursos hidráulicos*; e *Ingeniería hidráulica en México*, segunda época.

Ediciones especiales y números extraordinarios

La revista ***Tecnología y Ciencias del Agua*** podrá publicar números especiales por sí misma o en colaboración con otras revistas, asociaciones profesionales o casas editoriales de reconocido prestigio relacionadas con el recurso agua. En este caso, todos los trabajos deberán pasar por el proceso de arbitraje establecido en esta Política Editorial.

Asimismo, la revista ***Tecnología y Ciencias del Agua*** podrá publicar artículos por invitación, en reconocimiento a la trayectoria profesional de destacados investigadores.

En ambos casos se cuidará la calidad de los contenidos técnicos y las aportaciones científicas.

Código de ética

El quehacer de la revista ***Tecnología y Ciencias del Agua*** se basa en principios de imparcialidad, objetividad y honestidad.

Tecnología y Ciencias del Agua está registrada en los siguientes índices y resúmenes (abstracts) nacionales e internacionales:

• Thomson Reuters Science Citation Index® (*ISI*) • Expanded Thomson Reuters Research Alert® (*ISI*) • *Índice de revistas mexicanas de investigación científica y tecnológica* del Consejo Nacional de Ciencia y Tecnología (Conacyt) (2013-2018) • Sistema de Información Científica Redalyc (Red de Revistas Científicas de América Latina y El Caribe, España y Portugal), Universidad Autónoma del Estado de México • *EBSCO* (Fuente Académica Premier NISC; Geosystems, como Marine, Oceanographic and Freshwater Resources) • *ProQuest* (Cambridge Scientific Abstracts) • *Elsevier* (Fluid Abstracts: Process Engineering; Fluid Abstracts: Civil Engineering) • *CAB Abstracts*, CAB International • *Latindex* (Sistema Regional de Información en Línea para Revistas Científicas de América Latina, el Caribe, España y Portugal), Universidad Nacional Autónoma de México • *Periódica* (Índice de Revistas Latinoamericanas en Ciencias), Universidad Nacional Autónoma de México • *Catálogo Hela* (Hemeroteca Latinoamericana), Universidad Nacional Autónoma de México • *Actualidad Iberoamericana*, CIT-III, Instituto Iberoamericano de Información en Ciencia y Tecnología.

Otras fuentes

También puede encontrarse su acervo en *Google académico*.

Contenido

Artículos técnicos

Contents

Technical articles

IMTA
Instituto Mexicano de Tecnología del Agua

http://www.imta.gob.mx/tyca